Imperial College London

Functional Characterisation of Interferon Stimulated Genes in Respiratory Viral Infection

David C. Busse

Department of Medicine, Imperial College London

Thesis submitted for the degree of Doctor of Philosophy

“The truth is rarely pure and never simple”

— Oscar Wilde, The Importance of Being Earnest

Abstract

A key element of host antiviral defence is cell intrinsic immunity, driven by an array of interferon stimulated genes (ISGs), few of which have been properly characterised. However, the breadth of ISG antiviral mechanisms suggests this gene network can target nearly every stage of a viral life cycle.

Respiratory syncytial virus (RSV) is responsible for a vast number of infections, primarily in infants. Intriguingly, most infants requiring hospitalisation with a severe RSV infection present with no known risk factor. It was hypothesised that ISGs induced by RSV infection represent potential genetic risk factors that could influence virus control and disease severity between individuals.

The IFN-induced transmembrane (IFITM) family of ISGs are broadly antiviral and thought to target virus entry. The data presented here expand our understanding of IFITM1 function by demonstrating that antiviral activity is dependent upon plasma membrane localisation. The *in vivo* relevance of IFITM1 was also probed in a monogenic knockout mouse model, for the first time demonstrating that the loss of IFITM1 alone is sufficient to result in a loss of viral control and enhanced disease severity.

Next, the role of IFN-induced protein 44 (IFI44) proteins was explored as these ISGs are especially poorly characterised and are highly induced by RSV infection. There are conflicting data on the antiviral activity of IFI44 and IFI44L during RSV infection. This study presents evidence that these genes are antiviral, impacting an early point of the viral life cycle associated with reduced polymerase activity. Finally, the loss of IFI44 *in vivo* was shown to result in increased RSV disease severity.

Acknowledgements

I would like to express my gratitude to my supervisor Dr John Tregoning for his ceaseless and invaluable support, guidance, and motivation throughout this PhD. His supervision has taught me how to approach problems, deal with difficulty, and how to employ all the other facets of being a good research scientist. He has provided an excellent work atmosphere for which I am especially grateful. The time as part of his group has been immensely enjoyable and rewarding.

I would also like to thank my second supervisor Prof. Paul Kellam for his guidance throughout this project.

I would like to thank all members of the Tregoning group past and present with whom I have had the pleasure of working with, especially Dr Ekaterina Kinnear and Dr Helen Groves, for providing not just technical assistance but constant support and necessary humour during my PhD. Thanks is due to all members of the department for their assistance during these three years, especially Mr Chris Pinder and Dr Irene Bassano.

I would also extend thanks to all collaborators for their work, technical assistance, and provision of key reagents including Prof. Richard Randall, Dr Marcus Dorner, Dr Jean-François Éléouët, and Dr Yanping Guo.

Finally, this PhD would have been impossible without the incomparable support of my partner Megan and my family. Their ability to motivate me through the multitude of difficult moments was nothing short of ineffable.

This work was funded by a studentship awarded by the Wellcome Trust.

Declarations

Declaration of Originality

This thesis consists of one's own work, with all else properly referenced.

Copyright Declaration

Word count excluding bibliography: 50,161

Table of Contents

List of Figures and Tables

Abbreviations

AIM2	Absent in melanoma 2
AM	Alveolar macrophage
AMP	Adenosine monophosphate
AP-2	Activating protein 2
APOBEC3G	Apolipoprotein B mRNA editing enzyme catalytic polypeptide-like 3G
BALB/C	Bagg albino mouse strain
BALF	Bronchoalveolar lavage fluid
BCA	Bicinchoninic acid
BPD	Bronchopulmonary dysplasia
BSA	Bovine serum albumin
BUNV	Bunyamwera orthobunyavirus
C57BL/6	Black line-6 mouse strain
CCL	C-C motif chemokine ligand
CGAS	Cyclic GMP-AMP synthase
CHD	Congenital heart disease
CHIKV	Chikungunya virus
CIL	Conserved intracellular loop
CLR	C-type lectin receptor
CRISPR	Clustered regularly interspaced palindromic repeats
CXCL	C-X-C motif chemokine ligand
D10	DMEM supplemented with 10% FCS

DAMP	Danger associated molecular pattern
DAPI	4',6'-diamidino-2-phenylindole
DC-SIGN	Dendritic cell-specific intercellular adhesion molecule 3-grabbing non-integrin
DDHCTP	3'-deoxy-3',4'-didehydro-cytidine triphosphate
DENV	Dengue virus
DMEM	Dulbecco's modified eagle medium
DMSO	Dimethyl sulfoxide
ECMV	Encephalomyocarditis virus
EDTA	Ethylenediaminetetraacetic acid
ELISA	Enzyme-linked immunosorbent assay
ER	Endoplasmic reticulum
FACS	Fluorescence activated cell sorting
FCS	Foetal calf serum
FLUC	Firefly luciferase
FMO	Fluorescence minus one
GAPDH	Glyceraldehyde 3-phosphate dehydrogenase
GAS	Gamma-activated sequence
GBP	Guanylate binding protein
GDP	Guanosine diphosphate
GE	RSV gene end sequence
GFP	Green fluorescent protein
GLUC	Gaussia luciferase
GMP	Guanosine monophosphate

GPI	glycosylphosphatidylinositol
GRNA	Guide RNA
GS	RSV gene start sequence
GTP	Guanosine triphosphate
GTPASE	GTP hydrolase
HA	Haemagglutinin
HBV	Hepatitis B virus
HCMV	Human cytomegalovirus
HCV	Hepatitis C virus
HIV-1	Human immunodeficiency virus-1
HMPV	Human metapneumovirus
HPSE	Heparanase
HRP	Horseradish peroxidase
HSPG	Heparan sulphate proteoglycan
HSV-1	Herpes simplex virus-1
ICAM	Intercellular adhesion molecule
IFI44	IFN induced protein 44
IFI44L	IFN-induced protein 44-like
IFI6	IFN induced protein 6
IFIT	IFN-induced protein with tetratricopeptide repeats
IFITM	IFN-induced transmembrane protein
IFN	Interferon
IFNAR1/2	Interferon alpha and beta receptor subunit 1/2

IFNGR1/2	Interferon-γ receptor 1/2
IFN-I	Type one interferon
IFN-II	Type two interferon
IFN-III	Type three interferon
IFNLR1/IL10R2	Interferon lambda receptor-1/IL-10 receptor beta subunit
IL	Interleukin
IRES	Internal ribosome entry site
IRF	Interferon regulatory factor
ISG	Interferon stimulated gene
ISG20	Interferon stimulated exonuclease gene 20
ISRE	Interferon-sensitive response element
JAK	Janus-activated kinase
KO	Knockout
L	RSV large polymerase
LGP2	Laboratory of genetics and physiology 2
LRTI	Lower respiratory tract infection
L-SIGN	Liver/lymph node-specific intercellular adhesion molecule 3 grabbing non-integrin
M	RSV Matrix protein
MAVS	Mitochondrial antiviral-signalling protein
MDA-5	Melanoma differentiation-associated protein 5
MDCK	Madin-Darby Canine Kidney Epithelial Cells
MEM	Minimum essential medium

MTS	3-(4,5-dimethylthiazol-2yl)-5-(3-carboxymethoxyphenyl)-2-(4-sulfophenyl)-2H-tetrazolium
MX	Myxovirus resistance protein
N	RSV Nucleoprotein
NDV	Newcastle disease virus
NF-KB	Nuclear factor kappa B
NK	Natural Killer
NLR	NOD-like receptor
NOD	Nucleotide-binding oligomerisation domain
NS1	RSV Non-structural protein 1
NS2	RSV Non-structural protein 2
OAS	2'-5'-oligoadenylate synthase
ORF	Open reading frame
P	RSV Phosphoprotein
PAGE	Polyacrylamide gel electrophoresis
PAMP	Pathogen associated molecular pattern
PBS	Phosphate buffered saline
PCR	Polymerase chain reaction
PDC	Plasmacytoid dendritic cell
PIV	Parainfluenza virus
PKR	Protein kinase R
PRR	Pattern recognition receptor
R10	RPMI supplemented with 10% FCS
RDRP	RNA-dependent RNA polymerase

RFP	Red fluorescent protein
RLR	RIG-I-like receptor
RNP	Ribonucleoprotein
RPMI	Roswell Park Memorial Institute medium
RSV	Human respiratory syncytial virus
RV	Rhinovirus
RVFV	Rift valley fever virus
SDS	Sodium dodecyl sulphate
SH	RSV Small hydrophobic protein
SIRNA	Small-interfering RNA
SP-A	Surfactant protein-A
SP-C	Surfactant protein-C
SP-D	Surfactant protein-D
STAT	Signal transducer and activator of transcription
STING	Stimulator of interferon genes
TDRD	Tudor domain-containing protein
TIR	Toll/interleukin-1 receptor homology domain
TLR	Toll-like receptor
TM	Transmembrane
TNF-A	Tumour necrosis factor-alpha
TRIM	Tripartite motif
URTI	Upper respiratory tract infection
VEEV	Venezuelan encephalitis virus

VSV	Vesicular stomatitis virus
WNV	West Nile virus
WT	Wild-type
ZAP	Zinc finger antiviral protein

Chapter 1

Introduction

1 Introduction

1.1 Respiratory Viral Infections

1.1.1 Global Prevalence

Respiratory infections are estimated to be the fifth leading cause of death globally, and the leading infectious cause of death in those under the age of 5 years. This observation was noted in some of the earliest studies of global disease burden in infants [1]. A more recent study of 195 countries (1990-2015) estimated that lower respiratory tract infections (LRTI) caused 2.74 million deaths in 2015, of which 704 000 were children under the age of 5 years [2]. Bacterial lung infection was the major cause of death in children with pneumococcal pneumonia accounting for 55.8% alone. Viral infections were more often associated with non-fatal infections. RSV accounted for 15.4% of all infections with influenza the cause in 10.4% of LRTI cases in all ages [2].

1.1.2 Signs and Symptoms

There is a broad range of viral pathogens that can infect the airways. Infections of the respiratory system are categorised as either upper respiratory tract infections (URTI) where the pathogen and pathology are limited to the upper respiratory tract and trachea, and LRTIs where the infection spreads to the lower airways and respiratory tract. The upper respiratory tract consists of the nasal passages, sinuses, and pharynx [3]. The lower respiratory tract consists of the passageways that air transits upon exiting the upper respiratory tract including the trachea, bronchi, the smaller bronchioles, and finally the alveoli and alveolar sacs that are the essential sites of gas exchange [3].

URTIs are generally self-limiting conditions commonly presenting as pharyngitis, epiglottitis, laryngotracheitis, and of course the common cold with symptoms such as cough, hoarseness, earache, and tenderness [4]. They may be accompanied by fever. LRTIs are more serious and are associated with higher rates of mortality and morbidity. They include clinical presentations such as bronchitis, bronchiolitis, and pneumonia although there is no internationally agreed definition for these presentations. Bronchitis can refer to infections involving the large-airways whereas bronchiolitis and pneumonia can refer to infections of the small airways or alveolar sacs respectively [4]. Symptoms can include breathlessness, wheeze, severe cough, tachypnoea, and respiratory distress. Infants are the main group susceptible to LRTI [5].

1.1.3 Common Respiratory Viral Infections in Infants

The majority of respiratory viral infections are caused by a common set of viral pathogens: respiratory syncytial virus (RSV), influenza virus, and rhinovirus (RV) [6]. Co-infection can occur with both viral or bacterial pathogens, with up to 50% of severe respiratory viral infections thought to be exacerbated by pneumococcal pneumonia [2]. Other viruses that can cause respiratory tract infections include human metapneumovirus (HMPV), parainfluenza viruses (PIV), bocavirus, adenovirus, and enterovirus [6].

1.1.4 Diagnosis of Respiratory Viral Infections

There are several methods for determining the causative viral agent of a respiratory infection including virus culture, antigen detection (immunofluorescence), polymerase chain reaction (PCR) tests, and detection of virus-specific antibodies by a functional assay (serology) [4]. PCR-tests and others based on detection of nucleic acids can be

multiplexed and are faster than other available methods. They also are significantly more sensitive. However, PCR detection of viral infection may not in fact determine the causative agent, there are reports of detection of viral RNA in asymptomatic children [7] and viruses including rhinovirus and enterovirus have been persistently detected after episodes of acute infection [8]. In mice, RSV is also persistently detected in lung tissue following resolution of infection [9].

It is important to note that viral diagnosis is normally only sought if a patient requires admission to hospital [4]. For most common respiratory viruses there are no effective antiviral treatments and so therapy is mainly supportive. As such there is often no need for a specific diagnosis, although it can assist with preventing nosocomial co-infections by appropriately partitioning patients infected with different viruses [4]. It is also important to encourage confirmation of viral rather than bacterial infection as this can reduce the rate of antibiotic usage in cases where they would be unnecessary [4].

1.1.5 Treatment of Respiratory Viral Infections

Respiratory viral infection can result in airway obstruction and inflammation. Supportive therapy where there are no available effective antivirals often aims to combat these two elements. Bronchodilators such as epinephrine have been used and are reported to reduce symptoms but do not appear to reduce the duration of hospitalisation [10]. Multiple studies have found no benefit specifically in treatment of infant bronchiolitis [11-13]. Corticosteroids are commonly employed to reduce airway inflammation, although again there are conflicting reports as to their efficacy in LRTI cases [4].

1.1.6 Respiratory Syncytial Virus Epidemiology

RSV is the most common cause of acute respiratory infection in infants and this thesis aims to expand our understanding of how the host controls this ubiquitous infection. RSV is a prevalent viral pathogen which infects the majority of infants within the first two years of life [14]. Within those first two years RSV is the most common cause of lower respiratory tract infection (LRTI) [15]. Bont *et al* estimated that RSV is the causative agent of 12-63% of all acute respiratory infections and is responsible for 19-81% of respiratory infections where an infant requires hospitalisation [16]. As such, RSV accounts for a staggering number of healthcare engagements and hospitalisations around the world. One study reported that, in a population of 0-5 year-old infants (n=5067) across three counties of the United States of America in 2002-2004, RSV was responsible for 18% of emergency department visits and 15% of consultations with community-based doctors [17]. Globally in 2015 RSV infections are estimated to have resulted in 48000-74500 deaths of infants aged younger than five years [18]. Most of these fatal cases are thought to occur in developing countries.

1.1.7 Signs and Symptoms of Clinical Respiratory Syncytial Virus Infection

Infants are the dominant population that present with clinically relevant RSV infections [5]. The virus is spread through respiratory droplets and has an incubation period of 3-5 days. Most RSV infections are self-limiting and mild URTIs [4]. These cases may present with the myriad symptoms associated with a common cold. In addition, infants with an URTI may have a fever, earache along with a red bulging of the tympanic membrane, and show increased lethargy along with poor feeding [4]. Clinical examination may reveal inflammation of the inside of the nose (rhinitis) and pharynx (pharyngitis).

Respiratory viral infection such as RSV can progress to a more debilitating LRTI in around 33-40% of infants [4, 15]. This may require therapeutic intervention and in around 1-2% of infants developing a LRTI hospitalisation may also be required [17]. This is often the point at which virological investigation is undertaken and RSV diagnosed as the causative agent [4]. Although there have been several extrapulmonary manifestations described for RSV-LRTIs such as seizures and cardiac failure [19], the majority of symptoms are limited to the respiratory system. These include wheeze, a more severe cough, breathlessness, and abnormally rapid breathing (tachypnoea) [4]. Clinical observations include but are not limited to wheeze and crackle upon auscultation of the chest, indrawing of the chest wall caused by a loss of pressure in the chest cavity, and rarely cyanosis (bluish colour to extremities due to lack of oxygen) [4].

1.1.8 Antiviral Therapy

There are currently no approved curative therapies for RSV infection and a single prophylactic therapy. Palivizumab is a humanised monoclonal antibody that binds to a conserved epitope in the RSV F protein approved for prophylactic administration in at-risk infants [20]. While Ribavirin is licenced for use to treat ongoing RSV infection it is regarded as ineffective and not routinely included in recommendations [20]. Recommended interventions, including hydration and oxygen supplementation, are purely supportive. There are multiple lines of investigation ongoing into the development of effective curative therapies for RSV infection. Such strategies include developing immunoglobulins, nucleoside analogues, small-interfering RNAs (siRNA), and fusion inhibitors targeting the RSV F protein [20].

1.2 Risk Factors for Severe RSV Infection

Only a minority of RSV-infected individuals develop a LRTI and of those only a subset require intervention for a potentially fatal infection [4]. Severity of RSV infections can be monitored by the requirement for hospitalisation, supplemental oxygen, mechanical ventilation, and duration of hospitalisation. There are several described risk factors that attempt to explain why an individual may be predisposed to develop a more severe form of RSV infection. These include host factors such as age, premature birth [17], or immunosuppression [21]. There are also several described genetic components, primarily in genes involved in innate immunity [22], that are thought to contribute to an individual's propensity to develop a severe RSV infection. Environmental factors can also contribute to a person's immunological status and ability to fight off an infection [23]. Finally, viral factors such as a change in replication competency may also influence pathogenicity and increase the risk of a severe infection. Higher viral load has been shown to associate with severity of infection and requirement for intensive care admission [24]. Interestingly, the majority (85%) of infants requiring hospitalisation present with no known risk factor for developing a severe RSV infection [25]. As such we believe there are additional genetic factors, as yet undescribed, that contribute to this inter-individual disease severity.

1.2.1 Age and Premature Birth

Age is the primary risk factor for developing severe RSV infection [17]. The airways of neonates, especially those born prematurely, are reduced in diameter and there is a higher area-to-volume ratio in their still developing airways [26]. The reduced luminal diameter of infant airways make them more prone to obstruction than adults [27]. Neonates also mount a hypo-responsive immune response characterised by

dampened cytokine production, reduced innate cell numbers, a dysregulated Th2-skewed T cell response, and poor humoral responses resulting in reduced production of high affinity antibody [28].

In a cohort of infants under the age of 2 years, age was found to associate with requirement for hospitalisation and intensive care admission [24]. A study of hospitalised children with RSV bronchiolitis reported age (< 2 months) as the most significant determining requirement for mechanical ventilation [29]. Premature birth (generally defined as a gestational age of 33-37 weeks) has been significantly associated with RSV LRTI, hospitalisation, and increased requirement for mechanical ventilation, intensive care admission, and supplemental oxygen across a variety of studies [30-32]. A meta-analysis of published and unpublished studies from 1995-2015 reporting on cohorts of children younger than five years of age with RSV-associated LRTI suggest an odds ratio of 1.96 (95% confidence interval 1.44-267), increasing to 2.79 (95% confidence interval 2.19-3.55) when considering subjects with a gestational age of less than 33 weeks [33]. Lower admission weight is also commonly reported to associate with RSV hospitalisation and severe infection [24, 29].

1.2.2 Immunosuppression

Infants with congenital or acquired immunodeficiency, following transplantation or immunosuppressive therapy have been reported in a variety of studies to be at a greater risk of developing an RSV LRTI. A study of 293 RSV-positive immunocompromised patients reported that both adult and infants were more likely to be hospitalised when immunocompromised [34]. This risk was increased in the infant patients. Several studies have also reported prolonged viral shedding alongside increased hospitalisation rates in immunocompromised cohorts (reviewed in [21, 35]).

1.2.3 Cardiopulmonary Conditions

Congenital heart disease (CHD) is an umbrella term for abnormalities in heart structure and function that are present from birth. CHD has been associated with increased requirement for medical interventions and higher RSV-associated morbidity and mortality [36, 37]. These observations have led to palivuzumab prophylaxis being recommended for children under 2 years of age with significant CHD [35]. Bronchopulmonary dysplasia (BPD) is a condition primarily associated with premature birth as it develops following mechanical ventilation or supplemental oxygen. BPD is also associated with an increased rate of RSV hospitalisation and higher rates of mortality [38]. Cystic fibrosis has been associated with increased RSV-related hospitalisation [25] and reduced lung function following RSV infection [39].

1.2.4 Immunoglobulin Levels

In full-term infants less than 6 months of age, the presence of high titres of maternally derived anti-RSV neutralising antibodies is inversely correlated with the frequency of RSV LRTI [40]. Similarly, in pre-term infants reduced transfer of maternal antibodies is associated with severity of RSV infection [41]. There is a suggestion that the titre and contribution of maternally derived antibodies is dependent upon the time during the RSV season at which birth occurs [35]. Following birth, lack of breastfeeding has also been associated with a predisposition to developing severe RSV infection, likely due to reduced transfer of anti-RSV antibodies and other factors [35]. Antibodies are effectively transferred to the foetus during pregnancy and as such maternal immunisation is currently seen as a viable option to provide neonates with 3-6 months of protection [42].

1.2.5 Environmental and Demographic Risk Factors

Multiple non-medical factors have been linked to RSV LRTI and disease severity such as parental education level [43] (although several studies have been unable to confirm this association, reviewed in [35]), multiple gestations [44], day-care attendance [23], male sex, and birth in first half of the RSV season. Household crowding has also been associated with increased risk of infant hospitalisation following RSV infection in studies from a range of developing and developed countries [45].

1.2.6 Genetic Risk Factors

Genetic associations with severe RSV LRTI have been reported in a variety of genes, primarily related to innate immunity. SNPs in genes encoding surfactant proteins *SPA* [46]*, SPD* [47], and *SPC* [48] have been associated with severe RSV LRTI in infant patient populations. In addition SNPs in *TLR4*, *CXC3R*, and genes encoding chemokines IL-4, and IL-8 have been associated with severe RSV LRTI [49]. One study of 470 hospitalised children and 1,008 control subjects found the innate immune genes *VDR*, *IFNA5*, *NOS2*, and *JUN* associated with hospitalisation [22]. *JUN* encodes the AP-1 transcription factor required for optimal interferon (IFN)-β induction following pattern recognition receptor (PRR) activation. The association of an IFN-α-encoding gene and *JUN,* a key regulator of IFN-β induction, highlight the potential importance of the type I IFN (IFN-I) system during RSV infection in infants. To date, *MX1* is the only ISG that has been associated with an increased risk of severe RSV infection in a study of human infants [50]. Interestingly, these genetic risk factors are mostly in genes related to the innate immune response and sensing of the virus. In order to understand how these might have an effect, it is necessary to understand how the virus infects cells.

1.3 Respiratory Syncytial Virus Virology

1.3.1 Respiratory Syncytial Virus Genome Organisation

RSV was first identified in the 1950s, first in chimpanzees [51] and then in human infants [52]. RSV is an enveloped virus with a negative-sense non-segmented RNA genome of 15 kilobases [53]. RSV is classified in the *Orthopneumovirus* Genus within the family *Pneumoviridae* and *Mononegavirales* Order [54]. There are currently two subgroups of RSV, A and B. The genome sequence of these subgroups diverge along the entire length of the sequence but most strongly in the gene encoding the large glycoprotein G, involved in viral attachment [53]. The viral genome encodes 11 proteins from 10 genes due to two overlapping open reading frames (ORF) in the M2 gene. The genes in order from the 3' end are 3′ NS1-NS2-N-P-M-SH-G-F-M2-L 5'. The virion itself can be found in either spherical or filamentous forms and is enveloped in a host plasma membrane-derived lipid bilayer studded with three viral transmembrane surface glycoproteins that form disparate homo-oligomers [53]. These are the large glycoprotein (G), the fusion protein (F), and the small hydrophobic protein (SH).

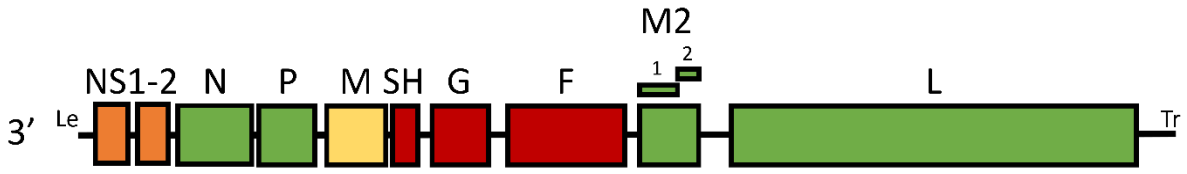

Figure 1.1. RSV genome organisation. RSV RNA genome schematic with gene boxes coloured according to function. Orange = non-structural. Green = Nucleocapsid and replication. Yellow = Matrix. Red = Envelope. Le = leader region. Tr = Trailer region.

1.3.2 Host Cell Entry by RSV

Ciliated epithelial cells are the primary site of RSV replication and entry into these cells is thought to occur initially across the apical membrane [55]. The G protein has been reported to bind a number of cellular receptors including annexin II [56], toll-like receptor (TLR)-4 [57], intercellular adhesion molecule 1 (ICAM-1) [58], heparan sulfate proteoglycans (HSPG) [59], and the CX3C chemokine receptor 1 (CX3CR1) [60]. HSPGs are not detectable on the apical surface of ciliated human airway epithelial cells and so this entry mechanism is likely to be a process that only occurs in synthetic culture systems [61]. Mice lacking CX3CR1 had reduced viral load in one study of adult mice [60] but a subsequent study in new-born mice saw no impact on viral burden [62]. Interestingly, viable mutants lacking the G gene are infectious, suggesting that G is not required for cell entry but may merely enhance binding to the cell surface [63].

The F protein has been reported to bind cell surface nucleolin [64]. Endogenous nucleolin expression is capable of conferring RSV susceptibility to cells not normally supportive of RSV infection [64]. Interestingly, only a small proportion of nucleolin is found on the cell surface with the majority localising to the nucleolus [64]. The F protein is also thought to bind to TLR4, although it has been suggested that it is the intracellular signalling induced by TLR4 binding that enhances RSV entry instead of TLR4 playing a direct role in virus internalisation [65].

Following receptor binding the viral nucleocapsid must be delivered to the cytoplasm. RSV is thought to be internalised through direct fusion with the plasma membrane, as the process is independent of endosome acidification which is commonly required to induce conformational changes in viral fusion proteins required for membrane fusion [66]. However, studies have also noted that RSV can be internalised by macropinocytosis [67] and clathrin-mediated endocytosis which delivers the viral

particle to Rab5^{+} endosomes prior to fusion of the viral envelope with the endosomal membrane and nucleocapsid escape [68].

It has since been proposed [66] that RSV entry is a two-step mechanism whereby (1) the virus binds to receptors on the cell surface at cholesterol-rich domains where the F protein mediates the initial steps of membrane fusion, forming a hemifusion where the outer leaflets of the two interacting membranes are fused [69, 70]. This is followed by (2) macropinocytosis or clathrin-mediated endocytosis and a second proteolytic cleavage event in the F protein triggers the final stages of membrane fusion [66]. This hypothesis is supported by observations that hemifusion occurs at the plasma membrane [66], that Rab5 is required for infection, and that the RSV F protein requires a second proteolytic-cleavage event in an endocytic compartment [67].

1.3.3 RSV Replication

The genome is encapsidated in the viral nucleoprotein (N) which forms a left-handed helical ribonucleoprotein (RNP) [71]. To produce viral proteins the negative-sense genome is transcribed to produce 5' capped and 3' poly(A)-tailed messenger RNA (mRNA) transcripts primed for translation by the infected host cell machinery. The viral RNA-dependent RNA polymerase (RdRp) binds the genome at the 3' end and either produces a full-length complementary copy known as the antigenome, which is immediately encapsidated by N, or mRNA transcripts [72]. The RdRp is made up of three viral proteins: N, phosphoprotein (P), and large polymerase (L) [73]. Each gene is flanked by gene start (GS) and gene end (GE) sequences that are recognised by the viral RdRp and signal either initiation or termination of transcription. The RdRp is unable to re-engage transcription at a gene not at the 3' end so the prevalence of gene transcription is biased towards genes located at the 3' of the viral genome [53]. M2-1, translated from the first ORF of the M2 mRNA, is essential to increase the processivity

of the viral RdRp and decrease the rate of premature transcription termination [74]. This efficient transcription requires the congregation of RdRp and M2-1 at cytoplasmic inclusion bodies.

1.3.4 RSV Assembly and Budding

Newly synthesised viral genomes associate with the N protein and form a RNP with the L and P proteins. These RNPs are trafficked to the plasma membrane in an M protein dependent manner [75]. Upon translation, the viral glycoproteins are trafficked through the secretory pathway to the cell surface. The M protein associates with lipids of the plasma membrane [76], the cytoplasmic domain of the G protein [77], and the viral proteins assemble into infectious virion filaments before separation from the cell surface by membrane scission [78]. In polarised cells, release of virus occurs at the apical surface [55]. Understanding of how the interactions between M and the other viral proteins drive assembly and budding, as well as the transport of viral RNPs from their cytoplasmic location to the plasma membrane is limited, although the actin cytoskeleton is thought to play a role [79].

1.4 Innate Immune Responses During RSV infection

1.4.1 Physical Barriers to Infection in the Respiratory System

The respiratory system has the unique immunological challenge faced by environment-facing tissues of maintaining sensitivity and appropriate tolerance while being constantly exposed to inhaled particles, microorganisms, and other stimulatory antigens. Physical barriers to infection are an essential element of the respiratory tract and other mucosal sites.

The architecture of the lung itself provides an entry barrier to certain pathogens. The branching airways become increasingly smaller in diameter and in the lower airways this restricts entry of pathogens greater than 2-3 μm in diameter [80]. Airway mucus plays an integral role in capturing pathogens entering the respiratory tract and preventing adhesion or invasion of the epithelial cell layer. For example, influenza infection is reliant on neuraminidase activity to prevent inhibition of infection by the mucus layer which contains heavily glycosylated mucins bearing the sialic acid moieties recognised by haemagluttinin [81]. The beating of cilia on airway epithelial cells drives mucociliary transport, moving mucus up the respiratory tract where it can be removed. The cough reflex is an effective shearing and expulsive force that can both damage and clear invading pathogens or infected mucus [82].

Mucus contains a variety of antimicrobial peptides some expressed constitutively, and others induced by infection. For example, lysozyme in mucus can degrade peptidoglycan on the surface of bacteria [83], while lactoferrin binds and sequesters iron required for bacterial growth [84]. LL37 is the only human cathelicidin and is produced by epithelial cells and neutrophils during RSV infection where it has been shown to be antiviral [81]. Defensins are AMPs with broad-spectrum activity against bacterial pathogens and some reported antiviral activity, for example human beta defensin 2 (HBD2) is secreted by epithelial cells in response to RSV infection *in vitro* and reportedly inhibits virus entry [85]. Peroxides are also found in mucus and result in the production of antibacterial oxygen radicals [80].

In the alveolar spaces' surfactant proteins are secreted into a thin liquid layer that lines the epithelium. They principally act to reduce surface tension to increase efficiency of gas exchange but surfactant proteins A (SP-A), C (SP-C) and D (SP-D) also have roles in host defence [86]. These proteins are members of the collectin protein family

and have a C-terminal lectin domain that allows them to bind to and opsonize pathogens, both bacterial and viral. This facilitates the recognition and phagocytosis of the bound pathogen by phagocytes such as macrophages [86]. Mice deficient for SP-A [87], SP-C [88], and SP-D [89] are more susceptible to RSV infection as well as infection with a variety of bacteria [86].

1.4.2 Pattern Recognition Receptors

Once the physical barriers to infection have been crossed and a pathogen begins to interact with host cells it is then recognised by the innate immune system. This recognition is mediated by an array of PRRs found on the cell surface and intracellularly in both immune and non-immune cell types [90]. PRRs recognise pathogen derived macromolecules termed pathogen-associated molecular patterns (PAMPs) [91] and damage-associated molecular patterns (DAMPs) which are cellular products that are produced in response to damage and cell stress [92]. Cell surface bound PRRs include the TLRs, C-type lectin receptors (CLRs), scavenger receptors, and G-protein coupled receptors. Intracellular PRRs include the RIG-I-like receptor (RLR) family, nucleotide-binding oligomerisation domain (NOD)-like receptors (NLRs), additional RNA helicases, AIM2-like receptors, and several TLRs. PRRs recognise specific PAMPs and so not all PRRs are relevant during infection with an RNA virus such as RSV.

PRRs expressed on airway epithelial cells, fibroblasts, and antigen presenting cells (APCs) present in the respiratory system are essential for the early detection of RSV infection [90]. PRR activation results in intracellular signalling cascades that drive the production of pro-inflammatory and antiviral molecules which initiate and organise the initial response to infection, as well as shaping the subsequent adaptive response [90]. TLRs, RLRs, NLRs and CLRs have all been implicated in the recognition of RSV [90].

1.4.3 TLR Recognition of RSV

The TLR family remains the most extensively studied group of PRRs. TLRs recognise a broad-spectrum of pathogens including viruses, bacteria, protozoa, and fungi [93]. They are membrane-bound glycoproteins with an extracellular or luminal ligand-binding domain and a cytoplasmic signalling Toll/interleukin-1 receptor homology (TIR) domain. Ligand binding induces TLR oligomerisation and clustering of signalling domains which allows signal transduction [94]. TLR1, TLR2, TLR4, and TLR6 recognise lipids and lipoproteins [93]. TLR3, TLR7, TLR8, and TLR9 bind nucleic acids [93]. TLR3 recognises dsRNA, TLR7 and TLR8 recognise ssRNA [93]. TLR2, TLR3, TLR4, and TLR7 have been implicated in the recognition of RSV PAMPS during infection [90]. TLR4 is thought to recognise the RSV F protein [57, 65] and is associated with proper Natural Killer (NK) cell function, inflammatory cytokine production [95], and subsequent viral clearance in mouse models of infection [57]. TLR2 is upregulated in RSV-infected airway epithelial cells and TLR2 deficient mice display reduced expression of pro-inflammatory cytokines, reduced neutrophil recruitment, and increased titre of RSV in lung tissue [96]. TLR7 can recognise RSV ssRNA if the virus is endocytosed, or when genomic RNA is taken up into endosomes after cytoplasmic entry [90]. TLR3 likely recognises dsRNA replication intermediates that are taken up into the endosome. Silencing of TLR3 reduces chemokine and IFN-β production during RSV infection *in vitro* [97]. TLR3 [98] or TLR7 [99] depletion during murine infection increases mucus production but does not affect viral load.

1.4.4 RLR Recognition of RSV

RLRs include the prototypic RIG-I, MDA-5, and LGP2. They are RNA binding proteins with a central DexD/H box helicase domain responsible for ligand binding [100]. As cytoplasmic RNA sensors RLRs are constitutively exposed to host cell RNA and as

such must bind specific species of RNA not found in host RNA [101-103]. RIG-I binds short uncapped 5'-triphosphate [102] and 5'-diphosphate RNA species [103], whereas MDA-5 binds longer species of dsRNA [104]. All RLRs contain a C-terminal zinc-binding domain and, in RIG-I and MDA-5 only, tandem caspase activation and recruitment domains at the N-terminus [100]. The C-terminal zinc-binding domain acts as a repressor domain, interacting with the tandem activation domains to repress signalling [105]. Interaction of the helicase domain with an RNA ligand triggers a conformational change that inhibits the activity of the repressor domain, allowing for RLR signalling that culminates in the production of IFN, via activation of IFN-regulatory factors (IRF) 3 and 7, and the pro-inflammatory transcription factor NF-κB [100]. LGP2 lacks the N-terminal signalling domain and is thought to act as a regulator of RLR signalling [106, 107].

MDA-5 and RIG-I are both upregulated upon RSV infection [100, 108]. During RSV infection *in vitro*, RIG-I silencing reduces NF-κB and IRF3 activation, and subsequent IFN and cytokine production, suggesting RSV RNA is recognised by RIG-I [97]. It was initially reported that MDA-5 did not detect RSV [109], however more recent data suggests MDA-5 is a relevant PRR during RSV infection [110]. In particular, MDA-5 has been reported to be essential to maintain activation of IRF3 during airway epithelial cell infection. In MAVS deficient mice the production of IFN and other pro-inflammatory cytokines is severely reduced during RSV infection [111-113].

1.4.5 NLR Recognition of RSV

NLRs are cytoplasmic PRRs that recognise DAMPS as well as microbial products and viral RNAs [90]. NOD2 recognises the ssRNA RSV genome and triggers MAVS signalling that is required for IRF3 and IFN-β production during RSV infection *in vitro*

[114]. NOD2 deficient mice have a defective IFN-I response and reduced viral clearance.

1.4.6 CLR Recognition of RSV

CLRs are glycan-binding receptors found on the surface of a range of cell types. The RSV G protein has been reported to interact with two CLRs, CD209 (DC-SIGN) and CD299 (L-SIGN) [115]. DC-SIGN expression is limited to dendritic cells and some macrophage populations whereas L-SIGN is only found expressed on endothelial cells [116]. The interaction of the G protein with either DC- or L-SIGN was not essential for virus entry but was associated with dampened dendritic cell activation and reduced IFN production [115].

1.4.7 The Interferon Family of Cytokines

Activation of PRRs and subsequent signalling results in the production of an array of cytokines and chemokines that are essential for shaping the response to RSV infection [28, 90]. One key group of cytokines are the IFNs, which are essential for an effective anti-viral response during a variety of infections including RSV [117, 118].

Isaacs and Lindenmann first coined the term Interferon and identified the activity of these factors in two seminal studies published in 1957 [119, 120]. Heat-inactivated influenza virus was used to stimulate chorio-allantoic membrane (a vascular membrane found in eggs) before this membrane was washed and infected with live virus. This pre-treatment of the membrane with inactivated virus was able to significantly reduce the subsequent live infection. As this interference occurred after removal of the heat-inactivated initial viral inoculum, Isaacs and Lindenmann suggested that interference was mediated by a non-viral factor, which they named Interferon [119, 120].

Extensive work purifying and characterising IFN species has revealed three distinct subclasses of IFN proteins in humans. Type I IFNs (IFN-I) consist of IFN-β, 13 species of IFNα, IFN-κ, IFN-ε, and IFN-ω. IFN-β is produced by the majority of cells whereas IFN-α subtypes are mainly produced by haemopoietic cells [121]. IFN-γ is the prototypic and only type II IFN (IFN-II) and is produced solely by immune cells such as B lymphocytes, natural killer cells, $CD8^+$ cytotoxic T lymphocytes, and antigen presenting cells monocytes, macrophages, and dendritic cells [122]. Type III IFNs (IFN-III), of which there are three members normally expressed in humans (IFN λ1-3 also known as IL-29, IL-28A, and IL-28B respectively) and a pseudogene *IFNL4*, are the most recently identified subtype of IFNs [123]. Both IFN-II and IFN-III share little homology with IFN-I but each subclass functions in a remarkably similar way. Each IFN subclass has an array of functions during viral infection; (1) the initiation of an antiviral state in local cells by promoting differential gene expression; (2) immune modulation including enhancement of antigen presentation, activation of certain cell types such as macrophages, and enhancing/altering cytokine production; (3) enhancement of the adaptive immune response [124, 125]. It is the antiviral effector proteins induced by IFN activity that are the focus of this thesis.

1.4.8 Type I Interferon Production During RSV Infection

RNA viruses induce IFN-I production primarily through two signalling pathways after PRR ligation, MAVS-associated signalling and TLR driven signalling. RLR signalling via MAVS results in IRF3 and IRF7 phosphorylation and nuclear translocation, whereas TLR signalling results in only IRF3 activation. Phosphorylated IRF3 can form homodimers or heterodimers with phosphorylated IRF7. These IRF dimers, along with AP-1 and NF-κB, activate IFN-I transcription [100], although IFN-β transcription is thought to be mainly induced by IRF3 homodimers [90]. Gene knockdown has

suggested that RLR signalling is responsible for initial IFN-I induction and upregulation of TLR3 in airway epithelial cells infected with RSV [97]. TLR3 signalling then drives IFN-I production later in infection.

There are potentially multiple sources of IFN-I during RSV infection *in vivo* including RSV-infected epithelial cells and APCs. Both IFN-α and IFN-β are produced by mouse respiratory epithelial cell lines *in vitro*, although their contribution *in vivo* is not well characterised [126]. Goritzka *et al* have shown that lung-derived murine epithelial cells ($CD45^{lo}EpCAM^{hi}CD31^{lo}$) do not transcribe *Ifnα6* 18 hours after infection, and report no detectable expression of either *Ifnα5* or *Ifnβ* mRNA in $CD45^{-}$ lung cells 4-12 hours after RSV infection [127]. This study by Goritzka *et al* demonstrated that production of IFN-I at the site of infection appears to originate predominantly from alveolar macrophages (AM) [127]. Plasmacytoid dendritic cells (pDC) are an essential producer of IFN-I during influenza infection in mice and are recruited to the nasal mucosa during RSV infection and produce IFN-α [128]. However, Jewell *et al* have demonstrated that in pDC-depleted BALB/c mice, levels of IFN-α are unaffected during RSV infection suggesting the contribution of pDCs may be redundant in otherwise immunocompetent mice [126].

A recent study of a cohort of infants with RSV LRTI reported that infants with more severe infection (n=12) had reduced IFN-I levels in nasopharyngeal aspirate versus moderately ill infants (n=18) [129]. Whatever the mechanism responsible for reduced IFN production, this study suggests IFN-I may contribute to viral control in human infection. Critically, IFN-I responses are often receding by the time RSV-infected infants present to clinicians. This makes determining the true kinetics of IFN-I during infant RSV infection challenging and increases reliance on mouse models of infection.

1.4.9 Antagonism of IFN-I Responses by RSV

The capacity of IFN responses to control RSV infection is highlighted by the observation that RSV encodes multiple IFN antagonists. IFN-I inhibition is primarily mediated by the NS1 and NS2 proteins of RSV, which are encoded by genes at the 3' end of the viral genome and as such are highly expressed [53]. NS1 is thought to interfere with RLR signalling through a variety of mechanisms, including disrupting the RIG-I-MAVS interaction required for signalling [130]. In addition, NS1 has been shown to inhibit TRIM25-mediated ubiquitination of RIG-I which is required for activation of this PRR [131]. NS2 also interacts with RIG-I to perturb signalling and the resultant IFN-I transcription [132]. TLR3-induced IRF3 activation is also inhibited by NS2 [132].

Interestingly, the G protein has also been reported to inhibit IFN-I responses [133]. The G protein contains a CX3C chemokine-like motif which is able to interact with CX3CR1, a fractalkine receptor expressed on epithelial cells and pDCs. This impairs the production of IFN-α from these cells [133].

Finally, the N protein has been reported to inhibit the phosphorylation of the eukaryotic translation initiation factor 2 alpha, evading the activity of a key antiviral protein up-regulated in response to IFN-I, protein kinase R (PKR) [134]. During RSV infection genomic RNPs localise to granules and inclusion bodies in the cytoplasm [135]. In these inclusion bodies the N protein has been shown to interact with the RNA sensor MDA-5, reducing its activity and IFN-I induction [136]. The encapsidation of viral RNA by the N protein also serves to sequester the genome from host RNA sensors, reducing IFN induction and the subsequent antiviral response [136].

1.4.10 Interferon Signalling

Each subclass of IFN binds a specific cognate cell surface receptor. Type I IFNs bind a heterodimeric receptor IFNAR1/2 found on the cell surface of all nucleated cells [124]. IFN-γ binds IFNGR1/2 and IFN-III proteins bind IFNLR1/IL10R2 complexes. Each IFN receptor type signals via the Janus-activated kinase (JAK)/signal transducer and activator of transcription (STAT) signalling pathway, although there are differences in the signalling intermediaries between the IFN subclasses [137].

IFN-I initially bind IFNAR1 in a monomeric form on the cell surface which promotes heterodimerisation of IFNAR1 and IFNAR2 [138]. This allows for cross-phosphorylation of kinases associated with cytosolic domains of IFNAR1 and IFNAR2, JAK1 and TYK2, and phosphorylation of residues in the cytoplasmic domains of the receptor chains [124, 139]. This phosphorylation generates binding sites for additional signalling proteins STAT1 and STAT2 [139]. Recruited STAT1 and STAT2 are then phosphorylated and form a heterodimer that complexes with IRF9 [140, 141]. This trimeric complex is known as ISGF3 and translocates to the nucleus of IFN-I stimulated cell and induces differential gene expression, including the upregulation of Interferon-stimulated genes (ISGs) by binding promoter Interferon-sensitive response elements (ISREs, consensus sequence TTTCNNTTTC) [142, 143]. Along with this canonical IFN-I JAK-STAT signalling it has been reported that IFN-I stimulation induces the formation of two additional STAT complexes, pSTAT1pSTAT1 and pSTAT3pSTAT3 [144]. These complexes are also transcriptionally active and induce differential gene expression by binding promoter elements known as Gamma-activated sequence (GAS, consensus sequence TTCNNNGAA) [145]. IFN-II signalling also results in the formation of pSTAT1 homodimers and upregulation of genes with GAS promoter elements [144]. IFN-III signalling is thought to induce similar JAK-STAT

signalling to IFN-I, resulting in ISGF3 translocation [146]. The regulation of gene expression is key to the antiviral roles of all subclasses of IFN.

Responses to IFN stimulation are both context and cell-type dependent. Cellular signals induced by PRR signalling, ISG expression, and by pathogens all contribute to modulation of JAK-STAT signalling and the overall response to IFN [121]. This can be through changes to expression levels, post-translational modifications of the receptor subunits, upregulating expression of factors that interact with STAT complexes, or altering the chromatin states at target gene sites [121]. Finally, regulation of translation can further fine-tune the IFN response by altering the pattern of transcribed RNAs that are translated [121].

1.5 Interferon-modulated Genes

1.5.1 Types of Interferon-Modulated Genes

In this thesis I will use the term Interferon stimulated genes (ISGs) to describe genes with ISRE/GAS promoter elements that are induced directly as a result of JAK-STAT signalling and ISGF3 or STAT homodimer transcriptional activation. In addition to these ISGs there are an array of Interferon-modulated genes (IMGs) that are indirectly differentially regulated during the IFN response [118]. Both IMGs and ISGs are also induced by IRFs, which are themselves ISGs, fashioning an effective amplification loop [118]. One study has suggested that some 20% of known ISGs are regulated by IRF8 alone [147]. There is also a subset of IMGs that are repressed by IFN signalling which may constitute an important element of the response, although the focus of research has always been on those genes that are upregulated by IFN activity. Some ISGs are activated by alternative signalling pathways such as IL-1 signalling [148] to further complicate the system. Another recent interest has been understanding the

non-coding genetic elements, long non-coding RNA and microRNA, that are differentially regulated during the IFN response [118].

The true number of ISGs and IMGs is not known. Multiple microarray studies gave the first indication of the number of ISGs, in the region of 300-450 genes in human cells [118]. Schoggins recently noted that the majority of studies attempting to determine the repertoire of ISGs relied upon a fold-change cut-off value to identify ISGs [118]. This may have reduced the number of identified genes as some ISGs have been reported to have a small but significant fold change in expression. Cut-offs have varied from 1.5 to 5-fold induction, exacerbating disparity between studies. The development of RNA sequencing technology has expanded our capacity to profile differentially regulated genes. One recent study, utilising RNA sequencing and a statistical cut-off, reported that near 10% of the human genome was differentially regulated in response to IFN-I [149].

Whatever the true number of ISGs in the human genome, only a minority of genes and their encoded proteins have been thoroughly characterised. However, ISGs targeting nearly every step of the viral life cycle have been identified (Fig 1.2).

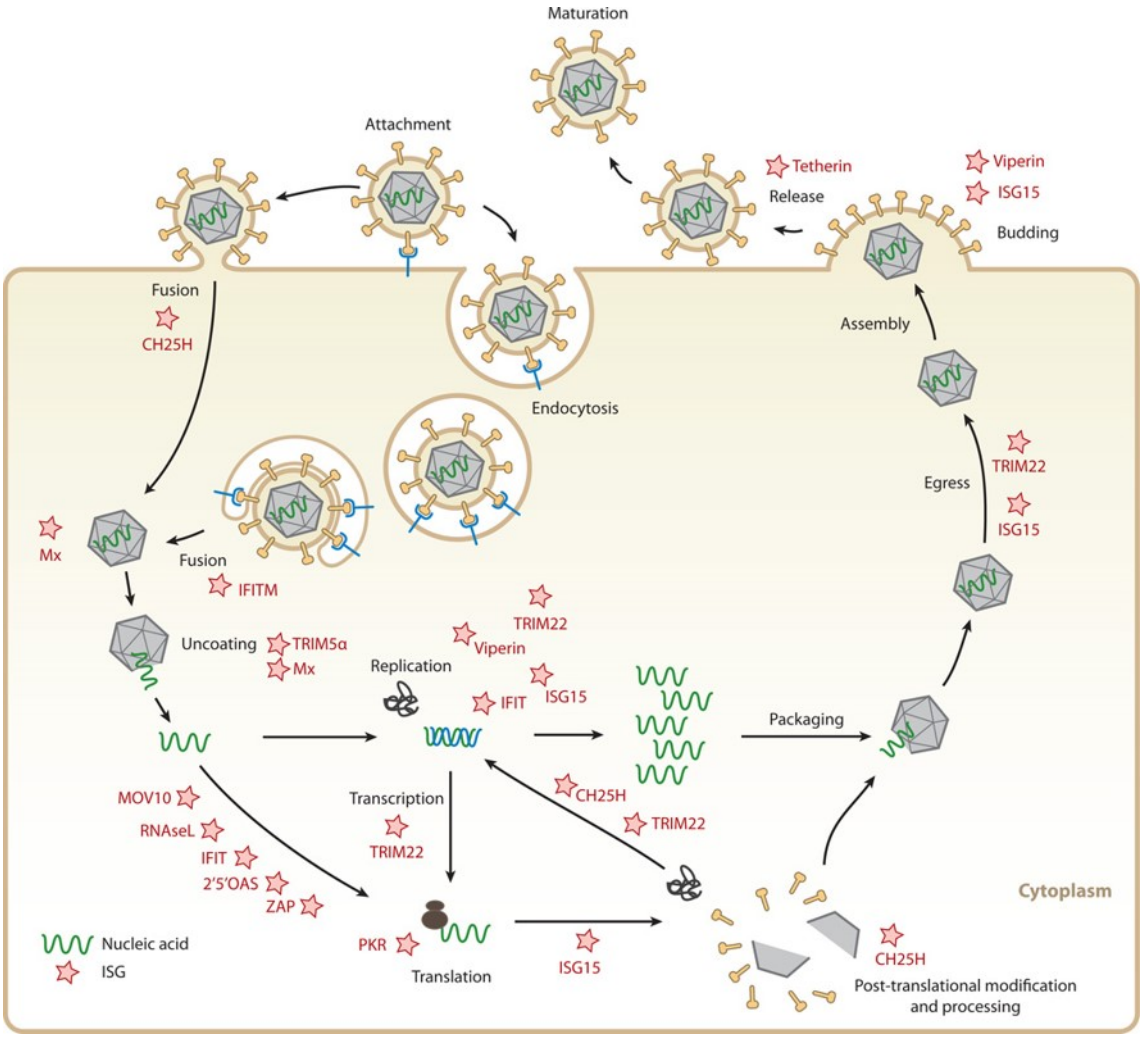

Figure 1.2. Antiviral ISGs. ISG products target different stages of the viral life cycle from entry through to assembly and release. ISGs noted are those with a described antiviral mechanism at the time of publication (2014). Reproduced with permission of Annual Review of Immunology, from "Interferon-stimulated genes: a complex web of host defences", Schneider *et al*, 32, 2014. Permission conveyed through Copyright Clearance Center, Inc.

1.5.2 ISGs Targeting Viral Attachment, Entry, and Trafficking

The first stage of any viral life cycle begins with attachment, entry, and subsequent localisation of viral genome and machinery to a specific intracellular compartment for replication. These initial stages are attractive targets for antiviral ISGs as they can be effective before the infection has too much of an impact on the cell.

1.5.2.1 Attachment

To date, there is only one ISG that is suggested to interfere with viral attachment. *HPSE* encodes heparanase and has been shown to inhibit multiple RNA viruses from the *Togaviridae*, *Flaviviridae*, and *Paramyxoviridae* families [150, 151]. Heparanase enzymatically cleaves side chains from HSPGs which are commonly used for virus attachment, including by RSV *in vitro* [59]. However, this mechanism of action remains speculative and further work is required to determine whether viral attachment is affected by expression of heparanase or whether this enzyme mediates alternative antiviral strategies [118].

1.5.2.2 Entry

Viral entry is targeted by multiple ISGs, the most well-characterised of which are the broadly antiviral IFITM proteins which are thought to inhibit a stage of membrane fusion [152]. The IFITM family is discussed in detail later in this chapter. Additional entry inhibitors are encoded by the ISGs *NCOA7* [153] and *CH25H* [154]. *CH25H* encodes cholesterol 25-hydroxylase which blocks membrane fusion by catalysing production of 25-hydroxycholesterol. *CH25H* restricts an array of enveloped viruses including influenza [154]. In addition, there are several IMGs, upregulated in response to IFN stimulation but without ISRE/GAS promoter elements, that encode effectors reported to restrict virus entry. These include *TM9SF2*, *SNN*, and *RIN2* [155].

1.5.2.3 Trafficking

Myxovirus resistance protein (MX)-1 and MX2 are dynamin-like guanosine-triphosphate hydrolases (GTPases) that inhibit virus trafficking to the nucleus prior to replication [118]. MX1 has been thoroughly characterised and reported to restrict variety of RNA viruses such as influenza, human immunodeficiency virus 1 (HIV-1), rabies virus, vesicular stomatitis virus (VSV), measles virus, sindbis virus, and reovirus [156]. MX1 appears to have multiple antiviral mechanisms and affect different viruses at different stages of their life cycle. Antiviral activity of MX1 is generally thought to be dependent upon the capacity of the protein for GTP binding, GTP hydrolysis, and oligomerisation [157]. However, this does not seem to be the case for restriction of hepatitis B virus (HBV) which does not require GTPase activity and involves sequestration of the HBV capsid into perinuclear compartments [158]. MX1 also inhibits replication of Bunyavirus genomes by sequestering the N protein into perinuclear complexes [159]. MX proteins bind nucleocapsid structures to prevent trafficking as well as initial viral mRNA synthesis in some cases such as VSV and parainfluenza virus infection [160, 161]. MX2 is localises to the cytoplasmic exterior of nuclear pores where it inhibits the import of the HIV-1 genome complex [157]. Additional ISG effectors that target viral entry and trafficking are listed in Table 1.1.

ISG	TARGETED VIRUSES	MECHANISM OF ACTION
CH25H	Ebola virus, influenza, rift valley fever virus (RVFV), VSV, HIV-1, Nipah viruses, lassa virus [154, 162, 163].	Inhibition of virus membrane fusion, inhibition of viral glycoprotein glycosylation.
ADAP2	Dengue virus (DENV), VSV [164].	Promotes alternative virus uptake pathway resulting in aberrant localisation of virions.
NCOA7	HIV-1, influenza, hepatitis C virus (HCV) [153].	Enhances acidification of virus-containing endosomes, inhibits virus membrane fusion, promotes lysosomal protease activity.
TRIM5A	HIV-1 [165].	Promotes virion capsid degradation, promotes IFN-β transcription.

Table 1.1. ISGs that restrict virus entry and trafficking.

1.5.3 ISGs Targeting Viral Transcription

ISGs can reduce viral gene expression by inhibiting transcription or translation. RNA virus transcription is an attractive target as many viruses are totally dependent upon activity of their polymerase, and the human genome is not thought to encode a typical RNA-dependent RNA polymerase [166]. Several ISGs have been shown to impact viral transcription during RNA virus infection including *SAMHD1* and those listed in table 1.2. SAMHD1 is interesting as it is the only deoxynucleoside triphosphate triphosphohydrolase (dNTPase) expressed in human cells [155]. The primary antiviral mechanism of SAMHD1 is thought to be dNTP depletion [167], although it has been suggested it may have other functions [168].

ISG	TARGETED VIRUSES	MECHANISM OF ACTION
RBBP6	Ebola virus [169].	Inhibits VP30-mediated promotion of transcription.
PML	HIV-1 [170, 171], herpes simplex virus 1 (HSV-1) [172], human cytomegalovirus (hCMV) [172], encephalomyocarditis virus (ECMV) [173], influenza [170], VSV [170], Poliovirus [170], rabies virus [170].	Multiple proposed mechanisms. Transcription inhibition by association with viral genomes (HIV-1, HSV-1, hCMV), reverse transcription inhibition (HIV-1), viral polymerase sequestration (ECMV).
IFI6	hCMV [174].	Impairs viral gene transcription
MX1	Broad antiviral activity reviewed in [156]	Inhibits transcriptional elongation and trafficking of viral RNPs.
APOBEC3G	HIV-1 [155].	Hypermutation of RNA genomes.
OAS1-3	RSV [175, 176], West Nile virus (WNV) [177]. Broad antiviral activity reviewed in [178].	Promotes RNase L activity resulting in degradation of host and viral RNAs.
GBP3	Influenza [179]	Inhibits viral polymerase activity

Table 1.2. ISGs that restrict virus transcription.

1.5.4 ISGs Targeting Viral RNA Translation

There are several approaches ISGs can use to inhibit translation, either by reducing activity of the host translational machinery or by preventing engagement of viral mRNA with this machinery. In addition, ISG effectors such as TRIM69 [180] or ISG15 [181] can directly regulate viral protein activity by promoting their degradation. The IFIT (IFN-induced proteins with tetratricopeptide repeats) family of proteins appear to adopt multiple strategies for inhibiting translation of viral mRNAs. In humans the IFIT family

consists of IFIT1, IFIT2, IFIT3, and IFIT5. IFIT1 and IFIT2 bind eukaryotic initiation factor (eIF) 3 which inhibits the translation of 5' capped RNAs or those with specific internal ribosome entry sites (IRES) [182]. As for many ISG effectors, IFIT1 and IFIT2 have additional mechanisms, including binding to viral RNAs with a Cap^0 structure, where the first nucleotide after the cap is not methylated. This binding prevents the mRNA from interacting properly with the translational initiation complex. IFIT proteins have been shown to be antiviral in the context of several *Herpesviridae*, *Flaviviridae*, *Coronaviridae*, *Papillomaviridae*, *Paramyxoviridae*, *Rhabdoviridae*, *Poxviridae*, and *Togaviridae* viruses [182].

PKR (double-stranded RNA-dependent protein kinase R, encoded by *EIF2AK2*) was one of the first ISG effectors shown to respond to dsRNA during viral infection and to have a characterised antiviral mechanism of action [183]. PKR is activated by binding dsRNA of at least 33 base pairs long which causes PKR to dimerize and auto-phosphorylate [184]. This active form of PKR then phosphorylates the key translation initiation factor eIF2α inhibiting translation of both viral and host mRNAs. PKR has been shown to restrict a broad range of viruses including both DNA and RNA viruses. Influenza, ebola virus, RVFV, hCMV and other viruses encode PKR antagonists in order to evade PKR-mediated translational shut down that effectively inhibits viral gene expression [184]. Additional ISG effectors targeting viral RNA translation are listed in Table 1.3.

ISG	TARGETED VIRUSES	MECHANISM OF ACTION
ZAP	Broad antiviral activity reviewed in [155].	Binds and promotes degradation of viral RNAs. Amplifies RLR signalling, increasing IFN production.
SLFN11	HIV-1 [185].	Binds transfer RNAs (tRNA) and inhibits HIV-1-induced changes to pool of available tRNAs.
SAT1	Chikungunya virus (CHIKV), Zika virus [186].	Inhibits polyamine synthesis.
C19ORF66	DENV [187], HIV-1 [188].	Interferes with viral RNA and cellular mRNA-binding proteins (DENV). Inhibits ribosomal frameshifting required for Gag-Pol translation (HIV-1).

Table 1.3. ISGs that restrict virus RNA translation.

1.5.5 ISGs Targeting Genome Amplification

Viral genome replication can occur in a variety of cellular compartments and some viruses will modulate host compartments to create suitable environments for replication such as DENV. There are a variety of ISG effectors that target genome replication through distinct mechanisms (Table 1.4). One mechanism is the incorporation of chain terminator molecules into newly synthesised viral RNA such as 3'-deoxy-3',4'-didehydro-cytidine triphosphate (ddhCTP), the production of which is catalysed by Viperin (*RSAD2*) [189]. Somewhat similarly, APOBEC3G inhibits retroviral infection by hypermutating retroviral genomes [155]. This ISG effector has

also been reported to simply bind viral genomes, directly repressing replication [190]. SAMHD1 is thought to deplete the pool of available dNTPs, impacting both reverse transcription, transcription, and genome replication [155]. Degradation of viral genomes and RNA instead of interference with replication or function is mediated by ISG effectors such as 2'-5'-oligoadenylate synthase (OAS)1-3 [175], zinc finger antiviral protein (ZAP) [155], and interferon stimulated exonuclease gene 20 (ISG20) [191]. The final mechanism by which ISG effectors have been reported to restrict viral genome amplification is by interfering directly with the site of replication. For example IFI6 is thought to localise to the endoplasmic reticulum (ER) and prevent formation of ER-membrane invaginations that are the site of Flavivirus replication [192].

ISG	TARGETED VIRUSES	MECHANISM OF ACTION
TRIM25	Influenza [193], sindbis virus [194].	Activates RIG-I. Binds influenza ribonucleoproteins to prevent transcription and replication [193]. Enhances ZAP activity [194].
TRIM32	Influenza [195]	Ubiquitinates PB1 subunit of the influenza polymerase.
TDRD7	Sendai Virus (SeV), RSV, parainfluenza virus-3 (PIV3) [196]	Inhibition of virus-induced autophagy
GBP3	Influenza [179]	Inhibits viral polymerase activity

Table 1.4. ISGs that restrict virus genome replication.

1.5.6 ISGs Targeting Virion Assembly and Egress

Completion of the viral life cycle requires assembly of new viral particles containing genome and exit from the infected host cell. This is a complex, varied, and multi-step process presenting multiple opportunities for ISG effectors to function. However, there are far fewer ISGs in this category than those targeting other stages of the viral life cycle. Of course, the entire complement of ISG effectors in the human genome has not been characterised. The majority of these ISGs, listed in Table 1.5, encode HIV-1 or retroviral restriction factors, although activity against other enveloped viruses such as influenza has been reported for Tetherin (*BST2*) [155] and Viperin (*RSAD2*) [197].

ISG	TARGETED VIRUSES	MECHANISM OF ACTION
BST2	HIV-1, influenza, VSV, HBV, LASV [155].	Inserts a glycosylphosphatidylinositol (GPI) anchor into viral envelopes preventing release from the cell surface.
RSAD2	Influenza [197].	Disrupts lipid raft formation
GBP5	HIV-1 [198].	Restricts incorporation of Env into viral particles
CNP	HIV-1 [199]	Restricts incorporation of Gag into viral particles
SERPINE1	Influenza [200]	Inhibits glycoprotein maturation

Table 1.5. ISGs that restrict virus assembly and egress.

It is clear that the human genome harbours ISGs capable of countering nearly each step of a viral life cycle. Many ISG effectors appear to be multifunctional in that they utilise divergent mechanisms to restrict infection of multiple viruses. Those with multifunctionality, such as MX1 which has a broad range of antiviral activity, that target several distinct stages of the viral life cycle are especially intriguing.

1.5.7 Interferon-Stimulated Genes and RSV

Studies of clinical cohorts of infants with severe RSV LRTI have reported an association with impaired immune responses. Genetic associations with severe RSV LRTI in infants have predominantly been made to genes involved in innate immunity [22], including the ISG MX1 [50]. In addition, there are several studies reporting *in vitro* and *in vivo* restriction of RSV infection by ISG activity. These factors may represent undescribed genetic risk factors for severe RSV LRTI. It is important to note that RSV encodes effective IFN antagonists and has been reported to directly interfere with the activity of ISGs such as PKR [134]. As such, there are likely multiple ISGs that would restrict infection of RSV in the absence of these IFN antagonists.

IRF7 is a key IFN regulatory factor, that is also an ISG [201], involved in upregulation of IFN-I expression and RLR signalling during RSV infection [202]. *Irf7*$^{-/-}$ mice are unable to produce IFN-I [203] and display signs of enhanced RSV disease [204]. HPSE expression has been reported to restrict RSV infection [150]. The antiviral mechanism of HPSE has not been explored but it is thought to inhibit virus entry that utilises HSPG binding. However, as HSPGs are not detectable on the apical surface of ciliated human airway epithelial cells it seems unlikely that this ISG would be relevant during human *in vivo* infection [61]. Expression of OAS [176] and OAS-like [175] restrict RSV replication *in vitro* although the mechanism of action has not been confirmed. Cyclic GMP-AMP synthase (cGAS) is a cytosolic DNA sensor that restricts

RSV replication likely through increasing IRF3 activation and subsequent increased antiviral capacity of the infected cell [150]. ISG15 is upregulated in response to RSV infection and can be conjugated with target proteins, in a process known as ISGylation [181]. This promotes degradation of the conjugated proteins. Overexpression and knockout studies *in vitro* suggest an antiviral role for ISG15 during RSV infection [181]. Viperin has also been reported to inhibit RSV replication *in vitro* and in a chinchilla model of infection [205]. Tudor domain-containing protein-7 (TDRD7), which inhibits autophagy, restricts RSV infection *in vitro* [196]. RSV induces autophagy which results in reduced cell death [206], which may explain the inhibition of infection by TDRD7.

MX1 is the only ISG to date for which SNPs have been identified that influence disease severity in humans [50]. Interestingly, RSV is reportedly resistant to MX1 activity in Vero and U87 cells, although in this study the RSV A2 isolate used was resistant to IFN-I treatment [50]. Significant restriction of RSV has been observed in HEK293T (Vaughn A. and Busse D. unpublished) and HEp-2 cells [204] using an RSV A2 isolate that is restricted by the IFN-I response in a dose-dependent manner. MX1 is known to restrict trafficking of viral capsid structures and influence viral transcription but neither mechanism has been investigated during RSV infection [156].

RSV infection is restricted by expression of IFITM1-3 *in vitro* [207, 208], and infection severity is increased in *Ifitm3*$^{-/-}$ mice [209]. There remain unanswered questions regarding the factors influencing IFITM tropism and antiviral activity. This is one part of this thesis and is discussed in more detail in the following section.

1.6 IFN-Induced Transmembrane Proteins

1.6.1 The IFITM Family

The Interferon-induced transmembrane protein (IFITM) family are a group of antiviral factors amplified during the IFN response by the IFN I-III signalling. They were some of the first ISGs to be identified [210] but it took 12 years for the first studies to be published describing antiviral activity, initially the restriction of VSV by IFITM1 (then known as 9-27 protein) [211]. IFITMs are now thought to be able to restrict a broad range of viruses although their tropism and mechanisms of action are not fully elucidated. Interestingly, IFITM proteins are present at high constitutive levels in some cell types such as barrier epithelial cells [152]. This suggests IFITM proteins act as a first line of defence against certain viral infections.

In humans there are five *IFITM* genes (*IFITM1*, *IFITM2*, *IFITM3*, *IFITM5* and *IFITM10)* and a pseudogene *IFITM4P* encoded on chromosome 11 [152, 212]. Mice contain a similar locus on chromosome 7 encoding *Ifitm1-3, Ifitm5,* and *Ifitm6*. *Ifitm7* is found on chromosome 16 [212]. IFITM genes can be found across a range of vertebrate species such as bats [213], pigs [213], reptiles [214], and birds [215-217]. Unlike human IFITM1-3, IFITM5 is not thought to be IFN inducible and has yet to be shown to have a role in viral immunity [218]. There is little information available regarding the function of IFITM10 but intriguingly it is the most conserved IFITM protein among birds, reptiles, and mammals [212]. IFITM1-3 are the only IFITM proteins with reported antiviral activity.

1.6.2 Cellular Localisation and Membrane Topology

IFITM proteins are membrane-bound and have been proposed to restrict the passage of viral particles across lipid bilayers [219-221]. The IFITM family members are thought

to have similar structures consisting of the N-terminal domain and C-terminal domain bordering two antiparallel transmembrane domains with a connecting conserved intracellular loop (CIL) domain. The first transmembrane domain is termed the intramembrane domain and together with the CIL makes up a CD225 domain found in the around 300 members of the CD225/p4505 family [222]. IFITM3 and IFITM2 are very similar proteins with greater than 90% amino acid identity, whereas IFITM1 only shares 80.36 and 75.89% with IFITM2 and IFITM3 respectively (Fig 1.3). This is mainly due to a 21 amino acid truncation of the IFITM1 N-terminal domain (residues 1-36) and differences within the C-terminal domain (residues 108-125). IFITM proteins are part of a larger family called the Dispanins which have 10 other members in humans (*TMEM91*, *TMEM90B*, *DSPC2*, *TMEM90A*, *PRRT2*, *TMEM233*, *TUSC5*, *ACO23157*, *AL160276*, and *AC068580*) and are found in a variety of both eukaryotic and bacterial species [223].

Figure 1.3. Alignment of IFITM1-3 amino acid sequences. Protein sequences of human IFITM1 (NP_003632.3), IFITM2 (NP_006426.2), and IFITM3 (NP_066362.2) were aligned using Clustal Omega (https://www.ebi.ac.uk/Tools/msa/clustalo/). "*" identical residue, "." weakly similar residue, ":" strongly similar residue.

The IFITM2 and IFITM3 proteins are predominantly found across intracellular endosomal membranes, co-localizing with late endosome (CD63, Rab7) and lysosomal markers (CD63, LAMP1) [224], where it is thought they inhibit the cytosolic entry of viruses that use the endocytic pathway for entry [221]. The same year IFITM1 mRNA (termed 9-27) [210] was demonstrated to be IFN-inducible, the encoded protein was also described as a human leukocyte antigen, Leu-13, found on the cell surface of both B and T cells [225]. Additional studies have confirmed that IFITM1 is detectable on the cell surface [226, 227], although there have been multiple divergent topologies proposed for how IFITM1 is arranged across membranes. It is important to note that IFITM1 is not only found on the cell surface, it has also been identified on intracellular membranes, co-localising with early endosome marker Rab-5 [227, 228]. Interestingly, the intracellular localisation of IFITM1 is distinct from that of IFITM2 and IFITM3 [229, 230].

The IFITM2 and IFITM3 proteins have also been detected on the cell surface in multiple studies using exogenously expressed epitope-tagged proteins [220, 231, 232]. In cell culture systems the majority of IFITM2 and IFITM3 protein appears to localise to intracellular membranes [233]. However, IFITM3 has been observed to concentrate on the apical plasma membrane of ciliated epithelial cells in the murine airway [234], the primary site of RSV infection [55]. This may be a result of differences between human and mouse IFITM proteins but may also represent an inherent limitation of studying localisation in immortalised cell cultures grown in monolayer. In addition, exogenous expression of high levels of IFITM proteins or N-terminal epitope tags may disrupt proper targeting and result in elevated plasma membrane expression [152]. Both IFITM2 and IFITM3 contain a YXXF motif in their N-terminal domain thought to promote internalisation through interaction with the clathrin adaptor protein

AP-2, although this internalisation can be inhibited for IFITM3 through phosphorylation of Tyr20 [235]. IFITM1 has no such motif in the N-terminal domain, which may explain the predominant localisation to the plasma membrane.

A proposed topology for IFITM1 at the cell surface suggests both the N- and C-terminal domains are extracellular, with an intracellular CIL domain connecting the TM domains [231, 236]. However, Weston *et al* proposed an alternate topology where the N-terminal domain is cytoplasmic and the C-terminal domain is extracellular [226]. In a study published just a year later Li *et* al demonstrated that the N-terminal domain can be detected on both the cell surface and in the cytoplasmic compartment [227]. Using SCAM (substituted-cysteine accessibility method) [237] they further corroborate that the C-terminal domain can be detected in the extracellular space but also show that when IFITM1 is expressed on intracellular membranes the C-terminal domain is predominantly luminal [227]. Li *et al* suggest that IFITM1 may adopt multiple topologies, with a consistent extracellular/luminal C-terminal domain and a variable CIL/N-terminal domain orientation. Weston *et al* utilised an IFITM1 N-terminal domain specific antibody raised against the first 35 amino acids of human IFITM1. The first TM domain is predicted to begin with V37, as such it is possible that this antibody was unable to bind extracellular N-terminal domain due to the spatial organisation of the N-terminal domain while the protein is embedded in a membrane, or protein-protein interactions may have interfered with binding. As such, the orientation of the N-terminal domain remains controversial (Fig 1.4).

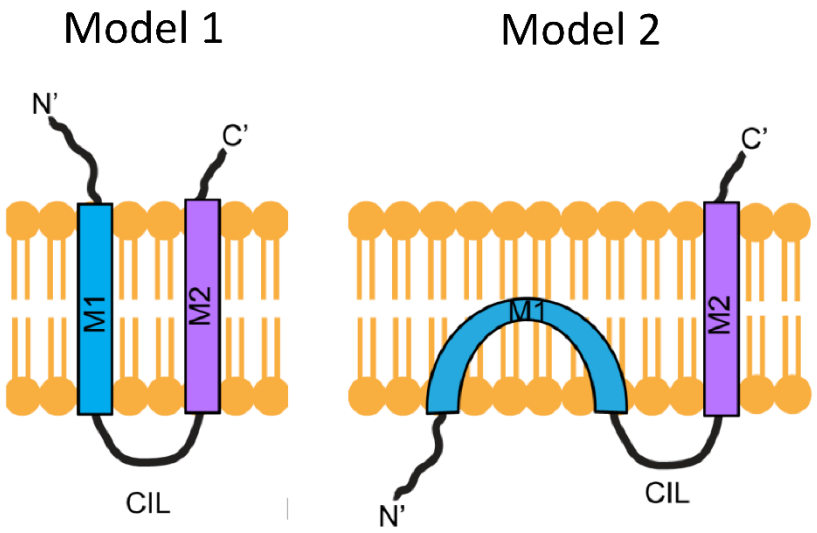

Figure 1.4. Proposed membrane topologies of IFITM1. Several topologies for IFITM proteins have been proposed. IFITM1 may adopt multiple topologies where the NTD and CTD are both found in the extracellular/luminal spaces (left) or with an extracellular/luminal C-terminal domain and intracellular/cytoplasmic N-terminal domain (right). Adapted from Weston *et al* [188]

1.6.3 Reported Antiviral Activity of IFITM1-3

IFITM1-3 have been studied in the context of a variety of infections and have been predominantly shown to restrict enveloped RNA viruses (Table 1.6). IFITM3 has perhaps the broadest range of reported antiviral activity but has also been the main focus of research into IFITM proteins.

1.6.4 RNA Virus Infection

IFITM2 and IFITM3 are generally able to restrict the infection of the same range of enveloped RNA viruses when they have been studied together. Interestingly, this is not the case for Zika Virus where unlike IFITM3, IFITM2 does not restrict infection [238]. To date, IFITM3 has only been shown to impact on a single non-enveloped RNA virus, Reovirus [239]. Unfortunately, there is no information as to whether this also occurs with IFITM1 or IFITM2 activity.

IFITM1 has been shown to restrict a variety of the same RNA viruses as both IFITM2-3 (Table 1.6) although there are some exceptions. IFITM1 is unable to restrict several members of the *Togaviridae* Semliki forest virus and sindbis Virus [240], as well as RVFV [229]. Differences in cellular sub-localisation may explain this apparent difference in antiviral tropism as IFITM1 has been shown to be able to inhibit cell-cell fusion induced by exogenous expression of the Semliki forest virus fusion protein complex, suggesting it would be capable of restricting Semliki forest virus entry at the plasma membrane [220].

Alongside the development of an *Ifitm3*$^{-/-}$ mouse strain, Lange *et al* developed a strain with the entire *Ifitm* locus on chromosome 7 deleted (*Ifitm1*$^{-/-}$*Ifitm2*$^{-/-}$*Ifitm3*$^{-/-}$*Ifitm5*$^{-/-}$ *Ifitm6*$^{-/-}$) referred to as *IfitmDel*$^{-/-}$. Both mouse strains have been shown to be more susceptible to influenza virus infection [232, 234, 241]. Both *Ifitm3*$^{-/-}$ and *IfitmDel*$^{-/-}$ mice exhibited more rapid and severe weight loss. Interestingly, *Ifitm3* has been demonstrated to bolster the adaptive immune response to influenza virus infection by preventing infection in tissue resident memory $CD8^+$ T cells [242]. *Ifitm3*$^{-/-}$ are also more susceptible to WNV [243] and alphavirus infection [244]. IFITM proteins were previously thought to be unable to restrict the infection of alphaviruses such as Venezuelan encephalitis virus (VEEV) and CHIKV but *Ifitm3*$^{-/-}$ mice have recently been reported to exhibit increased joint swelling, increased viral load, and elevated pro-inflammatory cytokines in a CHIKV model of viral arthritis, and increased susceptibility to lethal VEEV infection [244]. Everitt *et al* have previously demonstrated that *Ifitm3*$^{-/-}$ mice display enhanced RSV infection with increased weight loss and higher viral load in lung tissue than wild-type littermates [209]. However, it is unknown whether the individual loss of either IFITM1 or IFITM2 also enhances RSV disease in this murine model of infection.

We have recently demonstrated that IFITM1-3 expression restricts RSV A and B strains and a broader range of *Paramyxoviridae* than previously shown (Fig 1.5) [207]. This work was an essential starting point for the data presented in chapter 3 and established stably transduced cell lines used throughout. Smith *et al* generated stably transduced A549 (human lung epithelium) or Vero (Green monkey kidney epithelium) cells expressing IFITM1, IFITM2, or IFITM3. The Smith *et al* study demonstrated that IFITM1 has a broad range of activity against enveloped RNA viruses from the *Paramyxoviridae* family, reporting activity against parainfluenza virus-3, measles virus, mumps virus, HMPV, and Newcastle disease virus (NDV) for the first time [207]. Smith *et al* also noted significant restriction of RSV A and B strains by IFITM1 and only moderate restriction of each virus by IFITM3. IFITM1 also efficiently restricted influenza virus infection as demonstrated previously [232, 245]. In the Smith *et al* study, IFITM3 had no significant antiviral activity against either measles or mumps viruses and was only able to minimally reduce HMPV or NDV infection. IFITM2 was only able to moderately reduce RSV A and measles virus infection.

In the Smith *et al* study, IFITM1 was effective at restricting each virus of the *Paramyxoviridae* and *Pneumoviridae* tested, unlike IFITM2 or IFITM3. This may be due to the altered localisation of IFITM1 at the plasma membrane as these viruses predominantly utilise direct membrane fusion at the cell surface for entry especially *in vitro*. Dependency of IFITM1 on cell surface localisation would further support the hypothesis that IFITM proteins function at the site of membrane fusion [207]. Previous studies have demonstrated that IFITM3 inhibits HMPV infection [246], although the Smith *et al* study saw only a small impact on infection (~10%). Interestingly, HMPV is reported to utilise both clathrin-mediated endocytosis and direct fusion with the plasma membrane for cell entry. The ability of IFITM3 to restrict HMPV may be in part due to

HMPVs utilisation of this bifurcated entry strategy or a result of IFITM3 overexpression resulting in additional localisation to the plasma membrane.

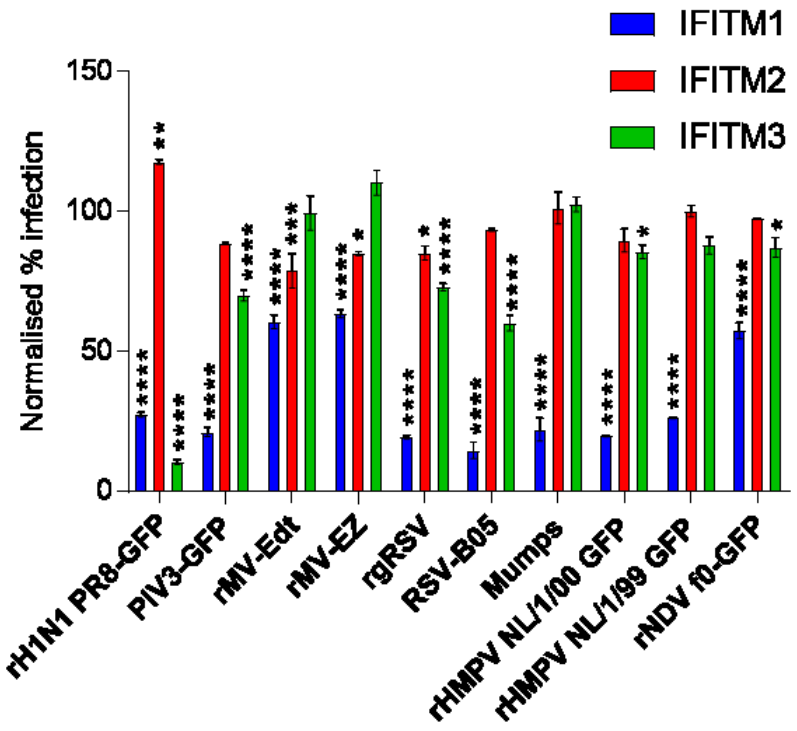

Figure 1.5. IFITM1 restriction of Paramyxoviridae and Pneumoviridae RNA viruses *in vitro*. Stably transduced Vero cells expressing IFITM1-HA were produced and screened for antiviral activity by S. Smith. Cells were infected for 24 hours before fixation and quantification of infection by flow cytometry. Influenza A virus PR8 (H1N1 PR8), parainfluenza virus-3 (PIV3-GFP), measles virus (rMV-Edt, rMV-EZ), RSV A2 (rgRSV), RSV B (RSV-B05), mumps virus (Mumps), Human metapneumovirus (rHMPV NL1/1/00 GFP, rHMPV NL/1/99 GFP), and Newcastle disease virus (rNDV). Significance to Vector transduced control cells by ANOVA, * $P < 0.05$, ** $P < 0.01$, *** $P < 0.001$, **** $P < 0.0001$. Data from Smith *et al*. J Virol (2019).

Virus Family	Virus Name	IFITM1	IFITM2	IFITM3	Reference
Orthomyxoviridae	Influenza A virus	+	+	+	[207, 219, 222, 232, 241, 245]
	Influenza B virus			+	[241]
Pneumoviridae	Respiratory syncytial virus	+	+	+	[207, 208]
Paramyxoviridae	Human metapneumovirus	+	NR	+	[207, 246]
	Measles virus	+	+	NR	[207]
	Newcastle disease virus	+	NR	+	[207]
	Parainfluenza virus-3	+	NR	+	[207]
Flaviviridae	West Nile virus	+	+	+	[232, 243]
	Dengue fever virus			+	[232]
	Yellow fever virus	+	+	+	[151]
	Zika virus	+	NR	+	[238]
	Hepatitis C virus	+	+	+	[247, 248]
	Omsk haemorrhagic fever virus	+	+	+	[232]
Togaviridae	Sindbis virus	NR	+	+	[240]
	Semliki forest virus	NR	+	+	[240]
	Venezuelan equine encephalitis virus			+	[244]
Rhabdoviridae	Vesicular stomatitis virus			+	[211, 231]
Filoviridae	Ebola virus	+	+	+	[245, 249]
	Marburg virus	+	+	+	[245, 249]
Bunyaviridae	Rift valley fever virus	NR	+	+	[229]
	La Crosse virus	+	+	+	[229]
	Crimean-Congo haemorrhagic fever virus	NR	NR	NR	[229]

Virus Family	Virus Name	IFITM1	IFITM2	IFITM3	Reference
Bunyaviridae	Hantaan virus	+	+	+	[229, 250]
	Andes virus	+	+	+	[229]
Arenaviridae	Lassa fever virus	NR	NR	NR	[232, 249]
Coronaviridae	Severe acute respiratory syndrome coronavirus	+	+	+	[245]
Retroviridae	Human immunodeficiency virus-1	+	+	+	[230]
	Murine leukaemia virus	NR	NR	NR	[232]
	Jaagsiekte sheep retrovirus	+	+	+	[220]
Reoviridae	Reovirus			+	[239]

Table 1.6. RNA viruses restricted by IFITM1-3. Each RNA virus with at least one published study investigating restriction by one or more IFITM proteins. + = restriction reported. NR = no restriction. Cells are left blank when referenced studies did not investigate the impact of a certain IFITM protein.

1.7 IFN-Induced Protein 44 Proteins

1.7.1 Identifying Novel ISGs to Characterise During RSV Infection

IFITM proteins are not the only ISGs that play a role in RSV restriction. To identify a discrete list of additional candidate ISGs to investigate in the context of RSV infection, McDonald *et al* undertook a meta-analysis of published transcriptomic and proteomic studies [204]. The authors of this study hypothesised that genes involved in control of infection would be more likely to be consistently upregulated during infection. Genes were given weighted scores based on the number of studies the ISGs were upregulated in and the type of study (*in vivo* > *in vitro*). Around 100 genes were identified that are consistently upregulated in response to RSV infection, a significant portion of which were ISGs with no known function during RSV infection. These ISGs were screened for antiviral activity using lentiviral expression and the following ISGs were found to inhibit RSV infection > 50%: *IFI6*, *IFI27, EIF2AK2*, *IFIT1*, *IFIT2*, *IFIT3*, *IFIT5*, *OASL*, *OAS1*, *OAS2*, *OAS3*, *MX1*, *IFITM3, USP18, ISG15, IFI44*, and *IFI44L*.

IFI44 (IFN-induced protein 44) and *IFI44L* (IFN-induced protein 44-like) were selected for my project initially due to the lack of described range of antiviral activity and mechanism of action.

1.7.2 The IFI44 Family

IFI44 and *IFI44L* are the prototypic members of the human IFI44 family. Both genes are encoded adjacently on chromosome 1. *IFI44* spans 14 kilobases whereas *IFI44L* is significantly larger covering 26 kilobases. IFI44 and IFI44L proteins share some 45% residue identity and are similarly sized at 444 and 452 amino acid residues respectively. IFI44 and IFI44L genes can be found in a range of vertebrates and invertebrates including mice, cows, dogs, bats, zebrafish [251], and oysters [252].

IFI44 was first identified as a cytoplasmic microtubular aggregate protein in hepatocytes of HCV-infected chimpanzees [253, 254]. Further analysis of the human *IFI44* gene identified an ISRE in the promoter region and characterised the genes nine exons and eight introns [255]. Kitamura *et al* demonstrated that *IFI44* expression is induced by IFN-I but not IFN-II. *IFI44L* also has an ISRE sequence in the promoter region and is IFN-I inducible. IFI44L is also translated from an mRNA made up of nine exons.

1.7.3 Predicted Protein Function and Cellular Localisation

IFI44 and IFI44L are thought to be cytoplasmic proteins [256], although IFI44 has been reported in the nucleus during HIV-I infection [257]. Immunoelectron microscopy originally identified IFI44 as a microtubular aggregate protein (one of its gene aliases is MTAP44), although no further characterisation on any interaction of IFI44 or IFI44L with the cytoskeleton has been published.

IFI44 and IFI44L are both predicted to contain a dynamin-like GTPase domain (Fig 1.4a) [256]. This domain contains five regions required for proper binding of guanosine diphosphate (GDP) and Mg^{2+} cofactors required for GTP catalysis [258]. Both proteins contain a putative G1 region (GXXXXGKS), initially identified in IFI44 by Hallen *et al* [256], that is predicted to bind the β-phosphate of GDP or GTP [258]. The terminal serine residue also contributes to Mg^{2+} binding. The G1-G4 regions of human IFI44 and IFI44L were annotated by McDowell *et al* while investigating diversification in immune gene families in invertebrates (Fig 1.6) [252]. However, the identification of the true G2 region is difficult as this consists of a single threonine residue involved in Mg^{2+} binding. Both IFI44 and IFI44L contain the aspartate and glycine residues of a G3 region involved in binding the terminal phosphate of GTP molecules and Mg^{2+} ions. The G3 DxxG motif is immediately followed by a hydrophobic leucine residue found in

other dynamin-like GTPases such as GBP1, instead of a catalytic glutamine residue seen in ras-like GTPase domains [258]. IFI44L also contains a TKxD motif predicted to function as a G4 region which mediates binding to the guanine base of GDP or GTP. However, IFI44 does not contain a complete G4 motif (THVD). G5 residues are not easily recognised as they are not as well conserved as G1-4 motifs [252].

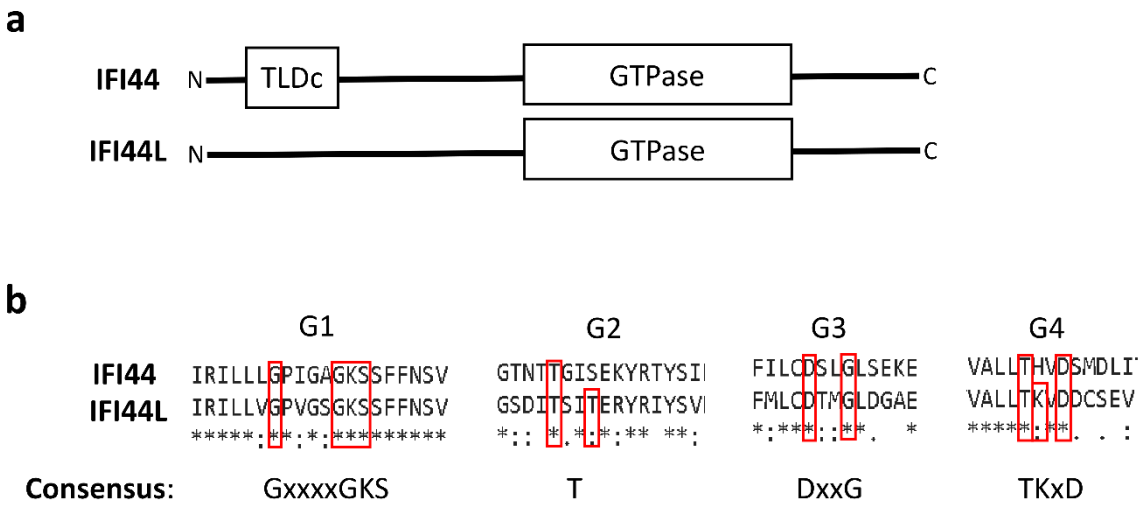

Figure 1.6. Predicted structure and domains of IFI44 proteins. (a) Predicted conserved domains found in human IFI44 and IFI44L. Domains identified with NCBI Conserved Domain Database. **(b)** Predicted regions of human IFI44 and IFI44L involved in GDP/GTP binding. Key residues in accordance with consensus sequence are highlighted in red boxes. Multiple potential threonine residues that may act as the G2 are highlighted. Sequences were aligned using Clustal Omega (https://www.ebi.ac.uk/Tools/msa/clustalo/). "*" identical residue, "." weakly similar residue, ":" strongly similar residue.

The IFI44 protein sequence also contains a predicted TLDc domain consisting of residues 28-87. This domain is also found in Rab GTPase-activating protein, LysM, and oxidation resistance proteins [259]. Interestingly, this domain is also found in NCOA7, an ISG demonstrated to restrict viral infection by inhibiting virus escape from endosomes, enhancing acidification of endosomes, and promoting lysosomal protease activity [153]. Both NCOA7 and oxidation resistance proteins have been reported to protect cells against oxidative damage [259]. RSV and many other viral infections induce formation of reactive oxygen species during infection [260]. IFI44 may play a role in protection from virus-induced oxidative stress.

IFI44 and IFI44L are reportedly anti-proliferative factors [256, 261]. Hallen *et al* suggested that the predicted GTP-binding capacity of IFI44 may contribute to its anti-proliferative activity, although this has not been investigated further. Analysis of IFI44L in hepatic cancer stem-like cells suggests that IFI44L affects proliferation, metastasis, and even drug resistance through modulation of Met/Src signalling [261]. This signalling pathway is involved in responding to hepatocyte growth factor and is often dysregulated in human cancers, including non-small cell lung cancer [262].

1.7.4 Reported Antiviral Activity of IFI44 Proteins

There is little published information on antiviral activity mediated by IFI44 and IFI44L. IFI44 expression has been reported to reduce replication of Bunyamwera orthobunyavirus (BUNV) around 10-fold *in vitro* [263]. Power *et al* have also reported that IFI44 restricts HIV-1 infection of HeLa and immortalised T cell lines [257]. IFI44 was shown to interact with viral DNA, following integration into the host genome, and reduce activity of viral promoter regions. Power *et al* also observed that IFI44 predominantly localised to the nucleus of HIV-1-infected T cell lines and HEK293 epithelial cells, unlike previous observations in melanoma-derived cell lines that IFI44

was cytoplasmic following IFN-I stimulation. This may suggest cell-type specific differences or, perhaps more likely, a virus-specific mechanism of action. This mechanism of action, which relies upon DNA-binding and nuclear localisation, does not explain how IFI44 is able to reduce RSV infection as observed previously [204]. RSV replicates wholly within the cytoplasm and forms no DNA intermediates during genome replication [53]. Similarly, BUNV has a negative-sense single-stranded RNA genome which is replicated in the cytoplasm without the formation of DNA intermediates [264].

Two high-throughput lentiviral-expression screens of ISG antiviral activity have included IFI44 and IFI44L [150, 151]. To screen ISG activity, Schoggins *et al* produced lentivirus particles using a bicistronic vector expressing an ISG and a red fluorescent protein (RFP) (Fig 1.7a). These lentivirus stocks are used to transduce HeLa, Huh7, and *STAT1*$^{-/-}$ fibroblasts 24 hours prior to infection with a variety of viruses including a GFP-expressing RSV, rgRSV (Fig 1.7b). After 6-72 hours (23 hours for rgRSV) the proportion of transduced cells that are infected is used to determine antiviral activity of the transduced ISG (Fig 1.7c).

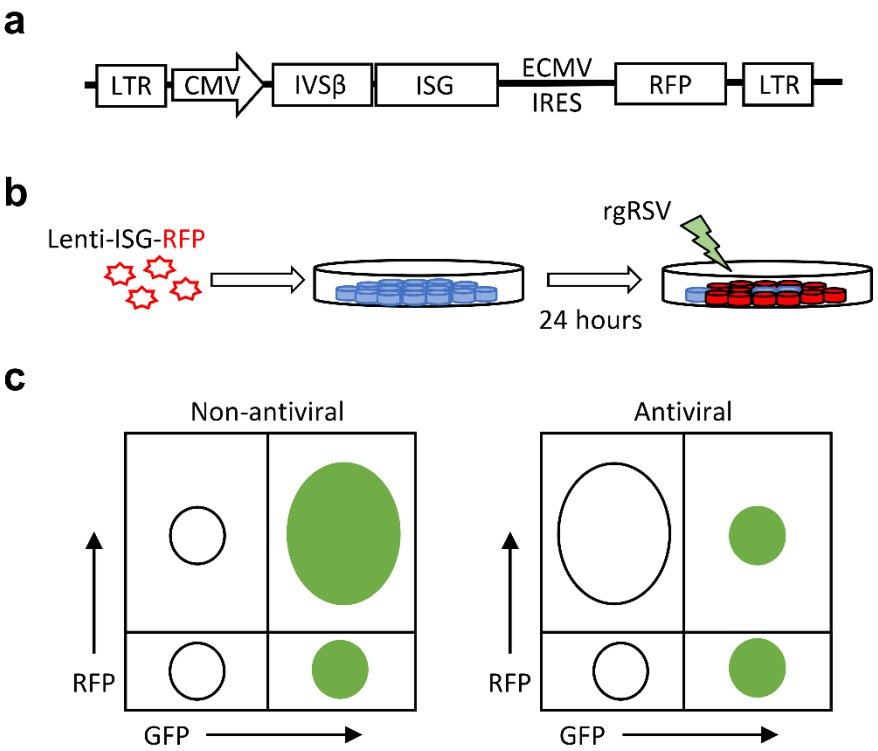

Figure 1.7. High-throughput screening of ISG activity. (a) Bicistronic lentiviral vector. **(b)** Schematic of transduction and infection protocol. **(c)** Predicted flow cytometry plots of transduced and rgRSV-infected cells with either an antiviral or non-antiviral ISG. Infected cells are shown as GFP^+ in green circles. Non-infected cells are shown as a white circle. Transduced cells are plotted in the upper quadrants. Adapted from Schoggins *et al.* Nature (2011).

The first screen by Schoggins *et al* reported mild (20-30%) restriction of HCV (28%), WNV (20%), and VEEV (30%) by IFI44 [151]. IFI44L did not have any impact on VEEV infection but was mildly antiviral during HCV (30%) and WNV (10%) infection. WNV and VEEV infection was assessed at an early time point (5.5-6 hours after infection), whereas HCV infection was assessed after 48 hours. However, Schoggins *et al* went on to show that IFI44L had a small but significant impact at an early point of HCV infection (12h). The timing of antiviral activity may suggest which stages of the viral life cycle are affected by IFI44 and IFI44L activity. A repeat of this initial high-throughput screen by Schoggins *et al* using additional DNA and RNA viruses reported

mild antiviral activity of IFI44 against PIV3 (21%) and HMPV (12%) [150]. IFI44L was only reported to impact Coxsackie B virus (17%), Poliovirus (25%), and NDV (22%) infection, with little activity against PIV3 (9%) and HMPV (7%).

Neither IFI44 nor IFI44L were shown to restrict RSV or BUNV infection [150]. Although lentiviral stocks were produced using the same lentiviral constructs as McDonald *et al* [204]. However, it is unclear if Schoggins *et al* titred lentivirus stocks prior to use. As lentiviral transduction can initiate TLR signalling and IFN-I production it follows that inoculation with varying numbers of lentiviral particles can result in differential antiviral capacity between samples [265, 266]. Further, application of different amounts of lentivirus particles results in different levels of transgene expression. As such, IFI44 or IFI44L transduction and subsequent expression was not properly normalised to a sample transduced with a vector control. Transgene expression was not confirmed by McDonald *et al* but lentivirus stocks were titrated in order to inoculate cells with either control or ISG-expressing lentivirus particles at the same multiplicity of infection [204]. Overall, these conflicting data require corroboration and follow-up experimentation to confirm any antiviral activity of IFI44 and IFI44L during RSV infection.

1.8 Hypothesis and Aims

Interferon-stimulated genes are a fascinating set of genes for which there is relatively little known, considering the number of ISGs. This thesis considers the hypothesis that there are additional ISGs that influence RSV infection. To investigate this, the ISGs *IFITM1*, *IFI44*, and *IFI44L* were characterised during RSV infection *in vitro* using both gain- and loss-of-function approaches. *In vivo* relevance of these genes was assessed using knockout mouse models of infection. The mechanism of action of these ISGs was probed to further our understanding of the range of ISG function.

1.8.1 IFN-Induced Transmembrane Protein 1

Studies by Smith *et al* have suggested that IFITM1 antiviral activity is dependent on plasma membrane localisation, and additional *in vitro* studies have suggested IFITM1 restricts RSV infection. RSV enters host cells following fusion events at the plasma membrane. As such, this chapter hypothesises that IFITM1 restriction of RSV is dependent on cell surface localisation. In addition, this chapter addresses the hypothesis that *Ifitm1* is a relevant ISG during RSV infection *in vivo* that influences disease severity.

The aims of this section of the thesis were to develop overexpression systems to assess IFITM1 function in the context of RSV infection *in vitro*, and to investigate whether alteration of IFITM1 localisation in these systems perturbed antiviral activity. Finally, this section aimed to further the understanding of *Ifitm1* activity *in vivo* during RSV infection in mice using a model of monogenic *Ifitm1* deficiency.

1.8.2 IFN-Induced Protein 44 and IFN-Induced Protein 44-Like

IFI44 and IFI44L are poorly characterised but are found up-regulated in a variety of viral infections. There is conflicting data as to whether these proteins restrict RSV infection *in vitro*. This chapter considered the hypothesis that these ISGs restrict RSV infection *in vitro* and have a role during *in vivo* infections. This chapter aimed first aimed to characterise the contribution of IFI44 and IFI44L to the control of RSV infection both *in vitro* and *in vivo*. Second, this chapter aimed to identify the mechanism of antiviral action.

To achieve these aims, the impact of IFI44 and IFI44L on RSV infection was examined using an optimised overexpression system. In addition, loss-of-function approaches were developed including siRNA and CRISPR-Cas9 gene editing. These tools were used to interrogate the function of IFI44 and IFI44L during RSV infection. Contribution of an identified GTPase domain in both IFI44 and IFI44L was investigated, along with other avenues informed by data from overexpression and loss-of-function studies. Finally, *Ifi44*$^{-/-}$ mice were used to assess the impact of *Ifi44* in an established whole organism model of RSV infection.

Chapter 2

Materials and Methods

2 Materials and Methods

2.1 *In Vitro* Cell Culture

2.1.1 Human Epithelial Cell Lines

A549, HEK293T/17, and HEp-2 human epithelial cell lines were thawed from cryostorage at 37°C in a water bath and transferred into T75 tissue culture flasks (Corning). Cells were maintained in Dulbecco's modified eagle medium (DMEM, Thermofisher) supplemented with 10% foetal calf serum (FCS, Sigma), 1% Penicillin/streptomycin (Sigma), and 1% L-glutamine (Thermofisher). Herein referred to as D10. Cultures were incubated in a humidified incubator at 37°C with 5% CO_2. Cells were routinely passaged by trypsinisation when >80% confluent. Cells were washed with 1 x phosphate-buffered saline (PBS) and incubated with 1 volume Trypsin-EDTA (Thermofisher) for 5 minutes at 37°C 5% CO_2. Trypsin activity was then neutralised with 3 x volume D10 and cells collected into 50 mL tubes (Falcon) and centrifuged at 500 x g for 5 minutes at 4°C. Cells were resuspended in D10 and counted by trypan blue exclusion before seeding into new flasks at an appropriate density to allow proliferation over 3-4 days.

2.1.2 Human THP-1 Cells

Human monocytic THP-1 cells were cultured in Roswell Park Memorial Institute (RPMI) medium (Sigma) supplemented with 10% foetal calf serum (FCS, Sigma), 1% Penicillin/streptomycin (Sigma), and 1% L-glutamine (Thermofisher). Herein referred to as R10. When cell density reached $1x10^6$ cells/mL cultures were split into new culture flasks.THP-1 cells were differentiated over 24 hours into phagocyte-type cells

by supplementation of culture medium with 20 ng/mL Phorbol 12-myristate 13-acetate (Sigma). Cells were rested for a further 24 hours in R10 prior to experimentation.

2.2 *In Vitro* Virology

2.2.1 Growing Respiratory Syncytial Virus

RSV A2 was a gift from P. Openshaw (Imperial College London). Stocks of RSV A2 or GFP expressing rgRSV [267] were produced by infecting HEp-2 monolayers and retaining cell supernatant after 48 hours. Prior to infection HEp-2 cells were seeded into T175 tissue culture flasks at a density of $5x10^6$ cells per flask and incubated for 24 hours. Cells were then washed once with 1 x PBS and infected with RSV A2 for 90 minutes, in a volume of 3 mL serum-free DMEM supplemented with 1% penicillin/streptomycin and 1% L-glutamine (herein referred to as D0), at a multiplicity of infection (m.o.i.) of 0.1 (0.1 plaque-forming units, pfu, per cell), assuming cell number had doubled. Following this the inoculum was removed and replaced with 30 mL D10. Cells were incubated for 24 hours. The serum content in the growth medium was reduced to 2% and cells incubated for a further 24 hours or until the observable cytopathy exceeded 50% of the cells in the culture. Medium was removed and sonicated for 20 seconds before being aliquoted into 1 mL vials and frozen in liquid nitrogen. Virus stocks were quantified by plaque assay prior to use.

2.2.2 RSV Plaque Assay

RSV titre was assessed through an immuno-plaque assay using biotinylated goat anti-RSV polyclonal antibody (Thermofisher, PA1-73019). HEp-2 cells were seeded into 96-well plates at a density of $2x10^4$ cells per well and incubated overnight. Virus stocks were then titrated by infecting these HEp-2 monolayers with doubling dilutions of viral

stocks in D0 starting at 1/100. The medium was removed from the HEp-2 cultures and replaced with 50 µL of a virus dilution. At least 8 dilutions were performed and assessed in triplicate. The cells were incubated at 37°C for two hours before the addition of 150 µL D10 to each well. After a further 24 hours the cells were washed in PBS and fixed with 100 µL methanol containing 2% H_2O_2 (Sigma) for 20 minutes at room temperature. Cells were then washed in 1% bovine serum albumin (BSA) in PBS. 100 µL of biotinylated anti-RSV antibody (1/400) in 1% BSA PBS was then added to each well and the plate incubated at room temperature for one hour. The cells were then washed twice with 1% BSA PBS. 100 µL of ExtrAvidin peroxidase (4 µg/mL, Sigma, E2886) in 1% BSA PBS was added to each well and the plate incubated for 30 minutes at room temperature. The cells were then washed twice with 1% BSA PBS. 50 µL of 3-amino-9-ethylcarbazole (Sigma) was added to each well and incubated for one to 24 hours at room temperature for colour development. To determine the concentration of each RSV stock or cell supernatant wells with 50-200 plaques were couned. Plaque-forming units (pfu) mL^{-1} were then calculated: number of plaques x dilution factor x 20.

2.2.3 Growing Influenza Virus

Sub-confluent Madin-Darby Canine Kidney (MDCK) epithelial cells were seeded in a T175 flask (Corning) and incubated for 24 hours in a humidified incubator at 37°C with 5% CO_2. 1 mL of H1N1 Influenza A/England/195 stock virus was thawed, added to 3 mL of RPMI without FCS (R0), and added to the MDCK culture for 1 hour. The cells were then washed with PBS and 10 mL R0 was added to the flask. Cells were incubated for 2-3 days until there was observable cytopathy. The cell supernatant was then removed, cleared by centrifugation at 528 x g for 5 minutes, and aliquoted into 1 mL vials before being frozen in liquid nitrogen. Stocks were quantified by plaque assay

prior to use. Virus stocks were kindly prepared by Ziyun Zhong and Dr Ekaterina Kinnear (Imperial College London).

2.2.4 Influenza Virus Plaque Assay

MDCK cells were cultured to >90% confluency in 12-well culture plates (Corning). Cultures were infected with serial dilutions of thawed virus stock in R0 for 1 hour in a humidified incubator at 37°C with 5% CO_2. The plates were agitated every 10 minutes to evenly disperse the viral inoculum over the culture. The cultures were then gently washed with 1 x PBS. To quantify the titre of the virus stock 1 mL of overlay was added to each well, consisting of 1/3 2% (w/v) Oxoid-purified agar, 2/3 overlay medium, with 0.001% Trypsin. Overlay medium consisted of H_2O, 15 mM HEPES, 0.3% BSA, 3 nM L-glutamine, 30 mM $NaHCO_2$, 0.01% dextran, 1.5% 10 x penicillin/streptomycin, and 15% minimum essential medium (10x, no glutamine). Once dried, the plates were incubated while inverted for 24-48 hours at room temperature. The cells were fixed in methanol and stained with 1% crystal violet. Plaques were counted to calculate titre as pfu mL^{-1}. Virus stocks were quantified by Ziyun Zhong and Dr Ekaterina Kinnear (Imperial College London).

2.2.5 *In Vitro* Infections

Cell monolayers were infected with RSV A2, rgRSV, or Influenza A virus (H1N1, A/England/195/2009) in D0 at least 24 hours after seeding. Inoculum volume was 2/5 the volume of growth medium used for each size of tissue culture plate. Where noted, viral inoculum was determined for each different cell line or treatment condition by calculating the number of viable cells in each well. Cells were infected for 90 minutes before the initial inoculum was removed and replaced with D10. Where noted in the

results section, cells were pre-treated with 500 IU mL^{-1} recombinant IFNα2α (PBL Assay Science) 16 hours prior to infection.

2.2.6 RSV Cell Binding Assay

Cells were seeded 24 hours prior to infection to be 80-90% confluent at the time of infection. Cells were equilibrated to 4°C for 30 minutes prior to infection. The numbers in each well for each cell line was determined by trypan blue exclusion before infection to ensure an accurate inoculum dilution. Cells were washed in ice-cold PBS and infected with RSV A2 at an m.o.i. of either 2 or 0.1 in a minimal volume of ice-cold D0. Cells were maintained at 4°C for 90 minutes with occasional agitation. Cells were then washed three times in ice-cold PBS before lysis in RLT buffer (Qiagen) with 10/1000 β-mercaptoethanol (Sigma) for analysis of viral RNA levels.

2.2.7 RSV Minigenome Assay

The RSV minigenome construct and plasmids expressing RSV proteins were a kind gift from Jean-Francois Eléouët (INRA, France). The minigenome plasmid pGEM3-Gaussia/Firefly encodes Gaussia luciferase (GLUC) downstream of the RSV leader sequence with a GE at the 5' end derived from the RSV M gene [74]. This M gene GE is followed by an SH GS and the Firefly luciferase (FLUC) ORF with an SH gene end sequence. HEK293T/17 cells were transfected at 90% confluence in 24-well plates (Corning) using Lipofectamine 3000® (Thermofisher). A DNA mixture was prepared containing 0.25 µg pGEM3-Gaussia/Firefly minigenome, 0.125 µg pCITE-L, 0.25 µg pCITE-P, 0.06 µg pCITE-M2-1, 0.25 µg pCITE-N, 0.12 µg pSV-β-Gal (Promega), and 0.25 µg pCAGGS-T7 (Addgene #65974). Negative controls were transfected with the DNA mix with pCITE-L replaced by pcDNA3.1. FLUC activity was measured after cell lysis in 1 x passive lysis buffer (Promega) for 45 minutes at room temperature with

frequent agitation. 10 µL of lysate was added to 50 µL luciferase assay substrate (Promega) and incubated in the dark at room temperature for 10 minutes. Luminescence was quantified using a FLUOstar omega spectrophotometer (BMG Labtech). β-Galactosidase levels were measured using the β-Galactosidase Enzyme Assay System (Promega) to normalise transfection efficiencies. Lysates were diluted 1:1 in 1 x reporter lysis buffer to a final volume of 40 µL. Lysate was incubated for 1 hour at 37°C after the addition of 40 µL 2 x assay buffer (200 mM Na_2HPO_4 buffer, 2 mM $MgCl_2$, 100 mM β-mercaptoethanol, 1.33 mg/mL ortho-Nitrophenyl-β-galactoside). To stop the reaction 150 µL 1 M Na_2CO_3 was added and absorbance measured at 420 nm on a FLUOstar omega spectrophotometer (BMG Labtech).

2.3 Molecular Biology

2.3.1 Short-Interfering RNA Transfection

A549 cells were reverse-transfected with endoribonuclease-prepared short-interfering RNA (esiRNA) constructs using Lipofectamine 3000® (Thermofisher) according to the manufacturers protocol. In brief siRNA were prepared in Opti-MEM® (Thermofisher) with Lipofectamine 3000® transfection reagent. RNA mixtures were incubated at room temperature for 15 minutes before distribution into empty tissue culture plates (1/6 of final well volume). During this incubation A549 cell suspensions were prepared and then added to appropriate wells. IFI44 was targeted with esiRNA-IFI44 (Sigma, EHU045601). IFI44L was targeted with esiRNA-IFI44L (Sigma, EHU030251). esiRNA targeting firefly luciferase was used as a non-targeting control (Sigma, EHUFLUC).

A549 cells were reverse transfected with single oligo siRNA (Sigma) using MISSION transfection reagent. siRNA was diluted to 6x the final required concentration in 1x volume D0 with 3 µL MISSION transfection reagent. This transfection mix was

incubated for 15 minutes at room temperature before addition to culture wells. A549 cell suspensions in fresh D10 medium were prepared and added to the appropriate wells (5x volume). MISSION siRNA universal negative control #1 (Sigma, #SIC001) was used as a non-targeting control. IFI44 was targeted by either si-IFI44-1 (Sigma, SASI_Hs01_00123752) or si-IFI44-2 (Sigma, SASI_Hs01_00123753). IFI44L was targeted by either si-IFI44L-1 (Sigma, SASI_Hs01_00079579) or si-IFI44L-2 (Sigma, SASI_Hs01_0079580).

2.3.2 Plasmid DNA and Cloning

For expression of IFI44 (NM_006417.5) and IFI44L (NM_006829.4) coding sequences were produced by GeneArt (Thermofisher) synthesis and cloned into the pcDNA3.1 expression vector (Thermofisher) using *BamH*I and *Xho*I restriction sites. For generation of stable cell lines IFI44 and IFI44L coding sequences were codon-optimised and synthesised (GeneArt) with additional sequence encoding a C-terminal myc (IFI44) or HA (IFI44L) epitope tag and inserted into pSIN-CSGW-Puro (a gift from P. Kellam, Imperial College London) using *BamH*I and *Not*I restriction sites. IFI44 (pTRIP-CMV-IVsb-IFI44-IRES-TagRFP) and IFI44L (pTRIP-CMV-IVsb-IFI44L-IRES-TagRFP) lentiviral constructs were a gift from M. Dorner (Imperial College London).

Single guide RNA (sgRNA) sequences were cloned into pSpCas9(BB)-2A-GFP (PX458) a gift from F. Zhang (Addgene plasmid #48138). sgRNA oligos were synthesised with *Bbs*I 5' and 3' overhang. To anneal and phosphorylate single-stranded oligonucleotides 100 µM of each paired single-stranded oligonucleotide were mixed and incubated with T4 polynucleotide kinase (New England Biolabs) in 1 x T4 ligation buffer (New England Biolabs) in a 10 µL reaction for annealing and phosphorylation with the following temperature cycle, 37°C for 30 minutes, 95°C for 5 minutes, ramp down to 25°C with a temperature change of 5°C per minute. PX458

was digested with *Bbs*I and the linear vector was purified using the QIAquick DNA extraction kit (Qiagen) according to the manufacturer's instructions following agarose gel electrophoresis. Annealed sgRNA oligonucleotides were subsequently ligated into PX458 using T4 DNA ligase (New England Biolabs).

2.3.3 Agarose Gel Electrophoresis

PCR products and plasmids were visualised after electrophoresis in a 1% agarose Tris-acetate EDTA gel with 1 x SYBR® safe DNA gel stain (Thermofisher). A 100-15000 bp ladder was used for reference (1 Kb Plus DNA ladder, Qiagen). DNA was separated at 100 V for 40-60 minutes and imaged using a GelDoc-IT2 (Analytik Jena).

2.3.4 DNA Transfection

Plasmid DNA was transfected into A549, HEK293T/17, and HEp-2 cell lines using Lipofectamine 3000®. Volumes of P3000 and Lipofectamine 3000® transfection reagent were optimised according to the manufacturers protocol using a plasmid encoding the red fluorescent protein tdTomato. DNA was prepared in Opti-MEM with P3000 (2 µL/µg DNA) and incubated at room temperature for 5 minutes. Lipofectamine 3000® transfection reagent was prepared in Opti-MEM and subsequently mixed 1:1 with a DNA mix. This transfection solution was incubated for a further 15 minutes at room temperature before being added drop-wise to appropriate wells of a tissue culture plate. Cells were seeded to be at 40% confluency at the time of transfection.

2.3.5 Lentivirus Production

Lentivirus stocks were produced from triple transfection of HEK293T/17 cells. Cells were routinely passaged to maintain health and optimal growth rates. Cultures were maintained for less than 20 passages for use in production of lentivirus. HEK293T/17 cells were seeded in 6-well plates (Corning) 24 hours prior to transfection and

transfected at >90% confluency. For each lentiviral stock wells were transfected in triplicate. A HIV-1-derived packaging construct p8.91, VSV-G coding plasmid pMDG.2, and lentiviral genome vector encoding the transgene of interest were combined in a ratio of 1:1:1, 2:5:5, or 1:5:10 for a total of 3 µg DNA in 125 µL Opti-MEM for a single well of a 6-well plate. P3000 reagent was added to the DNA mix (2 µL/µg DNA) and it was incubated for 10 minutes at room temperature. DNA solutions were subsequently added 1:1 to Opti-MEM with Lipofectamine 3000® transfection reagent (7 µL/well) and incubated for a further 15 minutes at room temperature before being added dropwise to the cells. Growth medium containing lentivirus was taken at 24 and 52 hours post-transfection. Media was pooled and filtered through a 0.22 µm filter. Stocks were either used directly for transduction or frozen on dry ice in 1 mL aliquots and stored at -80°C.

The concentration of lentiviral stocks encoding TagRFP was determined by flow cytometry. Cells were transduced with serial dilutions of lentivirus stock and the number of transducing units per mL of stock was calculated based on the number of transduced cells at a dilution where less than 20% of cells were transduced. Untransduced cells and 100% transduced cells were used as negative and positive controls to set appropriate analysis gates.

$$\text{Transducing units per mL} = (F \times (Co/V)) \times D.$$

Where F is the frequency of transduced cells, Co the number of cells in the well at the time of infection, V the volume of viral inoculum in mL, and D the dilution factor of the inoculum.

2.3.6 Lentivirus Transduction

For the generation of stable cell lines, A549 or HEK293T/17 cells were seeded into three wells of a six-well plate at 50% confluency 24 hours prior to transduction. For transient overexpression assays and to assay concentration of lentiviral stocks, A549 cells were seeded into 12 well plates at a density of $5x10^4$ cells per well 24 hours prior to transduction. To generate stable cells, cultures were transduced with 1mL of lentivirus stock. For transient transduction, cultures were inoculated with $2x10^5$ transducing units in 250 µL. Cells were centrifuged at 650 x g at room temperature for 30 minutes after addition of inoculum. Cultures were then incubated at 37°C for one hour prior to addition of D10 (2 x inoculum volume). For the generation of stable cell lines transduction was repeated after 8 hours and transferred into 12-well plates at 50% confluency 48 hours later. Stable cells were selected using puromycin or fluorescence activated cell sorting (FACS). For FACS selection, the top 2% of RFP^+ cells were sorted as single cells into two flat-bottomed 96-well plates (Corning). Cells were cultured for two weeks before the addition of fresh D10 and initial screening for RFP^+ colonies by fluorescent microscopy. RFP^+ cultures were expanded and assayed for transgene expression by qPCR and Western blotting.

2.3.7 CRISPR-Cas9 Gene Editing

Cell lines were transfected with PX458 constructs containing sgRNA sequences as described previously. The cells with the highest level of GFP expression (top 2% of single GFP^+ cells) were sorted as single cells using a Becton Dickinson Aria II. Monoclonal cultures were expanded over several weeks before analysis of gene editing. DNA was extracted using the QIAamp DNA mini kit according to the manufacturer's instructions (Qiagen). Sites targeted for Cas9-editing were amplified

using primers bordering the region (table 2.1) and editing assessed by agarose gel (1%) electrophoresis and sequencing (Eurofins Genomics).

Gene symbol	Primer orientation	Sequence (5'-3')
IFI44	Forward	GAGCTTACTGTCTGCCTTGA
IFI44	Reverse	GAAGAGCCCTCGAGATGTTT
IFI44L	Forward	GCCCTGGGTTATGCAAGAAAAC
IFI44L	Reverse	CACAATGGAGGTGGTTCTGATC

Table 2.1. Primer sequences used to amplify *IFI44* and *IFI44L* genomic DNA.

2.3.8 RNA Extraction

RNA was extracted from cell culture lysate using the RNeasy mini kit (Qiagen) according to the manufacturers protocol following lysis with RLT buffer with 10/1000 β-mercaptoethanol (Sigma) and centrifugation at 13 000 x g through a QIAshredder column (Qiagen). Between addition of lysis buffer and extraction samples were stored at -80°C as this increased RNA yield and purity as assessed by spectrophotometry.

2.3.9 Reverse Transcription of RNA

Equal amounts of RNA were converted to complementary DNA (cDNA) by reverse transcription of up to 2 µg of RNA with GoScript™ reverse transcriptase and random hexanucleotide primers (Promega) according to the manufacturer's instructions. RNA was added to GoScript™ reaction buffer (4 µL), GoScript™ enzyme mix (2 µL), and H_2O in a 20 µL reaction. The reaction was incubated at 25°C for 5 minutes, 42°C for

60 minutes, with a final denaturation step of 70°C for 15 minutes. cDNA was stored at 4°C for analysis the same or next day. Long-term storage was at -20°C.

2.3.10 Quantitative PCR of Human and Mouse mRNA Transcripts

Primer sequences and reaction conditions for each set are listed in table 2.2. Quantitative PCR (qPCR) of human and mouse mRNA transcripts was carried out with SYBR® Select master mix (Thermofisher). 2 µL of cDNA sample was added to the appropriate wells of a semi-skirted qPCR reaction plate (Agilent Technologies) before addition of the reaction mix which was prepared as a master mix. Both forward and reverse primers were added to a final concentration of 250 nM (1 µL of primer 5 µM stock solution) with 10 µL SYBR Select master mix and 6 µL nuclease-free H_2O (Qiagen) per reaction. Samples were analysed on a Stratagene Mx3005p (Agilent Technologies). Fluorescence values were normalised to a reference dye Rox and a threshold used to determine the threshold cycle (Ct) for each sample. Log2(foldchange) values were calculated by the ΔΔCt method [268]. Before use with experimental samples, primer sets were assessed for specificity by melt-curve analysis and for efficiency using a standard curve of cDNA samples with known concentration. Only primer sets with similar (90-110%) efficiency values were used for relative quantification.

Gene symbol	Species	Forward primer (5'-3')	Reverse primer (5'-3')	Reference
IFI44	Human	TGGTACATGTGGCTTTGCTC	CCACCGAGATGTCAGAAAGAG	[269]
IFI44L	Human	AAGTGGATGATTGCAGTGAG	CTCAATTGCACCAGTTTCCT	N/A
MX1	Human	GTGACGGATATGGTCCGGCT	TTGGCGGTTCTGTGGAGGTT	N/A
IFITM1	Human	ATCAACATCCACAGCGAGAC	CAACCATCTTCCTGTCCCTAG	[270]
GAPDH	Human	GGACCTGACCTGCCGTCTAG	TAGCCCAGGATGCCCTTGAG	[271]
Ifi44	Mouse	AACTGACTGCTCGCAATAATGT	GTAACACAGCAATGCCTCTTGT	[272]
Ifi44l	Mouse	AGTGACAGCCAGATTGACATG	CATTGTGGATCCCTGAAGAGAA	N/A
Ifitm1	Mouse	GACAGCCACCACAATCAACAT	CCCAGGCAGCAGAAGTTCAT	[273]
Ifitm3	Mouse	CCCCCAAACTACGAAAGAATCA	ACCATCTTCCGATCCCTAGAC	[274]
Gbp2b	Mouse	ACAACTCAGCTAACTTTGTGGG	TGATACACAGGCGAGGCATATTA	[275]
Ifnb	Mouse	TCAGAATGAGTGGTGGTTGC	GACCTTTCAAATGCAGTAGATTCA	[276]
Ifng	Mouse	TCAAGTGGCATAGATGTGGAAGAA	TGGCTCTGCAGGATTTTCATG	[277]
Ifnl2/Ifnl3	Mouse	AGCTGCAGGCCTTCAAAAAG	TGGGAGTGAATGTGGCTCAG	[276]
Gapdh	Mouse	AGGTCGGTGTGAACGGATTTG	TGTAGACCATGTAGTTGAGGTCA	[278]

Table 2.2. Primers used for quantitative PCR.

2.3.11 Quantitative PCR of RSV L Gene

RSV viral load was assessed by quantifying the copy number of total L gene RNA by qPCR following cDNA conversion of equal amounts of sample RNA. Semi-skirted 96-well qPCR reaction plates were loaded with 2 µL of sample cDNA or of a plasmid encoding the RSV L gene amplicon sequence, ranging from $1x10^9$ to $1x10^2$ copies of plasmid in each well. A master mix was then mixed for the total number of reactions consisting of 10 µL TaqMan Universal PCR Mastermix (Thermofisher), 3.6 µL forward primer (5'-GAA CTC AGT GTA GGT AGA ATG TTT GCA-3', final concentration 900 nM), 1.2 µL reverse primer (5'-TTC AGC TAT CAT TTT CTC TGC CAA T-3', final concentration 300 nM), 0.7 µL labelled probe (5'-FAM-TTT GAA CCT GTC TGA ACA TTC CCG GTT-TAMRA-3', final concentration 175 nM), and 2.5 µL nuclease-free H_2O per reaction. The plate was then analysed using a Stratagene Mx3005p with the following thermal cycle: 95°C for 10 minutes followed by 40 cycles of 95°C for 15 seconds and 60°C for 60 seconds. L gene copy number was then calculated based on Ct values of samples compared to that of the standard curve (analysis using MxPro software, Agilent Technologies). Copy number per microgram RNA was then calculated based on the input RNA of the reverse transcription reaction and qPCR sample volume.

2.3.12 Quantitative PCR of Influenza A Virus M Gene

Influenza A virus viral load was assessed by quantifying the copy number of total M gene RNA by qPCR, as for RSV L gene. The master mix was prepared with 0.4 µL forward primer (5'-AAGACAAGACCAATYCTGTCACCTCT-3', final concentration 33.3 nM), 0.4 µL reverse primer (5'-TCTACGYTGCAGTCCYCGCT-3', final concentration 33.3 nM), 0.8 µL labelled probe (5'-FAM-TYACGCTCACCGTGCCCAGTG-BHQ1-3', final concentration 66.6 nM), 10 µL

TaqMan Universal PCR Mastermix (Thermofisher), and 6.4 µL nuclease-free H_2O. The plate was then analysed using a Stratagene Mx3005p with the following thermal cycle: 95°C for 10 minutes followed by 40 cycles of 95°C for 30 seconds, 55°C for 60 seconds, and 72°C for 30 seconds. M gene copy number was then calculated based on Ct values of samples compared to that of the standard curve (analysis using MxPro software, Agilent Technologies). Copy number per microgram RNA was then calculated based on the input RNA of the reverse transcription reaction and qPCR sample volume.

2.3.13 SDS-PAGE and Western Blotting

Radio immunoprecipitation assay (Sigma) buffer was prepared to 1x concentration with cOmplete™ Ultra protease inhibitor cocktail (Sigma). Cells were washed with PBS prior to addition of lysis buffer. Cells were incubated on ice in lysis buffer with occasional agitation for 30 minutes. Lysates were then collected into microcentrifuge tubes and centrifuged at 13,000 x g for 5 minutes to pellet debris. Cleared lysates were stored at -20°C. For sodium dodecyl sulphate polyacrylamide gel electrophoresis (PAGE) lysates were quantified by bicinchoninic acid (BCA) assay (Thermofisher) using a BSA standard. Protein concentrations were equalised to 1 µg/µL in H_2O and Laemmli sample buffer at 1x final concentration (Bio-Rad). Samples were boiled for 10 minutes prior to loading. Proteins were separated using a 4-20% pre-cast Mini-Protean TGX gel (Bio-Rad) with 20 µL of sample per well at 120 V for 50-70 minutes, or until sample approached the gel boundary. A prestained 10-245 kilodalton (kDa) protein ladder was included for reference (Abcam, ab116028). Proteins were transferred onto a nitrocellulose membrane using the Trans-Blot turbo transfer system (Bio-Rad). Membranes were incubated in 5% milk PBS with 0.1% Tween 20 for 1 hour at room temperature prior to addition of primary antibody overnight at 4°C. Membranes

were probed using the following primary antibodies: IFI44 (Thermofisher, PA5-65370), IFI44L (VWR, ARP46166), and β-actin (Abcam, ab8227). Membranes were washed in PBST x 3 for 5 minutes and probed with anti-IgG HRP-conjugated antibodies (Dako) for 1 hour at room temperature. The PBST wash was repeated and antibody-bound proteins visualised by chemiluminescent detection. 1 mL of Luminata™ Crescendo Western HRP Substrate (Millipore) was added to each membrane for 1 minute at room temperature. Membranes were imaged using a Celvin® S detection system (Biostep).

2.3.14 Cellular Proliferation Assays

Cellular proliferation was assessed by measuring the number of viable cells using either Trypan Blue exclusion or a colorimetric assay. Cells were seeded at equal densities, allowed to proliferate for 24-48 hours and cells counted using a haemocytometer after dilution with Trypan Blue solution 1:1. Equal seeding was confirmed using this manual counting approach 6 hours after plating. CellTiter 96 Aqueous One solution (Promega) was used to assess the number of metabolically active cells in a well. Cells were seeded as above, counted at 6 hours to confirm equal plating, and allowed to proliferate for 24-48 hours prior to addition of 20 µL CellTiter 96 Aqeuous One reagent. Cells were incubated at 37°C 5% CO_2 in a humidified incubator for 4 hours before measuring absorbance at 490 nm on a FLUOstar omega spectrophotometer (BMG Labtech). The incubation time with CellTiter reagent was optimised prior to use and is discussed later in this chapter.

Finally, cell proliferation was assessed by CellTrace Violet dye perfusion. CellTrace Violet reagent was resuspended in DMSO according to the manufacturer's instructions and added to single cell suspensions in PBS ($1x10^6$ cells/mL) to a final concentration of 5 µM. During this staining, cells were incubated at room temperature in the dark for 20 minutes with occasional agitation. To remove excess dye, 5 x volume of D10 was

added to each sample and incubated for 5 minutes at room temperature. Samples were centrifuged for 5 minutes at 400 x g and supernatant removed. Cells were resuspended in appropriate volume of pre-warmed D10 and seeded at $5x10^5$ cells per well in triplicate in a 6-well plate. Cells were incubated for 72 hours prior to analysis by flow cytometry. Cells were removed from culture wells by trypsinisation as previously described and suspended in 4% paraformaldehyde for 20 minutes. Cells were then washed in 1% FCS PBS three times before analysis. Positive controls were stained and prepared immediately prior to analysis.

2.3.15 Lactate Dehydrogenase Release Assay

Cytotoxicity was assessed using the Cytotox 96 non-radioactive cytotoxicity assay (Promega). Cells were seeded in triplicate at $5x10^3$ cells per well of a 96-well plate in 100 µL D10 medium and incubated at 37°C 5% CO_2 in a humidified incubator for 24-48 hours. To calculate percentage cytotoxicity, 100% cytotoxicity controls were prepared from 3 additional wells of each cell line at each time point by the addition of 10 µL lysis buffer for 45 minutes. Wells containing only D10 were used as background controls. 50 µL of supernatant from each sample and control was added to 50 µL of Cytotox Reagent and incubated in the dark for 30 minutes at room temperature. 50 µL of Stop Solution was added and absorbance at 490 nm measured on a FLUOstar omega spectrophotometer (BMG Labtech). Background absorbance was subtracted from each value and percentage cytotoxicity calculated.

2.3.16 Site-Directed Mutagenesis

QuikChange II site-directed mutagenesis kit (Agilent Technnologies) was used to modify pTRIP-CMV-IVsb-IFI44-IRES-TagRFP or pTRIP-CMV-IVsb-IFI44L-IRES-TagRFP constructs. Primer oligonucleotides were designed according to the

manufacturer's instructions and synthesised by Eurofins Genomics. To generate the mutant plasmid a PCR reaction was prepared with the following reagents and made up to 50 µL with nuclease free H_2O: 125 ng of each primer oligonucleotide, 5 µL 10x reaction buffer, 10 ng plasmid template, 1 µL dNTP mix, 3 µL QuikSolution. Each reaction was then subjected to the following thermal cycler conditions: 95°C for 1 minute, 18 cycles of 95°C for 50 seconds - 60°C for 50 seconds - 68°C for 11 minutes, and a final extension step of 68°C for 7 minutes. The reaction was cooled on ice for 2 minutes before addition of 1 µL *Dpn*I. The reaction was mixed thoroughly and incubated at 37°C for 1 hour. 2 µL of this reaction was then used to transform XL10-Gold Ultracompetent cells (Agilent Technologies). 45 µL of competent cell suspension was incubated with 2 µL β-mercaptoethanol for 10 minutes prior to addition of the *Dpn*I-treated DNA. This mixture was then incubated on ice for 30 minutes before heat-shock at 42°C for 30 seconds. 500 µL Lysogeny broth was added to the cell suspension and the mixture incubated at 37°C for 1 hour at 225 rpm. 250 µL of the cell suspension was spread evenly on pre-warmed lysogeny broth-ampicillin plates and incubated overnight at 37°C. Mutagenesis was confirmed by sequencing (Eurofins Genomics).

Gene	Mutagenesis	Forward oligo (5'-3')	Reverse oligo (5'-3')
IFI44	Deletion of residues 193-201	CAAATACGAATTCTGCTGCTGTTTTTCAACTCAGTGAGGTCT	AGACCTCACTGAGTTGAAAAACAGCAGCAGAATTCGTATTTG
IFI44L	Deletion of residues 200-208	GGTTTCAGAAATTCGTATTCTTTTGGTGTTTTTCAATTCAGTCAAGTCTATTTTTC	GAAAAATAGACTTGACTGAATTGAAAAACACCAAAAGAATACGAATTTCTGAAACC

Table 2.3. Oligonucleotides used for site-directed mutagenesis.

2.4 *In Vivo* Procedures

2.4.1 Mice and General Phenotyping

Female BALB/c mice were obtained from Charles River at 7-9 weeks of age and kept in accordance with the United Kingdom Home Office guidelines in specific pathogen-free conditions. Mice were given food and water *ad libitum* and monitored daily for signs of illness. For gene knockout studies, knockout and C57BL/6N (WT) mice were housed at the Wellcome Trust Sanger Institute. Genetically modified animals were monitored for developmental defects and pipelined through the Wellcome Trust as described previously [279, 280]. BALB/c mice were culled via intraperitoneal administration of pentobarbitol. C57BL/6N mice were culled by cervical dislocation. All work was conducted with approval from the relevant Animal Welfare and Ethical Review Board and in accordance with the UK Animals (Scientific Procedures) Act 1986.

2.4.2 Intranasal RSV Challenge

Mice were infected intranasally under light isoflurane anaesthetic with RSV diluted in sterile PBS in a total volume of 100 µL per animal. Neonatal mice were infected with a weight-adjusted dose (assuming a 20 g adult mouse) in 20 µL sterile PBS. Mice were monitored until fully recovered from the anaesthesia and checked 6 hours after infection. Change in weight was monitored at the same time every day for at least seven days following infection. Control groups were administered with 100 µL sterile PBS.

2.4.3 Lung Cell Isolation

Lung tissue was collected in D10 and homogenised through a 70 µm membrane (Falcon). After centrifugation (500 x g, 5 minutes at 4°C) and collection of lung supernatant, red blood cells (RBCs) were lysed with ACK lysis buffer (Lonza). Cells were then centrifuged as previously, and cell pellets resuspended in appropriate volumes of D10 for either counting or antibody staining.

2.4.4 Bronchoalveolar Lavage

Bronchoalveolar lavage fluid (BALF) was collected by making a small incision in the trachea and flushing the lungs with 1 mL PBS. This was repeated 3 times with the same 1 mL PBS. BALF cells were collected by centrifugation at 13 000 x g for 1 minute. The cleared supernatant was collected for analysis. RBCs were lysed in ACK buffer and centrifugation repeated to collect cells for counting or antibody staining.

2.4.5 *Ex Vivo* Culture of Mouse Tissue

Lung, spleen, and liver tissue were excised post-mortem. Sections of equal size were distributed into 24-well tissue culture plates and submerged in 1 mL D10 alone or D10

supplemented with 1000 IU mL^{-1} recombinant IFNα2a. (PBL Assay Science) for 24 hours.

2.4.6 RNA Extraction from Lung Tissue

The left-hand lung lobe was taken for RNA extraction and qPCR analysis. RNA was extracted by phenol/chloroform precipitation. Lung tissue was homogenised in 1.5 mL tubes containing 2 ball bearings and 350 µL TRIzol reagent (Thermofisher) using a TissueLyzer (Qiagen) at 50 oscillations per second for 4 minutes. Homogenates were transferred to fresh 1.5 mL tubes and 150 µL additional TRIzol reagent was added. Following a 5-minute incubation at room temperature 100 µL chloroform was added. Tubes were mixed thoroughly by inversion and the aqueous phase removed into new 1.5 mL tubes after centrifugation at 13 000 x g for 15 minutes at 4°C. RNA was collected by isopropranol precipitation and washed in 70% ethanol following centrifugation at 13 000 x g for 10 minutes at 4°C. RNA was pelleted by centrifugation at 7500 x g for 7 minutes at 4°C before and air-dried before resuspension in nuclease-free H_2O pre-heated to 37°C. Samples were incubated at 55°C for 5-10 minutes prior to quantification by spectrophotometry using a Nanodrop 1000 spectrophotometer.

2.5 Immunological Techniques

2.5.1 Immunofluorescence Microscopy

Cells were seeded onto ultraviolet-sterilised glass cover slips in 24-well plates and allowed to continue growth for 24 hours. Culture medium was removed, and cells washed in 1 x PBS. Cells were then fixed in 4% paraformaldehyde (Thermofisher) for 20 minutes at room temperature prior to permeabilization in 0.1% Triton X-100 (Sigma) for 20 minutes. Cells were then washed in 1 x PBS three times (5 minutes, room

temperature). Cells were incubated for a minimum of 1 hour in 1% BSA PBS 0.1% Tween 20 prior to incubation with primary antibody solutions for 1 hour at room temperature. Anti-HA tag mouse IgG (Abcam, ab18181) was used to visualise IFI44L-HA. The prior wash step was repeated, and cells incubated with secondary antibody for 1 hour at room temperature (Abcam, ab96871). Cells were washed and coverslips mounted in ProLong Gold Antifade mountant solution with DAPI (4',6'-diamidino-2-pheylindole). Slides were allowed to dry for 24 hours in the dark at room temperature and were then stored at 4°C prior to analysis on an Eclipse Ti fluorescent microscope (Nikon).

2.5.2 Cytokine Enzyme-Linked Immunosorbent Assay

IL-1β, IL-6, IL-12 p70, and IFN-β were quantified in mouse lung tissue supernatant or BALF using R&D Systems Duoset ELISA kits according to the manufacturer's instructions. 96-well Nunc MaxiSorp™ flat-bottomed plates were coated with 100 µL capture antibody in PBS overnight. Plates were washed with PBS 0.05% Tween 20 three times before addition of reagent diluent (1% BSA PBS, 200 µL per well) for minimum 1 hour. Plates were washed again and samples or standards added to the appropriate wells. Plates were incubated for 2 hours at room temperature before a further wash step. Detection antibodies were resuspended in reagent diluent (1% BSA PBS) according to the specific lot instructions and 100 µL added to each well. Plates were incubated with detection antibody for 1 hour. Plates were washed again and 100 µL Streptavidin-Horseradish peroxidase (HRP), diluted according to lot specific instructions, was added to each well for 30 minutes at room temperature. Plates were washed again and 100 µL TMB substrate (Thermofisher) added to each well and incubated until appropriate colour had developed. The reaction was stopped with 100 µL 1M H_2SO_4 and absorbance at 450 nm was measured using a FLUOstar omega

spectrophotometer (BMG Labtech). Comparison to the linear portion of the standard curve for each plate was used to derive sample concentrations.

2.5.3 Luminex® Multiplex ELISA

Cytokine and chemokine responses to RSV infection was assessed in murine lung tissue supernatant using a multiplex magnetic screening Luminex® assay kit according to the manufacturer's instructions (R&D Systems). 25 µL of diluted magnetic microbeads conjugated to antibodies specific for GM-CSF, TNF-α, CXCL10, CCL3, CCL5, CXCL2, CXCL1, IL-5, CCL2, IL-1α, IL-1β, IL-12 p70, and CCL5 was added to each well of a Luminex plate. 25 µL of sample or standard were added to the appropriate wells and the plate was sealed and incubated for 2 hours at room temperature, with orbital shaking set to 800 rpm. A magnet was used to secure the magnetic beads at the bottom of the well during subsequent washing steps. Wells were aspirated and washed with provided wash buffer 3 times. 50 µL biotinylated secondary antibody cocktail was added to each well and the plate incubated as before for 1 hour. The wash step was repeated and 50 µL of Streptavidin-Phycoerythrin was added to each well and the incubation repeated as before for 30 minutes. The wash step was repeated before beads were resuspended in 100 µL wash buffer for analysis on a Bio-Plex® 200 system for analysis (Bio-Rad).

2.5.4 Flow Cytometric Analyses

Samples were analysed using a standard Becton Dickinson Fortessa LSR equipped with a 50 mW 405nm, 50 mW 488 nm, 50 mW 561 nm, and a 20 mW 633 nm laser with a ND1.0 filter in front of the forward scatter (FSC) photodiode. A minimum of $1x10^4$ events were recorded for each sample. BD FACSDiva™ CST checks were run each

day to increase precision. Table 2.4 details the conjugated antibodies used with supplier validation approaches are listed in table 2.5.

Prior to antibody staining adherent cells were trypsinised and resuspended in 1% FCS PBS. Lung cell isolation has been described previously. Prior to antibody staining *in vivo* derived mouse cell samples were centrifuged at 400 x g for 5 minutes at 4ºC and resuspended for minutes at 4ºC in live/dead Violet (Thermofisher, L34955). Cells were then centrifuged and resuspended in anti-CD16/CD32 antibody (BD Biosciences) and incubated for 30 minutes at 4ºC.

All samples were then centrifuged at 400 x g for 5 minutes at 4ºC and resuspended in 400 µL 1% FCS PBS containing diluted antibody/s. For intracellular staining of GFP, samples were instead resuspended in 1% FCS 0.01% Triton X-100 PBS with antibody. Cells were stained for 1 hour at 4ºC out of direct light for surface staining, or 20 minutes for intracellular staining. Samples were centrifuged again and washed x 2 in 1% FCS PBS. The cells were then fixed in 4% paraformaldehyde for 20 minutes and washed x 3 in 1% FCS PBS prior to analysis.

Antigen	Target Species	Antibody Conjugate	Clone/Description	Supplier	Product code
CD3e	Mouse	FITC	145-2C11	Thermofisher	11-0031
CD4	Mouse	PeCy7	GK1.5	Biolegend	100421
CD8	Mouse	APC-H7	53-6.7	BD Biosciences	560182
HA-tag	N/A	AlexaFluor 647	16B12	Biolegend	682404
GFP	N/A	Dylight 488	FM264G	Biolegend	338008

Table 2.4. Antibodies used for flow cytometry analysis

Antigen	Antibody Conjugate	Validation
CD3e	FITC	Flow cytometry – Murine splenocytes with isotype control, Immunofluorescence and Immunohistochemistry
CD4	PeCy7	Flow cytometry – Murine splenocytes with isotype control
CD8	APC-H7	Flow cytometry – Murine splenocytes with isotype control
HA-tag	AlexaFluor 647	Immunofluorescence – HA tag stably transfected CHO cells
GFP	Dylight 488	Flow cytometry – GFP transfected CHO cells

Table 2.5. Validation of antibodies used for flow cytometry analysis

2.6 Quality Control Procedures

2.6.1 Mycoplasma Detection

Cell lines were routinely assessed for mycoplasma contamination using a MycoAlert™ Mycoplasma Detection kit (Lonza). Assays were conducted by Mr Leon McFarlane (Imperial College London). 50 µL of cell line supernatant was mixed with equal volume MycoAlert™ reagent and incubated at room temperature for 5 minutes and 10 minutes with a luminescent reading taken at each point using a FLUOstar Omega plate reader. To determine levels of contamination the ratio of these values were then compared to that of a positive control (MycoAlert™ Assay Control Set, Lonza).

2.6.2 Primer Efficiency Validation

Prior to use the efficiency of qPCR primer pairs was optimised by testing various annealing temperatures. The chosen conditions resulted in a reaction efficiency of 90-110% for all human (Fig 2.1) or murine (Fig 2.2) primers.

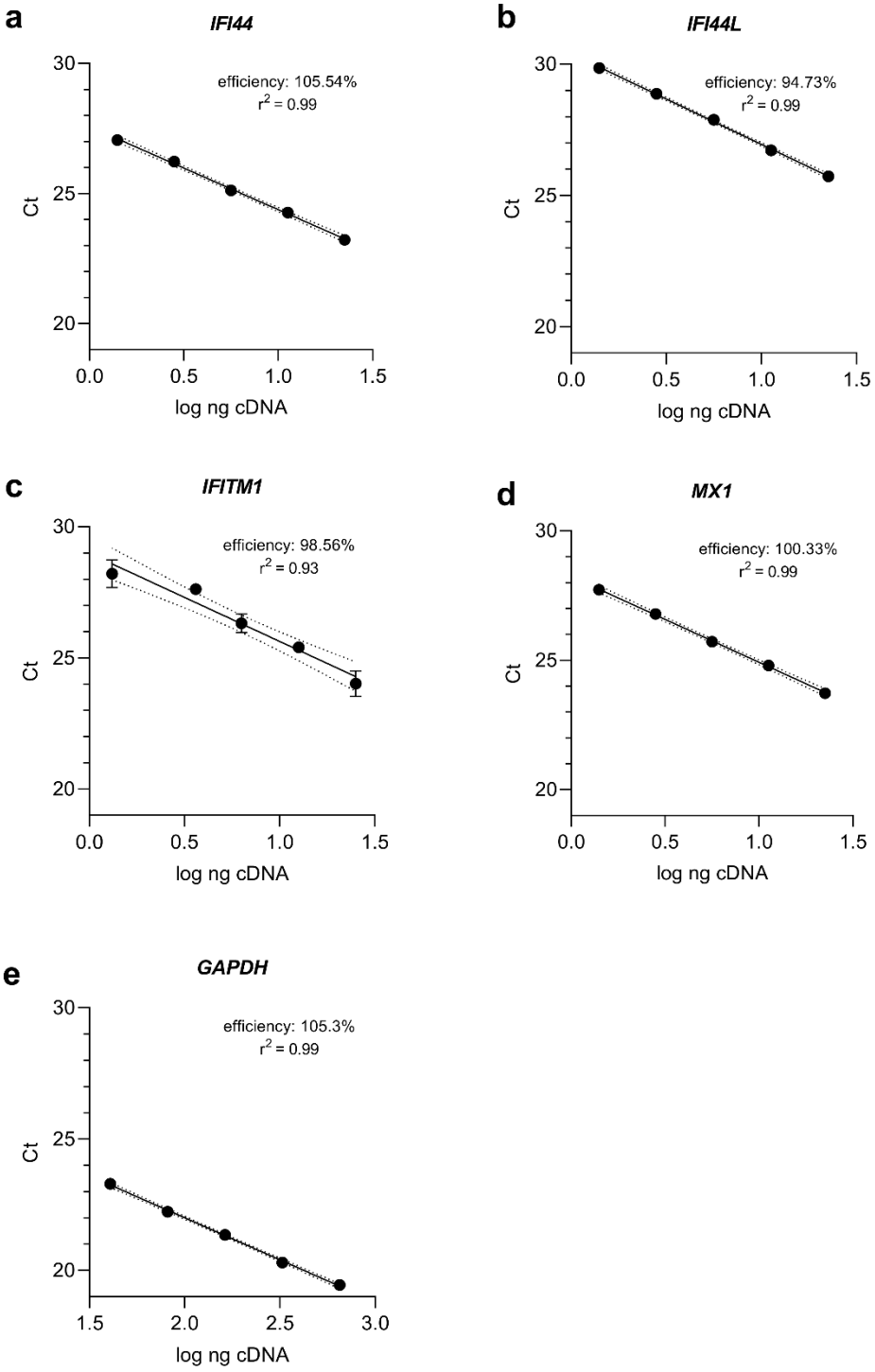

Figure 2.1. Efficiency of human qPCR primer pairs. (a) *IFI44,* **(b)** *IFI44L*, **(c)** *IFITM1*, **(d)** *MX1,* and **(e)** *GAPDH* primer pairs were used to amplify varying concentrations of human cDNA. Points represent the mean +/- SD. Best-fit (solid lines) +/- 95% confidence intervals (dotted lines) were generated by linear regression. Ct = threshold cycle. Efficiency of the reaction was calculated by:

$$Efficiency\ (\%) = \left(10^{\frac{-1}{Slope}} - 1\right) \times 100$$

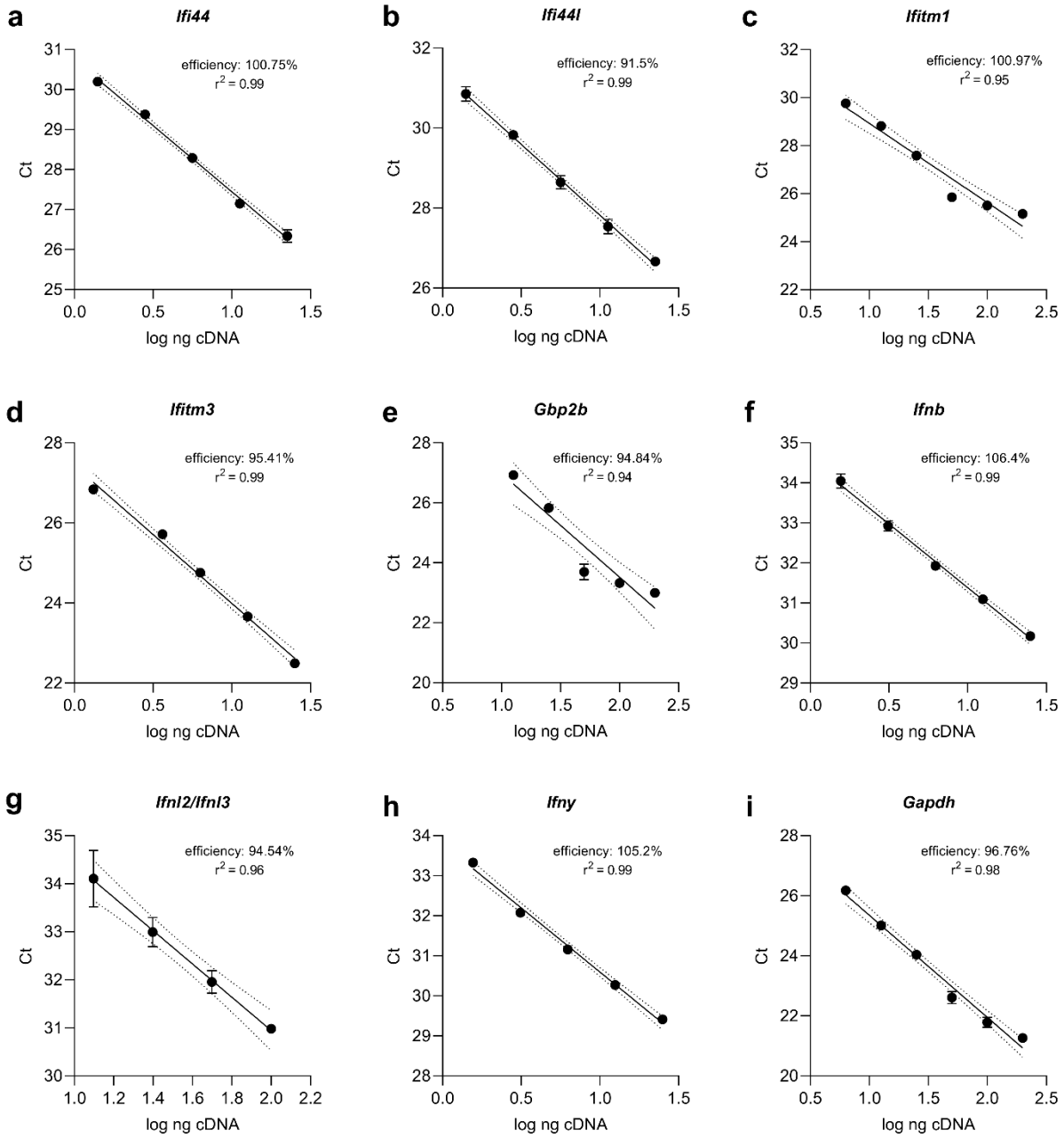

Figure 2.2. Efficiency of murine qPCR primer pairs. (a) *Ifi44,* **(b)** *Ifi44l*, **(c)** *Ifitm1*, **(d)** *Ifitm3*, **(e)** *Gbp2b*, **(f)** *Ifnβ*, **(g)** *Ifnλ2/Ifnλ3,* **(h)** *Ifnγ*, and **(i)** *Gapdh* primer pairs were used to amplify varying concentrations of murine cDNA. Points represent the mean +/- SD. Best-fit (solid lines) +/- 95% confidence intervals (dotted lines) were generated by linear regression. Ct = threshold cycle. Efficiency of the reaction was calculated by: $Efficiency\ (\%) = \left(10^{\frac{-1}{Slope}} - 1\right) \times 100$

2.6.3 CellTiter 96® Aqueous One Solution Assay Optimisation

To determine the most appropriate incubation period of CellTiter reagent with proliferating cell cultures, equal number of viable A549 cells were incubated with CellTiter reagent for 1-4 hours at 37ºC in a humidified 5% CO_2 incubator. The OD_{490} readings had a linear relationship over time (r^2 = 0.81, Fig 2.3a). Going forward, cultures were incubated for 4 hours with CellTiter reagent as this gave the most consistent data with the least deviation among replicate samples. Next, to test the range of cell densities that could be accurately assayed with CellTiter, $2.5x10^3$-$2x10^4$ A549 cells were seeded into wells of a 96-well plate in triplicate 24 hours prior to the addition of CellTiter reagent. OD_{420} readings showed that increasing numbers of cells was associated with an equivalent increase in OD_{490} (r^2 = 0.99, Fig 2.3b). For future assays $5x10^3$ cells per well were seeded and proliferation assayed over 48 hours in order to remain in the linear range of the assay.

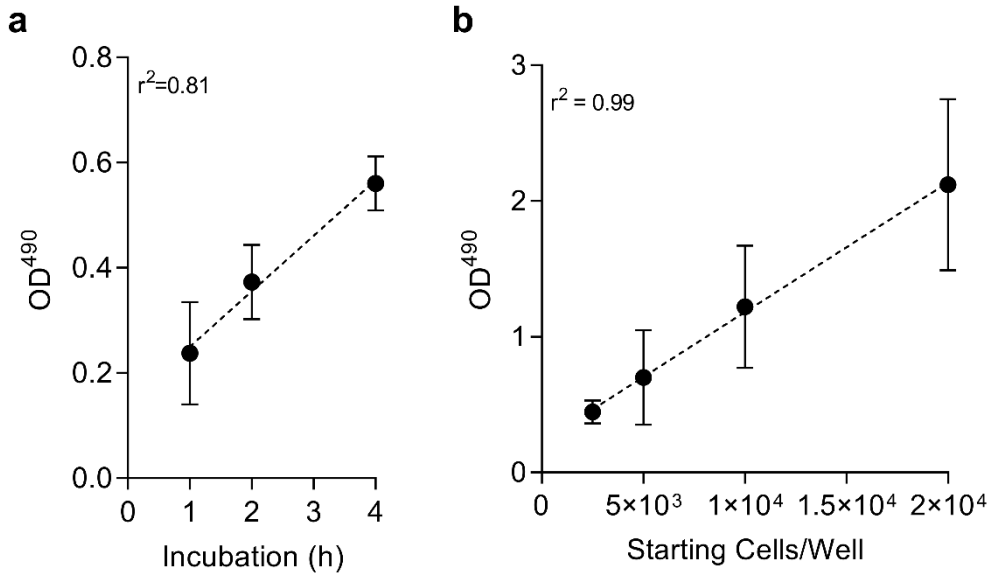

Figure 2.3. Optimisation of MTS assay for quantifying viable cell number. (a) Equal numbers of viable A549 cells were seeded and cultured for 6 hours prior to addition of MTS reagent for 1-4 hours. **(b)** $1x10^3$ to $2x10^4$ A549 cells were plated and allowed to proliferate for 24 hours prior to addition of MTS reagent for 4 hours. N=1. Points at the mean +/- SD. Dotted lines represent curves fitted with linear regression (Prism).

2.7 Data Analysis

2.7.1 GraphPad Prism 8

Data were analysed using GraphPad Prism 8 software (GraphPad) and statistical tests are described in the respective figure legends. For single variable analysis data were assumed to be normally distributed. When comparing two groups, statistics were generated by either unpaired t-test or ratio paired t-test when comparing multiple independent experiments assessing level of viral infection. When comparing more than two groups, statistics were generated by one-way ANOVA with Bonferonni's correction for multiple comparison, or ratio paired t-test. For multivariate analysis data

were assumed to be in a normal distribution and statistics were generated by two-way ANOVA. Linear regression was used to plot best-fit curves.

2.7.2 FlowJo

FCS file data was exported from BD FACSDiva™ (Bd biosciences) and analysed using FlowJo 10 software (Treestar). Majority cell populations were gated to exclude cell debris prior to double exclusion. Remaining events were then assessed for intracellular fluorescence or surface staining.

2.7.3 PCR Relative Quantification

To determine relative changes in gene expression cycle threshold (Ct) values were analysed by the ΔΔCt method [268]. GAPDH was used as a calibrator and all samples were run in duplicate. Mean Ct values of the calibrator gene were subtracted from mean Ct values of the target gene to give ΔCt. $2^{-\Delta Ct}$ was used to determine gene expression relative to that of the calibrator gene.

For analysis of fold change compared to a negative control, the mean ΔCt value of a control was then subtracted from the mean ΔCt value of an experimental group to give the ΔΔCt value. $2^{-\Delta\Delta Ct}$ = fold change in gene expression. To test statistical significance, mean ΔCt values were compared. Standard deviation (SD) was calculated from the standard deviation of the target (S_1) and calibrator Ct values (S_2) [281]:

$$SD = \sqrt{(s_1^2 + s_2^2)}^{1/2}$$

Chapter 3

Results

Interferon-Induced Transmembrane Protein 1 Restriction of Respiratory Syncytial Virus is Dependent Upon Cell Surface Localisation.

3 Interferon-Induced Transmembrane Protein 1 Restriction of Respiratory Syncytial Virus is Dependent Upon Cell Surface Localisation.

The data presented in this chapter contributed significantly to the following publication:

Interferon-induced Transmembrane Protein 1 restricts replication of virus that enter cells via the plasma membrane.

Sarah E. Smith, David C. Busse, Špela Binter, Stuart Weston, Carmen Diaz Soria, Brigitta M. Laksono, Simon Clare, Stefan Van Nieuwkoop, Bernadette G. Van den Hoogen, Mathew Clement, Morgan Marsden, Ian R. Humphreys, Mark Marsh, Rik L. de Swart, Rachel S. Wash, John S. Tregoning, Paul Kellam.

3.1 Chapter Abstract

Studies by Smith *et al* have suggested that IFITM1 antiviral activity is dependent on plasma membrane localisation, and additional *in vitro* studies have suggested IFITM1 restricts RSV infection. RSV entry occurs via direct fusion with the plasma membrane or in some cases hemifusion with the plasma membrane followed by macropinocytosis or clathrin-dependent endocytosis. Both mechanisms rely on interaction of the viral fusion protein with the cell surface membrane. As such, this chapter hypothesises that IFITM1 restriction of RSV is dependent on cell surface localisation. This study demonstrates that IFITM1 expression is capable of restricting RSV infection, and that loss of cell surface expression results in a loss of antiviral activity. Mutations in the conserved intracellular loop domain of IFITM1 are identified that perturb cell surface localisation and antiviral activity.

To date, studies of *Ifitm1 in vivo* have been limited to *IfitmDel*$^{-/-}$ mice lacking multiple *Ifitm* genes including *Ifitm1* and *Ifitm3*. To address the hypothesis that *Ifitm1* is a relevant ISG during RSV infection *in vivo* this chapter uses a monogenic *Ifitm1*$^{-/-}$ knockout mouse model. *Ifitm1*$^{-/-}$ display enhanced disease during RSV infection with increased weight loss, elevated viral load, and increased production of pro-inflammatory cytokines.

3.2 Results

3.2.1 RSV Infection is Restricted by IFN Treatment *in Vitro*

To investigate the responsiveness of different epithelial cell lines to IFN-I stimulation, and to identify an appropriate dose to induce an effective anti-RSV response, I treated A549, HEp-2, and HEK293T cells with 0-2000 IU mL^{-1} IFNα2a, 16 hours prior to RSV infection. Infection was assessed after 24 hours by qPCR. RSV L gene copy number was significantly reduced by all concentrations of IFN-I in each cell line when infected at m.o.i. 0.1 (Fig 3.1a-c). It is important to note that this qPCR is able to amplify both genomic cDNA (complementary to the forward primer) and antigenome/transcript cDNA species (complementary to the reverse primer) due to the use of random primers during the reverse transcription reaction. As such, this is not a measure of genome copies, transcription, or replication alone but a general measure of viral RNA. At a higher m.o.i. of 1 there was only significant reduction at 500-2000 IU mL^{-1} IFNα2a in HEp-2 (Fig 3.1d) and 293T cells (Fig 3.1e). These concentrations also reduced L gene copies in A549 cells infected at m.o.i. 1 but this trend was not statistically significant (Fig 3.1f).

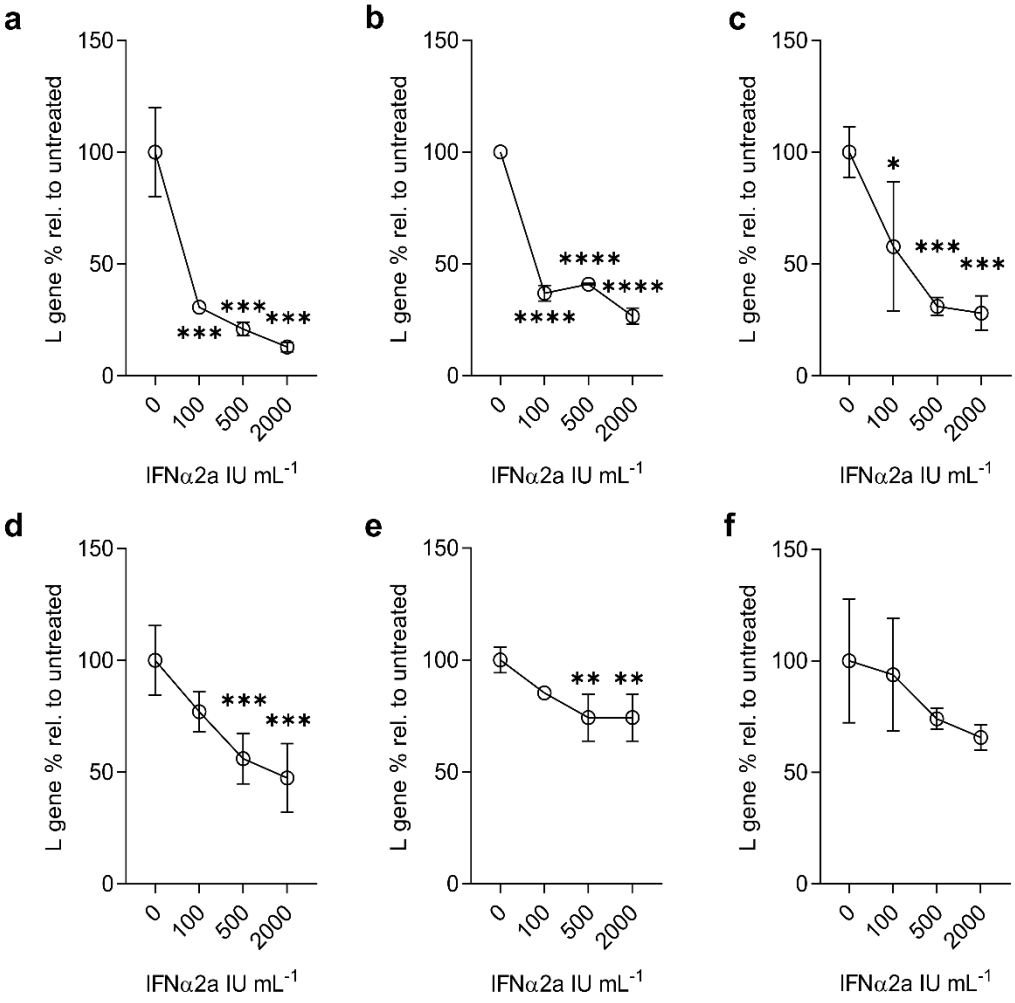

Figure 3.1. IFN treatment restricts RSV infection in vitro. (a) HEp-2, **(b)** HEk293T/17, and **(c)** A549 cells were seeded into 24-well plates and treated with doses of IFNα2a 16 hours prior to infection with RSV A2 at m.o.i. 0.1. L gene relative to untreated controls 24 hours after infection. N=3. **(d)** HEp-2, **(e)** HEk293T/17, and **(f)** A549 cells were seeded into 24-well plates and treated with doses of IFNα2α 16 hours prior to infection with RSV A2 at m.o.i. 1. L gene relative to untreated controls 24 hours after infection. N=3. Points at the mean +/- SD. Significance to untreated controls by ANOVA, * P <0.05, ** P < 0.01, *** P < 0.001, **** P < 0.0001.

3.2.2 IFITM1 is Upregulated in Response to RSV and IFN-l in Epithelial Cells

IFITM1 mRNA levels in response to IFN treatment (Fig 3.2a) or RSV infection (Fig 3.2b) were measured in A549 cells to verify that IFITM1 is responsive to either stimuli as previously reported. The use of a lung-derived epithelial cell line is important as this is the majority cell type at the site of RSV infection. IFNα2a treatment and RSV infection (m.o.i. 0.1) induced elevated expression of IFITM1 mRNA within 6 hours. Peak induction of IFITM1 expression by IFN treatment was seen after 12 hours. This level of expression was subsequently maintained for the next 12 hours. RSV infection led to increased *IFITM1* expression after 6 hours which increased further over the next 18 hours. These data demonstrate that IFITM1 is induced early during RSV infection and peaks within the first 24 hours.

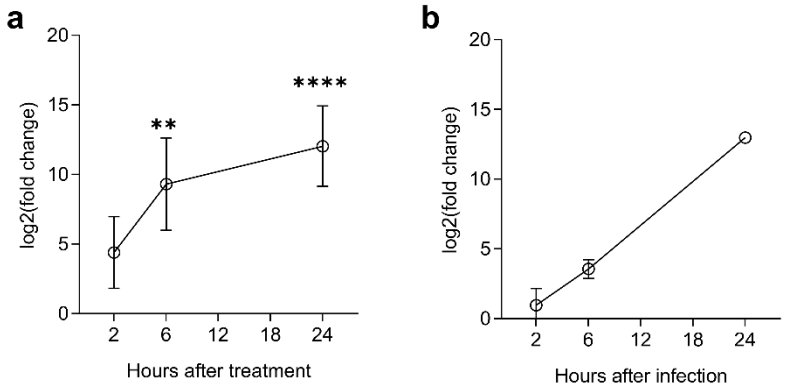

Figure 3.2. Induction of IFITM1 expression by IFN-l and RSV. A549 cells were **(a)** treated with 500 IU mL^{-1} IFNα2a for 2-24 hours, N=3, or **(b)** infected with RSV A2 (m.o.i. 0.1) for 2-24 hours, N=2. IFITM1 expression assessed by qPCR and relative quantification using GAPDH as the calibrator. Mean +/- SD. Significance to untreated controls at each time point by 2-way ANOVA. * P < 0.05, ** P < 0.01, *** P < 0.001, **** P < 0.0001.

3.2.3 IFITM1 is Constitutively Expressed in the Mouse Lung

The IFITM family have been reported to be constitutively expressed in several tissue types, commonly in barrier epithelial cells. To investigate this, tissue was collected from uninfected mice. *Ifitm1* RNA was detected in lung, liver, and spleen tissue from BALB/c mice suggesting constitutive expression (Fig 3.3a-b). Expression of *Ifitm1* mRNA was significantly induced by RSV infection after 24 hours (Fig 3.3a).

Expression levels were highest in the lung and lowest in the liver. For lung tissue, expression was found to be as high as 0.1 of *Gapdh* levels (Fig 3.3a-b). These data were normalised to expression of *Gapdh* which may influence comparison between tissue types if *Gapdh* is expressed at a lower or higher level. Unfortunately, unequal levels of RNA were converted into cDNA for qPCR analysis and so I cannot confirm whether there are differences in *Gapdh* levels between the different tissue types. To improve this analysis, it would be interesting to normalise the data to a different calibrator such as a different ISG or *IFITM* transcript, or multiple genes commonly used as calibrators such as actin or tubulin. This analysis is also limited in that it looks at tissue-wide expression levels and is unable to give cell type-specific information.

To attempt to observe tissue-specific induction kinetics I removed lung, liver, and spleen tissue from a single BALB/c mice and incubated weight adjusted tissue segments in D10 medium with or without 1000 IU mL^{-1} IFNα2a (Fig 3.3c). After 24 hours, levels of *Ifitm1* RNA were quantified relative to *Gapdh*. There was no observable increase in *Ifitm1* RNA in any tissue type, suggesting that either the dose of IFN was too low or the time for tissue perfusion was too short to observe *ex vivo* effects of IFN stimulation.

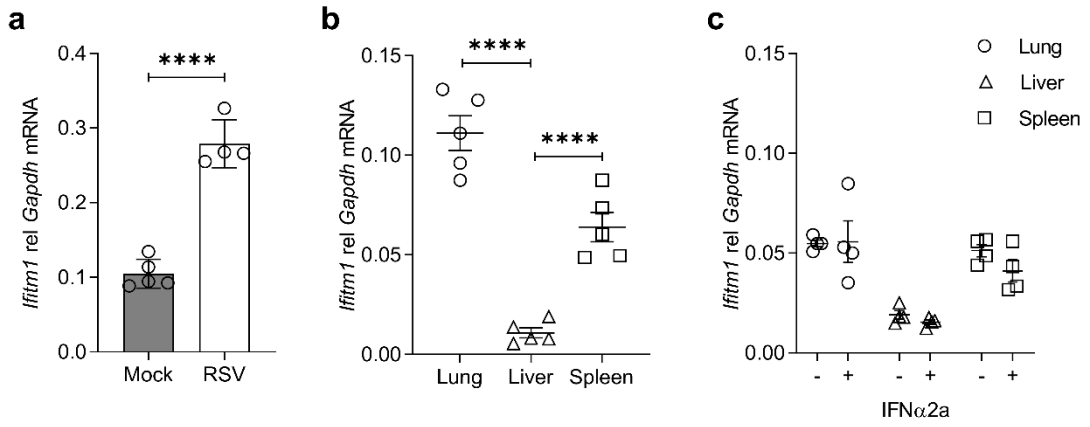

Figure 3.3. *Ifitm1* is constitutively expressed in the mouse lung. (a) *Ifitm1* expression relative to *Gapdh* in whole lung tissue of RSV infected mice or PBS-treated control mice (mock) 24 hours after infection. **(b)** *Ifitm1* expression relative to *Gapdh* in lung, liver, or spleen tissue from BALB/c mice infected with RSV for 24 hours. **(c)** *Ifitm1* expression relative to *Gapdh* in lung, liver, or spleen tissue extracted from a single BALB/c mice and treated *ex vivo* with 1000 IU mL^{-1} IFNα2a for 24 hours. Points represent individual animals or tissue samples of equal weight (**c**)**.** Line or bar at the mean +/- SEM. Significance by ANOVA, **** $P < 0.0001$.

3.2.4 IFITM Induction is Comparable Between Adult and Neonatal Mice

RSV infection is especially common in infants and the elderly [4]. The neonatal and infant immune response is thought to be different to that of adults with altered induction of key cytokines and subsequent dysregulated adaptive responses including Th2/17 polarisation of T cell responses [28, 282].

Neonatal mice have reduced IFN-I responses upon primary RSV infection, associated with reduced expression of IFNβ and IFNα from plasmacytoid dendritic cells [128], likely a result of defective IRF7 signalling [283]. To determine whether *Ifitm* genes are differentially regulated during neonatal infection we infected 7-day old neonatal mice or 10-week old adult mice (BALB/c) with RSV.

Neonatal mice continue to gain weight after RSV infection (Fig 3.4a), unlike adults (Fig 3.4b). Upon secondary infection as adults, mice infected as neonates demonstrated

increased weight loss relative to adults infected for the first time (Fig 3.4b). In addition, there was a trend of increased lung (Fig 3.4c) and BAL cell counts (Fig 3.4d), suggestive of increased inflammation. After primary infection, L gene copies were detected in both adults and neonates (2/3 neonates), although the level was lower in neonatal mice (Fig 3.4e). This may be the result of the weight adjusted dose. However, the upregulation of *Ifitm1* (Fig 3.4f) and *Ifitm3* (Fig 3.4g) expression was comparable between infected neonates and adults, even with a detectable decrease in IFNβ levels (Fig 3.4h-i). IFN-III mRNA was lower in neonatal mice following infection but were undetectable in PBS-treated control animals (Fig 3.4j).

The upregulation of *Gbp2b* was significantly reduced in neonates (Fig 3.4k). This gene is thought to be predominantly induced by IFN-II, although we have observed induction occurs following IFN-I treatment in A549 cells. These data suggest that ISG responses are dysregulated in neonates during primary RSV infection but *IFITM* responses are maintained.

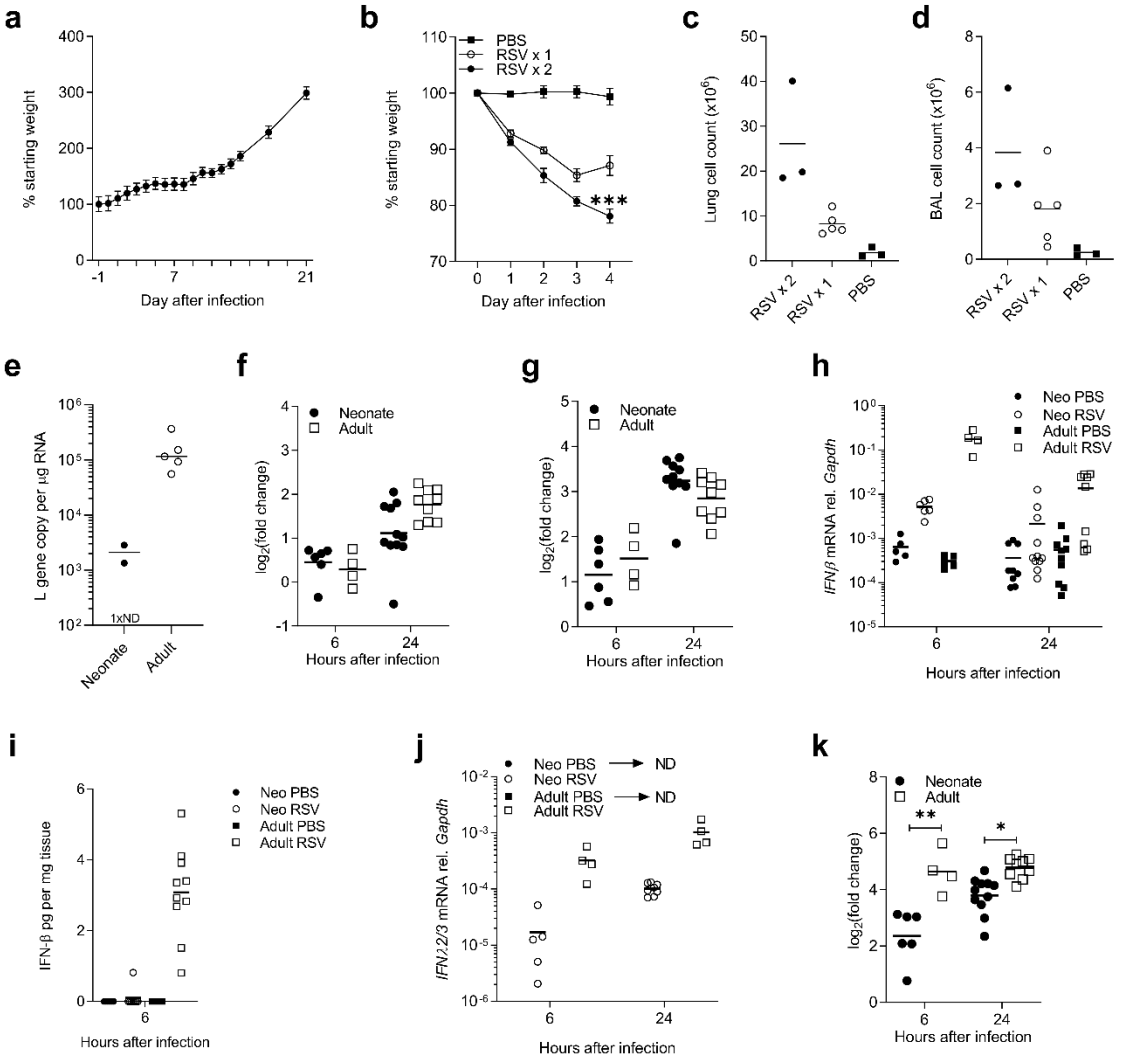

Figure 3.4. *Ifitm1* and *Ifitm3* induction during RSV infection is comparable between neonatal mice and adult mice. Adult mice were infected with 4x10^5 PFU RSV A2. Neonatal mice were given a weight-adjusted dose. **(a)** Weight change in infected neonates. N=3. **(b)** Mice challenged with RSV at 7 days of age were re-infected after 4 weeks (RSV x 2, N=6). Age-matched controls were infected with RSV (RSV x 1, N=5) or administered PBS only (N=3). Weight change over 4 days of infection. **(c)** Cell counts in lung or **(d)** BALF after 4 days. **(e)** L gene copy number in lung tissue 24 hours after RSV infection. **(f)** *Ifitm1* and **(g)** *Ifitm3* expression relative to PBS-treated controls in neonate or adult mice 6-24 hours after infection. **(h)** *IFN-β* expression 6-24 hours after infection. **(i)** IFN-β protein in lung tissue 6 hours after infection. **(j)** *IFN-λ2/3* expression 6-24 hours after infection. **(k)** *GBP2b* expression relative to PBS-treated controls 6-24 hours after infection. **a-b** points represent the mean +/- SEM, 1 independent experiment. **c-k** points represent individual animals, line at the mean, 2 independent experiments. Significance by ANOVA, * P <0.05, ** P < 0.01. *** P <0.001. nd = not detected.

3.2.5 Optimisation of Transfection for Overexpression Studies *in Vitro*

To assay the impact of IFITM1 and other ISGs on RSV infection I first aimed to maximise the efficiency of plasmid DNA transfection into HEp-2 cells as this is a faster protocol than the development of stable cell lines and has been used previously to demonstrate antiviral capability of some ISGs [208]. Increasing the volume of lipofectamine 3000 reagent in the transfection mix increased the transfection efficiency in a dose-dependent manner, as measured by microscopic analysis of tdTomato positive cells 24 hours after transfection (Fig 3.5). For future transfections in 24-well plates I used 1.5 µL of reagent per well. For different sizes of culture plates or dishes this volume was scaled appropriately.

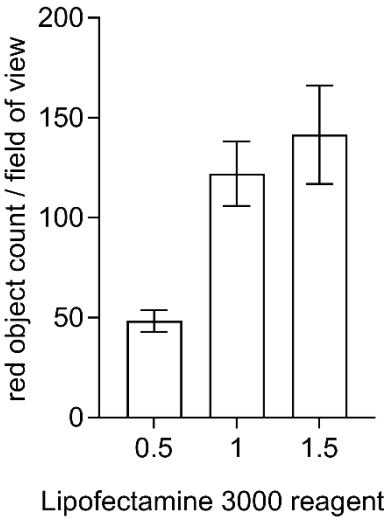

Figure 3.5. Transfection optimisation. HEp-2 cells were transfected with 1 µg of plasmid DNA expressing the red fluorescent protein TDTomato with increasing volumes of Lipofectamine 3000 reagent per well (µL). 24 hours after infection, transfection was assessed by counting the number of RFP^+ cells in at least 3 fields of view using a fluorescent microscope. N=1. Bar at the mean +/- SD.

3.2.6 Overexpression of IFITM1 Efficiently Restricts RSV Infection

Previous studies have demonstrated restriction of RSV, both in terms of the number of infected cells and the levels of viral RNA, by transient overexpression of IFITM1, IFITM2, and IFITM3 [208]. Prior to the development of the stable cell lines used in the remainder of this chapter I assessed the impact of IFITM1 overexpression on RSV infection by transfecting HEK293T/17 or HEp-2 cells with a construct expressing IFITM1 (pCMV-IFITM-HA) or an empty vector (pcDNA3.1). The proportion of rgRSV infected cells (GFP^+) was reduced following IFITM1 transfection (Fig 3.6a). In addition, we noted a significant reduction in luciferase activity following RSV-Luc infection (Fig 3.6b). Finally, WT RSV A2 virus was restricted in transfected HEp-2 cells, demonstrated by a reduction in virus titre in the cell supernatant (Fig 3.6c).

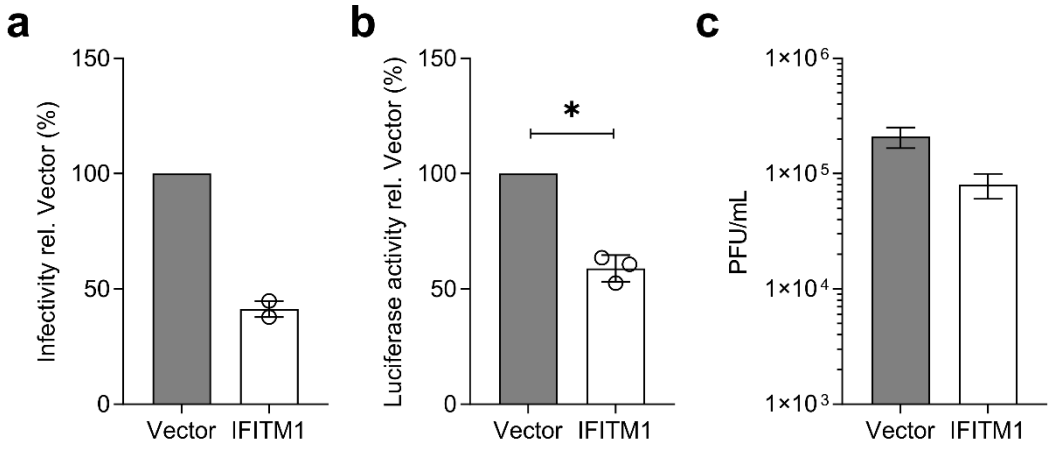

Figure 3.6. Overexpression of IFITM1 restricts RSV infection. (a) HEK293T/17 cells were transfected with pCMV-IFITM1-HA (IFITM1) or pcDNA3.1 (Vector) and infected with rgRSV (m.o.i. 1) for 24 hours (N=2). Infectivity assessed by flow cytometry relative to Vector-transfected. **(b)** HEK293T/17 cells were transfected as for **a** and infected with RSV-luc for 24 hours (N=3). Luciferase activity relative to Vector-transfected. **(c)** HEp-2 were transfected as for **a** and infected RSV-A2 for 24 hours (N=2). Viral titre in cell supernatant. Points represent individual experiments with a bar at the mean +/- SD. Significance by ratio paired t-test prior to data transformation. * P <0.05, ** P <0.01.

Transfection of empty control plasmid DNA was able to efficiently restrict RSV infection. This was identified as a key issue with the assay as it could reduce the dynamic range and the ability to detect the antiviral activity of mild to moderately antiviral ISGs. As part of improving this transient overexpression assay, I developed pcDNA3.1 derived constructs that encoded our ISG of interest IFITM1 and mScarlet from the same promoter using an Encephalomyocarditis virus (ECMV) internal ribosome entry site (IRES). This would allow for single construct transfection and accurate analysis of transfected cells that were actively transcribing RNA of our transfected ISG. This construct was able to express mScarlet either with or without an ISG sequence in the initial open reading frame (Fig 3.7a). Transfection of either pcDNA3.1 or pcDNA3.1-mScarlet reduced RSV infectivity in a dose-dependent manner in both A549 (Fig 3.7b, Fig 3.7d) and HEp-2 (Fig 3.7c, Fig 3.7e) cells. To try and identify how plasmid transfection was restricting RSV infection I assessed ISG induction after transfection. Interestingly, transfection of empty pcDNA3.1-mScarlet did not induce increased expression of *IFITM1*, or a range of ISGs tested (Fig 3.7d). However, as expected the transfection of pcDNA3.1-IFITM1-mScarlet was associated with a large increase in detectable *IFITM1* transcript. This may suggest that the restriction of RSV by plasmid transfection is not a result of IFN induction and ISG expression.

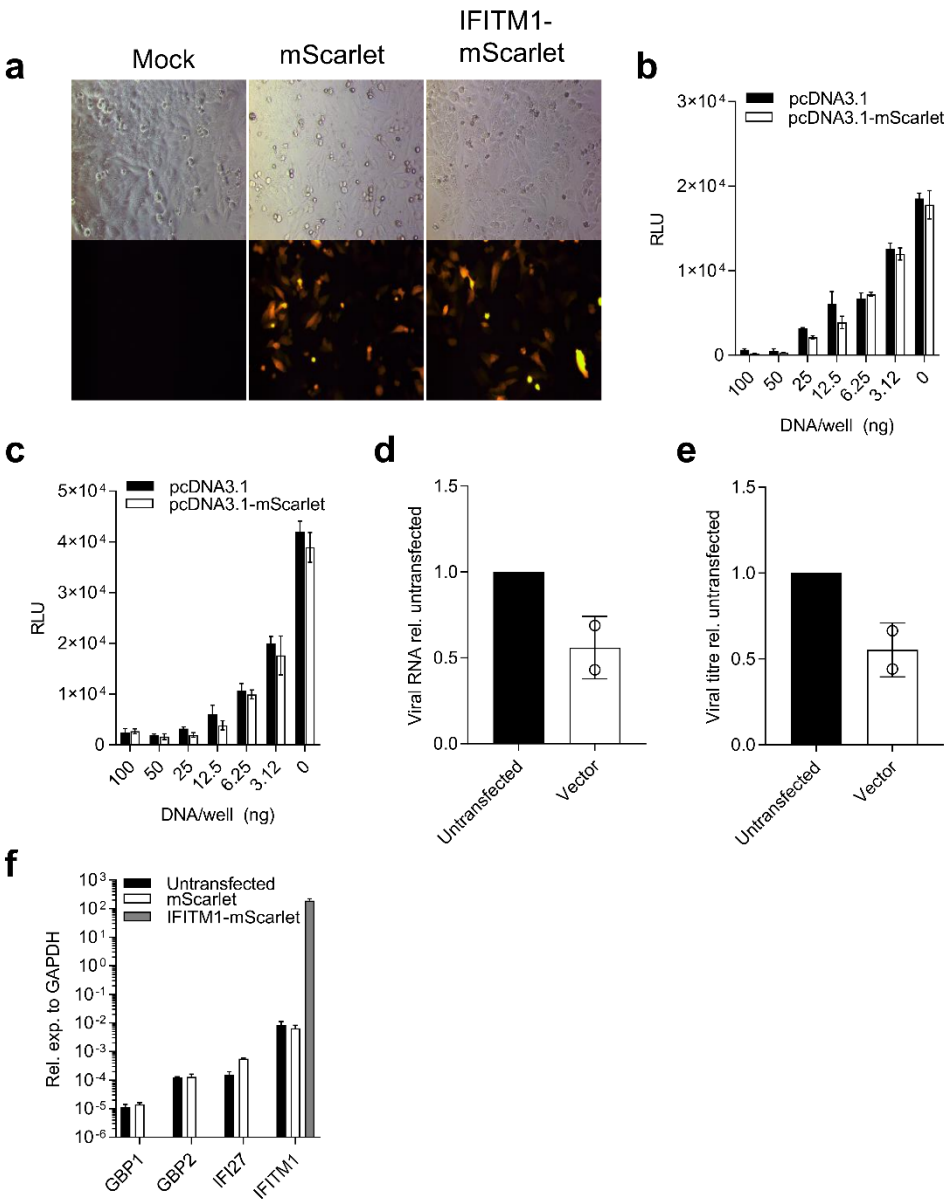

Figure 3.7. RSV infection is restricted by pcDNA3.1 transfection. (a) Fluorescent microscopy of HEp-2 cells transfected with pcDNA3.1-mScarlet, pcDNA3.1-IFITM1-mScarlet, or mock transfected. Imaged 24 hours after transfection. N=1. **(b)** A549 or **(c)** HEp-2 cells were transfected with up to 100 ng of either pcDNA3.1 or pcDNA3.1-mScarlet and infected with RSV-Luc after 24 hours. Infectivity was assessed by quantifying luciferase activity after a further 24 hours. RLU = relative luciferase units. N=1. **(d)** A549 cells were infected with RSV A2 (m.o.i. 1) 24 hours after transfection with 0.5 µg pcDNA3.1-mScarlet (vector). Viral RNA 24 hours after infection, relative to untransfected controls. N=2. **(e)** HEp-2 cells were treated as for **d** and viral titre in cell supernatant assessed after 48 hours, relative to untransfected controls. N=2. **(f)** Expression of ISGs GBP1, GBP2, IFI27, and IFITM1 mRNA relative to *GAPDH* in HEK293T/17 cells 24 hours after transfection with pcDNA3.1-mScarlet (white bars) or mock transfection (black bars). IFITM1 expression in cells transfected with pcDNA3.1-IFITM1-mScarlet is shown in grey. N=1. Bars at the mean +/- SD.

This observation suggested that the use of transient transfection was not suitable for assaying a range of ISGs as it could hinder the observation of antiviral effects of mild or moderately active ISGs. As such, the development of stable cell lines for these studies became a priority as these cells constitutively express the ISG of interest and there is no transient activation of immune signalling prior to infection. Stably transduced A549 cell lines were developed by Dr. Sarah Smith and Dr. Rachel Wash (Wellcome Trust Sanger Institute) by lentiviral transduction and puromycin selection [207]. IFITM1 sequences were derived from NP_003623.3 (NCBI) and a C-terminal haemagglutinin (HA) tag (YPYDVPDYA) was inserted to allow localisation studies (full sequence deposited in GenBank, reference MK288009). Expression of each wild-type or mutant IFITM1 in stably selected A549 cells was confirmed by Immunofluorescence and Western blotting.

3.2.7 The C-Terminus of IFITM1 is Detectable on the Cell Surface

As discussed previously, there are multiple suggested models of IFITM1 topology. Following studies in both A549 and Vero cells expressing IFITM1, Weston *et al* proposed that the C-terminus, and not the N-terminus, is detectable on the cell surface. To confirm the cell surface localisation of IFITM1, I corroborated the extracellular nature of the IFITM1 C-terminus by flow cytometry where the cells were not subjected to membrane permeabilising conditions. Cells transduced with the empty lentiviral vector were used as a negative control. IFITM1 transduced cells were stained under these conditions, demonstrating the accessibility of the C-terminal domain of IFITM1 on the cell surface (Fig 3.8). This approach is unable to determine if there are any conformations of IFITM1 in the plasma membrane that have an intracellular C-terminal domain and cannot differentiate between IFITM1 negative cells and those cells expressing IFITM1 intracellularly only.

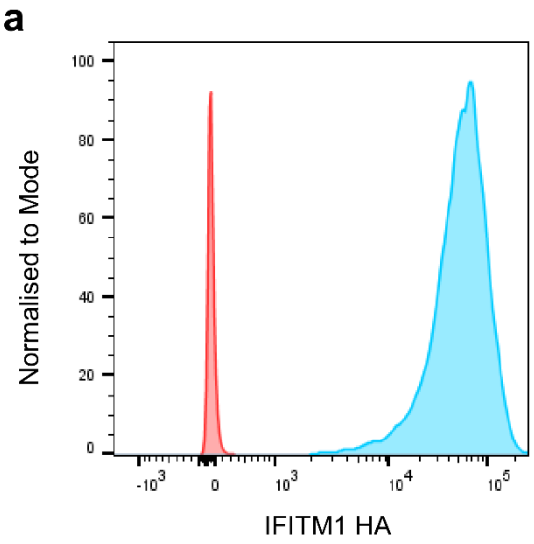

Figure 3.8. The C-terminal domain of IFITM1 is expressed on the cell surface. (a) IFITM1 detection on the cell surface of stably transduced A549 cells (blue) or cells transduced with empty vector (red). Cells were stained under non-permeabilising conditions with anti-HA antibody to bind the C-terminal HA tag of the transduced IFITM1.

3.2.8 Mutation of the CIL Domain Impacts IFITM1 Surface Expression

Stably transduced A549 cell lines were generated expressing mutant IFITM1 proteins with blocks of 6 residues in the CIL domain replaced with repeated alanine residues (Cell lines provided by S. Smith and R. Wash) (Fig 3.9a). Smith *et al* observed that the cellular localisation of these IFITM1 mutant proteins was altered [207]. These cell lines no longer displayed diffuse expression by immunofluorescence, instead expression of IFITM1 CIL mutants appears to be distinctly perinuclear, suggesting that these cells no longer express IFITM1 on the cell surface (Fig 3.9b). However, mutant IFITM1 #76 maintained a diffuse expression pattern, although there is a noticeable increase in a perinuclear compartment (Fig 3.9b). Three of the four (#63, #69, and #83) tested cell lines expressing mutant protein did not have detectable IFITM1 on the surface of the majority of cells (Fig 3.9c). The fourth cell line #76, while still maintaining detectable

IFITM1 on >75% of cells, had reduced quantities of IFITM1 on the cell surface relative to cells expressing wild-type IFITM1 as observed by the change in distribution of fluorescence intensity (Fig 3.9d). These observations were in concordance with the immunofluorescence images produced by S. Smith.

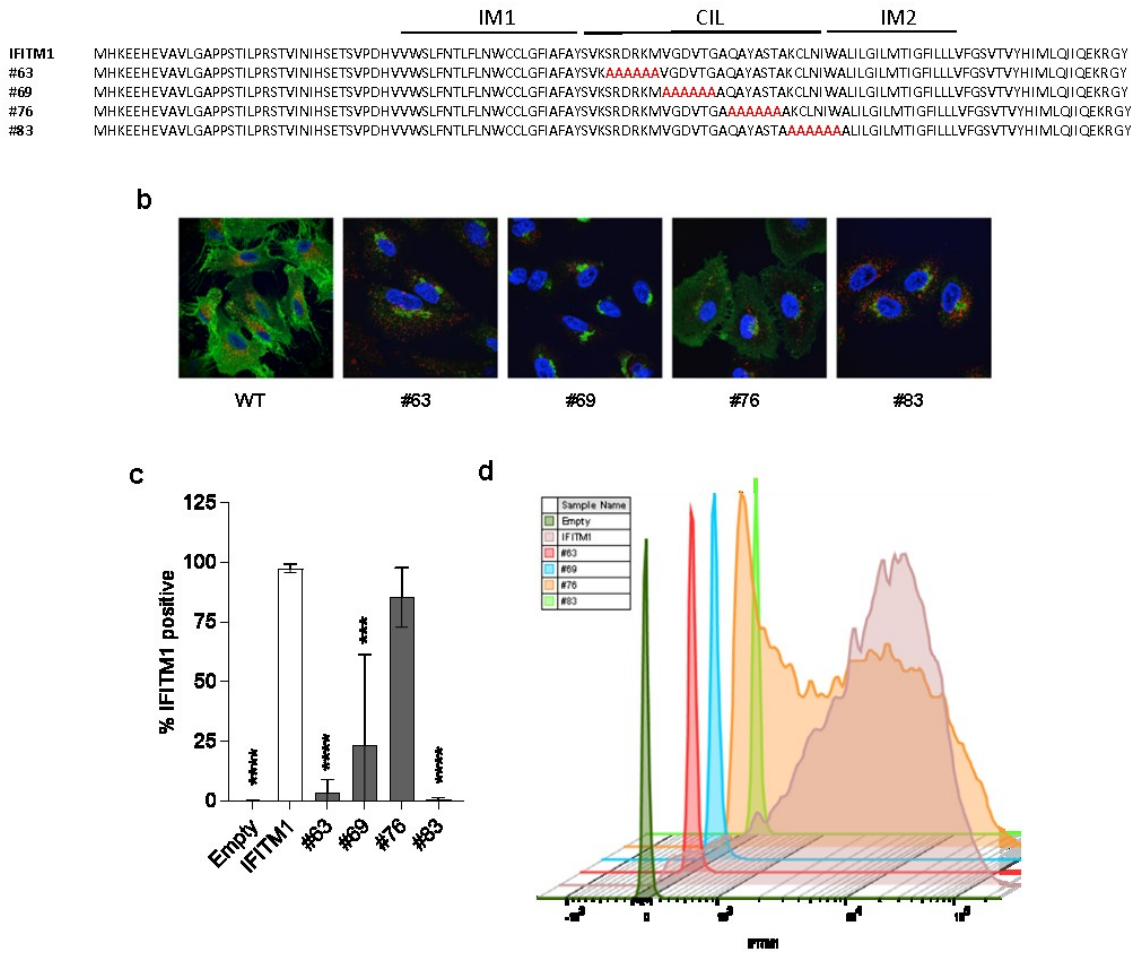

Figure 3.9. IFITM1 CIL mutants display reduced cell surface expression. (a) Amino acid sequence of IFITM1 WT and alanine scanning mutants with CIL mutations. The name of each mutant denotes the first residue replaced with an alanine. Regions replaced are highlighted in red. IM = intramembrane domain. CIL = conserved intracellular loop. **(b)** Stably transduced Vero cells expressing IFITM1 WT and CIL mutants. HA-tagged IFITM1 proteins shown in green, LAMP1 in red, and DAPI in blue. Microscopy by S. Smith adapted from Smith *et al* 2019. **(c)** Percentage of IFITM1 positive single cells determined by flow cytometry with stable expression of IFITM1 WT or IFITM1 CIL mutants. Significance relative to A549-IFITM1 WT by ANOVA. Mean +/- SD, N=3. **(d)** Representative IFITM1 (HA) histogram of A549 stably transduced cells expressing WT or CIL mutant IFITM1. N=3. * $P < 0.05$, ** $P < 0.01$, *** $P < 0.001$, **** $P < 0.0001$.

3.2.9 CIL Mutants Have Altered Ability to Restrict RSV Infection

Infectivity of cells expressing mutant IFITM1 was tested using rgRSV. Stably transduced cells expressing WT IFITM1 are capable of restricting RSV infection as observable by flow cytometry following rgRSV infection (Fig 3.10a). Cell lines expressing mutant IFITM1 however each displayed a significant loss of restriction relative to cells expressing WT IFITM1 (Fig 3.10a). Interestingly, #76 still maintained a mild level of restriction against RSV. These data suggest plasma membrane localisation is essential for IFITM1 activity during RSV infection.

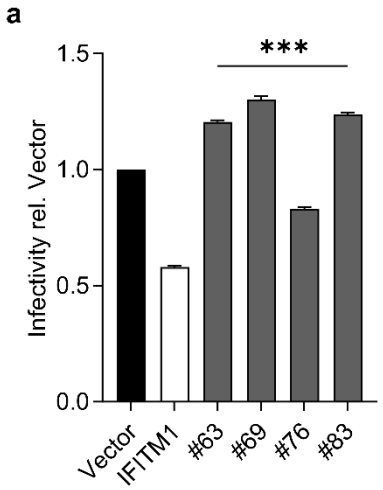

Figure 3.10. IFITM1 CIL mutants exhibit reduced restriction of RSV infection. (a) Stably transduced A549 cells were infected with rgRSV (m.o.i. 0.1) and infectivity analysed by flow cytometry after 24 hours. Infected (GFP+) cells relative to Vector-transduced control. Mean +/- SD, N=3. Significance to A549-IFITM WT by ANOVA. *** P < 0.001.

3.2.10 Disease severity is enhanced in a murine *Ifitm1*$^{-/-}$ model of RSV infection

To investigate the impact of IFITM1 in RSV infection *in vivo* we assessed infection in C57BL/6N *Ifitm1*$^{-/-}$ mice relative to WT controls. One of the two independent infections

was completed and presented as part of a thesis for the degree of Master of Research (Busse D, unpublished). It is included here for completion.

Previous studies have only characterised infection in *Ifitm3*$^{-/-}$ or *IfitmDel*$^{-/-}$ mice that lack all the *Ifitm* genes. *Ifitm1*$^{-/-}$ mice were phenotypically normal as assessed by the Wellcome Trust murine phenotyping pipelines. *IfitmDel*$^{-/-}$ and *Ifitm3*$^{-/-}$ mice also have no reported developmental defects or apparent phenotype [284]. *Ifitm1*$^{-/-}$ mice had significantly elevated weight loss 7 days after infection (3.11a), generally the peak of weight loss before recovery begins. Viral load is highest at day 4 of infection and there were increased levels of RSV L gene in lung tissue of the *Ifitm1*$^{-/-}$ mice relative to WT (3.11b). At this point there was also significantly increased cell counts found in the BALF of *Ifitm1*$^{-/-}$ mice relative to WT mice (Fig 3.11c), although there was only a trend towards an increase at day 7. Cell counts in lung tissue were similar between *Ifitm1*$^{-/-}$ mice and WT at day 4 but were significantly increased in the KO mice by day 7 (Fig 3.11d). These data from BALF and lung tissue are suggestive of increased inflammation [285], although we could not determine specific cell types and did not reserve tissue for histological examination. *Ifitm3*$^{-/-}$ mice infected with RSV had elevated numbers of $CD3^+$ cells in lung tissue by day 7 of infection [209]. This is a common feature of severe RSV disease in the murine model of infection and it would have been interesting to determine if the same phenotype is seen in *ifitm1*$^{-/-}$ mice [204]. In addition, *Ifitm3*$^{-/-}$ mice infected with RSV have dysregulated pro-inflammatory cytokine responses, notably in IL-1β and IFN-γ [209]. Here we observed a similar dysregulation and increase in IL-1β (Fig 3.11e) levels and IL-6 (Fig 3.11f). IFN-γ levels were not examined. Overall the phenotype presented by *Ifitm1*$^{-/-}$ mice during RSV infection appears to be one of increased disease severity and corroborates *in vitro* observations that *Ifitm1* plays an antiviral role during RSV infection.

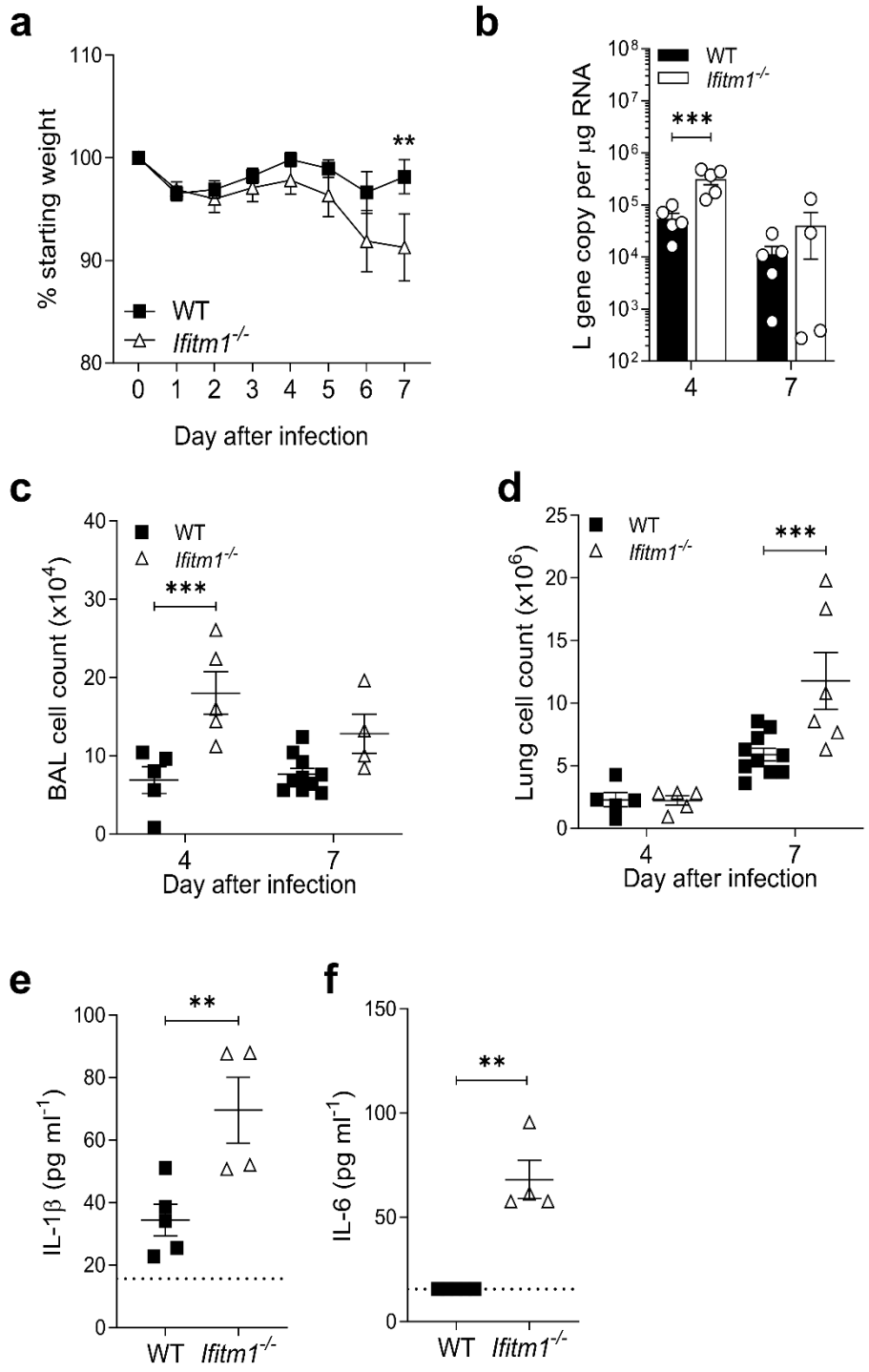

Figure 3.11. RSV infection of Ifitm1$^{-/-}$ mice. (a) Weight loss over 7 days of RSV infection. WT N=15, KO N=10. Points at the mean +/- SEM. **(b)** Viral load in lung tissue. **(c)** BALF and **(d)** lung cell counts 4 and 7 days after infection. **(e)** IL-1β and **(f)** IL-6 protein levels 7 days after infection. Points represent individual animals, with a line/bar at the mean +/- SEM **(b-f)**. Two independent experiments. Significance to WT controls by ANOVA **(a-d)** or unpaired T test **(e-f)**. * P <0.05, ** P < 0.01, *** P < 0.001.

3.3 Chapter Summary

In summary, this chapter focussed on the role of IFITM1 in RSV infection and investigated links between cell surface localisation and efficacy of antiviral activity. Further, this chapter demonstrated that single gene knockout of *Ifitm1* in a mouse model of RSV infection is associated with increased disease severity.

In vitro studies confirmed that IFITM1 can restrict RSV infection in several cell lines. Next, extracellular localisation of the C-terminal domain of IFITM1 was confirmed. IFITM1 CIL mutants had reduced cell surface localisation and reduced antiviral activity. The mutant which retained the highest level of restriction also maintained some level of cell surface expression, further suggesting that this localisation is central to the ability of IFITM1 to restrict RSV infection.

In vivo we observed that *Ifitm1* is constitutively expressed in the murine lung, spleen, and liver. Additionally, *Ifitm1* and *Ifitm3* expression is maintained in neonatal mice compared to adults, even in the context of a dampened IFN-I and IFN-III response. Finally, *Ifitm1*$^{-/-}$ mice display several characteristics of enhanced disease during RSV infection. This included increased weight loss, a higher level of viral RNA at the peak of infection, and a dysregulated pro-inflammatory cytokine response.

Chapter 4

Results

Interferon-Induced Protein 44 Proteins Restrict RSV Infection by Reducing Polymerase Activity.

4 Interferon-Induced Protein 44 Proteins Restrict RSV Infection by Reducing Polymerase Activity.

4.1 Chapter Abstract

This chapter addresses the hypothesis that IFI44 and related protein IFI44L are antiviral in the context of RSV infection.

Prior to starting my project, there were conflicting data on the antiviral activity of IFI44 and IFI44L during RSV infection *in vitro*. Several overexpression systems were developed and tested as part of the project. This resulted in the use of a lentivirus-based overexpression system to produce clonal stably transduced cell lines expressing IFI44 or IFI44L. Here, IFI44 and IFI44L significantly restricted RSV infection at an early point in infection. Loss-of-function assays including siRNA and CRISPR-Cas9-mediated gene knockout were developed and further indicated antiviral activity of IFI44 and IFI44L *in vitro*. Using a minigenome assay system, IFI44 and IFI44L were shown to reduce RSV polymerase activity. Antiviral activity was independent of the G1 region of a predicted GTPase domain in IFI44, suggesting GTP-binding is not required for anti-RSV activity.

Finally, this chapter addresses the *in vivo* relevance of IFI44 activity during RSV infection in a knockout mouse model. *Ifi44*$^{-/-}$ mice display enhanced disease during RSV infection with elevated viral load, reduced IL-1β production, and significantly increased weight loss.

4.2 Results

4.2.1 IFI44 and IFI44L are IFN-I and RSV Inducible in Epithelial and Monocytic Cells *in Vitro*

To demonstrate that IFI44 and IFI44L are upregulated in response to IFN-I and RSV, A549 cells were treated with 500 IU mL^{-1} recombinant IFNα2a protein or infected with RSV A2 (m.o.i. 0.1) for 2-48 hours.

The induction of gene expression was confirmed by qPCR in comparison to mock treated or mock infected cells. *IFI44* expression was upregulated in response to IFN treatment after just 2 hours (Fig 4.1a). Significant induction of *IFI44* expression was observed 6 hours after treatment. IFI44 expression then plateaued after 6 hours until at least 48 hours after treatment. *IFI44L* and *IFI44* expression were comparably induced after 6 hours of IFN treatment, but there was an additional increase only in *IFI44L* expression by 48 hours.

Following RSV infection, induction of both genes increased steadily over time (Fig 4.1b) as viral load increased (Fig 4.1c). Induction following RSV infection was slower than with IFN treatment, as seen previously for *IFITM1* (Fig 3.2).

Having confirmed upregulation of gene expression by observing increased levels of mRNA transcript, IFI44 and IFI44L protein levels were also shown to be increased following IFN-I treatment. A549 cells were treated with 0-1,000 IU mL^{-1} IFNα2a for 24 or 48 hours. IFI44 protein increased with either 500 or 1,000 IU mL^{-1} IFNα2a by 24 hours and was more strongly induced after 48 hours (Fig 4.1d). IFI44 protein was not detectable in untreated cells. IFI44L induction was not observable until 48 hours after treatment and was only clearly induced by 1000 IU mL^{-1} IFNα2a. Interestingly, IFI44L was detectable in unstimulated cells during this experiment and appeared to increase

in unstimulated cells over time. There was a trend of *IFI44* and *IFI44L* RNA expression increasing over time in mock treated cells, where cells received fresh pre-warmed D10 instead of D10 supplemented with IFNα2a (Fig 4.1e). Expression of either gene peaked around 12-24 hours after mock treatment, before decreasing by 48 hours. This may be due to changes in expression of these genes with changes in cell density and may have impacted how accurate this assay was at accurately determining change in gene expression from an unstimulated state at these time points.

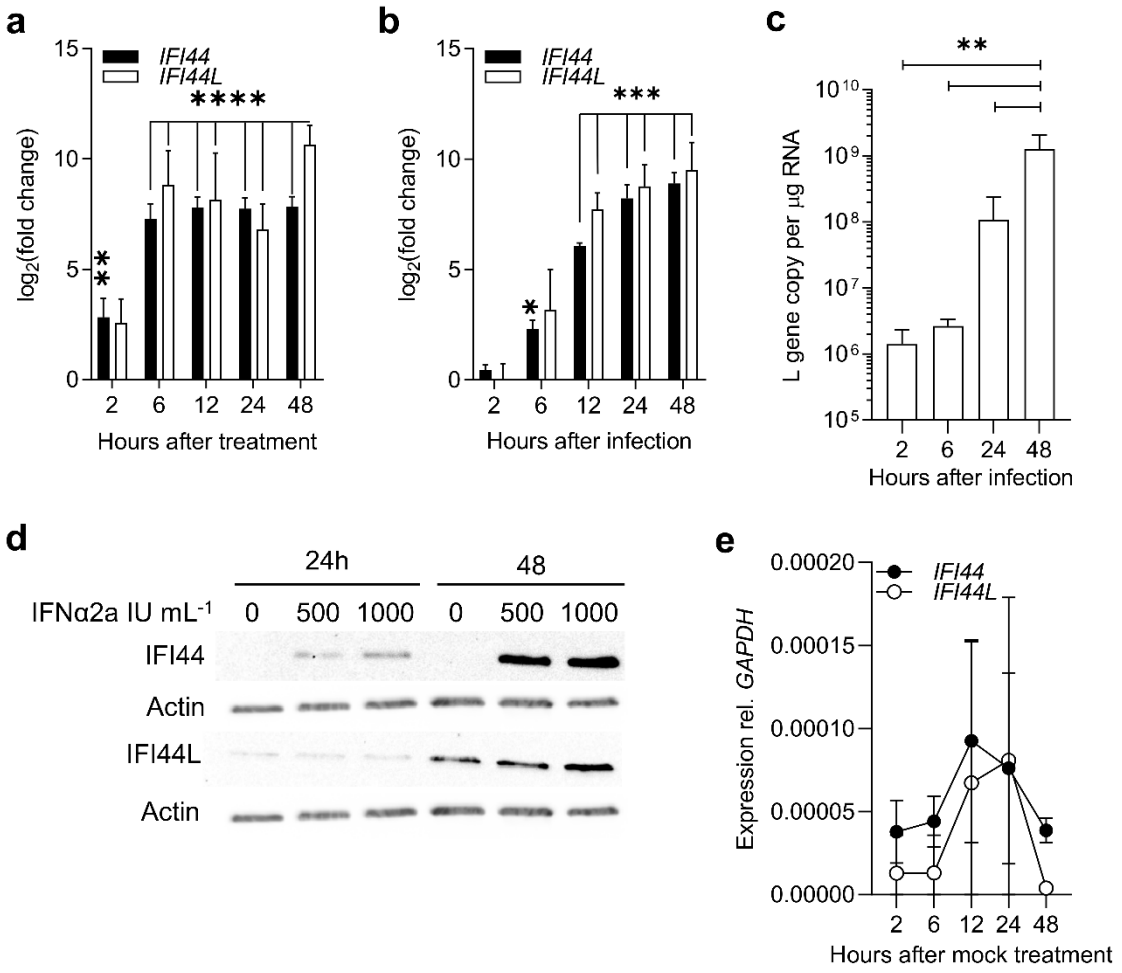

Figure 4.1. IFI44 and IFI44L are upregulated in response to either IFN or RSV. (a) A549 cells were treated with 500 IU mL^{-1} IFNα2a for 2-48 hours. IFI44 and IFI44L mRNA levels assessed by qPCR. Log2(foldchange) from untreated controls. N=3. **(b)** A549 cells were infected with RSV A2 (m.o.i. 0.1) for 2-48 hours and IFI44/IFI44L mRNA levels assessed by qPCR. Log2(foldchange) from mock infected controls. N=3. **(c)** L gene copy number in A549 cells infected with RSV A2 (m.o.i. 0.1). N=3. **(d)** IFI44 and IFI44L protein levels in A549 cells treated with 0-1000 IU mL^{-1} for 24 or 48 hours. N=2. **(e)** IFI44 and IFI44L mRNA levels in untreated control cells from **a**. Expression relative to *GAPDH* ($2^{-\Delta CT}$). N=3. Bars/points show the mean +/- SD. Significance assessed to untreated/uninfected controls or noted groups **(c)** by ANOVA (ΔCt values tested prior to data transformation). * P < 0.05, ** P < 0.01, *** P < 0.001, **** P < 0.0001.

IFI44 and *IFI44L* expression was then examined by qPCR in differentiated THP-1 cells, which have a macrophage-like phenotype. To confirm that RSV can infect these cells they were infected with rgRSV (m.o.i. 0.1) and GFP expression confirmed by microscopy after 24 hours (Fig 4.2a). *IFI44* and *IFI44L* expression was also increased in IFN-I-treated (Fig 4.2b) or RSV infected (Fig 4.2c) THP-1 cells, although this experiment was not repeated, and no statistical significance can be determined. However, these data suggest that these genes are activated by infection in monocytic cell lines as well as epithelium-derived cells.

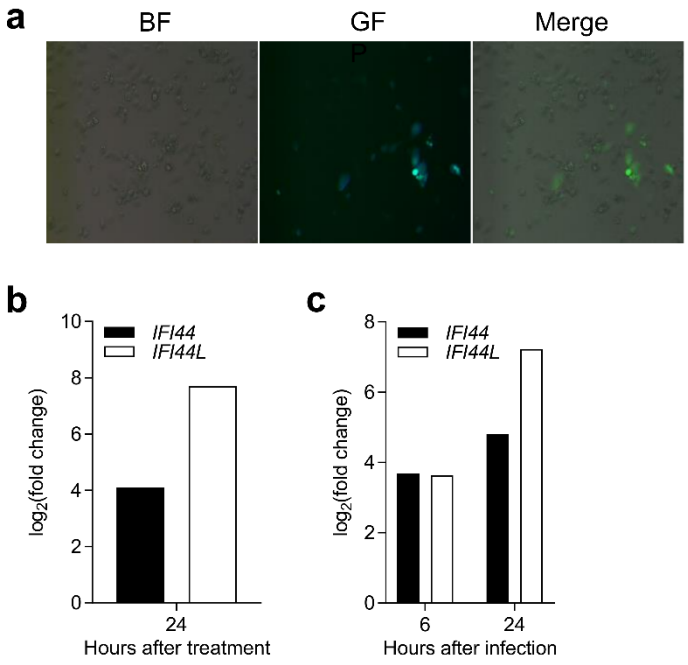

Figure 4.2. Differentiated THP-1 cells upregulate IFI44 and IFI44L in response to IFN and RSV. **(a)** Live fluorescence microscopy of differentiated THP-1 cells infected with rgRSV (m.o.i. 0.1) for 24 hours. BF = brightfield. GF = Green fluorescence. **(b)** Differentiated THP-1 cells were treated with 500 IU mL^{-1} IFNα2a or **(c)** infected with RSV A2 (m.o.i. 0.1) for 24 hours. *IFI44* and *IFI44L* mRNA levels assessed by qPCR, shown relative to uninfected or untreated controls. Bar at the mean, N=1.

4.2.2 *Ifi44* and *Ifi44l* are Induced by RSV Infection *in Vivo*

To investigate the expression kinetics of *Ifi44* and *Ifi44l* in a mouse model of RSV infection, BALB/c mice were infected intranasally with RSV and whole lung RNA extracted for qPCR analysis. RSV infection induced weight loss in adult (8-10-week-old) BALB/c mice which peaked at around day 7 after infection (Fig 4.3a). After this the animals began to regain weight as the infection was cleared, seen by decreasing levels of detectable viral RNA in the lung (Fig 4.3b), although they did not recover to pre-infection weights by day 14. Viral load peaks earlier than weight loss at around day 4 of the infection.

Ifi44 and *Ifi44l* mRNA were detectable by qPCR in uninfected mouse lung, spleen, and liver (Fig 4.3c). Basal *Ifi44* expression was highest in the spleen and lung, with only low levels seen in the liver. *Ifi44l* was also most highly expressed in the spleen but there were much lower levels seen in the lung and liver tissue. Basal levels of *Ifi44* and *Ifi44l* in murine lung tissue are >10-fold lower than *Ifitm1* mRNA (Fig 4.3d), an ISG thought to be constitutively expressed in barrier tissues such as the lung. In the absence of protein expression data, these observations were not sufficient to conclude whether or not IFI44 or IFI44L are constitutively expressed at physiologically relevant levels in murine tissues.

During RSV infection of adult BALB/c mice, both genes were significantly upregulated relative to PBS-treated control mice within 6 hours of infection (Fig 4.3e). The highest upregulation was observed 1 day after infection. It would have been interesting to look at additional acute time points after infection such as 12 and 18 hours, as well as 2 and 3 days, to properly characterise when maximal induction of these genes occurs and compare to viral RNA levels. Expression of *Ifi44* was still significantly upregulated

by day 4 of infection. Both genes returned to levels comparable to the PBS-treated controls by days 7 of infection.

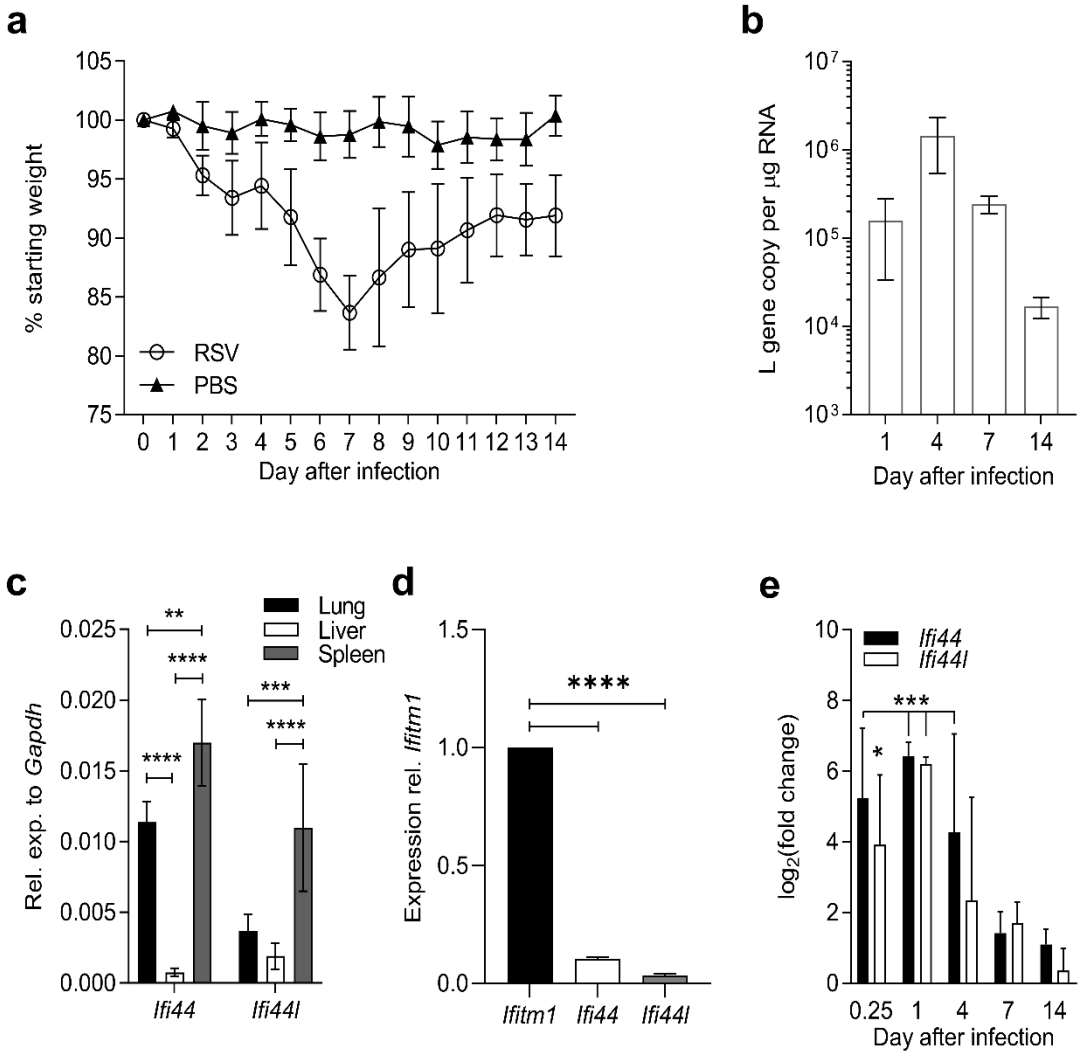

Figure 4.3. Ifi44 and Ifi44l are upregulated in response to RSV infection in mice. (a) 8-10-week-old female BALB/c mice were intranasally infected with $2x10^5$ pfu RSV A2. Weight change over 14 days of infection. **(b)** L gene copy number in whole lung tissue by qPCR. **(c)** Expression of *Ifi44* and *Ifi44l* relative to *Gapdh* ($2^{-\Delta CT}$) in lung, liver, and spleen of uninfected BALB/c mice. **(d)** Expression of *Ifi44* and *Ifi44l* relative to *Ifitm1* ($2^{-\Delta CT}$) in lung, liver, and spleen of uninfected BALB/c mice. **(e)** *Ifi44* and *Ifi44l* mRNA levels assessed by qPCR in whole lung tissue. Log2(foldchange) in expression relative to PBS-treated control mice. Bars/points show the mean +/- SD. N≥4 animals at each time point. Significance by ANOVA (ΔCT values tested prior to data transformation). * $P < 0.05$, ** $P < 0.01$, *** $P < 0.001$, **** $P < 0.0001$.

4.2.3 Transient Transfection of IFI44 or IFI44L

The first approach taken to investigate the impact of IFI44 or IFI44L expression on RSV infection was transient plasmid DNA transfection. In a previous chapter this approach was shown to be suboptimal due to restriction of RSV infection by the transfection of control vector alone. These data were obtained in parallel to those presented in chapter 3.

Human codon optimised IFI44 and IFI44L coding sequences were synthesised and cloned into the mammalian expression vector pcDNA3.1 by GeneArt (Thermofisher). Transcripts were detected in deoxyribonuclease (DNase)-treated RNA of transfected A549 cells (Fig 4.4a). Levels increased in a dose-dependent manner. To confirm the efficacy of the DNase treatment in removing residual plasmid DNA that would be detectable during qPCR, pcDNA3.1-IFI44 was modified by the removal of the CMV enhancer and promoter regions by *Spe*I digestion and subsequent re-ligation of the vector backbone to create pcDNA3.1-ΔCMV. Removal of the CMV region was confirmed by DNA gel electrophoresis following *Spe*I digestion of the pcDNA3.1-ΔCMV-IFI44 or pcDNA3.1-IFI44 (Fig 4.4b). The modified pcDNA3.1-ΔCMV-IFI44 had a single band pattern following digestion, confirming the removal of the CMV region. Finally, A549 cells were transfected with either a plasmid encoding tdTomato (pTDT), pcDNA3.1-ΔCMV-IFI44, pcDNA3.1-IFI44, or pcDNA3.1-IFI44L. RNA was extracted 24 hours later, DNase treated and converted to cDNA for qPCR analysis. Transfection of pcDNA3.1-IFI44 was associated with a 2-log increase ($P < 0.01$) in *IFI44* expression compared to pcDNA3.1-ΔCMV-IFI44 or pTDT (Fig 4.4c). However, transfection of pcDNA3.1-ΔCMV-IFI44 was associated with significantly higher levels of codon-optimised IFI44 than transfection of pTDT. As such there may have been residual expression of *IFI44* RNA from this vector or residual DNA after DNase treatment.

However, these data show that pcDNA3.1-IFI44 is likely transcribed to produce IFI44 RNA. pcDNA3.1-empty was used as the vector control for all remaining overexpression studies.

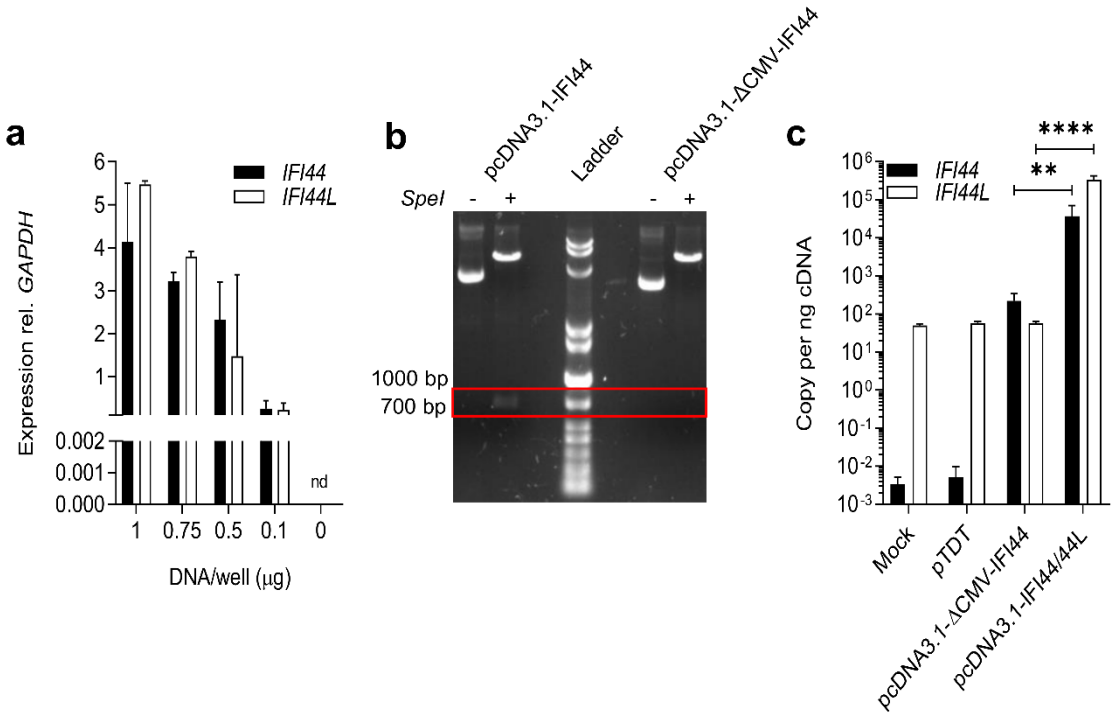

Figure 4.4. Detection of IFI44 and IFI44L transcription following plasmid transfection. (a) Expression of codon-optimised *IFI44* and *IFI44L* RNA in A549 cells transfected with 0.1-1 µg pcDNA3.1-IFI44 (black bars) or pcDNA3.1-IFI44L (white bars). On-column DNase treatment was used to remove plasmid DNA. Expression relative to *GAPDH* (2^{-dCT}). N=2. Mean +/- SEM. **(b)** Confirmation of CMV promoter deletion in pcDNA3.1-ΔCMV-IFI44. **(c)** Copy number of codon optimised *IFI44* or *IFI44L* RNA per ng cDNA in A549 cells transfected with 0.5 µg plasmid DNA. On-column DNase treatment was used to remove plasmid DNA. pTDT = plasmid encoding tdTomato. IFI44/44L = either pcDNA3.1-IFI44 or pcDNA3.1-IFI44L. N=3. Mean +/- SD. Significance by ANOVA. ** P < 0.01, **** P < 0.0001. nd = not detected.

A549, HEp-2, and HEK293T/17 cells were transfected with 0.5 μg pcDNA3.1-empty (vector), pcDNA3.1-IFI44, or pcDNA3.1-IFI44L and infected with RSV A2 (m.o.i. 1) 24 hours later. There was no significant difference in levels of viral RNA compared to vector transfected controls after 24 hours of infection with either IFI44 or IFI44L expression (Fig 4.5a-c). Next, cells were transfected as previously but infected with rgRSV (m.o.i. 1) and infectivity determined by flow cytometry. There was no significant difference in the percentage of infected cells after 24 hours with either IFI44 or IFI44L expression in each cell line (Fig 4.5d-f). These data suggest that IFI44 and IFI44L have no impact on RSV infection in this experimental set up. However, IFI44 or IFI44L protein expression was not confirmed, due to a lack of available antibodies at the time of the experiment, and an m.o.i. of 1 may be too high to observe an impact of mild or moderately antiviral ISGs. As shown previously, just 0.1 μg pcDNA3.1 DNA was sufficient to significantly restrict RSV infection *in vitro* warranting the development of stably transduced cell lines for overexpression studies.

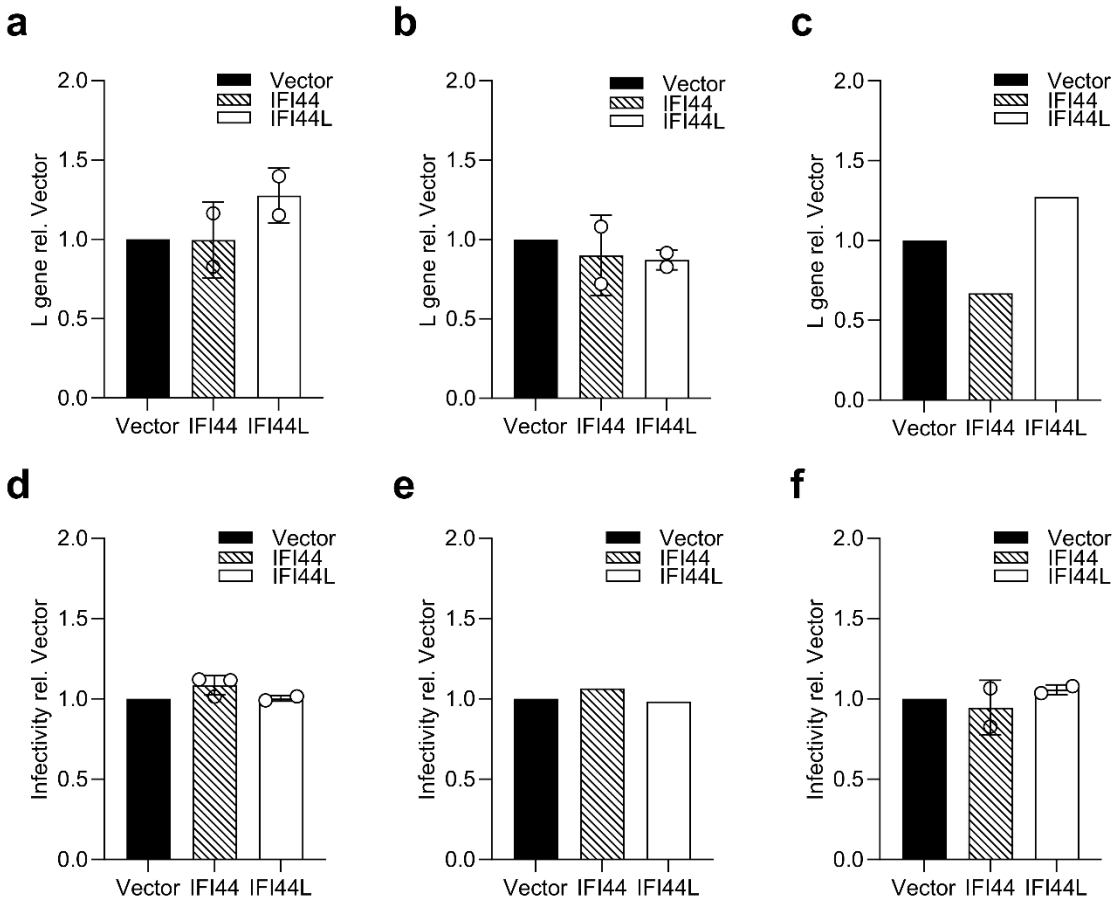

Figure 4.5. RSV infection is unaffected by transfection of IFI44 or IFI44L pcDNA3.1 plasmid constructs. (a) A549, **(b)** HEp-2, and **(c)** HEK-293T/17 cells were transfected with 0.5 µg pcDNA3.1 (vector), pcDNA3.1-IFI44 (IFI44), or pcDNA3.1-IFI44L (IFI44L) and infected with RSV A2 (m.o.i. 1) 24 hours later. After 24 hours infection was assessed by qPCR of the RSV L gene. **(d)** A549, **(e)** HEp-2, and **(f)** HEK-293T/17 cells were transfected as for **a-c** with the addition of pTdtomato (0.1 µg) and infected with rgRSV (m.o.i. 1) after 24 hours. 24 hours after infection the percentage of RFP^+ single cells that were GFP^+ was assessed by flow cytometry. Points represent individual experiments, bar at the mean +/- SD. Significance by paired ratio t-test prior to data transformation.

4.2.4 RSV Infection is Moderately Restricted by IFI44L in Stably Transduced Vero Cells

Stably transduced Vero cell lines were developed by Dr. Sarah Smith and Dr. Rachel Wash (Wellcome Trust Sanger Institute) by lentiviral transduction and puromycin selection. Expression of IFI44L-HA was confirmed by immunofluorescence microscopy, although this was not observed in every cell (data not shown). This may be due to the polyclonal nature of the transduced cells or a result of poor staining of either primary or secondary antibodies during slide preparation. Vero IFI44L-HA cells infected with rgRSV (m.o.i. 1) for 24 hours showed no significant difference in the percentage of cells infected relative to Vector transduced control cells (Fig 4.6b). However, when infected with RSV A2 (m.o.i. 1) there was a mild but significant decrease ($P < 0.05$) in viral RNA in IFI44L-HA cells (Fig 4.6c). To build on these results I aimed to generate stable A549 cell lines expressing either IFI44 or IFI44L. A549 cells are a more relevant cell line for the study of RSV infection and unlike Vero cells have a competent IFN system which may be essential for the study of ISGs whose antiviral mechanisms rely on other IFN-inducible factors.

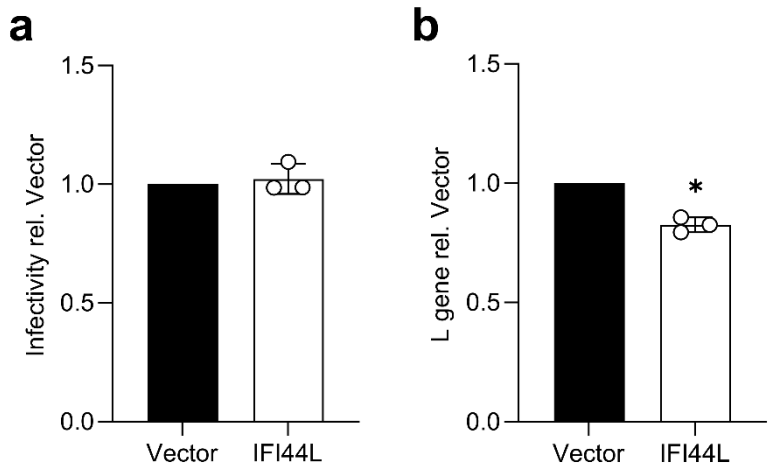

Figure 4.6. IFI44L moderately reduces RSV infection in stably transduced Vero cells. (a) Stably transduced Vero cells were infected with rgRSV (m.o.i. 1) for 24 hours and the percentage of infected (GFP^+) cells assessed by flow cytometry. **(b)** Stably transduced Vero cells were infected with RSV A2 (m.o.i. 1) for 24 hours and total L gene copy number assessed by qPCR. Bars show the mean +/- SD relative to vector-transduced control cells. Points show the mean of independent experiments. Significance assessed by ratio paired t-test prior to data transformation. * $P < 0.05$.

4.2.5 Generating pSIN-IFI44-Puro Stably Transduced A549 Cells

In order to produce stably transduced cell lines, it was essential to optimise the production of lentivirus in HEK293T/17 cells. Lentivirus was produced through triple transfection with p8.9 (packaging), pMDG2 (envelope), and a transfer plasmid encoding the gene of interest. Altering the ratio of these plasmids during transfection from 1:1:1 to 2:5:5 increased production of lentivirus to detectable levels using a qualitative p24 detection test (Fig 4.7a). A549 cells were transduced with the transfer plasmids pSIN-GFP-Puro or pSIN-IFI44-Puro and stably transduced cells selected by the addition of puromycin 48 hours later. Puromycin concentration was titrated and the minimum concentration that resulted in 100% cell death was selected for use (data not recorded). GFP expression was confirmed in the surviving cells transduced with pSIN-GFP-Puro (vector) but not with pSIN-IFI44-Puro (Fig 4.7b). Two weeks after

transduction, elevated *IFI44* RNA expression was detected in pSIN-IFI44-Puro transduced cells but not in vector transduced cells (Fig 4.7c). This expression appeared to wane after two more weeks in culture, although it remained higher than in WT or vector transduced cells. There was no detectable IFI44 protein expression in stably transduced A549 cells (14 days after transduction, D14) or cells transduced with pSIN-IFI44-Puro for 1 day (Fig 4.7d). In addition, there was no observable impact on RSV viral RNA levels either 24 or 48 hours after RSV A2 infection (m.o.i. 1) in these pSIN-IFI44-Puro stably transduced cells relative to vector controls (Fig 4.7e). Whilst this approach provided an opportunity to develop the protocol to produce lentivirus stocks it was not successful in assaying the impact of IFI44 due to the lack of detectable IFI44 protein expression using pSIN-IFI44-Puro.

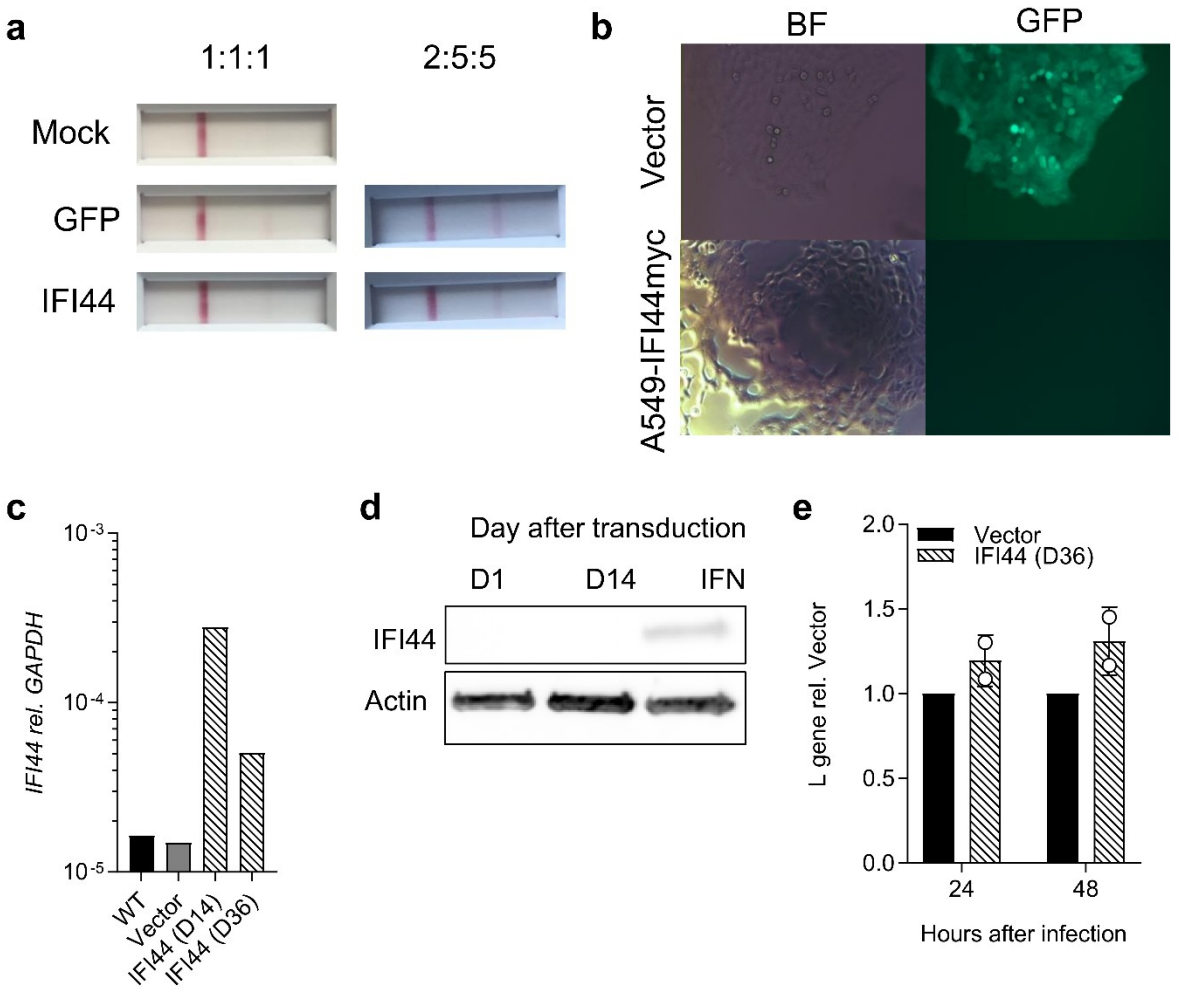

Figure 4.7. Production of stably transduced pSIN-IFI44-Puro A549 cells. (a) Lentivirus was produced by triple transfection with packaging, envelope, and transfer plasmid at a ratio of 1:1:1 or 2:5:5. Lentivirus concentration in cell supernatant was assessed qualitatively after 52 hours and is indicated by a second right-hand red bar. **(b)** Live fluorescence imaging of A549 cells transduced with either pSIN-GFP-Puro or pSIN-IFI44-Puro and selected with puromycin for two weeks. **(c)** *IFI44* mRNA expression relative to *GAPDH* (2^-ΔCt) following transduction and puromycin selection. D14: 14 days after transduction. D36: 36 days after transduction. Vector cells were transduced with pSIN-GFP-Puro. **(d)** IFI44 protein expression in A549 cells transduced with pSIN-IFI44-Puro for 1 day or for 2 weeks. IFN = A549 cells treated with 500 IU mL^{-1} IFNα2a for 24 hours. **(e)** Stably transduced A549 cells were infected with RSV A2 (m.o.i. 1) for 24 hours and levels of viral RNA assessed by RSV L gene qPCR. Points represent independent experiments. Bar at the mean +/- SD. Significance by paired ratio t-test prior to data transformation.

4.2.6 Production of pTRIP-Based Lentivirus

A previous study reported restriction of RSV infection in cells transduced with pTRIP-CMV-IVsb-IFI44-IRES-TagRFP or pTRIP-CMV-IVsb-IFI44L-IRES-TagRFP [204]. These constructs were kindly provided by M. Dorner (Imperial College London) and were next validated and used to develop an effective overexpression assay to study IFI44 and IFI44L during RSV infection.

pTRIP constructs include a synthetic intron sequence (IVsb) upstream of the ISG start codon that is thought to enhance expression of the downstream coding sequence [286, 287]. The ISG coding sequence is followed by an IRES and sequence encoding the red fluorescent protein TagRFP [288]. To confirm expression of IFI44 or IFI44L protein using these constructs, 293T cells were transfected for 24 hours. IFI44 protein was detected with transfection of pTRIP-CMV-IVsb-IFI44-IRES-TagRFP but not pTRIP-CMV-IVsb-FLUC-TagRFP (vector) encoding firefly luciferase (FLUC) (Fig 4.9a). IFI44L protein was not detectable following pTRIP-CMV-IVsb-IFI44L-IRES-TagRFP transfection (Fig 4.8a) although the cells were RFP^+ following transfection (Fig 4.8b). The IFI44L coding sequence in this construct was sequenced and found to be based on an outdated reference sequence (AAH15932.1) lacking the N-terminal 39 amino acids of IFI44L (NP_006811.2). As the antibody used was raised using a synthetic peptide consisting of the first 50 residues of IFI44L it was unable to confirm protein expression following IFI44L transfection.

Next, lentivirus stocks were generated by transfecting HEK293T/17 cells using a 2:5:5 ratio of packaging, envelope, and pTRIP DNA as described previously. A549 cells were then transduced with neat lentivirus-containing supernatants. High levels of IFI44 protein was detected in IFI44-transduced cell lysates (Fig 4.8c). A549 cells transduced with IFI44L were not RFP^+ and so the production of lentivirus was repeated with a ratio

of 1:5:10. The titre of the resultant lentivirus-containing supernatants was quantified by flow cytometry. Transduction with vector or IFI44 lentivirus stocks resulted in greater than 60% of cells being RFP^+ (Fig 4.8d). As such, the titre of Vector and IFI44 lentivirus stocks was calculated to be over $1x10^6$ transducing units (TU) per mL (Fig 4.8e). Transduction with IFI44L resulted in less than 20% of cells being transduced (RFP^+) and a calculated titre of $1.14x10^5$ TU mL^{-1}.

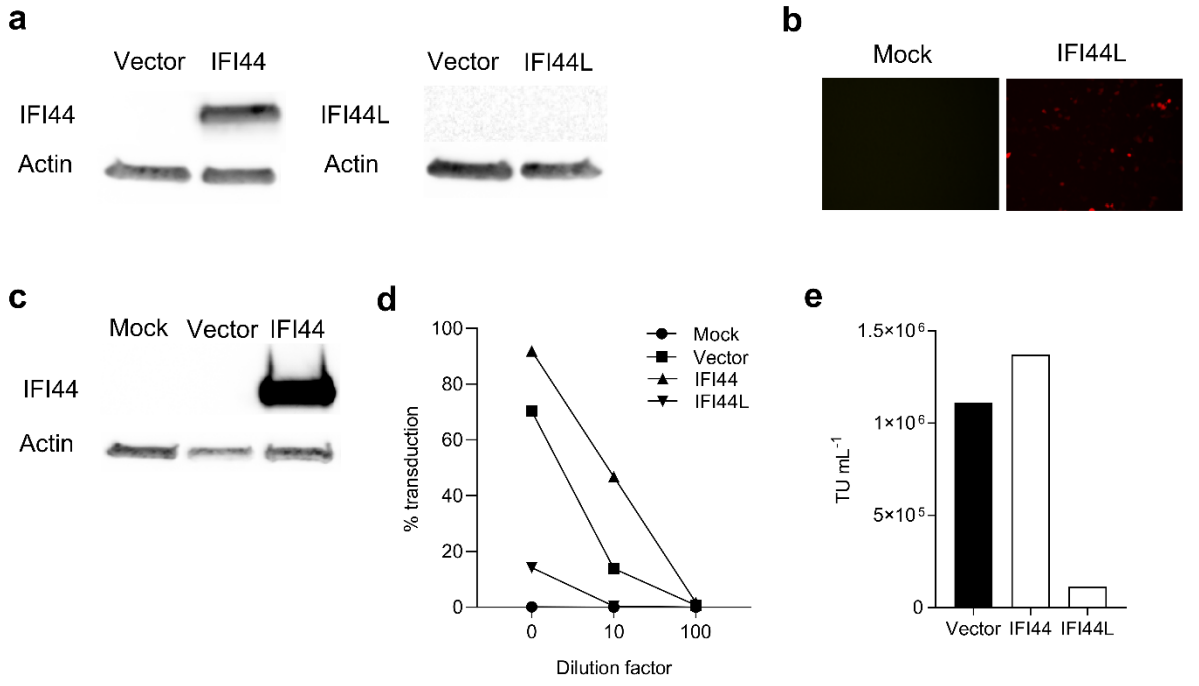

Figure 4.8. Optimisation of pTRIP lentivirus production. (a) IFI44 and IFI44L protein expression in HEK293T/17 cells 24 hours after transfection with 1 µg pTRIP-CMV-IVsb-FLUC-TagRFP (vector), pTRIP-CMV-IVsb-IFI44-TagRFP (IFI44), or pTRIP-CMV-IVsb-IFI44L-TagRFP (IFI44L). **(b)** TagRFP fluorescence 24 hours in HEK293T/17 cells after transfection with pTRIP-CMV-IVsb-IFI44L-TagRFP. **(c)** IFI44 protein expression in A549 cell lysate 24 hours after transduction with undiluted supernatant containing vector or IFI44 lentivirus. **(d)** Percentage RFP^+ A549 cells following transduction with lentivirus produced using a ratio of packaging, envelope, and transfer plasmids of 1:5:10. **(e)** Titre of lentivirus stocks used in **e**. TU = transducing units.

4.2.7 Gating Strategy for Infectivity Analysis

For the analysis of rgRSV infection of transduced cells (RFP^+) an initial homogenous population was gated to exclude cell debris (Fig 4.9). This was followed by doublet discrimination. RFP^+ and GFP^+ gates were determined using mock transduced or uninfected controls respectively. RFP^+GFP^+ cells were gated from RFP^+ single cells. The percentage of RFP^+ cells that were RFP^+GFP^+ was used to compare levels of infection between samples.

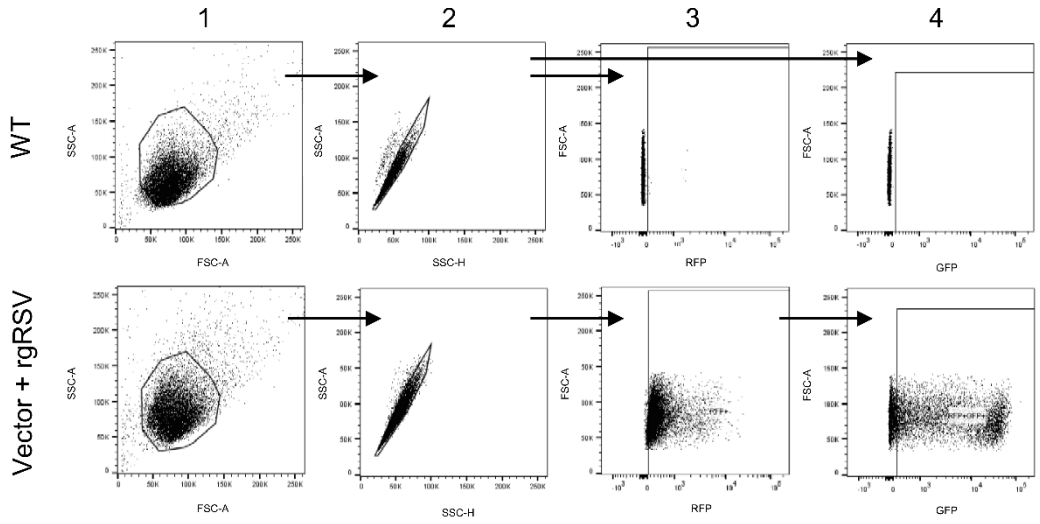

Figure 4.9. Infectivity assay gating strategy following pTRIP-based lentivirus transduction. A549 cells were transduced with pTRIP-CMV-IVsb-FLUC-TagRFP and infected with rgRSV after 24 hours. RFP and GFP fluorescence assessed 24 hours after infection. Uninfected WT cells included as negative controls. For gating of transduced and infected cells a majority population is first isolated (1) to remove cellular debris before doublet exclusion (2). Next, RFP^+ (3) and GFP^+ (4) gates are set using an unstained/uninfected control sample.

4.2.8 Transient Transduction of IFI44 Restricts RSV Infection

A549 cells were transduced with $2x10^5$ TU of FLUC (vector) or IFI44 lentivirus and subsequently infected 24 hours later with either RSV A2 or rgRSV (m.o.i. 0.8). There was a trend of lower RSV A2 viral RNA 24 hours after infection (Fig 4.10a). There was a significant decrease in the percentage of transduced cells that were infected with rgRSV ($P < 0.05$, Fig 4.10b) and a 30% decrease in median fluorescence intensity (MFI) of those infected cells, relative to infected cells transduced with the Vector control ($P < 0.001$, Fig 4.10c). This suggested that IFI44 was able to reduce RSV infectivity and reduce RSV replication.

As seen previously with transfection of plasmid DNA, lentiviral delivery of non-host DNA resulted in a restriction of subsequent RSV infection. This restriction was only slightly reduced by treating cells with the JAK-STAT signalling inhibitor ruxolitinib, although after one experiment statistical significance of this could not be determined. This effect of transduction on RSV infection may reduce the observable impact of transgene expression and reduce the range of the assay. As such, the development of stable cell lines was required to investigate the impact of IFI44 further, and to assess any impact of IFI44L expression due to the low titre of IFI44L lentiviral stocks.

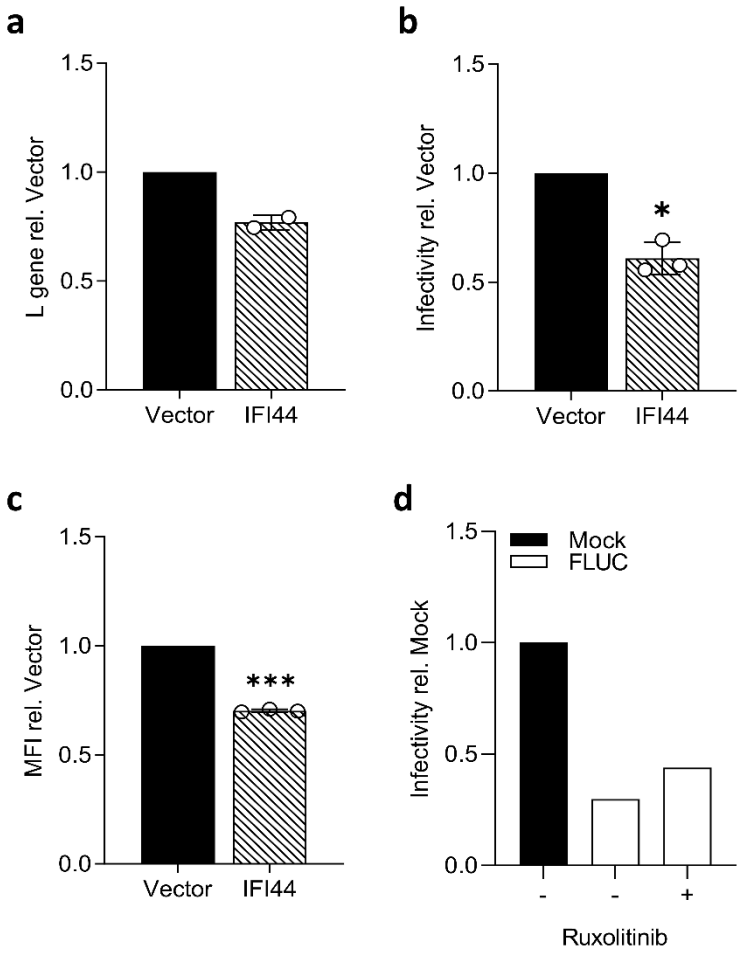

Figure 4.10. Transduction of IFI44 reduces RSV infection. A549 cells were transduced with $2x10^5$ TU lentivirus 24 hours prior to infection with **(a)** RSV A2 (m.o.i. 0.1) and infection assessed by RSV L gene qPCR after 24 hours (N=2), or **(b)** rgRSV (m.o.i. 0.1) and infection assessed by quantifying the proportion of transduced cells that were infected after 24 hours. N=3. **(c)** Mean GFP fluorescence intensity 24 hours after rgRSV infection. Data expressed relative to the vector control. N=3. **(d)** Infectivity of A549 cells transduced with $2x10^5$ TU FLUC lentivirus relative to mock transduced cells. Cells were infected with rgRSV (m.o.i. 0.1) 24 hours after transduction. At the time of transduction and rgRSV infection noted groups were also treated with 2 µg/mL ruxolitinib. N=1. Points represent independent experiments, bar at the mean +/- SD. Significance by ratio paired t-test prior to data transformation. * $P < 0.05$, *** $P < 0.001$.

4.2.9 Development and Validation of Stably Transduced A549 Cell Lines

To generate stably transduced cell lines fluorescent activated cell sorting (FACS) was used to plate single cells into each well of two 96-well plates 24 hours after transduction. The transduced cells with the top 2-10% RFP fluorescence were selected. This approach was required as the lentiviral constructs based on pTRIP do not contain a suitable antibiotic selection marker. After 3 weeks in culture expanded colonies were screened by microscopy for RFP expression. A single colony of FLUC vector transduced cells was isolated, two IFI44L transduced clones, and three IFI44 transduced clones. IFI44 protein expression was detectable in each IFI44 transduced clone at similar or higher levels than seen after treatment with 500 IU mL^{-1} IFNα2a for 24 hours (Fig 4.11a). The clone with the highest expression was selected for further study. IFI44L protein expression was not detected in any IFI44L, Vector, or IFI44 clone. IFI44L clone #1 was selected for further study as IFI44L clone #2 was deemed unsuitable due to altered morphology and poor growth.

After a further expansion period of 2 weeks, cells were again screened for RFP expression by flow cytometry. 99% of the selected IFI44 and IFI44L cells were still RFP^+, whereas only 91.5% of Vector transduced cells were RFP^+ (Fig 4.11b). *IFI44* and *IFI44L* mRNA levels were significantly increased in their respective cell lines either with or without IFN stimulation ($P < 0.01$, Fig 4.11c). The expression of *MX1* was also assessed by qPCR in these cell lines and no difference was seen in IFI44 or IFI44L cells relative to the FLUC control. However, after IFN treatment there was a trend towards increased levels of *MX1* RNA in IFI44L-expressing cells relative to WT. These data do not suggest that IFI44 or IFI44L regulate IFN responses.

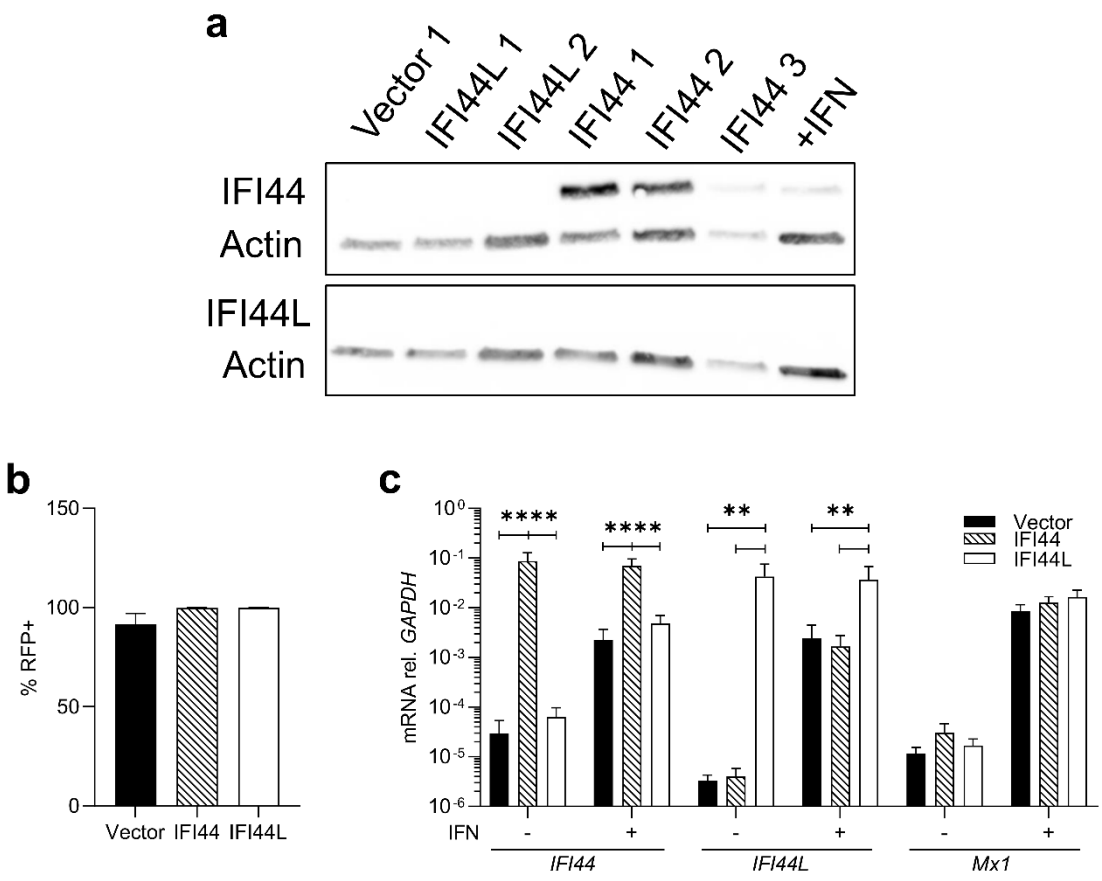

Figure 4.11. Confirmation of IFI44 or IFI44L expression in stably transduced clonal A549 cell lines. (a) IFI44 or IFI44L protein expression in clonal A549 lines 3 weeks after transduction. **(b)** Percentage of RFP^{+} single cells from the selected clones (vector #1, IFI44 #1, IFI44L#1) 3 weeks after transduction. **(c)** *IFI44*, *IFI44L*, *MX1* expression relative to *GAPDH* ($2^{-\Delta Ct}$) in the selected clones with or without IFNα2a treatment (500 IU mL^{-1}, 24 hours). Bar at the mean +/- SEM. Significance by ANOVA. ** P < 0.01, **** P < 0.0001.

4.2.10 Expression of IFI44 or IFI44L Reduces Cell Proliferation

Previous studies have reported that IFI44 and IFI44L reduce cell proliferation [256, 261]. To corroborate these reports, proliferation was assayed in stably transduced clonal cell lines using several approaches.

Initially, a colorimetric 3-(4,5-dimethylthiazol-2yl)-5-(3-carboxymethoxyphenyl)-2-(4-sulfophenyl)-2H-tetrazolium (MTS) assay measuring viable cell number through the reduction of MTS to the purple Formazan ((E,Z)-5-(4,5-dimethylthiazol-2-yl)-1,3-diphenylformazan) by cellular reducing agents such as NADPH and a provided electron coupling reagent (phenazine ethosulfate). These cellular reducing agents are produced by dehydrogenase enzymes active in metabolically active cells. $5x10^3$ viable cells were plated of each cell line and the number of viable cells quantified 24 hours later. Both IFI44 and IFI44L clonal cell lines had significantly less viable cells in each well relative to the Vector control ($P< 0.05$, Fig 4.12a).

Next, viable cell number was quantified manually 6-48 hours after plating by trypan blue exclusion. Counting the cells after just 6 hours confirmed there was no difference in the number of plated cells (Fig 4.12b). After 24 hours both IFI44 and IFI44L cell number had not increased, unlike the Vector control cells. By 48 hours, although both IFI44 and IFI44L cell lines had nearly doubled in number of viable cells there remained significantly less cells than in the Vector control wells ($P < 0.01$).

Each cell line was then perfused with CellTrace Violet dye and allowed to proliferate for 72 hours. The fluorescent dye forms covalent bonds with intracellular amines and with each cell division the dye in each daughter cell is diluted. After 72 hours, each cell line had a relatively uniform spread of CellTrace Violet fluorescence but both IFI44 and IFI44L cell lines had significantly increased mean fluorescence intensity values

relative to the Vector control cells ($P < 0.05$, Fig 4.12c-d). Fluorescence intensity was reduced in comparison to wild-type (WT) parental cells stained and immediately fixed for analysis confirming that each cell line had proliferated, and the dye had been diluted.

Finally, to confirm that the reduced rates of proliferation seen with IFI44 or IFI44L expression was not a result of increased cell death, a cytotoxicity assay was performed. The assay used measured the release of lactate dehydrogenase (LDH) into the cell supernatant by cells with a damaged cell membrane. Cytotoxicity levels were compared to 100% cytotoxicity controls for each cell line. There was no significant increase in cytotoxicity in either IFI44 or IFI44L cell lines (Fig 4.12e).

These data confirm previous observations that IFI44 proteins are anti-proliferative and that this is not caused by an increase in cell death.

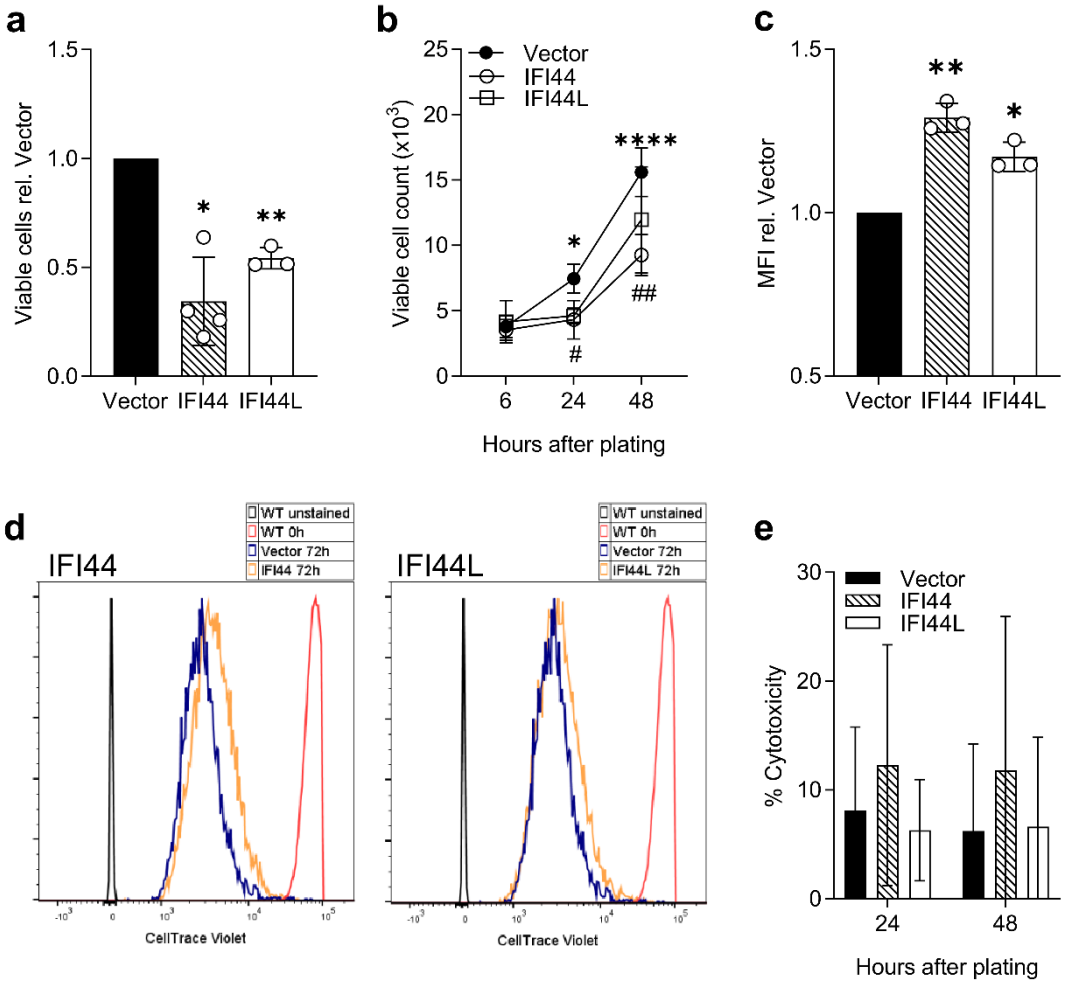

Figure 4.12. IFI44 and IFI44L reduce cellular proliferation. (a) A549 stably transduced clonal cell lines expressing IFI44, IFI44L, or transduced with FLUC vector were seeded at equal densities and viable cell number quantified 24 hours later using a colorimetric metabolic activity assay or after 6-48h by **(b)** trypan blue exclusion (* = IFI44, # = IFI44L). N≥3. **(c)** Stably transduced clonal A549 cell lines were stained with 5 µM CellTrace Violet. Cells were allowed to proliferate for 72 hours. Mean fluorescence intensity (MFI) quantified relative to vector. N=3. **(d)** Representative histograms of CellTrace Violet fluorescence from **c**. WT cells were stained with 5 µM CellTrace Violet or treated with vehicle only and immediately fixed prior to analysis for positive (red) and negative (grey) controls. **(e)** Cytotoxicity was assessed in vector, IFI44, or IFI44L A549 clonal cell lines by LDH release assay 24-48 hours after plating. N=3. Significance to vector controls assessed by ratio paired t-test prior to data transformation. Points represent a single independent experiment with a bar at the mean +/- SD. * P < 0.05, ** < P <0.01, *** P < 0.001, **** P < 0.0001.

4.2.11 IFI44 or IFI44L Stably Transduced Clonal Cell Lines Restrict RSV Infection

RSV infection was then assessed in validated stably transduced A549 clonal cell lines expressing either IFI44 or IFI44L. The impact of these factors on proliferation was taken into account when preparing viral inoculum for the following *in vitro* infections, by counting the number of viable cells for each cell line prior to infection. Initially, each cell line was infected with rgRSV (m.o.i. 0.1/0.01) for 24 hours. The percentage of infected cells at each m.o.i. was significantly reduced with either IFI44 or IFI44L expression relative to the Vector control ($P < 0.05$, Fig 4.13a-b). As seen with transient transduction there was also a significant decrease in median fluorescence intensity of GFP in IFI44 or IFI44L cells, although only at the higher m.o.i. of 0.1 ($P < 0.05$, Fig 4.13c). Cells were next infected with RSV A2 virus and viral RNA levels quantified after 24 hours. There was a ~50% decrease in viral RNA in either IFI44 or IFI44L cells ($P < 0.05$, Fig 4.13d). Viral titre in cell supernatant was assayed after 48 hours of RSV A2 infection and was significantly reduced by expression of both IFI44 proteins at m.o.i. 0.01 ($P < 0.05$, Fig 4.13e). There was also reduced (41% of vector control) viral titre in m.o.i. 0.1 cell supernatant with IFI44 expression although this was not statistically significant. IFI44L expression did significantly reduce viral titre in cell supernatant during an m.o.i. 0.1 RSV A2 infection (66% of vector control, $P < 0.01$).

These data suggest IFI44 proteins have an antiviral function during RSV infection. To confirm this, several loss-of-function assays were then developed.

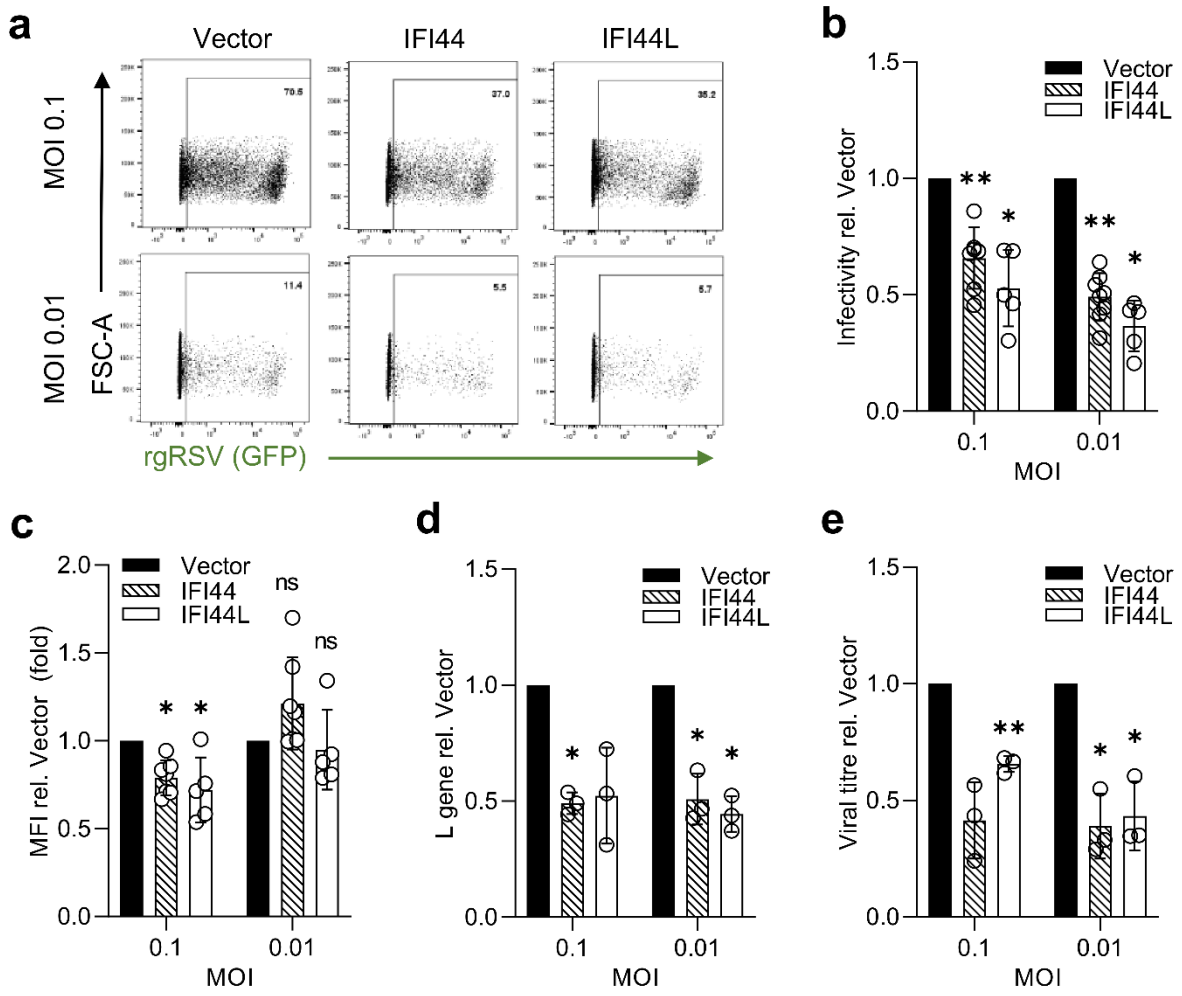

Figure 4.13. IFI44 and IFI44L overexpression restricts RSV infection. Stably transduced cell lines were infected with rgRSV (m.o.i. 0.1 or 0.01) and infectivity assessed after 24 hours. **(a)** Representative dot plot of GFP fluorescence in RFP^+ single cells. **(b)** Infectivity relative to vector control. **(c)** Median GFP fluorescence. **(d)** Stably transduced cell lines were infected with RSV A2 (m.o.i. 0.1 or 0.01) for 24 hours. Viral RNA was quantified by RSV L gene qPCR. **(e)** Cells were infected as for **d** and viral titre in cell supernatant assessed by plaque assay 48 hours after infection. Points represent the result of an independent experiment. Bars at the mean +/- SD. * represents significance relative to cells transduced with FLUC vector, assessed by ratio paired t-test**.** Analysis was done prior to data transformation. * $P < 0.05$, ** $P < 0.01$.

4.2.12 Knockdown of IFI44 and IFI44L Increases Susceptibility to RSV Infection

To examine whether loss of IFI44 proteins impacts RSV infection, short-interfering RNA (siRNA) were used to knockdown expression prior to infection. Endoribonuclease-prepared siRNA (esiRNA) are pools of short dsRNA oligonucleotides targeting a region of mRNA transcript common to all transcript variants of a gene of interest. esiRNA are produced from a long dsRNA molecule transcribed *in vitro* from a cDNA molecule generated from a full-length PCR amplicon of the target mRNA region. The long dsRNA molecule is treated with *Escherichia coli* RNase III to generate short esiRNAs with an average length of 21 base pairs. esiRNA pools targeting either IFI44 or IFI44L were produced by Eupheria Biotech (Sigma).

A549 cells were transfected with esiRNA targeting IFI44 (esi-IFI44) at a final concentration of 1-20 nM and IFI44 RNA levels determined by qPCR 48 hours after transfection. There was a trend towards reduced expression levels with concentrations of 10-20 nM (Fig 4.14a). 20 nM esi-IFI44 only resulted in a knockdown of 42% relative to cells transfected with a non-targeting (NT) control siRNA. Expression of *IFI44L* RNA was not quantified in these samples.

The impact of esiRNA-mediated IFI44 and IFI44L knockdown was assayed by transfecting cells with 50 nM esiRNA. Cells were treated with 500 IU mL^{-1} IFNα2a 24 hours later and subsequently infected with RSV A2 (m.o.i. 0.1) 16 hours after IFNα2a stimulation. Infection and expression of IFI44 or IFI44L expression was assayed after 48 hours. The higher concentration of 50 nM esi-IFI44 resulted in a 45% knockdown of IFI44 expression (Fig 4.14b) but also a 33% reduction in IFI44L expression (Fig 4.14c). A similar trend was seen for esi-IFI44L which reduced both IFI44 (Fig 4.14b) and IFI44L (Fig 4.14c) expression by 41%. Transfecting A549 cells with a 1:1 ratio of esi-IFI44 and esi-IFI44L for a final concentration of 50 nM resulted in a 55% reduction

in IFI44 (Fig 4.14b) and 38% (Fig 4.14c) reduction in IFI44L expression. These data show that the pools of esiRNA are not specific for either IFI44 or IFI44L, likely due to sequence similarities between the two genes. Transfection of esi-IFI44 was associated with a 2.5-fold increase in viral RNA (Fig 4.14d). Transfection of esi-IFI44L and a 1:1 ratio of both esi-IFI44 and esi-IFI44L was also associated with a 3-fold increase in viral RNA. Knockdown of IFI44 and IFI44L by esi-IFI44 also resulted in an increase in viral titre in cell supernatant relative to cells transfected with the NT control siRNA in one experiment (Fig 4.14e).

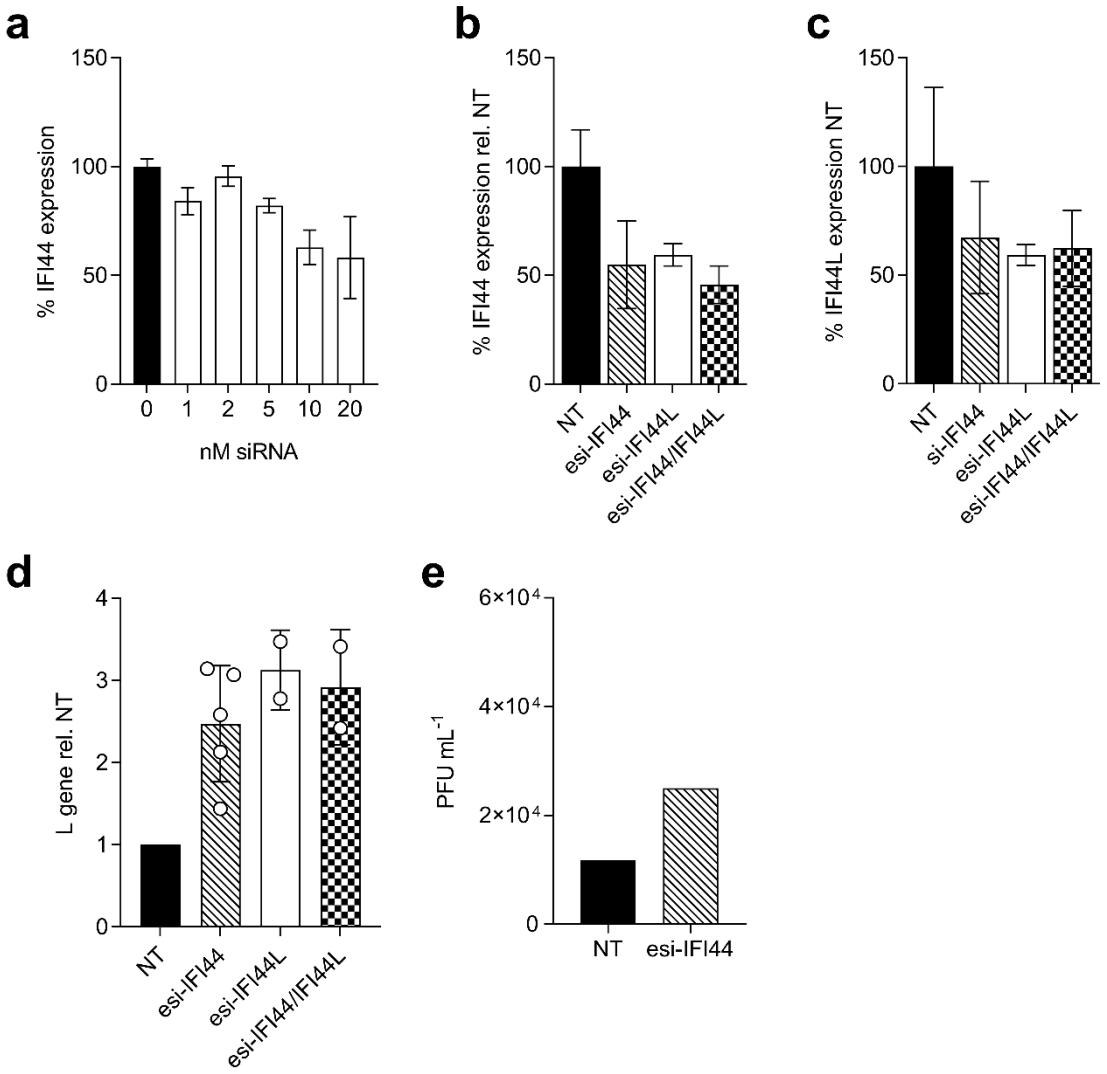

Figure 4.14. Knockdown IFI44 and IFI44L increases RSV infection. (a) A549 cells were transfected with 1-20 nM esiRNA-IFI44 (esi-IFI44) and treated with 500 IU mL^{-1} IFNα2a after 24 hours. *IFI44* expression relative to mock transfected controls was measured 48 hours after transfection. N=2. A549 cells were transfected with 50 nM esi-IFI44, esi-IFI44L, or a 1:1 combination of the two siRNA pools (esi-IFI44/IFI44L). 24 hours after transfection cells were treated with 500 IU mL^{-1} IFNα2a for 16 hours before infection with RSV A2 (m.o.i. 0.1) for a further 48 hours. **(b)** *IFI44* or **(c)** *IFI44L* expression relative to non-targeting (NT) siRNA transfected controls. N=2. **(d)** Levels of viral RNA quantified by RSV L gene qPCR. N≥2. **(e)** Viral titre in cell supernatant. N=1. Points represent the result of an independent experiment. Bars at the mean +/- SD.

4.2.13 Knockdown of IFI44 or IFI44L Alone Does not Increase RSV Infection

To improve the efficacy and specificity of the siRNA-mediated knockdown, single siRNA oligonucleotides were synthesised targeting either IFI44 or IFI44L. A549 cells were transfected with 12.5-50 nM siRNA and knockdown assessed after 48 hours. IFI44 expression was reduced >90% by either si-IFI44-1 (herein referred to as si-IFI44) or si-IFI44-2 at all concentrations (Fig 4.15a). Si-IFI44-2 also reduced IFI44L expression >90% and as such was used when targeting both genes for knockdown was required (herein referred to as si-IFI44/44L) (Fig 4.15b). Si-IFI44 was associated with a 40% knockdown of IFI44L at 25-50 nM (Fig 4.15b). IFI44L expression was not detected after transfection with 12.5 nM si-IFI44-1 which seems likely to be due to a handling error while preparing the qPCR reaction as this is the lowest concentration of si-IFI44-1 used. Si-IFI44L-1 and si-IFI44L-2 reduced IFI44L expression >80% but due to a reduced impact (~40% vs ~50%) on IFI44 expression si-IFI44L-1 (herein referred to as si-IFI44L) was selected for further use (Fig 4.15a-b). Importantly, cells transfected with non-targeting siRNA or mock transfected prior to subsequent IFN treatment and RSV A2 infection exhibited no significant difference in levels of RSV infection (Fig 4.15c). This confirmed the suitability of the control siRNA but also demonstrated an advantage of this siRNA approach over previous overexpression approaches requiring the delivery of DNA, which subsequently restricts RSV infection.

An identical approach to measure impact of siRNA on RSV infection was taken as for esiRNA, except A549 cells were transfected with siRNA at a final concentration of 12.5 nM. Here, si-IFI44 resulted in a significant reduction in IFI44 expression of >60% ($P < 0.01$, Fig 4.15d) but was also associated with increased expression of IFI44L ($P < 0.01$, Fig4.15e). si-IFI44L did not significantly impact IFI44 expression but did reduce IFI44L expression by 57% ($P < 0.05$, Fig 4.15e). si-IFI44/44L effectively reduced IFI44

and IFI44L expression by 82% ($P < 0.0001$) and 73% ($P < 0.01$) respectively (Fig 4.15d-e). Knockdown of both genes by si-IFI44/44L was associated with a significant > 3-fold increase in viral RNA levels ($P < 0.05$), whereas si-IFI44 and si-IFI44L were only associated with a slight non-significant increase (Fig 4.15f).

As overexpression of IFI44 proteins is associated with reduced cell proliferation, the proliferation of cells transfected with IFI44 or IFI44L siRNA was investigated using a colorimetric MTS assay described previously. A549 cells were transfected with 12.5 nM siRNA and treated or mock treated with 500 IU mL^{-1} IFNα2a 24 hours later. The number of viable cells were then measured by MTS assay after a further 24 hours. In the absence of IFN stimulation both si-IFI44 and si-IFI44/44L transfection was associated with significant reduction in proliferation ($P < 0.05$, Fig 4.15g). Transfection of si-IFI44L increased the number of viable cells but this was not statistically significant. The impact on viability and proliferation were not taken into account when calculating viral inoculums for the previous infectivity assay and as such the impact of si-IFI44/44L may have been exaggerated by a higher m.o.i. infection compared to NT-transfected controls. In addition, the impact of IFI44L knockdown may have been masked by infecting at a lower m.o.i. compared to NT-transfected controls.

Next, this infectivity assay was repeated using rgRSV (m.o.i. 0.1 and 0.01), with viral inoculum adjusted for cell number across different transfection conditions, and infectivity measured by flow cytometry 24 hours after infection. Knockdown efficiency was not assessed in these cells as all cells were used for flow cytometry. There was a small increase in the percentage of infected cells with si-IFI44L transfection at m.o.i. 0.1 (Fig 4.15h). At the lower m.o.i. of 0.01 there were no significant differences although both si-IFI44L and si-IFI44/44L resulted in increased infection.

It was interesting to note that si-IFI44 transfection was associated with increased levels of *IFI44L* expression during RSV infection. This may represent compensatory expression and may have hindered our ability to observe the impact of IFI44 loss on RSV infection. It would have been useful to repeat this experiment in Vero cells, to determine whether the increased induction of *IFI44L* was IFN-dependent. To further study the impact of IFI44 or IFI44L deficiency, clustered regularly interspaced short palindromic repeats (CRISPR)-CRISPR associated protein 9 (CRISPR-Cas9) gene editing was used to generate single and double knockout cell lines.

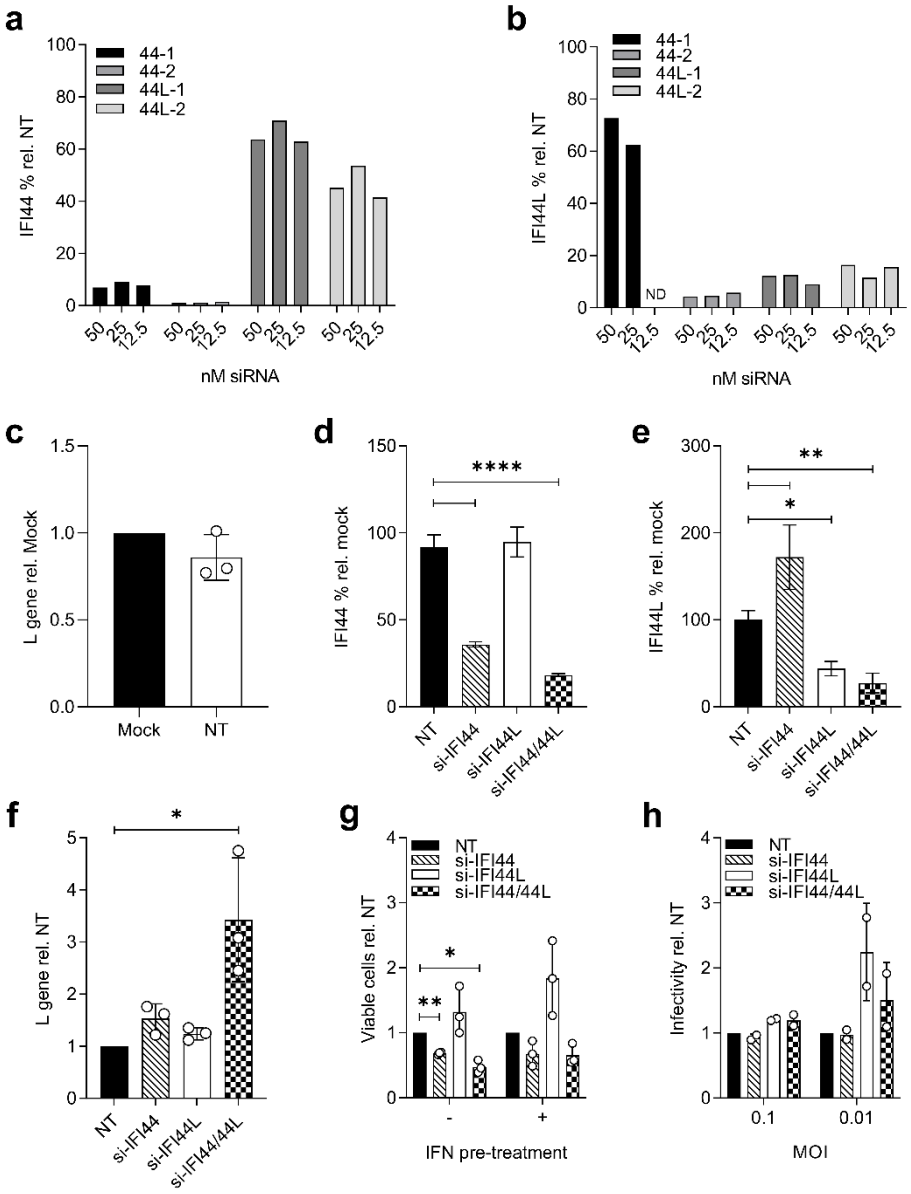

Figure 4.15 Knockdown of IFI44 or IFI44L alone is not sufficient to enhance RSV infection. A549 cells were transfected with 12.5-50 nM siRNA and 24 hours later treated with 500 IU mL^{-1} IFNα2a for 48 hours before quantifying **(a)** *IFI44* and **(b)** *IFI44L* mRNA. N=1. A549 cells were transfected with 12.5 nM si-IFI44, si-IFI44L, si-IFI44/IFI44L, or a non-targeting siRNA control (NT). 24 hours after transfection cells were treated with 500 IU mL^{-1} IFNα2a for 16 hours before infection with RSV A2 (m.o.i. 0.1) for a further 48 hours. **(c)** Infectivity of NT-transfected cells relative to mock transfected. N=3. **(d)** *IFI44* or **(e)** *IFI44L* expression relative to non-targeting (NT) siRNA transfected controls. N=3. **(f)** Levels of viral RNA quantified by RSV L gene qPCR. N=3. **(g)** Number of siRNA-transfected viable A549 cells assessed by colorimetric metabolic activity assay 24 hours after 500 IU mL^{-1} IFNα2a treatment. **(h)** A549 cells were treated as for **d-f** but infected with rgRSV (m.o.i. 0.1 or 0.01) for 24 hours. Infectivity relative to NT-transfected control. Points represent independent experiments with bars at the mean (+/- SD). Significance by ANOVA **(d-e)** or ratio paired t-test, analysis prior to data transformation. * P <0.05, ** P < 0.01, *** P < 0.001, **** P < 0.0001.

4.2.14 Generating CRISPR-Cas9 Edited Knockout Cell Lines

CRISPR-Cas9 gene editing uses a guiding RNA sequence to target a Cas9 endonuclease to a specific DNA target sequence. The guide RNA (gRNA) sequence contains 19 bp of targeting sequence which must be followed by a protospacer adjacent motif (PAM) sequence specific to the Cas9 enzyme in use. This requirement for a PAM sequence limits which genomic DNA sequences can be targeted for editing. The plasmid pSpCas9-2A-GFP (PX458) was chosen for use as this construct can encode both a single gRNA (sgRNA) along with the Cas9 enzyme and transcriptionally linked GFP for cell selection (Fig 4.16a). The Cas9 enzyme encoded by this construct was derived from *Streptococcus pyogenes* and requires a PAM sequence of NGG.

Two gRNA sequences for either *IFI44* or *IFI44L* were designed and cloned into PX458. The use of two gRNA sequences can be used to produce cells containing a specific deletion of intervening sequence but has also been shown to increase the efficacy of gene targeting [289]. *IFI44* and *IFI44L* exons were screened for PAM sequences in order to identify potential gRNA target sites. Sequences were chosen in exons 4 and 5 of *IFI44* (Fig 4.16b) and exons 3 and 4 of *IFI44L* (Fig 4.16c). The 19 bp upstream of the PAM sequences were used as gRNAs. These gRNA bordered sequence encoding a predicted GTP-binding loop. These regions of *IFI44* or *IFI44L* were targeted due to the potential relevance to functionality of the encoded proteins. It was thought that it may be possible to generate clonal cell lines with either complete gene knockout, through the introduction of a stop codon following homologous recombination, or a specific deletion of this potentially relevant region using the same gRNA sequences. The selected target sequences allowed the inclusion of a 5' G nucleotide in the gRNA sequence which has been reported to increase expression of gRNA from the human U6 promoter [290]. In addition, the selected gRNA sequences had < 50% GC content

and contained no stretches of ≥ 4 repeated nucleotides that could reduce specificity. Each gRNA sequence was found to have been previously reported in a genome-wide library of gRNA sequences, GeCKO V2 where gRNA were selected that had low predicted off-target potential [291]. gRNA sequences were screened using CRISPR Finder (https://www.sanger.ac.uk/htgt/wge/). Each selected gRNA had no predicted off-target activity against targets with 0-2 mismatches and <5 targets with 3 mismatches, apart from IFI44 gRNA 2 which had 11 predicted targets with 3 mismatches.

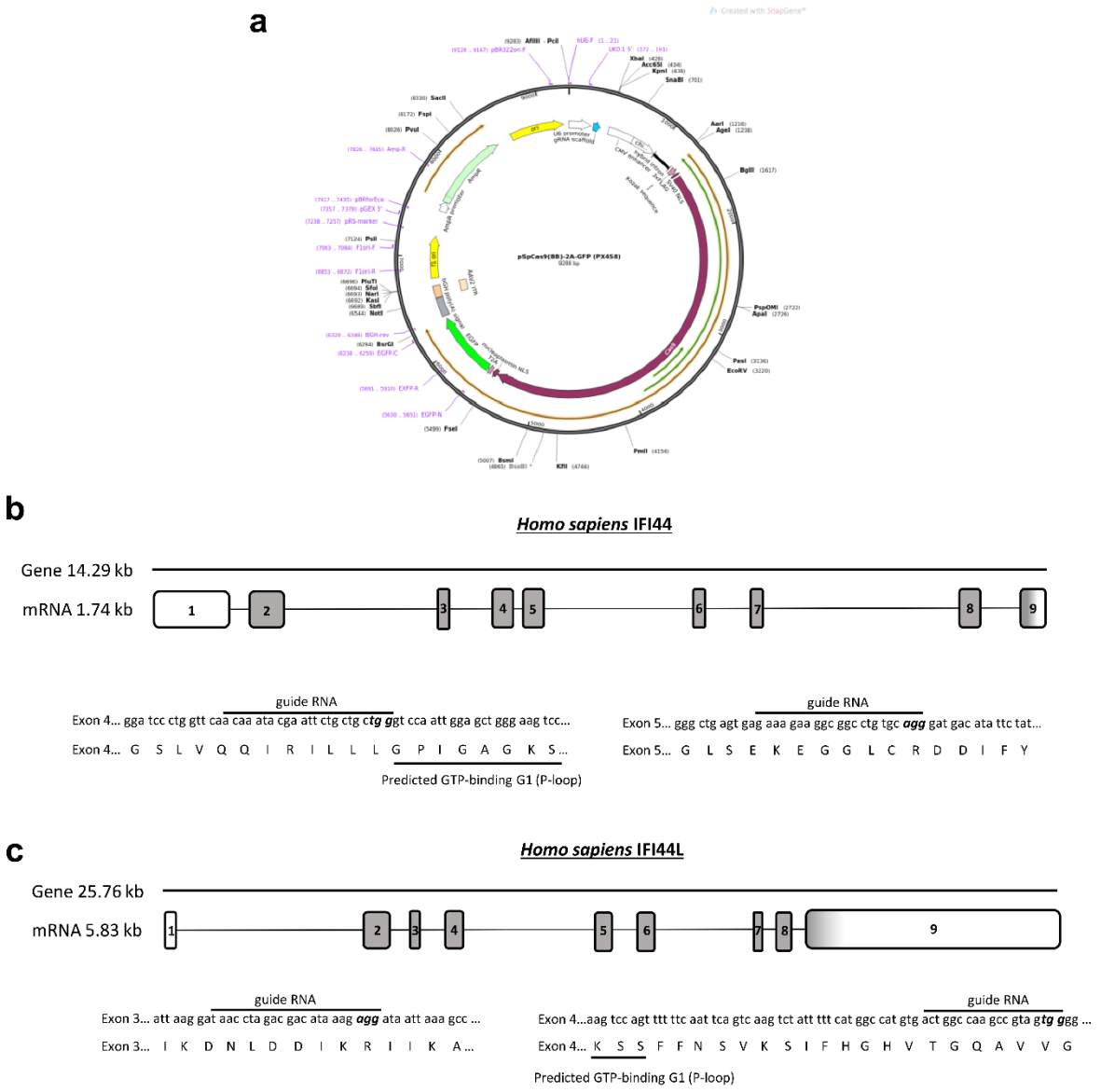

Figure 4.16. Strategy for generation of CRISPR-Cas9-edited IFI44 or IFI44L knockout cell lines. (a) Plasmid map of pSpCas9-2A-GFP (PX458). Guide RNA sequences were cloned into this vector downstream of a U6 promoter and gRNA scaffold sequence. **(b)** *IFI44* or **(c)** *IFI44L* mRNA organisation and regions of exons targeted by gRNA sequences with encoded amino acid residues below. Exons are shown as boxes, shaded to show translated regions versus untranslated regions (white). Predicted GTPase G1 motif in each protein is highlighted.

Insertion of gRNA sequences to generate PX458-IFI44-1, PX458-IFI44-2, PX458-IFI44L-1, and PX458-IFI44L-2 was confirmed by Sanger sequencing. HEp-2 cells were then transfected with either PX458 alone, PX458-IFI44-1 and PX458-IFI44-2, or PX458-IFI44L-1 and PX458-IFI44L-2. GFP expression was observed in all transfected cells which was assumed to coincide with Cas9 expression (Fig 4.17a). To generate clonal cell lines with the greatest potential for gene-editing to have taken place, cells with the top 2% GFP fluorescence were sorted as single cells into 2 96-well plates (Fig 4.17b). The approach and design of gRNA sequences was initially validated using HEp-2 cell lines and then subsequently used to develop knockout A549 cell lines for assessing any impact on RSV infection.

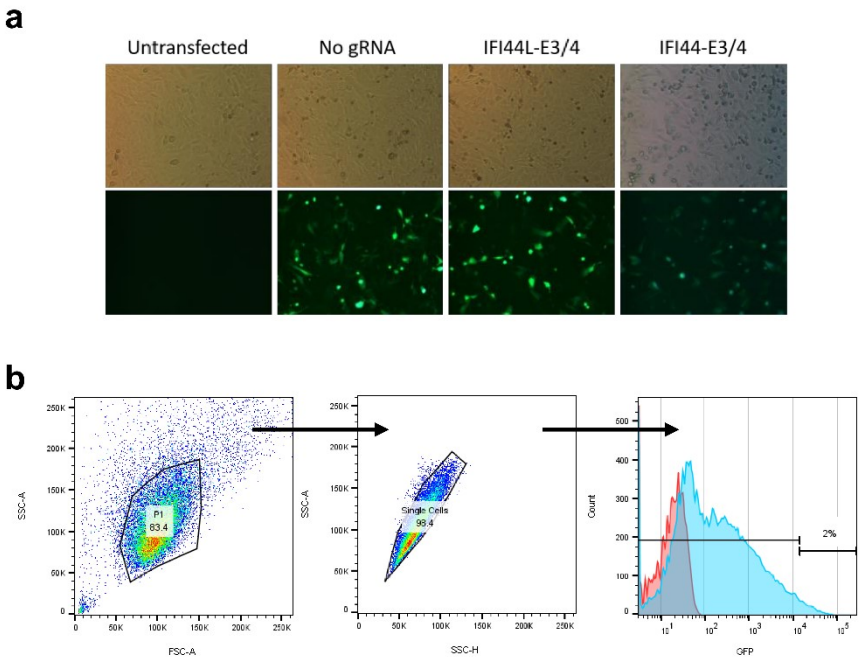

Figure 4.17. PX458 transfection and FACS sorting. (a) HEp-2 cells were transfected with PX458 constructs containing the noted gRNA sequences. GFP fluorescence imaged 24 hours after infection. **(b)** Example of isolation of PX458-transfected cells with the top 2% GFP fluorescence levels. A majority population was gated initially to remove debris prior to doublet exclusion.

4.2.15 Validation of HEp-2 Knockout Cell Lines

To validate on-target activity of Cas9 in expanded clones, genomic DNA was extracted, and the region targeted for editing was amplified by PCR. The primers for this reaction were designed to amplify a wild-type amplicon of 648 bp (*IFI44*) or 1228 bp (*IFI44L*), including both intronic and exonic sequence (Fig 4.18a). HEp-2 cells are diploid cell lines and so the complete loss of a wild-type amplicon was used to identify clones with biallelic gene-editing activity. A single ΔIFI44 clone (Fig 4.18b) and three ΔIFI44L (Fig 4.18c) clones were identified which did not amplify a WT amplicon. Each clone amplified a single product of either 200 (*IFI44*) or 300 (*IFI44L*) bp suggesting Cas9 activity had resulted in bi-allelic deletions in each clone.

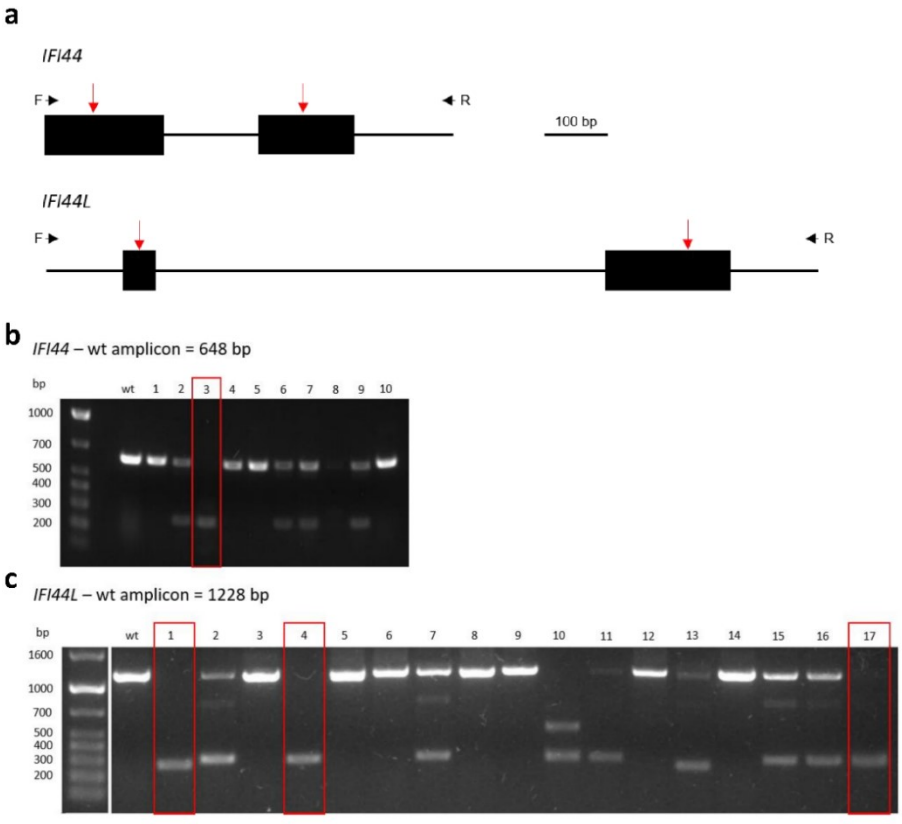

Figure 4.18. Screening HEp-2 clonal cell lines for CRISPR-Cas9 editing activity. (a) Graphical representation of Cas9-targeted regions of *IFI44* (top) and *IFI44L* (bottom). Exons are represented by black rectangles connected by intronic sequence (black line). gRNA targets are highlighted by red arrows. Black arrows are PCR primer locations. Targeted regions of **(b)** *IFI44* or **(c)** *IFI44L* genomic DNA were amplified by PCR using the primers in **a**. Clonal populations with loss of the WT amplicon are highlighted with red boxes.

The mutant amplicon products were then sequenced by Sanger sequencing (Eurofins Genomics). Analysis of HEp-2 ΔIFI44 #3, ΔIFI44L #4, and ΔIFI44L #17 amplicons was not possible due to poor sequencing quality. The HEp-2 ΔIFI44L #1 amplicon contained sequence from both exon 3 and exon 4 of *IFI44L* (Fig 4.19). Compared to WT sequence this amplicon revealed a deletion event that removed the intronic sequence between exon 3 and 4, as well as the majority of exon 4 sequence. Overall these changes were predicted to encode a mutant IFI44L protein with an altered stretch of residues (160-169) followed by a large deletion (170-241). The changes to the starting codons of exon 3 and exon 4 may also disrupt splicing of the transcript and the resulting protein product.

At the time of this work antibodies to detect endogenous IFI44 or IFI44L proteins were not available. Validation of protein loss and additional sequencing data is required to properly validate these modified HEp-2 cells for use. Preferably a next-generation sequencing approach would be employed to accurately determine sequences of each gene copy present and investigate any off-target effects. However, this project was successful at establishing the workflow required to isolate Cas9-edited clonal cell lines and confirmed the on-target effect of the selected gRNA sequences. This process was further refined during the development of A549 knockout cell lines.

HEp-2 ΔIFI44L clone #1

Genomic DNA sequencing

***IFI44L* Exon 3**

Wild-type	GA ATT AAG GAT AAC CTA GAC GAC ATA AAG AGG ATA ATT AAA GCC AGA GA
ΔIFI44L #1	TG CTA TGT TTA TTT CCT ATA GGA ATA AA-

***IFI44L* Exon 4**

Wild-type	G CAC AGA AAT AGG CTT CTA GCA GAC ATC AGA GAC TAT AGG CCC TAT GCA GAC TTG GTT TCA GAA ATT CGT ATT CTT TTG GTG GGT CCA GTT GGG TCT GGA AAG TCC AGT TTT TTC AAT TCA GTC AAG TCT ATT TTT CAT GGC CAT GTG ACT GGC CAA GCC GTA GTG GGG TCT GAT ATC ACC AGC ATA ACC GAG CGG
ΔIFI44L #1	…C ACC AGC ATA ACC GAG CGG

IFI44L Protein

Wild-type	aa160-241	GIKDNLDDIKRIIKAREHRNRLLADIRDYRPYADLVSEIRILLVGPVGSGKSSFFNSVKSIFHGH VTGQAVVGSDITSITER	
ΔIFI44L #1	aa160-176	VLCLFPIGINTSITER	65 residue deletion

Figure 4.19. Sequence analysis of HEp-2 ΔIFI44L clone #1. Genomic DNA sequencing of a single amplicon isolated from the CRISPR-Cas9 targeted region of *IFI44L*. The gRNA target sequence is highlighted in red. Altered bases are underlined, hyphens indicate gaps in the sequence. All sequence shown is exonic.

4.2.17 Generation and Validation of A549 Knockout Cell Lines

Clonal A549 KO cells were selected as described previously, with the addition of cells transfected with PX458-IFI44-1 and PX458-IFI44L1 to generate A549 ΔIFI44ΔIFI44L cell lines. Unlike HEp-2 cells, A549 cells are commonly polyploid. As such, when the targeted genomic region was amplified by PCR neither ΔIFI44 or ΔIFI44L clones amplified just a single mutant amplicon. However, the presence of a mutant band at all suggested that the cells had harboured active, targeted Cas9 enzyme following transfection and so the larger WT amplicon seen in each clone may still contain edited sequence. A549 ΔIFI44ΔIFI44L clones were selected that contained neither WT or

mutant amplicons of either *IFI44* or *IFI44L* (Fig 4.20). Five ΔIFI44, 2 ΔIFI44L, and 3 ΔIFI44ΔIFI44L clones were chosen for further study (Fig 4.20).

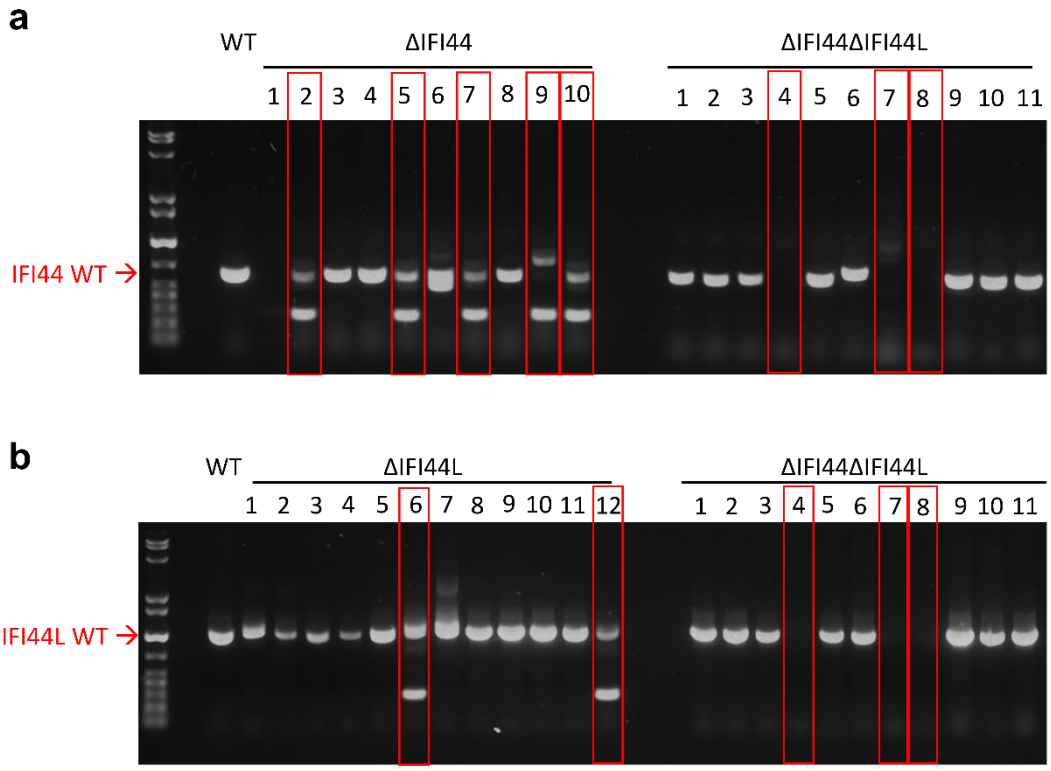

Figure 4.20. Screening A549 clonal cell lines for CRISPR-Cas9 editing activity. (a) *IFI44* or **(b)** *IFI44L* genomic DNA were amplified by PCR from WT, ΔIFI44, ΔIFI44L, and ΔIFI44ΔIFI44L cell lines. Clonal populations with either complete loss of the WT amplicon or appearance of a smaller band, suggestive of CRISPR-Cas9 editing activity, are highlighted with red boxes.

The selected clones and the parental polyclonal WT cells were treated with 1000 IU mL^{-1} IFNα2a for 24 hours and expression of IFI44 and IFI44L assessed by qPCR and Western blotting. There were no significant differences in *IFI44* transcript levels in all ΔIFI44 clonal lines (Fig 4.21a), although there was a non-significant reduction of 40-50% in #5 and #10. There was also no significant difference in *IFI44L* transcript levels in either ΔIFI44L clone (Fig 4.21b), although there was a non-significant 100% increase in #6 and a 50% decrease in #12. The CRISPR-Cas9 approach did not aim to remove the entire coding sequence of either gene and so transcription may carry

on regardless of gene editing. WT cells expressed detectable levels of either IFI44 or IFI44L protein suggesting requisite IFN stimulation (Fig 4.21c). None of the ΔIFI44 or ΔIFI44L clones expressed detectable levels of IFI44 or IFI44L respectively. Expression of either IFI44 or IFI44L was undetectable in each ΔIFI44ΔIFI44L clone.

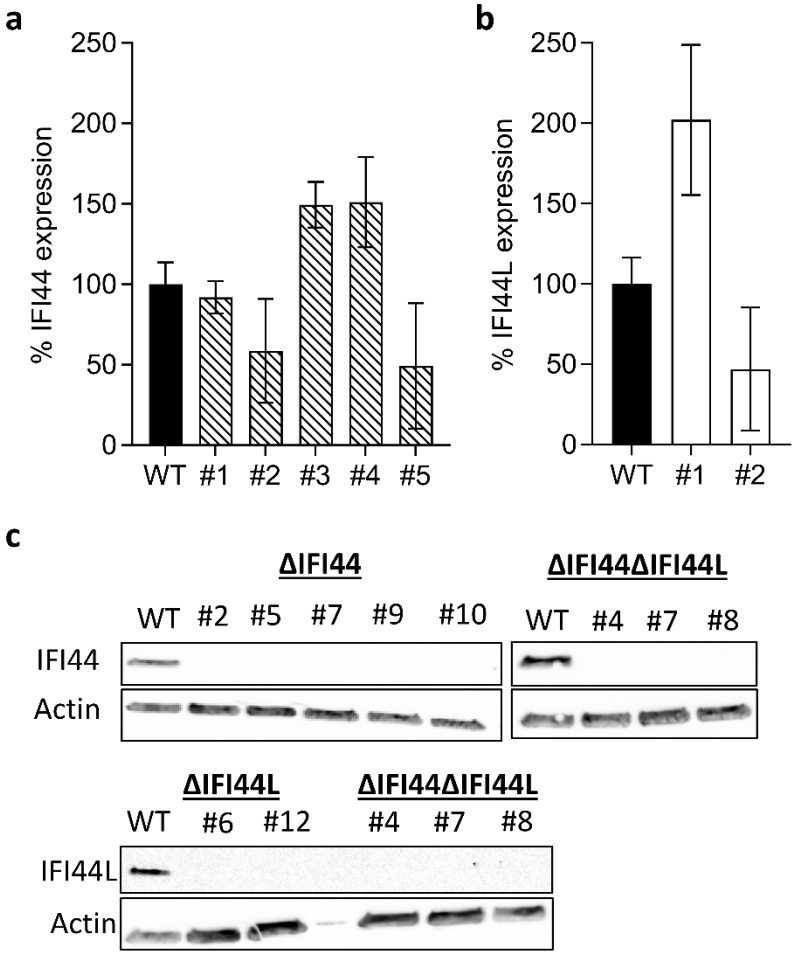

Figure 4.21. IFI44 and IFI44L expression in A549 CRISPR-Cas9-edited cell lines. Candidate A549 CRISPR-Cas9-edited cell lines were treated with 1000 IU mL^{-1} IFNα2a for 24 hours and **(a)** *IFI44* or **(b)** *IFI44L* mRNA expression quantified relative to parental WT cells by qPCR. Bars at the mean +/- SEM. N=2. **(c)** Candidate A549 CRISPR-Cas9-edited cell lines were treated as above and IFI44 and IFI44L protein expression assessed by Western blotting. N=1. Significance by ANOVA.

A549 ΔIFI44 #5 and ΔIFI44L #12 clonal lines were further validated by sequencing. As before, primers amplifying the targeted region of either *IFI44* or *IFI44L* were used to produce genomic DNA for sequencing (Fig 4.22a). PCR of genomic DNA from the selected A549 ΔIFI44 clone only amplified a single WT *IFI44L* band, suggesting that no deletion event had occurred in this gene when using *IFI44*-targeting gRNA. Similarly, the A549 ΔIFI44L #12 clone only showed a single WT *IFI44* amplicon. Sequencing of these WT amplicons further confirmed that no gene editing had taken place in the gene which was not targeted (data not shown). However, this analysis cannot address the potential for other off-target sequence edits.

Analysis of the larger of the two *IFI44* amplicons from A549 ΔIFI44 #5 revealed extensive changes to the sequence immediately downstream of the gRNA-1 (exon 4) target resulting in the formation of several exonic in-frame stop codons (Fig 4.22b). This allele was predicted to produce a protein product of 218 amino acids, with the final 27 residues different from the WT protein. The smaller amplicon revealed a deletion event had taken place which also resulted in a frameshift and stop codon formation. This allele was predicted to encode a 198 amino acid product maintaining the first 190 amino acids of the WT IFI44 protein. However, this sequencing cannot confirm whether additional edits took place in the gene sequence resulting in further aberrations in protein expression. A polyclonal antibody mixture was used to detect IFI44 expression. The immunogen for these antibodies was a recombinant peptide consisting of residues 311-408. As such, these data could not confirm whether or not this cell line produces a truncated IFI44 protein of less than 311 residues in length.

Analysis of the larger of the two *IFI44L* amplicons from A549 ΔIFI44L #12 suggested a frameshift mutation had occurred immediately following the target sequence for IFI44L gRNA-1 (exon 3) resulting in stop codon formation (Fig 4.22c). This allele was

predicted to encode a protein product of 178 amino acids, maintaining the first 168 residues of WT IFI44L protein. The second smaller amplicon identified a deletion event had occurred between the two gRNA-targeted sequence regions in exon 3 and exon 4. This was predicted to result in a protein product of 391 residues, lacking residues 169-230. However, this analysis was unable to predict the effect of the deletion of the intervening intronic sequence on transcript splicing and subsequent translation. A monoclonal antibody raised using a peptide consisting of the N-terminal 50 residues of IFI44 was used to demonstrate lack of protein expression in this clone. This antibody has been validated previously and IFI44 protein was detectable in comparably treated parental WT cells. As such, this antibody could bind truncated proteins maintaining N-terminal sequence. These data suggest that A549 ΔIFI44L #12 is a functional *IFI44L* knockout.

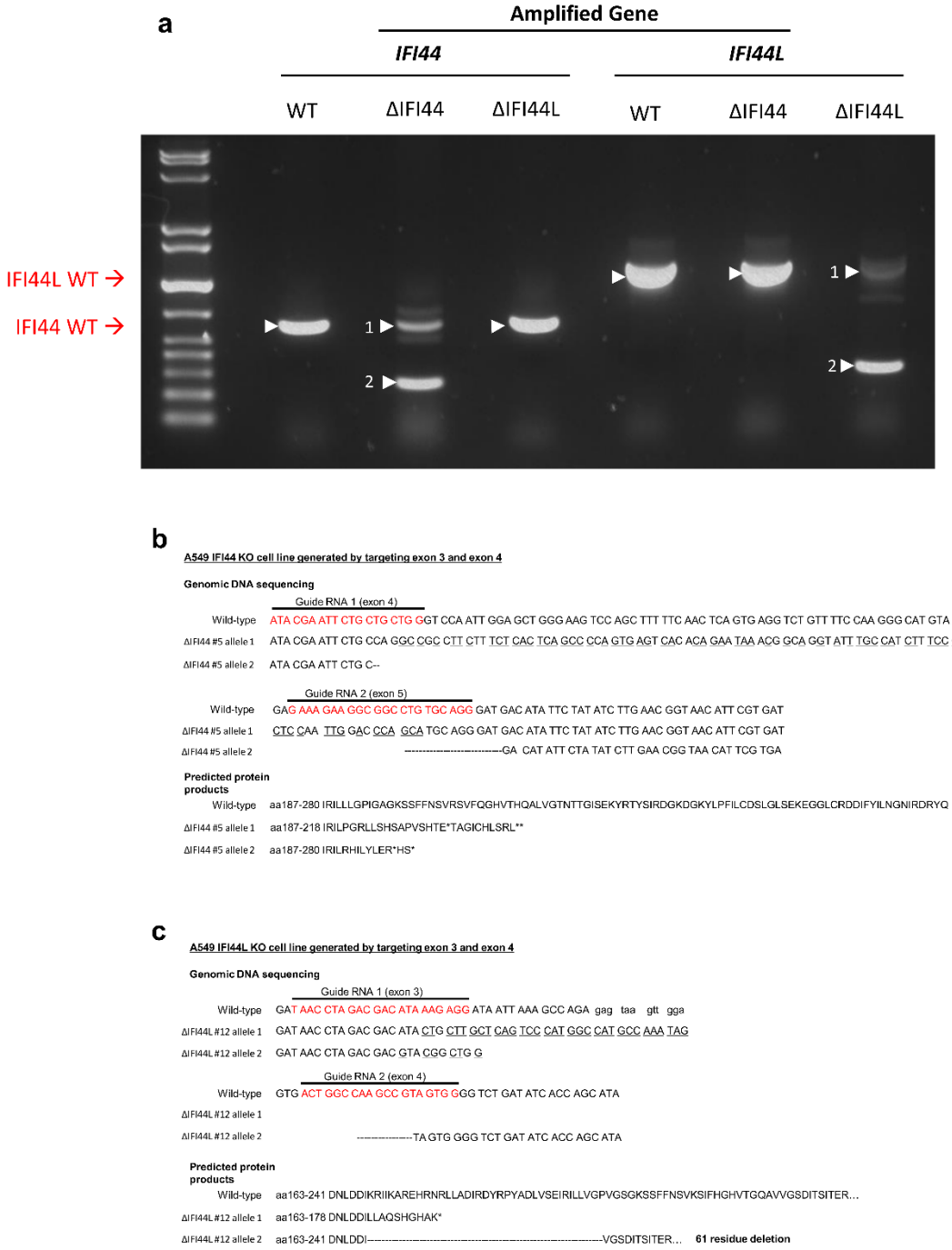

Figure 4.22. Sequence analysis of A549 ΔIFI44 and ΔIFI44L cell lines. (a) CRISPR-Cas9-targeted regions of *IFI44* and *IFI44L* genomic DNA were amplified by PCR in WT, ΔIFI44, and ΔIFI44L cell lines. The bands highlighted by white arrows were isolated for sequencing. Numbers correspond to allele number in **b-c**. Genomic DNA sequencing of amplicons isolated from the CRISPR-Cas9 targeted region of **(b)** *IFI44* and **(c)** *IFI44L* in the corresponding KO clones. The gRNA target sequence is highlighted in red. Altered bases are underlined, hyphens indicate gaps in the sequence. Intronic sequence is in lowercase. * = predicted translational stop.

4.2.18 Knockout of IFI44 or IFI44L Increases Cell Proliferation

Proliferation of sequenced single gene KO clones A549 ΔIFI44 #2 and A549 ΔIFI44L #2 was compared to parental WT A549 cells, along with A549 ΔIFI44ΔIFI44L #3. Even in the absence of IFN-I treatment, over 48 hours in culture each KO cell line demonstrated increased proliferation relative to WT cells by MTS assay ($P < 0.05$, Fig 4.23a). Manual counting also confirmed that each cell line expanded at a faster rate than WT cells, although this was only statistically significant for A549 ΔIFI44L #2 (Fig 4.23b). Interestingly, this suggested that basal levels of IFI44 and IFI44L are relevant for cell proliferation, although these data cannot rule out clonal differences being the cause of altered proliferation. When cells were treated with 500 IU mL^{-1} IFNα2a, and viable cell number determined over the following 48 hours, only the ΔIFI44L and ΔIFI44ΔIFI44L clones expanded at a faster rate than WT cells (Fig 4.23c). This may be as the IFI44L present in the ΔIFI44 clone was sufficient to maintain proliferation rates relative to WT cells. As seen with IFI44 knockdown previously, levels of IFI44L may be elevated in these cell lines following IFN-I treatment. The same effect on IFI44 in the absence of IFI44L has not been observed. Cytotoxicity was not increased in any knockout clone (Fig 4.23d). Following IFN-I treatment and 24 hours of RSV infection (m.o.i. 0.1), there was no significant difference in levels of *MX1* RNA in any KO cell line, although there was a trend towards reduced expression in cells lacking *IFI44L* (Fig 4.23e).

The altered proliferation rates of the selected KO clones further corroborate the reported anti-proliferative function of IFI44 and IFI44L and suggests that basal levels are capable of influencing proliferation in A549 cells.

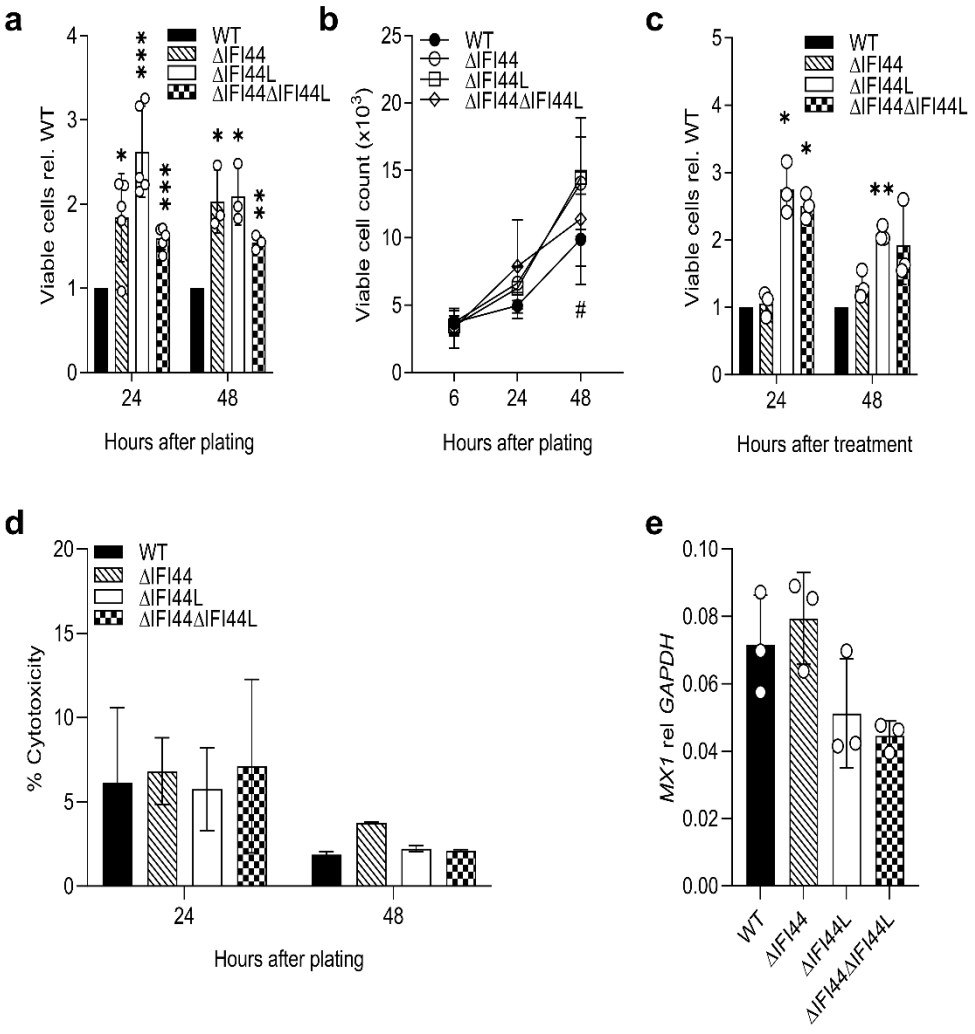

Figure 4.23. IFI44 and IFI44L knockout increases cellular proliferation. (a) A549 WT, ΔIFI44, ΔIFI44L, or ΔIFI44ΔIFI44L cell lines were seeded at equal densities and viable cell number quantified by a metabolic activity assay after 24-48 hours or **(b)** by trypan blue exclusion after 6-48 hours (# = ΔIFI44L rel. WT). **(c)** A549 WT, ΔIFI44, ΔIFI44L, or ΔIFI44ΔIFI44L cell lines were seeded at equal densities and treated with 500 IU mL^{-1} IFNα2a after 6 hours. Viable cell number was quantified 24-48 hours after treatment by metabolic activity assay. **(d)** Cytotoxicity was assessed in WT and ΔIFI44, ΔIFI44L, or ΔIFI44ΔIFI44L A549 cell lines by LDH release assay 24-48 hours after plating. N≥2. **(e)** *MX1* RNA after 16 hours IFNα2a treatment and 24 hours RSV A2 (m.o.i. 0.1) infection. Bars at the mean +/- SD, **a**, **c, e** points represent individual experiments. **b** points at the mean +/- SD. Significance to WT controls by ratio paired t-test (**a-c**) prior to data transformation, or ANOVA (d). */# = P < 0 .05, ** P < 0.01, *** P < 0.001.

4.2.19 Knockout of IFI44 or IFI44L Increases Cell Susceptibility to RSV Infection

RSV infection was assessed in A549 ΔIFI44 #5, A549 ΔIFI44L #12, A549 ΔIFI44ΔIFI44L #8, and parental WT cells. First, cells were treated with 500 IU mL^{-1} IFNα2a prior to infection with rgRSV for 24 hours (m.o.i. 0.1/0.01). There was a significant increase in the percentage of detectably infected cells (GFP^+) in ΔIFI44 cells at either m.o.i. 0.1 or m.o.i. 0.01 ($P < 0.05$, Fig 4.24a). There was only a ~5% increase in the percentage of infected ΔIFI44L cells at m.o.i. 0.1 ($P < 0.05$) and a 2-fold increase at m.o.i. 0.01, although this was not significant after just 2 independent experiments. The mean percentage of infected ΔIFI44ΔIFI44L cells was comparable to that of ΔIFI44 cells at either m.o.i., although the increase relative to the WT cells was not statistically significant.

Next, A549 KO cell lines and parental WT controls were infected with RSV A2 (m.o.i. 0.1) following IFN-I treatment and levels of viral RNA assessed after 24 hours. Here, each KO cell line was associated with significant increases in viral RNA > 1.5-fold ($P < 0.05$, Fig 4.24b). The loss of both IFI44 and IFI44L was not associated with a further increase in viral RNA relative to the single gene KO cell lines. After 48 hours RSV A2 infection, levels of live virus in the cell supernatant was quantified by plaque assay. Each KO cell line was associated with elevated viral titre, although this was only statistically significant for ΔIFI44L and ΔIFI44ΔIFI44L clones ($P < 0.05$, Fig 4.24c). Viral titre was highest following infection of the double gene KO cell line.

HEp-2 parental WT cells, HEp-2 ΔIFI44 #3, and HEp-2 ΔIFI44L #1 were infected with RSV A2 (m.o.i. 0.1) for 24 hours after 16 hours IFNα2a treatment (500 IU mL^{-1}). Levels of viral RNA were increased over 2-fold in HEp-2 ΔIFI44L #1 cells in this one experiment (Fig 4.24d).

Overall these data corroborate previous observations using siRNA-mediated knockdown, that loss of either IFI44 or IFI44L is associated with increased RSV RNA during infection. These data also report an increase in viral titre during infection of ΔIFI44 or ΔIFI44ΔIFI44L cells. Intriguingly, there was no consistent observation of whether or not loss of both genes further enhanced susceptibility of cells to infection.

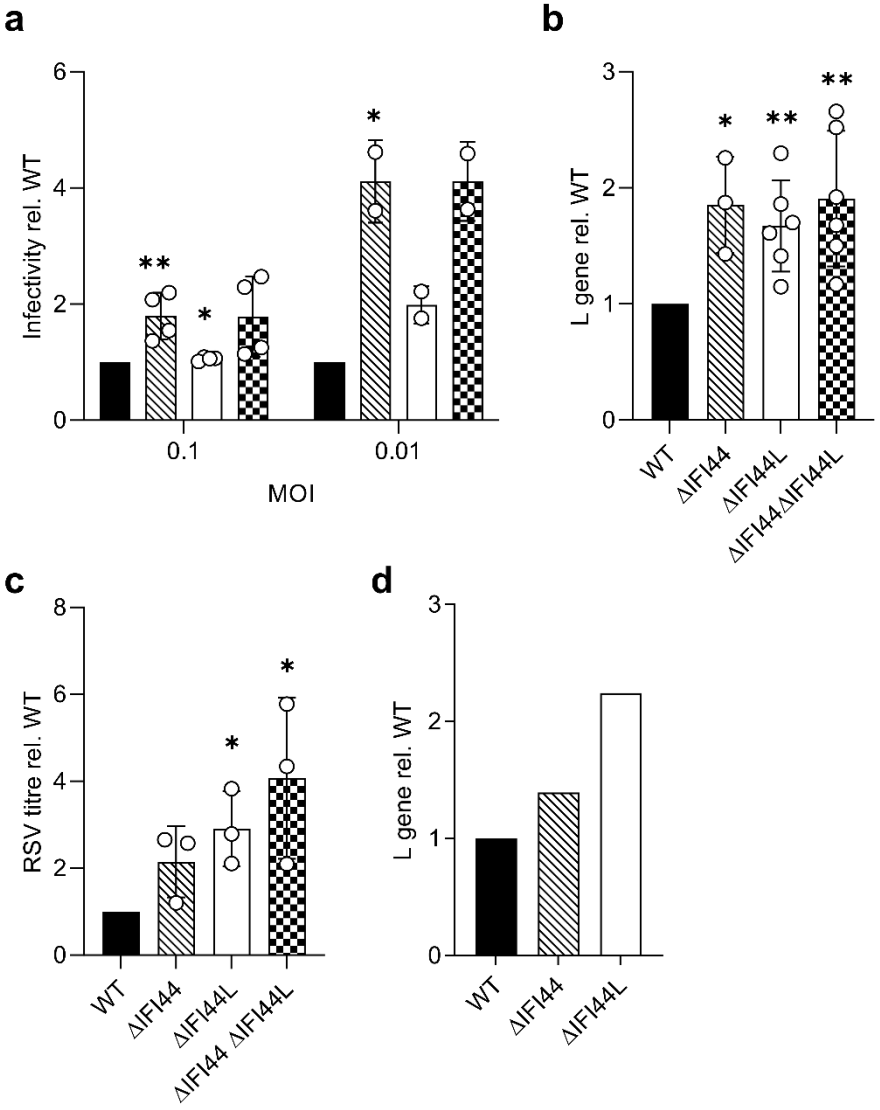

Figure 4.24. RSV infection is enhanced in IFI44 and IFI44L knockout cell lines. A549 WT, ΔIFI44, ΔIFI44L, or ΔIFI44ΔIFI44L cell lines were treated with 500 IU mL^{-1} IFNα2a for 16 hours prior to infection with **(a)** rgRSV (m.o.i. 0.1 or 0.01) for 24 hours. Infectivity relative to vector control by assessing the proportion of RSV-infected cells. **(b)** WT and KO A549 cells were treated as for **a** and infected with RSV A2 (m.o.i. 0.1) for 24 hours. Viral RNA assessed by RSV L gene qPCR. **(c)** WT and KO A549 cells were treated and infected as for **b**, levels of viral titre in cell supernatant was assessed 48 hours after infection. **(d)** HEp-2 WT, ΔIFI44, and ΔIFI44L cell lines were treated with 500 IU mL^{-1} IFNα2a for 16 hours prior to infection with RSV A2 (m.o.i. 0.1) for 24 hours. Viral RNA assessed by RSV L gene qPCR. N=1. Points represent independent experiments with a bar at the mean +/- SD. Significance to WT controls by ratio paired t-test, prior to data transformation. * $P < 0.05$, ** $P < 0.01$.

4.2.20 IFI44 and IFI44L Impact Influenza Infection *in Vitro*

Work presented in this chapter has developed effective tools to investigate the impact of IFI44 and IFI44L during viral infection *in vitro*. These stably transduced and gene KO cell lines were next used to investigate any impact of IFI44 or IFI44L during influenza infection. Like RSV, influenza is a respiratory RNA viral infection with public health relevance. Influenza infection is responsible for significant morbidity and mortality around the world [2]. However, there are key differences between the life cycles of these two viruses. Influenza predominantly enters host cells via the endocytic pathway [292], whereas RSV is thought to utilise both direct plasma membrane fusion and endocytic uptake. In addition, influenza has a segmented genome that is replicated in the nucleus and not the cytoplasm [292]. These differences may preclude different ISG effectors from being able to restrict infection of both viruses.

Stably transduced clonal cell lines were infected with influenza (H1N1, A/England/195/2009) at an m.o.i. of 0.8 or 0.1 for 24 hours. Levels of influenza M gene RNA were reduced more than 50% at either m.o.i. in IFI44 expressing cells relative to Vector transduced controls, although this was not statistically significant over two independent experiments (Fig 4.25a). Interestingly, there was no clear trend in IFI44L expressing cells. A549 KO clonal cell lines were pre-treated with 500 IU mL^{-1} IFNα2a for 16 hours prior to influenza infection (m.o.i. 0.1). After 48 hours of infection, levels of viral RNA in ΔIFI44 and ΔIFI44L cells were comparable to WT controls. Knockout of both IFI44 and IFI44L was associated with a significant 4-fold increase in levels of M gene RNA relative to WT controls ($P < 0.01$, Fig 4.25b). This may suggest IFI44 and IFI44L mediate redundant roles during influenza infection. It would have been interesting to assay infection in stably transduced Vero cells to confirm whether

overexpression of IFI44, in the absence of a complete IFN-I and ISG response, was capable of restricting influenza infection.

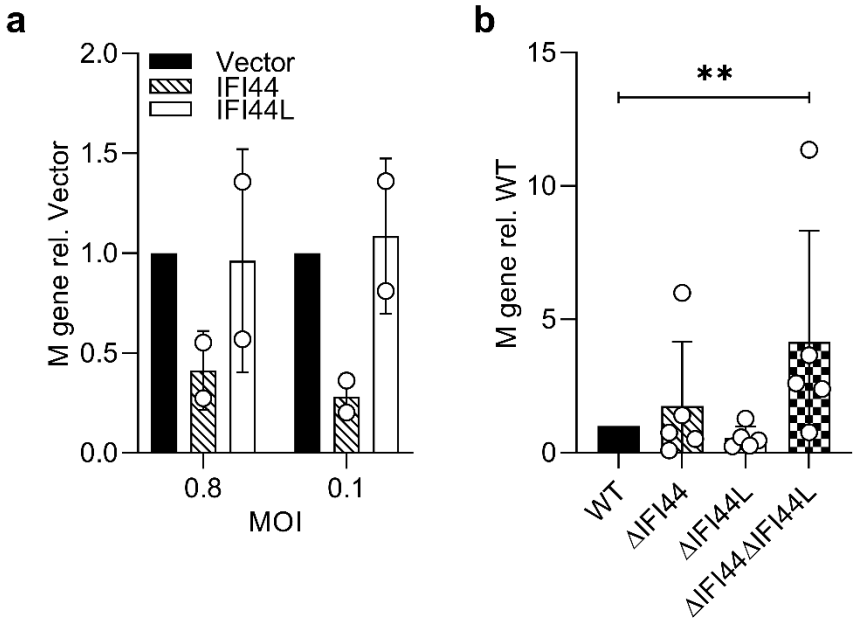

Figure 4.25. Impact of IFI44 and IFI44L during influenza infection. (a) Stably transduced A549 cell lines were infected with influenza (H1N1, A/England/195/2009) at m.o.i. 0.1 for 24 hours. Levels of viral RNA assessed by influenza M gene qPCR. **(b)** A549 WT, ΔIFI44, ΔIFI44L, or ΔIFI44ΔIFI44L cell lines were treated with 500 IU mL^{-1} IFNα2a for 16 hours prior to infection with influenza as for **a**. Levels of viral RNA were assessed after 48 hours by influenza M gene qPCR. Points represent independent experiments with a bar at the mean +/- SD. Significance to vector or WT controls by ratio paired t-test prior to data transformation. ** $P < 0.01$.

4.2.21 IFI44 and IFI44L Impact an Early Point of RSV Infection

Previous assays have taken a snapshot of infection after 24 or 48 hours. To determine where in the viral life cycle IFI44 and IFI44L impact on RSV infection, it was important to get a better understanding of infection kinetics and study infection at different time points.

A549 cells were infected with rgRSV (m.o.i. 0.1) for 8-32 hours before flow cytometry analysis of GFP expression (Fig 4.26a). After 8 hours 9.04% of cells were GFP^+. These infected cells had only low levels of GFP^+ expression. By 24 hours, the percentage of GFP^+ cells had increased to 39.1%. Here there was a broad distribution of GFP fluorescence with some cells having very low expression as at 8 hours of infection, and a clear population with high levels of expression. It was not possible to determine whether the cells with low levels of GFP fluorescence after 24 hours represented newly infected cells. After 32 hours, the spread of GFP fluorescence was more uniform than at 24 hours. This may be due to initially infected cells releasing new virions, increasing the number of newly infected cells and reducing the proportion of cells with high levels of GFP expression.

To investigate the impact of IFI44 and IFI44L within the first replication cycle of RSV, infection in stably transduced cell lines was assessed after 8 hours. IFI44 expression was associated with a significant reduction in the percentage of infected cells 8 hours after infection (Fig 4.26b-c). This reduction was comparable to that seen previously at 24 hours. The impact of IFI44L was not statistically significant, although the percentage of infected cells was reduced by >40%. These data suggest that both IFI44 and IFI44L can impact early stages of infection prior to the release of progeny virions and a second round of infection.

To further investigate this, HEp-2 KO clonal cell lines were treated with 500 IU mL^{-1} IFNα2a for 16 hours and subsequently infected with rgRSV (m.o.i. 3) for 6 hours. Infection was assessed by microscopy, whereby the number of GFP^+ cells were counted in four randomly selected fields of view (f.o.v.). In this single experiment, both ΔIFI44 and ΔIFI44L cell lines had increased numbers of infected cells, further suggesting that IFI44 and IFI44L can impact RSV infection at an early stage *in vitro* (Fig 4.26d).

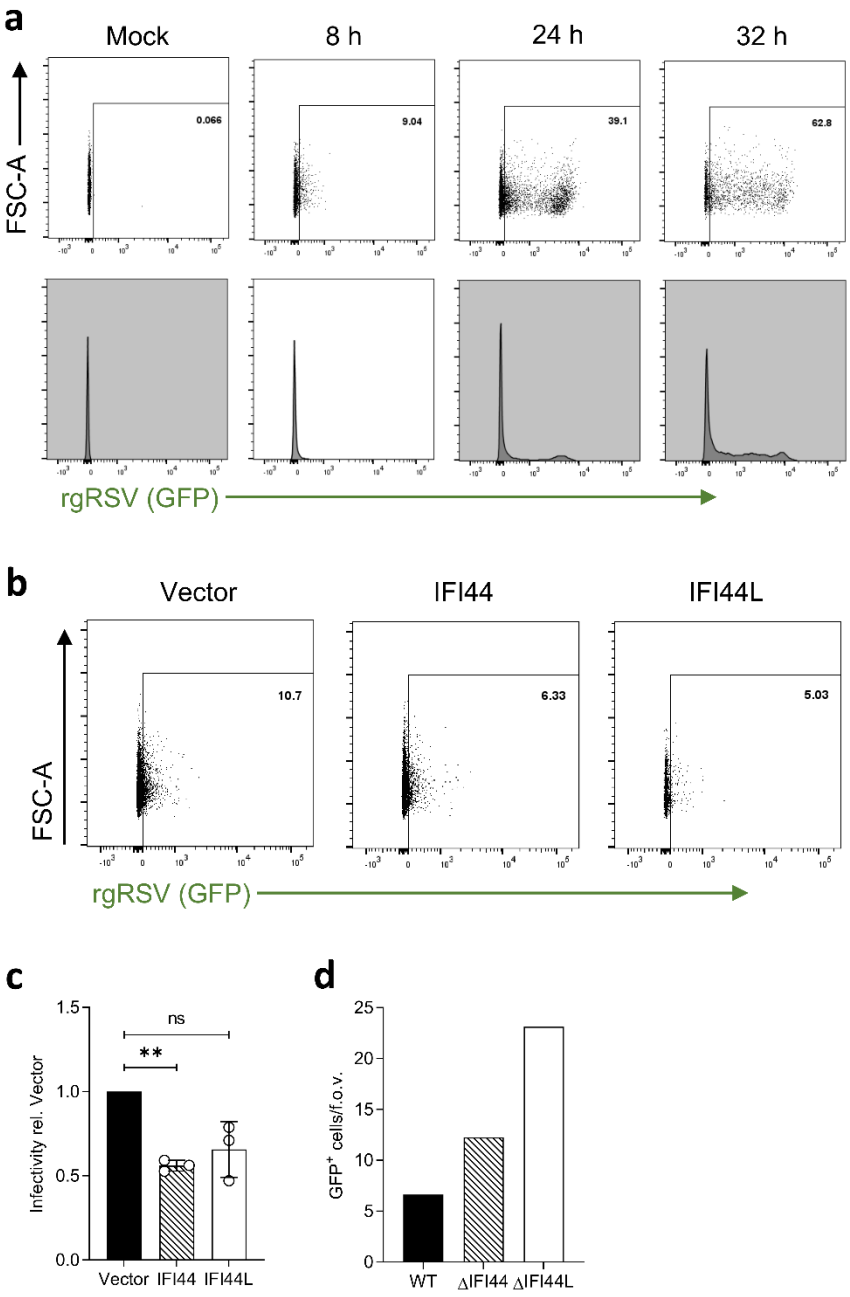

Figure 4.26. IFI44 and IFI44L impact an early stage of RSV infection. (a) A549 cells were infected with rgRSV (m.o.i. 0.1) and the proportion of infected cells assessed by flow cytometry after 8-32 hours. Dot plots show GFP fluorescence of single cells with respective histograms below. **(b)** Stably transduced A549 cell lines were infected with rgRSV (m.o.i. 0.1) for 8 hours. Dot plots show GFP fluorescence of single cells. Representative plots from 3 independent experiments, quantified in **c**. N=3. **(d)** HEp-2 WT, ΔIFI44, and ΔIFI44L cells were treated with 500 IU mL^{-1} IFNα2a for 16 hours and then infected with rgRSV (m.o.i. 3) for 6 hours. The number of GFP^+ cells were assessed manually using a fluorescence microscope and. Four random fields of view (f.o.v.) were counted for each cell line, data presented as the mean. N=1. Points represent independent experiments, with a bar at the mean +/- SD. Significance to vector controls by ratio paired t-test, prior to data transformation. ** $P < 0.01$. ns = not significant.

4.2.22 IFI44 and IFI44L Do Not Impact RSV Attachment

A cold-bind assay was used to determine whether IFI44 or IFI44L interfere with RSV attachment to the surface of target cells. Cells were incubated with RSV A2 (m.o.i. 2) for 1 hour at 4°C, where virions can bind the cell surface but are not internalised. After 1 hour unbound inoculum were removed by three washes with ice-cold PBS. IFI44 and IFI44L-expressing cell lines had comparable levels of viral RNA bound to the cell surface as vector transduced controls, suggesting these ISGs do not affect virus binding (Fig 4.27). Levels of detectable RSV RNA in each clonal cell line were comparable to the parental WT cells. For additional confirmation it would have been interesting to analyse RSV protein levels instead of total L gene RNA.

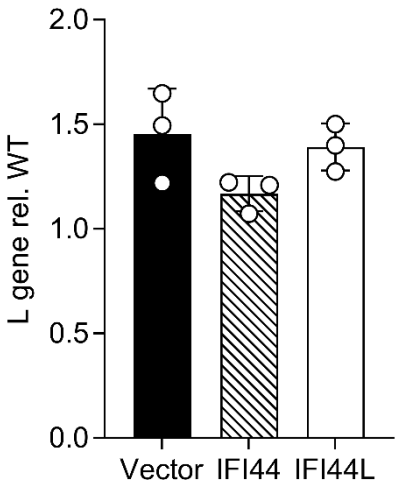

Figure 4.27. IFI44 and IFI44L do not impact RSV cell attachment. Stably transduced A549 cell lines were incubated with RSV A2 (m.o.i. 2) for 1 hour at 4°C then harvested for analysis of RSV L gene copy number relative to parental WT cells. Points represent independent experiments, with a bar at the mean +/- SD. Significance by ratio paired t-test prior to data transformation.

4.2.23 IFI44 Reduces RSV Replication in a Minigenome Assay

A common stage of the viral life cycle targeted by ISG effectors is replication of the viral genome, as well as transcription of viral genes. Here, an RSV minigenome assay (gift from J.F. Eleouet, INRA) was used to assess the impact of IFI44 or IFI44L on RSV replication and transcription. Cells were transfected with a minigenome construct pGEM2-Gaussia/Firefly which was transcribed by a co-transfected T7 DNA-dependent RNA-polymerase to produce a negative-sense sub-genomic RSV replicon (Fig 4.28a). From the 3' end this replicon consists of a Leader sequence, an ORF encoding Gaussia luciferase (GLUC) bordered by NS1 gene start (GS) and M gene end (GE) sequences, a second ORF encoding FLUC bordered by SH GS and SH GE sequences, and finally a Trailer sequence. The Leader sequence is required for initiation of both viral transcription and production of a full-length positive-sense replicon copy [293]. The complement of the Trailer sequence subsequently directs synthesis of negative-sense replicon copies [294]. Cells were co-transfected with constructs expressing the viral proteins required for replication and transcription: M2-1, L, P, and N. Finally, cells were also transfected with a β-galactosidase-expressing plasmid and pCAGGS-T7 to express the DNA-dependent RNA-polymerase T7. β-galactosidase transcription was driven by a host polymerase and measurement of β-galactosidase activity was used to normalise transfection efficiency.

Transfection efficiency of A549 cells and HEK293T/17 cells was compared to determine the appropriate cell line for use with this assay. Unlike HEK293T/17 cells, A549 cells are difficult to transfect at a high efficiency. It was hypothesised that A549 cells would be unsuitable for use with this assay due to poor transfection efficiency. First, A549 and HEK293T/17 cells were transfected with pTRIP-CMV-IVsb-FLUC-IRES-TagRFP and luciferase activity quantified 24 hours later. Luciferase activity was

readily detectable in the HEK293T/17 cells but not detectable in A549 cell lysate (Fig 4.28b). This may have been due to poor lysis of the A549 cells but extending the incubation time in lysis buffer, increasing agitation during lysis, and freeze-thaw cycles were unable to improve this process to the point where luciferase activity was detectable following FLUC transfection (data not shown). In addition, when HEK293T/17 cells and A549 cells were transfected with the minigenome system and a β-galactosidase-expressing plasmid, β-galactosidase activity was significantly higher in HEK293T/17 cell lysate ($P < 0.01$, Fig 4.28c). The negative control for this assay was transfection with each plasmid required for the minigenome system apart from pCITE-L, encoding the RSV polymerase. Luciferase activity was undetectable in HEK293T/17 cells transfected with the minigenome system without pCITE-L (Fig 4.28d).

Stably transduced HEK293T/17 clonal cell lines expressing IFI44 or IFI44L were developed using pTRIP-CMV-IVsb-IFI44-IRES-TagRFP or pTRIP-CMV-IVsb-IFI44L-IRES-TagRFP lentivirus as described previously. Four HEK293T/17 clones were selected with stable expression of IFI44 protein (Fig 4.28e). HEK293T/17 IFI44 #2 was selected for further use as this clone had the highest transfection efficiency, as demonstrated by β-galactosidase activity (Fig 4.28f). A single IFI44L clone was recovered following transduction and clonal expansion. Expression of IFI44L protein could not be confirmed and mRNA was not quantified. Minigenome activity was significantly reduced by 44% in HEK293T/17 IFI44 #2 relative to parental WT HEK293T/17 cells ($P < 0.05$, Fig 4.28g). There was a similar reduction observed in IFI44L expressing cells, although this result was not statistically significant due to increased variation between experiments.

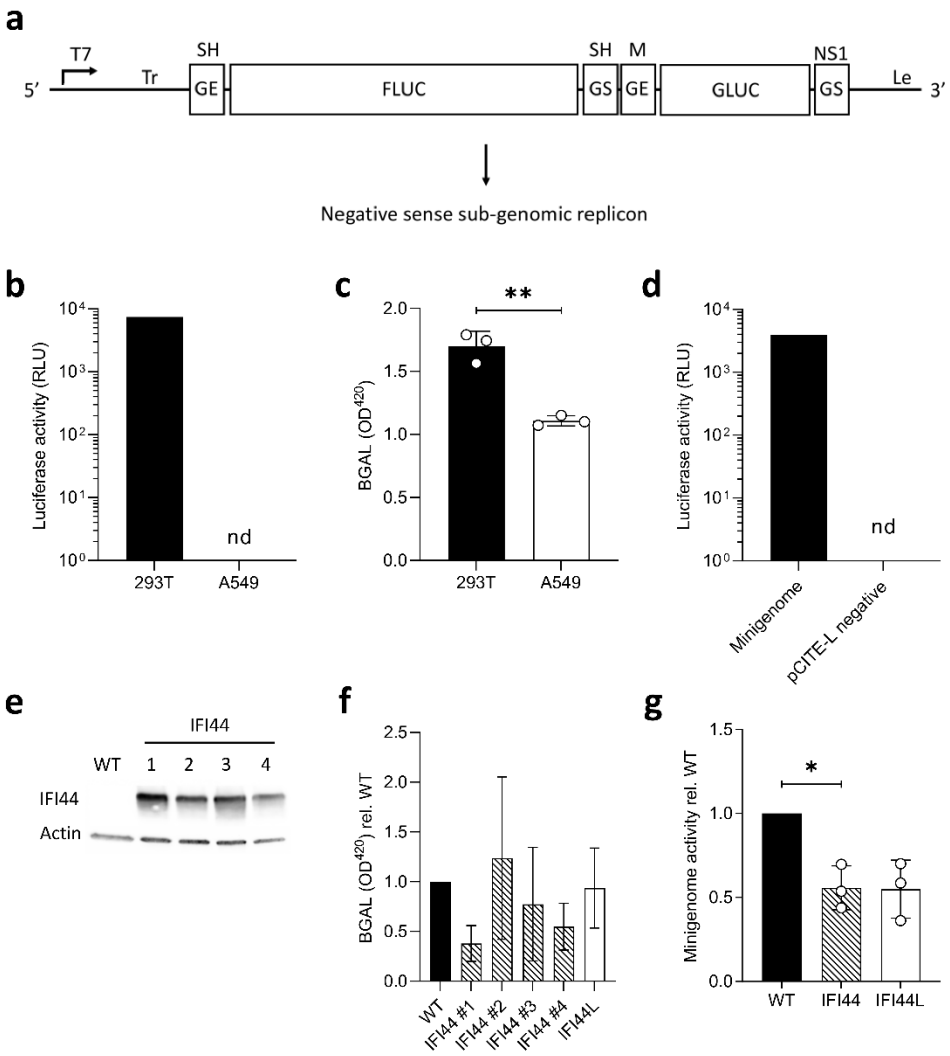

Figure 4.28. Minigenome activity is reduced by IFI44 or IFI44L expression. (a) Schematic of pGEM2-Gaussia-Firefly minigenome plasmid. Tr = RSV A2 trailer sequence. GE = Gene end sequence. FLUC = Firefly luciferase. GS = Gene start sequence. GLUC = Gaussia luciferase. Le = RSV A2 leader sequence. **(b)** HEK293T/17 and A549 cells were transfected with pTRIP-CMV-IVSb-FLUC-IRES-TagRFP and luciferase activity assessed after 24 hours. RLU = relative light units. N=1. **(c)** HEK293T and A549 cells were transfected with a β-galactosidase (BGAL)-expressing construct and RSV minigenome system including RSV proteins M2-1, N, P, and L. BGAL activity assessed after 24 hours. N=3. **(d)** HEK293T/17 cells were transfected with the RSV minigenome system. The construct expressing the RSV polymerase (pCITE-L) was replaced with pcDNA3.1 in pCITE-L negative. Minigenome activity was assessed by quantifying FLUC activity after 24 hours. N=1. **(e)** IFI44 protein expression in stably transduced clonal HEK293T/17-IFI44 cell lines and parental polyclonal HEK293T/17 cells. N=1. **(f)** BGAL activity in clonal HEK293T/17-IFI44 cell lines and parental WT quantified 24 hours after transfection. N=3. **(g)** Minigenome activity in stably transduced IFI44 and IFI44L HEK293T/17 cell lines relative to parental WT cells 24 hours after minigenome transfection. Data normalised to BGAL activity. Points represent independent experiments with bars at the mean +/- SD. Significance to WT controls by ratio paired t-test prior to data transformation. * $P < 0.05$, ** $P < 0.01$. nd = not detectable.

4.2.24 A Predicted GTP-binding Region of IFI44 is Dispensable for Antiviral Activity

To investigate the functional relevance of the predicted ability of IFI44 and IFI44L to bind GTP site-directed mutagenesis was used to produce pTRIP constructs expressing IFI44 or IFI44L lacking the G1 motif in the predicted GTPase domain of either protein. It was hypothesised that GTP binding by IFI44 or IFI44L may reduce RSV polymerase activity by reducing the available pool of cytoplasmic nucleotides. Oligonucleotides were designed that overlapped the region to be deleted in either plasmid (Fig 4.29a). For IFI44 this region consists of residues 193-201. For IFI44L this region encompasses residues 200-208. The deletion of the G1-coding DNA sequence removed an *Ava*II restriction site (Fig 4.29b).

Plasmids with the planned deletion were identified by the loss of a DNA fragment following incubation with *Ava*II. Nine IFI44 and six IFI44L plasmids were recovered with this restriction digest pattern (Fig 4.30a). Selected constructs were verified by sequencing to ensure no additional mutations had occurred (Fig 4.30b).

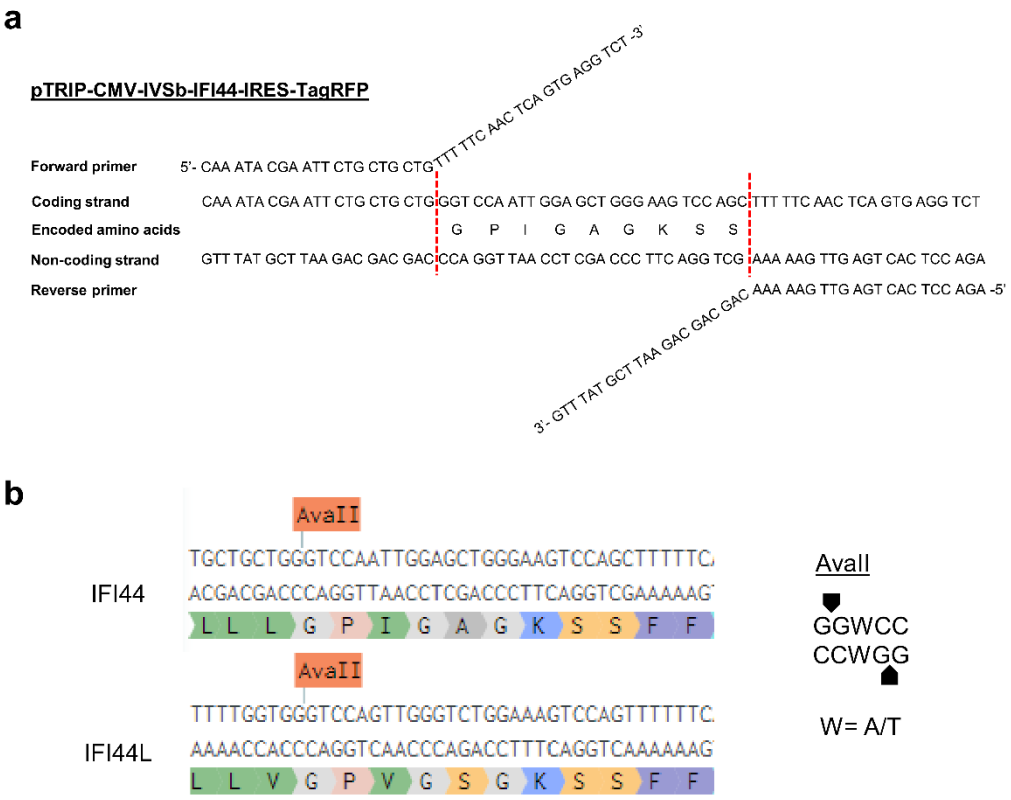

Figure 4.29. Site-directed mutagenesis to generate a lentiviral IFI44Δ193-201 expression construct. (a) Schematic of pTRIP-CMV-IVSb-IFI44-IRES-TagRFPand forward and reverse oligonucleotides designed to remove sequence encoding residues 193-201 of IFI44. **(b)** Sequence encoding G1 region of IFI44 and IFI44L in pTRIP-CMV-IVSb-ISG-IRES-TagRFP constructs. Site targeted for digest by the restriction enzyme *Ava*II.

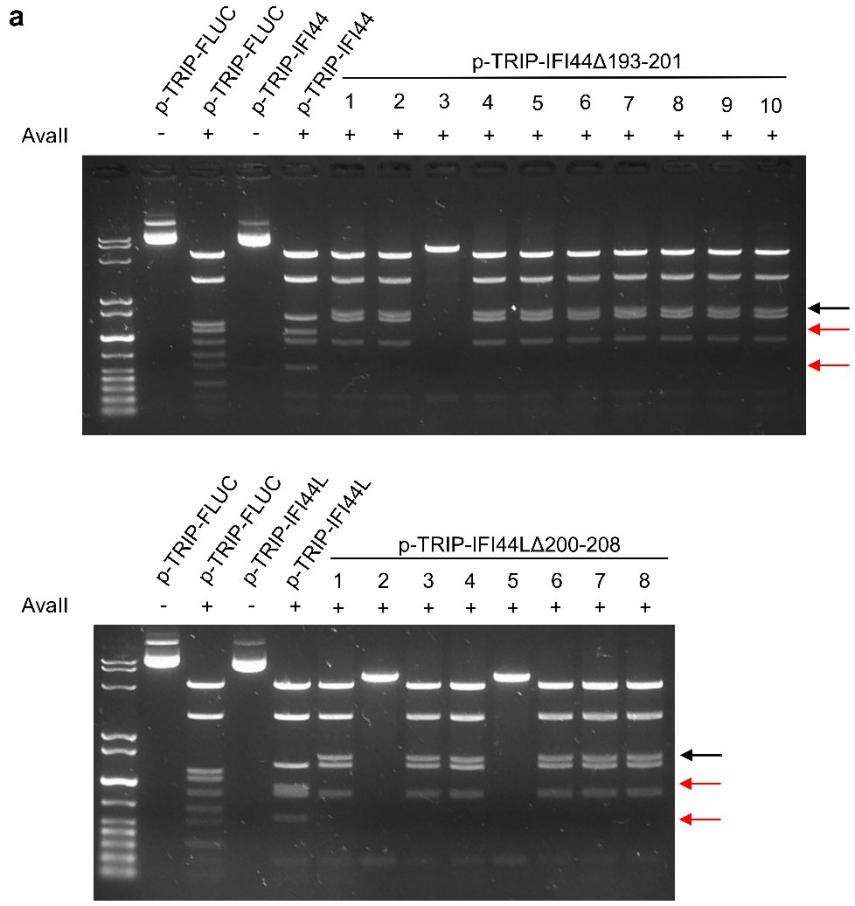

Figure 4.30. Confirmation of sequence deletion by site-directed mutagenesis. (a) pTRIP-CMV-IVSb-X-IRES-TagRFP (pTRIP) constructs encoding firefly luciferase (FLUC), IFI44, IFI44L, IFI44Δ193-201, and IFI44LΔ200-208 were digested with *Ava*II for 2 hours and fragment pattern after electrophoresis used to confirm deletion of sequence targeted by site-directed mutagenesis. Red arrows highlight bands present in WT but not in edited plasmids. Black arrows highlight bands present in edited but not WT plasmids. **(b)** pTRIP-IFI44Δ193-201 plasmid #1 and pTRIP-IFI44LΔ200-208 # 3 were sequenced and aligned with the sequence of the WT plasmid by Clustal Omega. * identical residues. Amino acids encoded by deleted region shown below (IFI44/IFI44L).

IFI44$_{\Delta 193\text{-}201}$ plasmid #1 and IFI44L$_{\Delta 200\text{-}208}$ #3 were used for further work. IFI44$_{\Delta 193\text{-}201}$ protein expression was detectable in HEK293T/17 cells transfected for 24 hours (Fig 4.31). Expression was slightly lower than that of the WT protein. Site-directed mutagenesis was again used to insert sequence encoding a C-terminal HA tag. However, sequencing of the generated plasmids could not confirm insertion of the intended sequence. As such, detection of WT IFI44L or IFI44L$_{\Delta 200\text{-}208}$ protein expression following transfection or lentiviral transduction was still not possible.

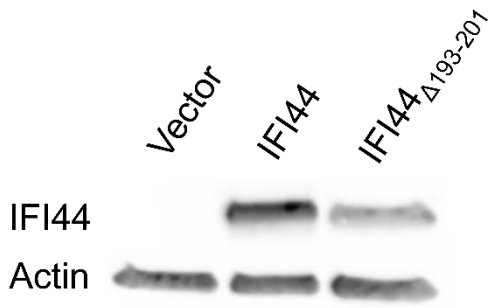

Figure 4.31. Expression of IFI44Δ193-201. HEK293T/17 cells were transfected with pTRIP-CMV-IVSb-FLUC-IRES-TagRFP (vector), pTRIP-CMV-IVSb-IFI44-IRES-TagRFP (IFI44), or pTRIP-CMV-IVSb-IFI44Δ193-201-IRES-TagRFP (IFI44Δ193-201). IFI44 protein expression by Western blotting 24 hours after transfection. N=1.

A549 were transduced with equalised inoculums of vector (FLUC), IFI44, or IFI44$_{\Delta 193\text{-}201}$ lentivirus and protein expression assessed after 24 hours. Here levels of the mutant protein appeared to be much lower than the WT protein, as the bands appeared equal in density but the WT loading control was not detectable, suggesting a much lower quantity of protein had been loaded overall (Fig 4.32a). Transduced cells were infected with rgRSV (m.o.i. 0.8) and the proportion of infected cells was assessed after a further 24 hours. IFI44 WT transduction significantly reduced infection by 25% ($P < 0.01$). A

similar reduction was seen with transduction of IFI44$_{\Delta 193\text{-}201}$ ($P < 0.05$), suggesting the deleted region is not essential for antiviral activity of IFI44 (Fig 4.32b). To confirm this observation, the experiment was repeated with a lower m.o.i. of 0.1 or 0.01, as used for previous overexpression studies. In a single experiment, IFI44$_{\Delta 193\text{-}201}$ again reduced infectivity to similar or lower levels than seen with transduction of IFI44 WT (Fig 4.32c).

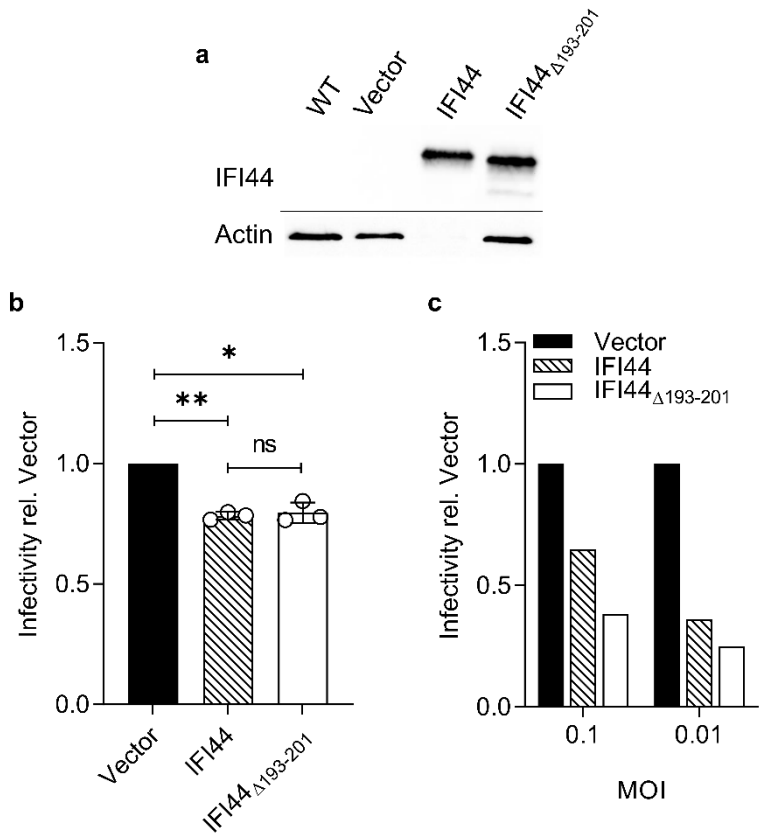

Figure 4.32. IFI44Δ193-201 reduces RSV infection. A549 cells were transduced with 2x10^5 TU lentivirus and **(a)** levels of IFI44 expression quantified after 24 hours. N=2. **(b)** After 24 hours, transduced cells were infected with rgRSV (m.o.i. 0.8) for a further 24 hours. Infectivity assessed by determining the proportion of transduced cells that were infected by flow cytometry. N=3. **(c)** A549 cells were transduced as above with the addition of 2 μg/mL ruxolitinib and infected with rgRSV (m.o.i. 0.1 or 0.01) after 24 hours. Infectivity was assessed as for **b**. N=1. Points represent independent experiment, bars at the mean +/- SD. Significance by ratio paired t-test prior to data transformation. * $P < 0.05$, ** $P < 0.01$. ns = not significant.

Stably-transduced clonal A549 cell lines expressing either IFI44$_{\Delta 193\text{-}201}$ or IFI44L$_{\Delta 200\text{-}208}$ were produced by FACS selection as described previously for cell lines expressing WT IFI44 or IFI44L. After 3 weeks in culture >90% of A549 IFI44$_{\Delta 193\text{-}201}$ or A549 IFI44L$_{\Delta 200\text{-}208}$ cells were RFP^{+} suggesting stable integration and expression of the lentiviral construct (Fig 4.33a). *IFI44* (Fig 4.33b) and *IFI44L* (Fig 4.33c) mRNA was detectable at high levels in both clonal lines at this passage. However, expression of IFI44$_{\Delta 193\text{-}201}$ had no impact on RSV infectivity (Fig 4.33d). Although, expression of IFI44$_{\Delta 193\text{-}201}$ was associated with a reduction in viral RNA in a single experiment (Fig 4.33e). Proliferation was also unaffected by expression of IFI44$_{\Delta 193\text{-}201}$ (Fig 4.33f). Protein expression was assessed to confirm whether this cell line was expressing the mutant IFI44. No mutant IFI44 protein was detectable (4-weeks after transduction, Fig 3.43g) and *IFI44* mRNA levels had returned to comparable levels to the vector transduced control 7-weeks after transduction. (Fig 4.33h). Similarly, expression of IFI44L$_{\Delta 200\text{-}208}$ in a stably-transduced clonal A549 cell line had no impact on infectivity (Fig 4.33i), although a reduction in viral RNA was noted in a single experiment (Fig 4.33j). Expression of mutant IFI44L also had no impact on proliferation (Fig 3.43k). Having previously observed antiviral activity comparable to that of the WT IFI44 protein, with transient expression of IFI44$_{\Delta 193\text{-}201}$, and being unable to confirm protein expression in either IFI44 or IFI44L mutant stably transduced cell lines, it seems likely that these cell lines are not expressing relevant levels of protein after expansion from single cells. As such, I was unable to confirm the relevance of the IFI44L G1 region, although it likely plays a similar role as in IFI44.

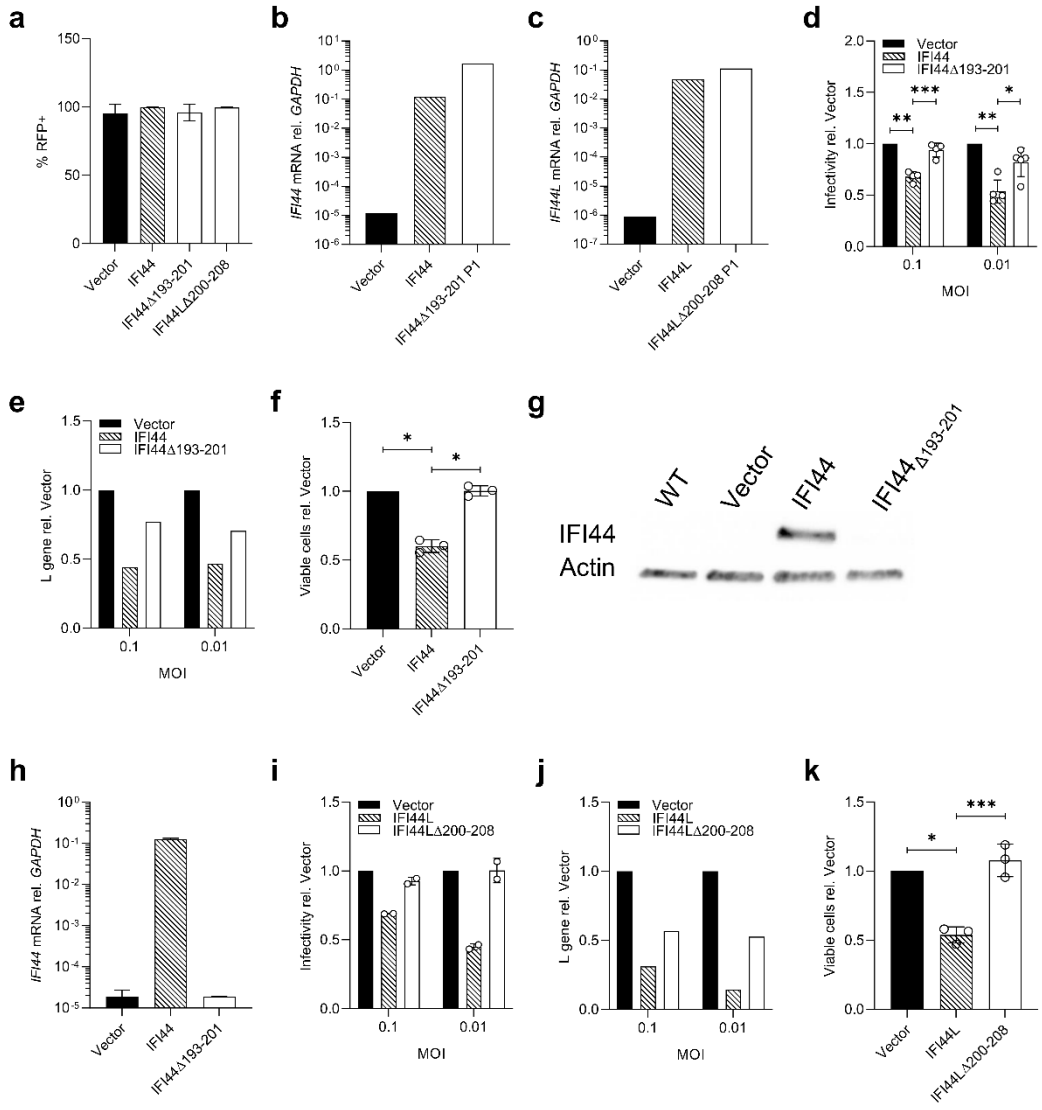

Figure 4.33. Stable Transduction of IFI44Δ193-201 or IFI44LΔ200-208. (a) Percentage of RFP^+ cells in clonal stably-transduced cell lines 3 weeks after transduction. *IFI44* **(b)** or *IFI44L* **(c)** mRNA expression 3 weeks after transduction. **(d)** Stably transduced cell lines were infected with rgRSV (m.o.i. 0.1 and 0.01) for 24 hours and infectivity assessed by proportion of GFP^+ infected cells relative to a vector transduced cell line. N=4. **(e)** Stably transduced cell lines were infected with RSV A2 (m.o.i. 0.1 and 0.01) for 24 hours. Levels of viral RNA relative to vector transduced control cells. N=1. **(f)** Viable cell number 24 hours after plating by MTS assay. N=3. **(g)** IFI44 protein expression in stably transduced clonal cell lines. A549 $IFI44_{\Delta 193\text{-}201}$ lysate taken 4 weeks after transduction. N=1. **(h)** *IFI44* mRNA in stably transduced clonal cell lines. A549 $IFI44_{\Delta 193\text{-}201}$ lysate taken 7 weeks after transduction. N=2. **(i)** Cell lines were infected as for **d**. N=2. **(j)** Cell lines were infected as for **e**. N=1. **(k)** Proliferation of stably transduced IFI44L cell 24 hours after plating by MTS assay. N=3. Significance to noted groups by paired ratio t-test prior to data transformation. * $P < 0.05$, ** $P < 0.01$, *** $P < 0.001$, **** $P < 0.0001$.

4.2.25 Contribution of the IFI44L N-Terminus to Protein Function

Mutagenesis strategies to generate N-terminal deletion mutants of IFI44 and IFI44L were designed to delete the entire region preceding the predicted GTPase domain. In IFI44 this included the predicted TLDc domain. During the time available only a pTRIP construct encoding IFI44L$_{\Delta 2\text{-}171}$ was produced.

A single stably transduced clonal cell line was recovered following transduction and FACS selection of the top 2% of transduced cells. *IFI44L* mRNA was elevated in this stably-transduced cell line and comparable to levels in the IFI44L WT-expressing cell line (Fig 4.34a). Expression of IFI44L$_{\Delta 2\text{-}171}$ was associated with reduced proliferation relative to the vector transduced cell line ($P < 0.05$, Fig 4.34b), although proliferation was also significantly higher than in the WT IFI44L-expressing cell line ($P < 0.05$). Interestingly, a similar pattern was observed in RSV infectivity, where expression of IFI44L$_{\Delta 2\text{-}171}$ was associated with a reduced proportion of infected cells relative to vector transduced controls but increased infection relative to cells expressing WT IFI44L (Fig 4.34c). These data suggest that the N-terminal region of IFI44L may have some role in the antiviral and antiproliferative activity of the protein, but it is not wholly essential. However, it is important to note that protein expression could not be confirmed in these cell lines due to lack of an effective antibody. As such, I could not confirm that levels of IFI44L protein expression were comparable between clonal lines and so these data should be interpreted with caution.

Mutagenesis approaches to generate IFI44 and IFI44L C-terminal deletion mutants, as well as mutants lacking the entire GTPase region, were designed but were not completed in time for inclusion in this thesis.

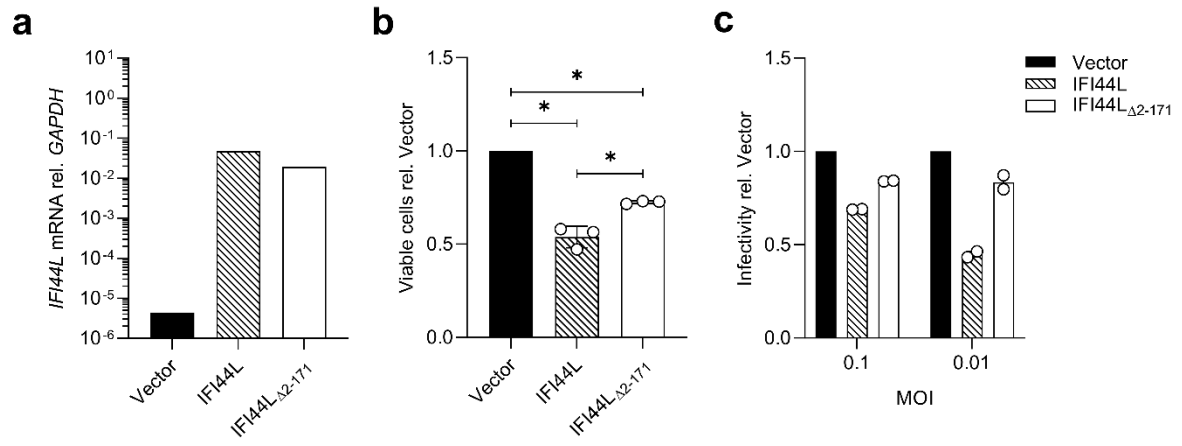

Figure 4.34. IFI44LΔ2-171 Has Reduced Antiviral and Antiproliferative Activity. (a) Percentage of transduced (RFP$^+$) cells 3 weeks after transduction. N=1. **(b)** Proliferation of stably transduced IFI44L cell 24 hours after plating by MTS assay. N=3. **(c)** Stably transduced A549 clonal cell lines were infected with rgRSV (m.o.i. 0.1 and 0.01) for 24 hours. Infectivity assessed by proportion of infected (GFP$^+$) cells relative to vector transduced control cells. N=2. Bars at the mean +/- SD. Significance by ratio paired t-test, prior to data transformation. * P < 0.05, ** P < 0.01. ns = not significant.

4.2.26 RSV Disease Severity is Enhanced in IFI44 Deficient Mice

C57BL/6N *Ifi44*$^{tm1b(komp)Wtsi}$ (*Ifi44*$^{-/-}$) mice were bred and housed by the Wellcome Trust Sanger Institute [295]. The Wellcome Trust phenotyping pathways identified several abnormalities in these *Ifi44*$^{-/-}$, including abnormal behaviour, decreased prepulse inhibition, and enlarged lymph nodes (phenotype data were retrieved from the Mouse Genome Database [296]). Multiple independent RSV infections were undertaken to establish any disease phenotype in these knockout mice.

Interestingly, cells from the C57BL/6 strain of inbred mice are seemingly unable to transcribe *Ifi44l* mRNA [297], likely due to a deletion of the 5' gene region including the translational start site. *Ifi44l* mRNA was undetectable in either WT C57BL/6N or *Ifi44*$^{-/-}$ mice four days after RSV infection (Fig 4.35). *Ifi44* mRNA was detectable in both WT and KO mice, albeit at significantly lower levels in *Ifi44*$^{-/-}$ mice ($P < 0.0001$, Fig 4.35).

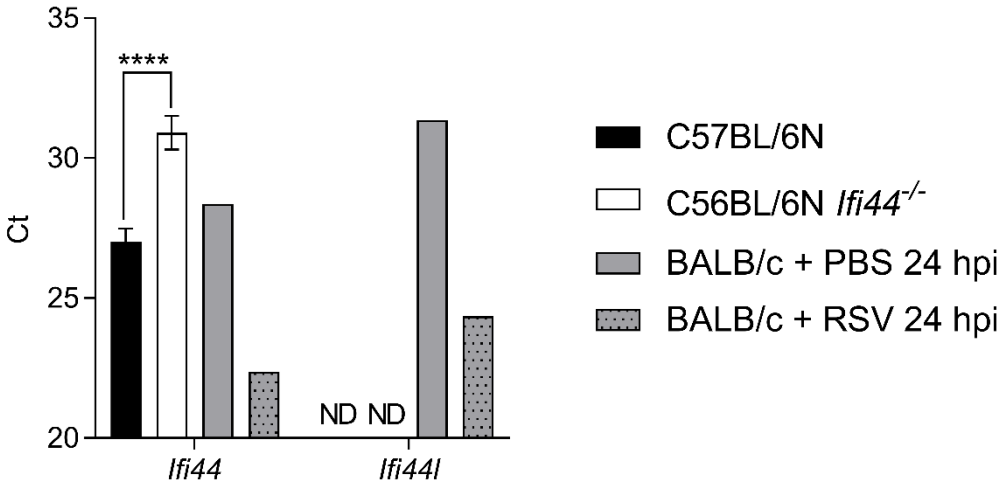

Figure 4.35. C57BL/6N mice do not express detectable levels of *Ifi44l*. 7-week-old female C57BL/6N or C57BL/6N *Ifi44*$^{tm1b(komp)Wtsi}$ (*Ifi44*$^{-/-}$) mice were infected with RSV A2 for 4 days. 9-week-old BALB/c mice were infected with RSV A2 for 24 hours or given PBS intranasally. *Ifi44* and *Ifi44l* mean cycle threshold (Ct) values +/-SEM. C57BL/6N or *Ifi44*$^{-/-}$ N=4 animals per group. Bars at the mean +/- SD. BALB/c N=1 animal per group. Significance by ANOVA, **** $P < 0.0001$. ND = not detectable.

Initially, female 7-week-old mice were infected with $5x10^5$ pfu RSV A2 and monitored for 4 days. Here, there was no apparent difference in weight change (Fig 4.36a) but *Ifi44*$^{-/-}$ mice had significantly higher levels of viral RNA in their lung tissue after 4 days (Fig 4.36b). There was no significant difference in cellular infiltration detected in either the lung homogenate (Fig 4.36c) or bronchoalveolar lavage fluid (BALF, Fig 4.36d). There was a significant decrease in concentration of IL-1β in the lung homogenate of *Ifi44*$^{-/-}$ mice (Fig 4.36e). However, Neither IL-6 nor IL-1β were readily detectable in BALF (Fig 4.36f). CXCL10 was also reduced in *Ifi44*$^{-/-}$ mice at day 4, although there were no significant differences in other measured analytes (Fig 4.36g). To investigate whether *Ifi44*$^{-/-}$ mice have altered IFN responses levels of *Ifnγ* and *Ifnb* were measured by qPCR (Fig 4.37a-b). No difference was seen between KO and WT mice. *Muc5ac*, reportedly enhanced in infants with severe RSV bronchiolitis [129], was also not differentially expressed relative to WT mice (Fig 4.37c).

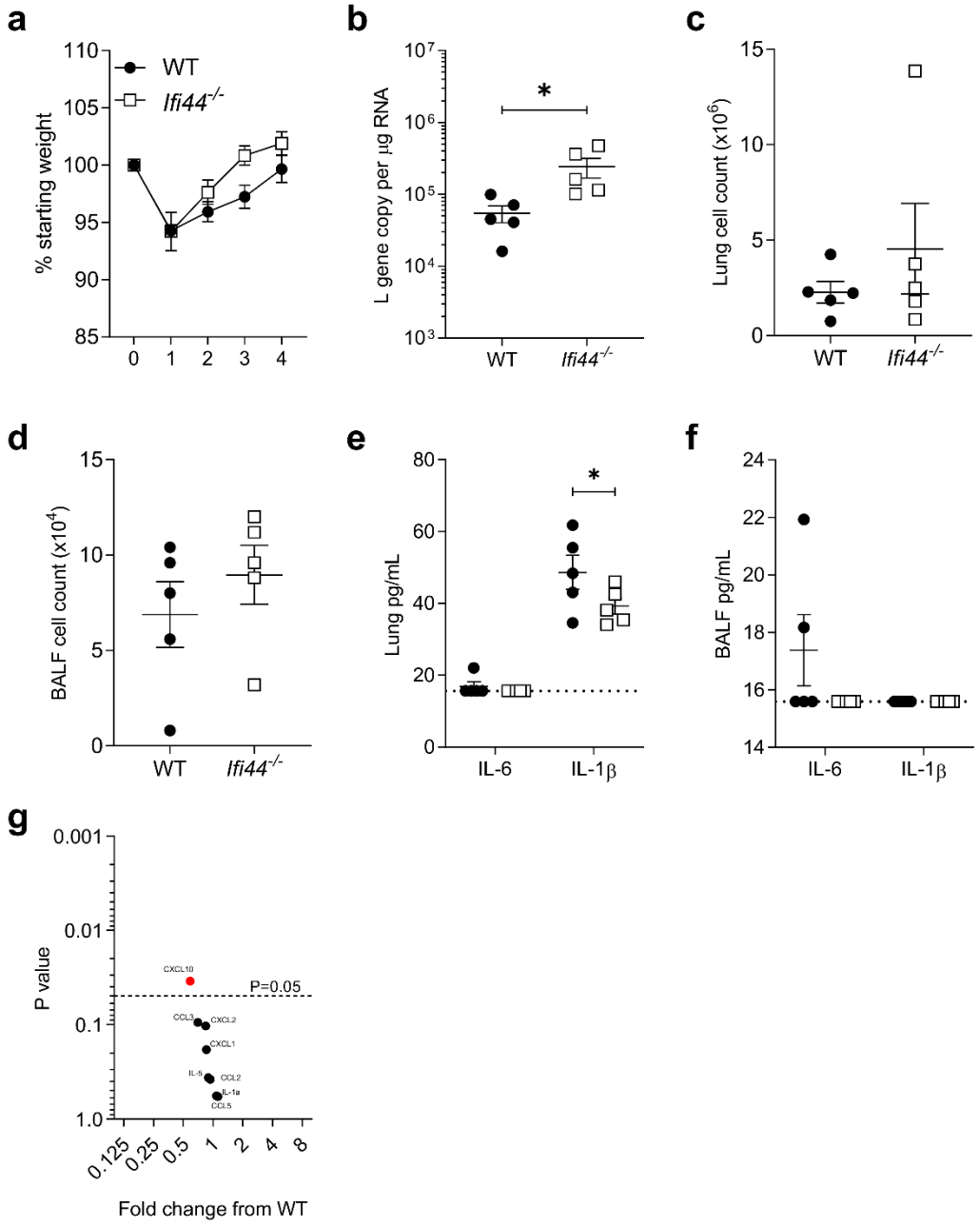

Figure 4.36. Viral load is increased in IFI44 knockout mice. C57BL/6N wild-type (WT) or C57BL/6N *Ifi44*$^{tm1b(komp)Wtsi}$ (*Ifi44*$^{-/-}$) mice (7-week-old females) were infected intranasally with pfu RSV A2 for 4 days. **(a)** Change in weight over four days of infection. Points represent the mean +/- SEM. **(b)** Levels of RSV L gene in lung tissue at day 4. **(c)** Lung or **(d**) BALF cell counts at day 4. Levels of IL-6 and IL-1β in **(e)** lung tissue or **(f)** BALF at day 4. **(g)** Fold change of cytokine and chemokine levels from WT in lung tissue at day 4 by multiplex ELISA. Red dots represent significant differences (P < 0.05). N=5 animals per group. **b-f** points represent individual animals. **a**+**g** points represent the mean. Line at the mean +/- SEM. Significance by unpaired t-test (**b**) or ANOVA (**e**). * P < 0.05.

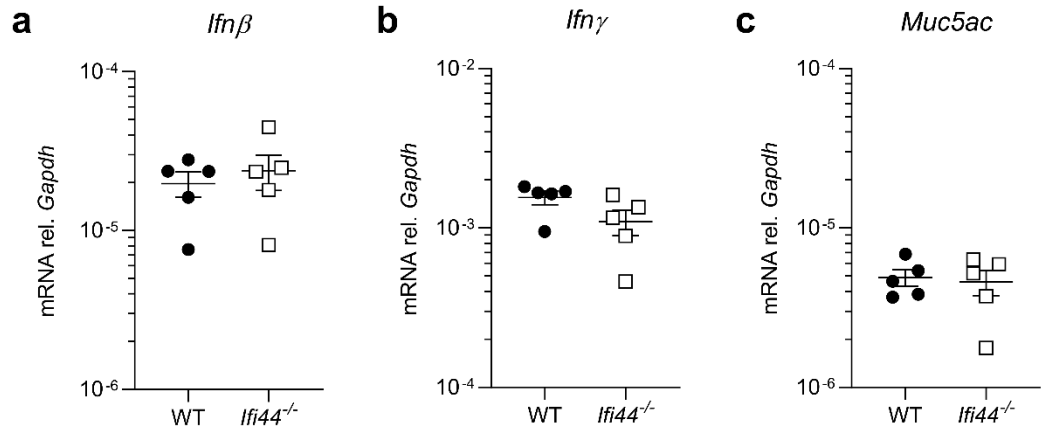

Figure 4.37. IFN and mucin expression in *Ifi44* knockout mice during RSV infection. C57BL/6N wild-type (WT) or C57BL/6N *Ifi44*$^{tm1b(komp)Wtsi}$ (*Ifi44*$^{-/-}$) mice (7-week-old females) were infected intranasally with pfu RSV A2 for 4 days. **(a)** *Ifnγ*, **(b)** *Ifnβ*, and ***(c)*** *Muc5ac* mRNA levels relative to *Gapdh* ($2^{-\Delta Ct}$) in lung tissue. N=5 animals per group. Points represent individual animals, line at the mean +/- SEM.

This initial experiment also included a cohort of mice infected for 7 days. However, proper analysis of weight change, cell numbers, and cytokine levels was hampered by the difference in sex and age amongst groups. Comparing all KO and WT mice there was no significant difference in weight change over 7 days of infection (Fig 4.38a). However, when comparing age-matched groups (7-weeks) of male WT and female KO mice there was significantly increased weight loss in the KO mice relative to WT (Fig 4.38b). Of course, this could be a result of differences in RSV disease amongst male and female mice. Additionally, when comparing sex-matched groups of older female WT (14-weeks) or younger female KO (7-weeks) mice the opposite phenotype was observed, with WT mice losing significantly more weight at days 6 and 7 of infection (Fig 4.38c). No difference was observed in BALF or lung homogenate cell counts with either age or sex-matched WT controls (Fig 4.39a-f). Levels of IL-6 and IL-1β were too low for detection in BALF and IL-6 was also undetectable in lung tissue

(data not shown). There was no significant difference in IL-1β levels in lung tissue when compared to all WT controls (Fig 4.39g) or sex-matched controls (Fig 4.39i). However, there was a slight but significant decrease when *Ifi44*$^{-/-}$ mice were compared to age-matched controls (Fig 4.39h). Due to the lack of appropriate control groups and subsequent difficulty interpreting the data the infection was repeated with age and sex-matched controls.

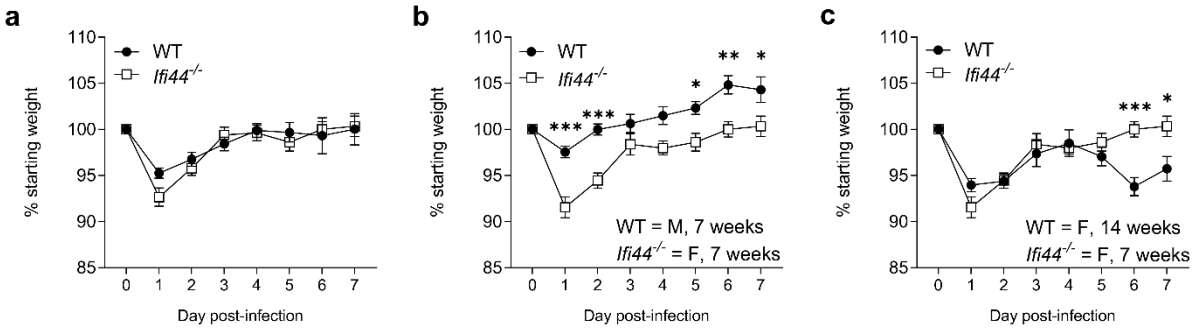

Figure 4.38. Change in weight over 7 days of RSV infection in IFI44 knockout mice with unmatched WT controls. C57BL/6N wild-type (WT) or C57BL/6N *Ifi44*$^{tm1b(komp)Wtsi}$ (*Ifi44*$^{-/-}$) mice were infected intranasally with RSV A2 for 7 days. **(a)** Weight change over 7 days comparing all *Ifi44*$^{-/-}$ (7-week-old females, N=7) and all WT mice. **(b)** Weight change over 7 days comparing all *Ifi44*$^{-/-}$ (7-week-old females, N=7) and age-matched (7-week-old males, N=5) WT mice. **(c)** Weight change over 7 days comparing all *Ifi44*$^{-/-}$ (7-week-old females, N=7) and sex-matched (14-week-old females, N=5) WT mice. Points represent the mean +/- SEM. Significance by ANOVA. * P < 0.05, ** P < 0.01, *** P < 0.001.

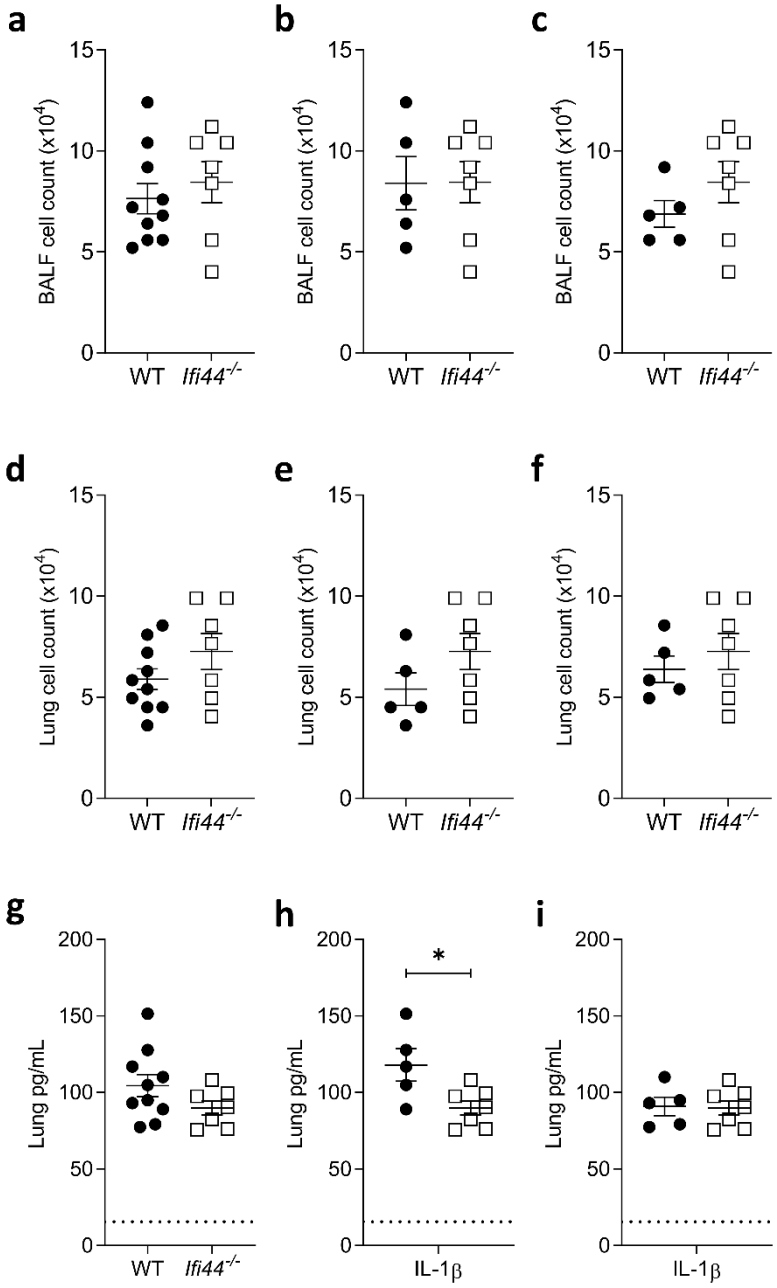

Figure 4.39. Cell infiltration and pro-inflammatory cytokine responses at day 7 of RSV infection in IFI44 knockout mice with unmatched WT controls. C57BL/6N wild-type (WT) or C57BL/6N *Ifi44*$^{tm1b(komp)Wtsi}$ (*Ifi44*$^{-/-}$) mice were infected intranasally with RSV A2 for 7 days. BALF cell counts with all *Ifi44*$^{-/-}$ mice (7-week-old females, N=7) compared with **(a)** all, **(b)** age-matched (7-week-old males, N=5), and **(c)** sex-matched (14-week-old females, N=5) WT controls. Lung cell counts with all *Ifi44*$^{-/-}$ mice (7-week-old females, N=7) compared with **(d)** all, **(e)** age-matched (7-week-old males, N=5), and **(f)** sex-matched (14-week-old females, N=5) WT controls. IL-1β levels in lung tissue of all *Ifi44*$^{-/-}$ mice (7-week-old females, N=7) compared with **(g)** all, **(h)** age-matched (7-week-old males, N=5), and **(i)** sex-matched (14-week-old females, N=5) WT controls. Dotted line at limit of detection. Points represent individual animals with a line at the mean +/- SEM. Significance by unpaired t-test, * $P < 0.05$.

For all subsequent mouse infections, a new stock of RSV A2 was used (PP3K). This stock was initially tested in 9-11-week old female C57BL/6J mice. Infection with 100 µL undiluted virus stock results in significant weight loss from just 1 day after infection (Fig 4.40). For studies in KO mice, the dose was reduced to a 1:1 dilution, equivalent to $1x10^5$ pfu as measured by plaque assay *in vitro*, although the degree of weight loss suggests that this *in vitro* titre may be inaccurate.

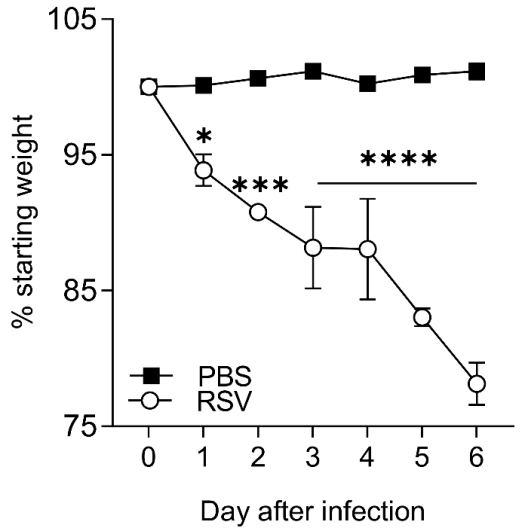

Figure 4.40. In vivo Confirmation of RSV-Induced Weight Loss with RSV A2 stock PP3K. 9-11-week old female C57BL/6J mice were infected intranasally with $2x10^5$ pfu RSV A2 (stock PP3K) in 100 µL. Weight change over 6 days of infection. Mean +/- SEM, N=3 animals per group. Significance to PBS-treated controls by ANOVA. * P < 0.05, ** P < 0.01, *** P < 0.001, **** P < 0.0001.

When using age and sex-matched controls, *Ifi44*$^{-/-}$ mice had significantly increased weight loss over days 5-7 of infection (Fig 4.41a). There was no significant difference in levels of viral RNA after 7 days, although levels in KO mice were reduced on average (Fig 4.41b). There was also no difference in cell number in either the lung homogenate (Fig 4.41c) or BALF (Fig 4.41d). Multiplex analysis of cytokines and chemokines revealed low levels of analytes in both WT and KO mice, with no

significant difference between these groups (Fig 4.41e). In addition, there was no significant difference in levels of *Ifnγ* (Fig 4.41f) or *Ifnb* (Fig 4.41g) expression between WT and KO mice.

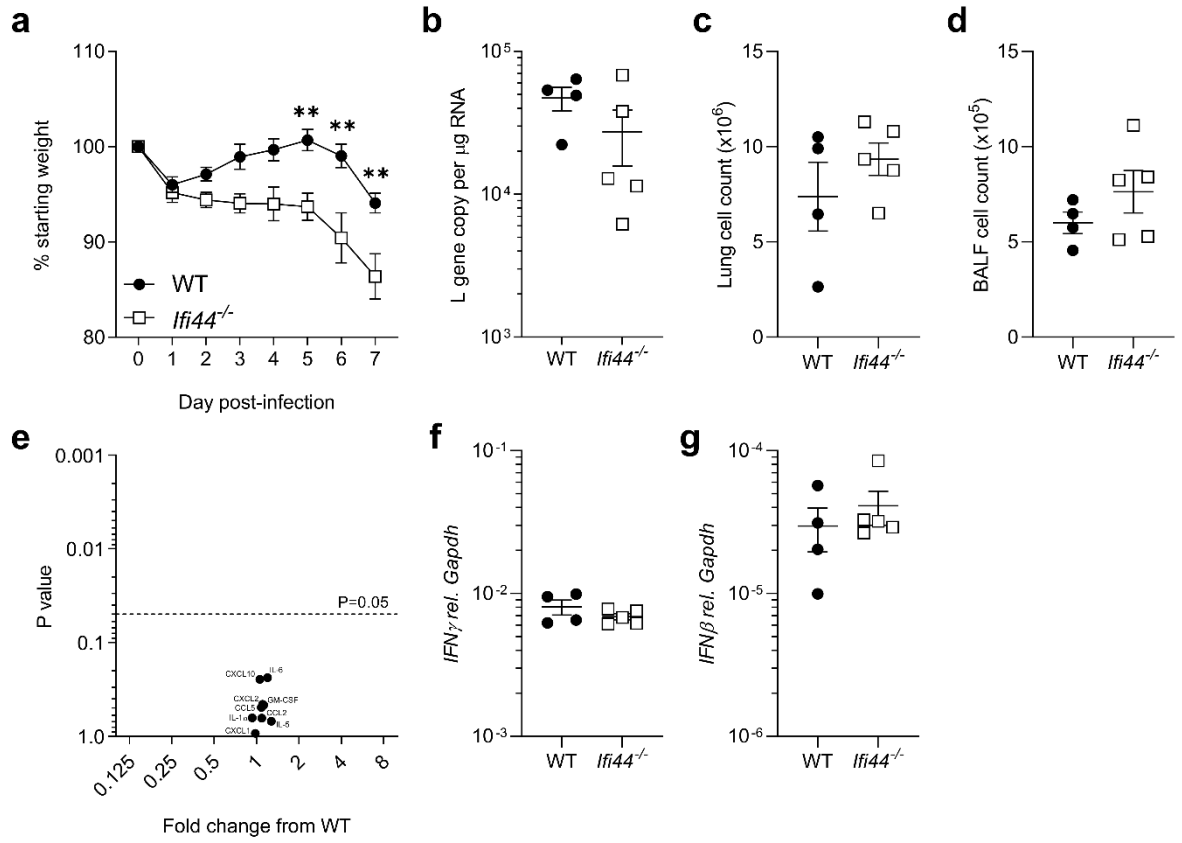

Figure 4.41. Weight loss is enhanced in IFI44 knockout mice compared with matched WT controls. 18 to 20-week-old female C57BL/6N wild-type (WT) or C57BL/6N *Ifi44*$^{tm1b(komp)Wtsi}$ (*Ifi44*$^{--}$) mice were infected intranasally with RSV A2 for 7 days. **(a)** Weight change over 7 days. **(b)** Levels of RSV L gene in lung tissue at day 7. **(c)** Lung or **(d**) BALF cell counts at day 7. **(e)** Fold change of cytokine and chemokine levels from WT in lung tissue at day 7 by multiplex ELISA. Red dots represent significant differences (P < 0.05). **(f)** *Ifnγ* and **(g)** *Ifnβ* mRNA levels relative to *Gapdh* ($2^{-\Delta Ct}$) in lung tissue at day 7. N≥4 animals per group. **b-g** points represent individual animals. **a** points represent the mean. Line at the mean +/- SEM. Significance by ANOVA, * P < 0.05, ** P < 0.01.

Both $CD4^+$ and $CD8^+$ T cells have been shown to play a role in RSV clearance from the mouse lung [298]. Dysregulated T cell responses can contribute to enhanced RSV disease and were investigated in *Ifi44*$^{-/-}$ mice. To identify T cells in cell populations derived from whole lung tissue, the whole lymphocyte population was gated prior to double exclusion (Fig 4.42). Next live cells were gated using a Live/Dead stain and unstained controls. $CD3^+$ live cells were gated next using fluorescence minus one (FMO) controls. Finally, $CD4^+$ and $CD8^+$ cells were gated from the $CD3^+$ cell population using FMO controls.

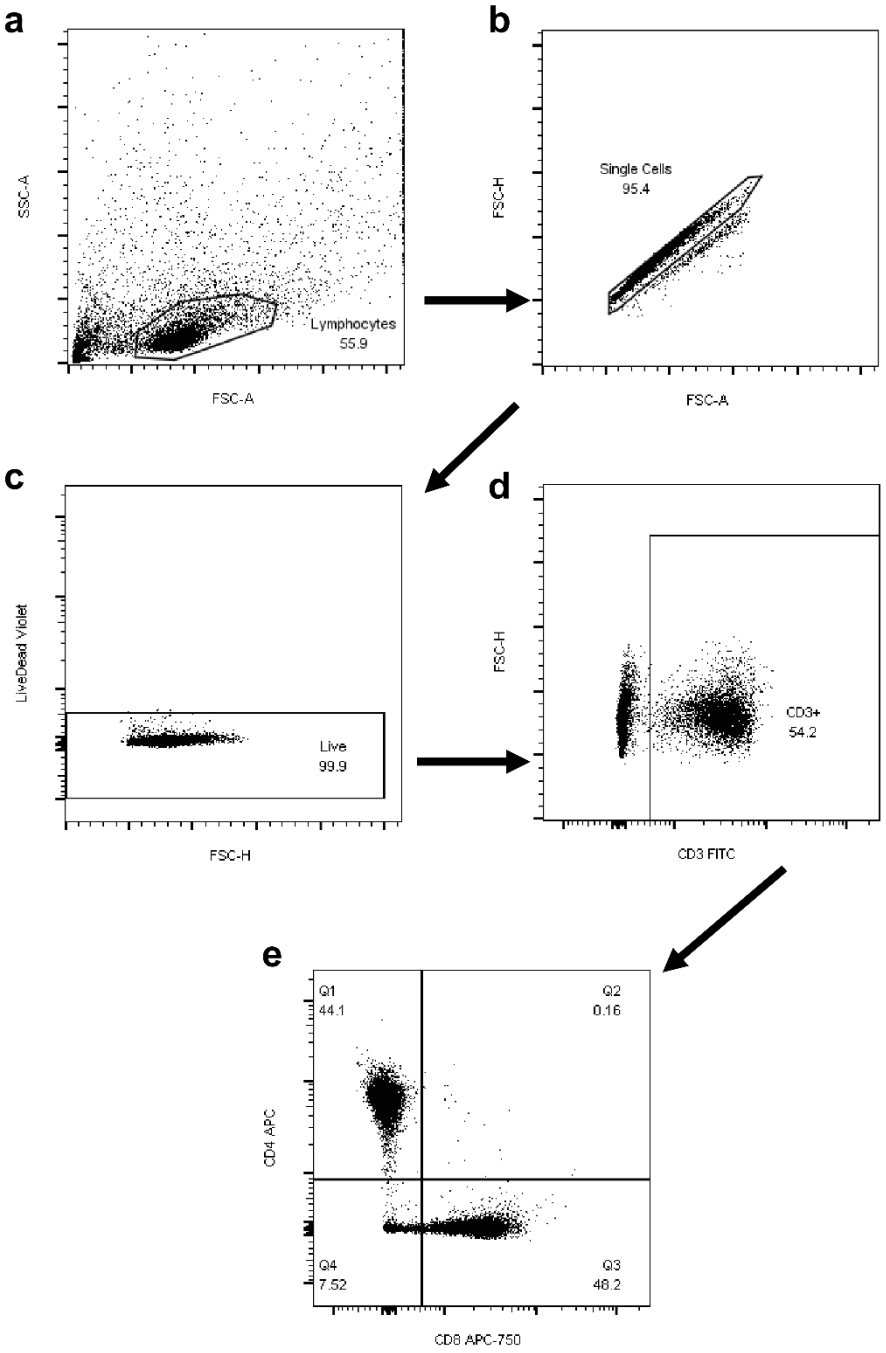

Figure 4.42. Gating Strategy for CD4+ and CD8+ T Cells in Live Lung Cells. The lymphocyte population is gated initially **(a)**, followed by doublet exclusion **(b)**. Live cells were gated using Live/Dead staining **(c)** before $CD3^+$ T cells were gated **(d)**. T cells were then separated into $CD4^+CD8^-$ (Q1) and $CD4^-CD8^+$ (Q3) populations. Each gate was based on comparison to a fluorescence minus one control sample.

Age and sex-matched 14 to 16-week-old female WT and *Ifi44*$^{-/-}$ mice were infected with 1x10^5 pfu RSV for 7 days. There was no significant difference in weight loss (Fig 4.43a) or cell number in the lung homogenate (Fig 4.43b) or BALF (Fig 4.43c) in this experiment. In *Ifi44*$^{-/-}$ mice the proportion of lung cells that were CD3$^+$CD8$^+$ T cells was increased compared to WT ($P < 0.001$, Fig 4.43d). Total numbers of CD4 and CD8 T cells were calculated by combining the percentage of live lung cells with the total cell counts from lung homogenate. Here, there was a reduced number of CD4$^+$ T cells ($P < 0.001$, Fig 4.43e) and no significant difference in total number of CD8$^+$ cells. This experiment had a limited number (N=3) of KO mice and also saw no significant difference in weight loss as seen previously, as the WT mice also lost almost 10% of total body weight over the 7-day infection. This experiment should be repeated, with improved characterisation of T cell subsets, to more effectively assess the T cells response in WT and *Ifi44*$^{-/-}$ mice during RSV infection.

Overall these data suggest *Ifi44*$^{-/-}$ mice suffer enhanced RSV disease relative to WT controls with increased viral replication early in infection and dysregulation of IL-1β and CXCL10 responses. In one case this was associated with increased weight loss seen from days 5-7, although *Ifi44*$^{-/-}$ display no defect in viral clearance.

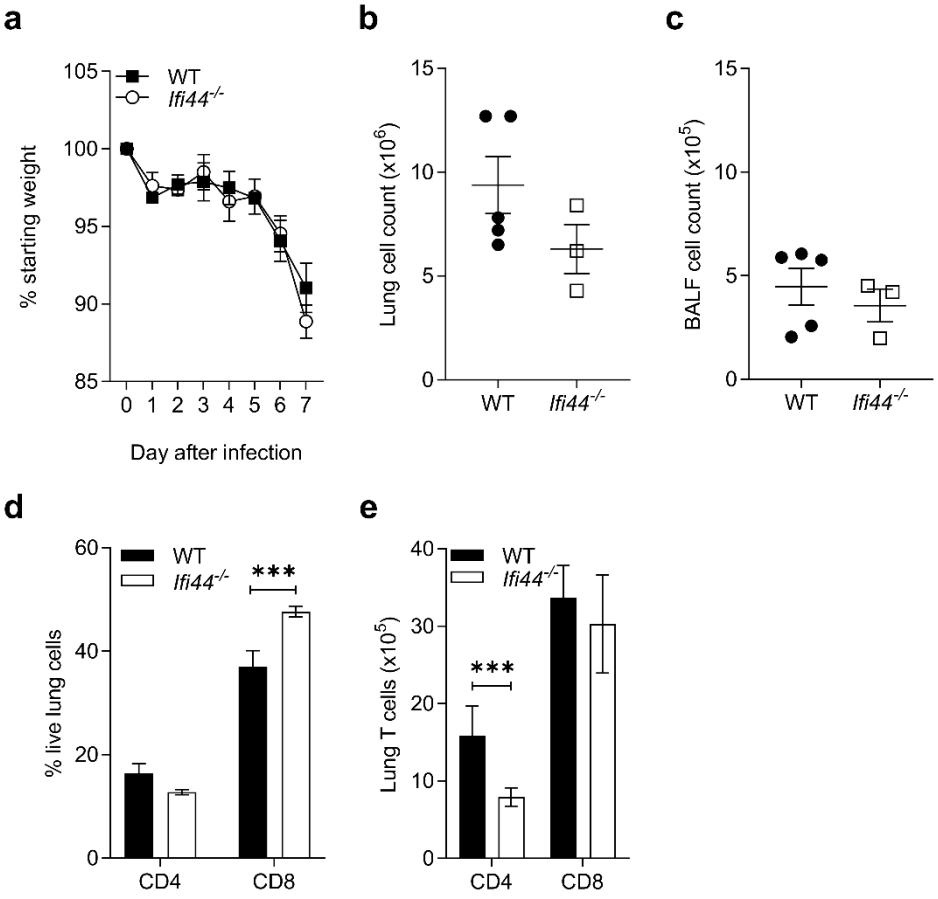

Figure 4.43. The T cell response is altered during RSV infection of *Ifi44*$^{-/-}$ mice. 14 to 16-week-old female C57BL/6N wild-type (WT) or C57BL/6N *Ifi44*$^{tm1b(komp)Wtsi}$ (*Ifi44*$^{-/-}$) mice were infected intranasally with RSV A2 for 7 days. **(a)** Weight change over 7 days. **(b)** Lung or **(c)** BALF cell counts at day 7. **(d)** Percentage of $CD3^+CD4^+$ and $CD3^+CD8^+$ cells in lung at D7 of infection. **(e)** Total number of $CD3^+CD4^+$ or $CD3^+CD8^+$ cells calculated by combining data from **d** and **b**. N≥3 animals per group. **b-g** points represent individual animals. **a** points represent the mean. Bars/Lines at the mean +/- SEM. Significance by ANOVA, * $P < 0.05$, ** $P < 0.01$.

4.3 Chapter Summary

The work contributing to this chapter has expanded our understanding of how the ISGs IFI44 and IFI44L are induced during RSV infection where they restrict replication at an acute point. IFI44 and IFI44L were consistently upregulated in response to RSV infection in epithelial and monocytic cells *in vitro*. Similarly, *Ifi44* and *Ifi44l* were rapidly induced upon RSV infection in mice.

After development and optimisation of an overexpression assay, IFI44 and IFI44L were both shown to significantly restrict RSV infection as measured by the proportion of infected cells, levels of viral RNA, and the resultant level of recoverable viral particles in cell supernatant. These observations were further confirmed using siRNA and CRISPR-Cas9 gene editing to study RSV infection in the absence of either one or both ISGs. Knockout of *IFI44* or both genes was associated with an increase in susceptibility to infection, whereas knockout of either IFI44 or IFI44L significantly increased levels of viral RNA. Importantly, there was no further enhancement of RSV infection with the knockout of both genes, suggesting these genes may have redundant function. Although, only knockout of both *IFI44* and *IFI44L* was associated with an increase in influenza virus RNA during infection.

IFI44 and IFI44L were both shown to impact an early stage of RSV infection, suggesting a mechanism impacting initial stages of the viral life cycle. Virus attachment was not impaired by IFI44 or IFI44L expression. Use of a minigenome assay demonstrated that these ISGs reduce polymerase activity, although whether this is a direct or indirect mechanism affecting the viral polymerase, the cellular environment, or additional viral proteins, remains unexplored. Deletion of a G1 motif, predicted to contribute to GTP-binding, was dispensable for the antiviral activity of

IFI44. Although further study is required to confirm whether IFI44 proteins bind and hydrolyse GTP, and subsequent loss of binding in G1 mutant proteins.

Finally, I used an *Ifi44*$^{-/-}$ mouse model to investigate the role of IFI44 *in vivo*. Interestingly the commonly used inbred strain of mice C57BL/6 are *Ifi44l* deficient. The loss of *Ifi44* was associated with enhanced RSV disease. *Ifi44*$^{-/-}$ mice had significantly increased weight loss during one infection and levels of viral RNA in the lungs of *Ifi44*$^{-/-}$ mice were higher than WT mice at day 4, when viral replication peaks. These mice also had a dysregulated cytokine response with reduced IL-1β and CXCL10, important factors for instigating an appropriate pro-inflammatory response and immune cell recruitment respectively. The dampened CXCL10 response may explain the reduced number of $CD4^+$ T cells observed in a subsequent infection of *Ifi44*$^{-/-}$ mice.

Overall data presented in this chapter confirms the *in vitro* and *in vivo* relevance of IFI44 proteins as host factors involved in the control of RSV infection. As such, they may represent interesting factors for research into developing novel antiviral therapeutics or better identifying those individuals susceptible to severe RSV infection.

Chapter 5

Discussion

5 Discussion

5.1 Tools to Study ISG Activity *In Vitro*

5.1.1 Intrinsic Antiviral Capacity of Foreign Nucleic Acid

A central element of this thesis was the development of effective biological tools and assays to identify antiviral ISGs *in vitro*. During this process it became apparent that the delivery of nucleic acids, either by transfection or lentiviral transduction, was able to induce an antiviral state within cells that restricted subsequent RSV infection. This section discusses this issue and how it may affect the usability of these traditional approaches for the identification of pathologically relevant ISGs.

In this study, the transfection of plasmid DNA or lentiviral transduction resulted in subsequent restriction of RSV infection. However, transfection of short 21 base pair duplex siRNA molecules did not result in any significant change in levels of viral RNA (Fig 4.15c). RIG-I detects blunt-ended dsRNA of around 21 base pairs in length, but the siRNA used have deoxythymidine overhangs which may have reduced activation of RIG-I [299]. MDA-5 is also activated by blunt-ended dsRNA suggesting overhang inclusion may also reduce activity of this receptor. Reducing the length of these siRNA duplexes further to around 19bp could also reduce recognition by other RNA sensors such as TLR3 [300].

Transfection of plasmid DNA has been shown to activate the cytosolic nucleic acid sensor cGAS [174] which has been shown to restrict RSV infection [150]. This was previously thought to be a result of increased IFN production as a result of STING (Stimulator of IFN genes) activation by cGAS activity. However, the expression of several ISGs was not induced following plasmid DNA transfection into HEp-2 cells (Fig

3.7d). In addition, restriction of RSV infection following lentiviral transduction was still observed in cells treated with ruxolitinib (Fig 4.10d), which inhibits JAK-STAT signalling. However, these observations do not wholly rule out IFN as the causative pathway of RSV restriction following cell delivery of DNA. The concentration of ruxolitinib used was based on previously published studies [301] but inhibition of IFN responses was not confirmed. Interestingly this may suggest a DNA sensing response to an RNA virus. Study of whole transcriptome responses to non-host DNA would be interesting to determine the pathway responsible for viral restriction. This could identify novel host restriction factors or targetable pathways for the development of novel antivirals.

Antiviral activity of IFITM1 after plasmid transfection was still apparent (Fig 3.6) and a mild but significant impact of IFI44 on RSV infection was observed following lentiviral transduction (Fig 4.10b). However, the identification of mild or moderately antiviral ISGs, or those that promote the same antiviral signalling pathway instigated by transfection or transduction, may be hindered by cell stimulation resulting from the introduction of foreign nucleic acids. The use of *Stat1*$^{-/-}$ [150, 151], *cGAS*$^{-/-}$ [302], or *STING*$^{-/-}$ cell lines has been proposed as a means of alleviating this issue. The use of Vero cell lines, deficient in IFN-I production, has also been used to identify ISG function [207]. However, these approaches may again hinder identification of indirectly antiviral ISGs that promote antiviral signalling events reliant on intermediates such as STAT1. Stably transduced or knockout cell lines can reduce this issue, but they are not necessarily conducive for the high-throughput screening approaches required for research to tackle the large numbers of ISGs with no defined function. Using siRNA libraries with minimally stimulatory siRNA appears to be a good option, however efforts

should be made to validate on-target effects of the siRNA and reduce the impact of off-target knockdowns.

5.2 Antiviral Activity of IFITM1

5.2.1 Mutation of the IFITM1 CIL Domain Alters Subcellular Localisation

IFITM proteins contain two transmembrane domains which border a connecting CIL domain. Flow cytometry analysis of C-terminally HA-tagged IFITM1 mutants with stretches of the CIL domain replaced with alanine residues demonstrated that cell surface localisation, assessed by extracellular detection of the C-terminus, is reliant on the CIL domain (Fig 3.9). Immunofluorescence microscopy by Smith *et al* also showed a perinuclear localisation of most IFITM1 CIL mutants [207]. Interestingly, IFITM1$_{\Delta 76\text{-}81}$ (with the altered residues replaced with alanines) retained some cell surface expression of the C-terminus and a more diffuse expression pattern by microscopy. How alteration of the IFITM1 CIL domain impacts on cell surface localisation has yet to be completely defined.

Mutations in the IFITM3 CIL domain have also been shown to result in perinuclear localisation [222]. Interestingly, John *et al* did not observe altered localisation with mutation of the C-terminal end of the IFITM3 CIL domain [222], whereas mutation of comparable residues (IFITM1$_{\Delta 83\text{-}88}$) of IFITM1 resulted in aberrant perinuclear localisation (Fig 3.9b) [207]. CIL domain alteration could impede the ability of the bordering transmembrane domains to insert and orientate properly in the membrane, resulting in reduced cell surface expression. However, the observation that transmembrane-bordering residues in IFITM3 do not affect localisation suggests this is not the case and that it is specific regions and residues of the CIL domain that are involved in regulating proper localisation.

IFITM proteins are post-translationally modified with the addition of palmitoyl groups to certain cysteine residues in a process called S-palmitoylation. This palmitoylation has been shown to occur on human IFITM3 cysteine residues in the N-terminal transmembrane domain and a single residue in the CIL domain (C105) [303]. Palmitoylation of murine IFITM1 has been reported on two conserved cysteine residues in the first transmembrane domain, a conserved cysteine in the C-terminal end of the CIL domain, and one cysteine residue in the C-terminal domain [236]. However, Hach *et al* did not investigate localisation of murine IFITM1 proteins lacking palmitoylation on these residues [236]. Alanine replacement of the single cysteine residue in the CIL domain of human IFITM1 (C84) results in re-localisation to the lysosome [248]. S-palmitoylation at the Golgi membrane has been shown to sort proteins for anterograde transport [304], and so the loss of this post-translational modification may result in IFITM proteins undergoing retrograde transport from the Golgi to the ER. Localisation to the ER may explain the perinuclear distribution of IFITM mutants lacking cysteine residues predicted to be S-palmitoylated.

Interestingly, as C84 is the only cysteine residue in the CIL of IFITM1, this does not explain the impact on localisation of mutations spanning residues 63-81 (Fig 3.9). John *et al* have noted that mutation of R85 in the CIL domain of IFITM3 results in perinuclear localisation [222]. This residue is not palmitoylated, although arginine residues can be methylated, phosphorylated, undergo citrullination, carbonylation, and ADP-ribosylation [305]. This all suggests that there may be additional key residues or post-translational modifications in IFITM CIL domains involved in proper trafficking and localisation events. As such, additional investigation into single residue contributions to localisation and their post-translational modifications is required to fully elucidate the regulation of IFITM1 localisation to the cell surface by the CIL domain.

5.2.2 IFITM1 CIL Mutation Ablates Anti-RSV Activity

IFITM1 CIL mutants had significantly reduced antiviral activity during RSV infection (Fig 3.10). Here, mutation of residues 76-81 resulted in only partial loss of antiviral activity, whereas each other CIL mutant (IFITM1$_{\Delta 63\text{-}68}$, IFITM1$_{\Delta 69\text{-}74}$, IFITM1$_{\Delta 83\text{-}88}$) showed a complete loss of restriction. This may be due to the IFITM1$_{\Delta 76\text{-}81}$ protein retaining some level of cell surface expression (Fig 3.9). IFITM proteins are thought to interfere with a stage of viral entry [222, 229, 230, 232, 235, 239] and these data suggest IFITM1 activity is dependent upon localisation to the plasma membrane.

The ability of IFITM proteins to restrict virus entry was first suggested by Brass *et al* after they observed restriction of Influenza A virus infection within the first 12 hours of infection of either U2OS or A549 cell lines [232]. They then demonstrated that by expressing Influenza virus glycoproteins on the surface of a virus not normally restricted by IFITM1-3 (MLV) they could induce restriction, suggesting an impact on a viral glycoprotein-dependent stage of cell entry. Similarly for HIV-1, inducing expression of IFITM2 and IFITM3 following virus entry has no significant impact on virus replication, and virion fusion assays demonstrate only IFITM2 and IFITM3 significantly reduce HIV-1 entry [230].

There are of course several hypotheses for how the IFITMs inhibit virus entry. Receptor downregulation was suggested but as yet there is no evidence that IFITMs reduce expression of receptors for IFITM-susceptible viruses influenza and severe acute respiratory syndrome coronavirus [232, 245]. There are also no reports that IFITM proteins reduce virus attachment at the cell surface or trafficking into endosomes following endocytosis [221, 239].

Another hypothesis is that IFITM proteins directly inhibit passage of viruses across cellular membranes by acting at the site of fusion. This was proposed by multiple previous studies [230, 232, 245] but direct evidence for this was first presented by Li *et al* in 2013 [220]. This study observed that IFITM proteins could inhibit membrane fusion induced by a variety of viral membrane fusion proteins, also restricting syncytia formation. Membrane fusion is an ordered step-wise process that generally begins with a trigger, commonly pH change or receptor binding, that induces a conformational change in the viral membrane fusion protein [70]. This allows a fusion peptide to interact with the target host membrane. The now attached membranes begin to pull together as the fusion protein goes through another conformational change. Initially only the opposed proximal layers of each membrane become merged forming a structure known as a hemifusion [69, 70]. This is followed by fusion pore formation as the other layers of each membrane become fused [70]. The viral membrane fusion protein enters its final conformation which prevents the reversal of the process and sealing of the pore. Li *et al* reported that IFITM proteins restricted hemifusion in the context of influenza virus infection and suggested that this was a result of an alteration in membrane fluidity induced by IFITM expression [220]. Desai *et al* however demonstrated that restriction of influenza virus occurred at the point of pore formation [219]. Interestingly, mutation of hydrophilic residues in the N-terminal transmembrane domain is not though to alter localisation of the protein but does ablate the ability of IFITM1 to restrict influenza virus [306]. Chesarino *et al* suggest that this amphipathic helix in IFITM1 and IFITM3 stabilises membranes surrounding viral hemifusions which prevents pore formation.

This study has shown that IFITM1 antiviral activity during RSV infection requires cell surface localisation, further suggesting that IFITM1 inhibit viral membrane fusion at

the site of fusion. If IFITM proteins are required to localise at the site of virus-membrane fusion, forced expression of IFITM proteins to the plasma membrane may expand the range of activity to additional viruses. This has not yet been reported and it may be that dense localisation at certain plasma membrane locale, such as lipid rafts, is required for this. However, mutation of a C-terminal sorting signal in IFITM1 alters the subcellular distribution of IFITM1, increasing localisation to multivesicular bodies which enhanced restriction of Jaagsiekte sheep retrovirus pseudovirions which localise to the same compartment [227]. In addition, a plasma membrane-localised IFITM3 mutant, IFITM3$_{Y20A}$, does more robustly inhibit cell-cell fusion mediated by influenza virus HA [306]. Although this mutant has not been reported to restrict any viruses previously unaffected by IFITM3, this would be an interesting experiment to confirm the requirement for IFITM localisation to the site of fusion.

To further understand the mechanism of action of IFITM1 and other IFITM proteins it will be essential to study the interaction of these factors with the viral fusion pore. Super-resolution microscopy and co-immunoprecipitation with subsequent mass spectrophotometry could be used to confirm whether there is a direct interaction between IFITM proteins, viral proteins, or additional host factors at the site of fusion.

5.2.3 RSV Infection is Controlled by IFITM1 *in Vivo*

The results of this study demonstrate for the first time that *Ifitm1* alone plays a significant role in the control of RSV infection *in vivo*. Viral load was increased at the peak of infection in KO mice, which likely resulted in the increased levels of cells recruited to the lung tissue and enhanced expression of pro-inflammatory cytokines IL-1β and IL-6 (Fig 3.11). These data support our *in vitro* observations that IFITM1 alone can efficiently restrict RSV infection.

Ifitm3 has also been shown to be important for the control of RSV infection with a similar phenotype of enhanced weight loss, viral load, and higher levels of IL-1β [209]. In addition, *Ifitm3*$^{-/-}$ mice infected with RSV had increased numbers of CD3^{+} cells in lung tissue and elevated IFN-γ levels. It would be interesting to determine whether this is a feature also seen during RSV infection of *Ifitm1*$^{-/-}$ mice.

IFITM1 and IFITM3 are expressed in distinct cellular localisations with IFITM1 found predominantly on the plasma membrane and IFITM3 found on endocytic compartments. If IFITM1 function is primarily mediated at the plasma membrane independently of IFITM3 disease severity could be further enhanced in an *Ifitm3*$^{-/-}$ *Ifitm1*$^{-/-}$ mouse strain. Although IFITM3 has been shown to restrict TLR responses of murine cells, limiting pathogenesis of mCMV *in vivo* without directly restricting viral entry. It may not be possible to separate these disparate functions contributing to pathogenesis in a double IFITM knockout model [307].

5.3 Limitations and Future Work: IFITM1

5.3.1 CIL Mutant Localisation

Localisation of IFITM1 CIL mutants was confirmed using an antibody binding a C-terminal HA epitope tag. Using flow cytometry, IFITM1 CIL mutants were shown to have reduced cell surface localisation. However, it is possible that IFITM1 retained cell surface localisation in a topology with an intracellular C-terminal domain. Several studies have confirmed the extracellular localisation of the IFITM1 C-terminal domain [226, 227] and microscopy by S. Smith also suggests that CIL mutants had reduced cell surface localisation. However, this microscopy did not take full z-stacks to provide a 3-dimensional view of localisation. Confirmation of localisation using an antibody

targeting endogenous IFITM1, an N-terminal tag, and confocal microscopy could be used to improve this analysis of IFITM1 CIL mutant localisation.

5.3.3 Single Nucleotide Mutagenesis of CIL Domain

Confirmation of S-palmitoylation of human IFITM1 cysteine residues, and their impact on localisation would further our understanding of IFITM1 regulation. In addition, there could be additional residues within the CIL domain that affect localisation. The approach of alanine replacement of blocks of six residues could be improved by producing single residue mutant proteins. This would allow for single residue resolution of how the CIL domain impacts localisation and would allow identification of the type of post-translational modification that may be responsible.

5.3.4 CIL-Independent Mis-Localisation

Mis-localisation of intracellular IFITM1 has been observed by altering a C-terminal sorting signal [227]. However, the impact on cell surface localisation in this mutant protein was not characterised. Smith *et al* has generated a panel of mutant IFITM1 proteins with alanine blocks replacing residues throughout the entire protein. This library could be used to generate stably transduced cell lines to examine the impact on surface localisation of alteration of this C-terminal sorting signal. In addition, it would be interesting to examine whether mutations in close proximity to the transmembrane domains of IFITM1 in either the C- or N-terminal domains had an impact on localisation, similar to seen with mutations in the CIL domain.

5.3.4 Human Studies

Having investigated the importance of IFITM1 *in vitro* and now *in vivo*, a next step to determining the relevance for human infection is the identification of human SNPs associated with a predisposition to severe RSV LRTI.

Two *IFITM3* SNPs have been associated with severe influenza infection [241, 281, 308]. The role of the SNP rs12252-C remains controversial as studies of Caucasian populations where the C allele is rare generally find no association with significant infection [309-314] whereas multiple studies of Chinese patients where the C allele is more common have reported an association [250, 315-317]. The second *IFITM3* SNP (rs34481144-A) to be linked to severe Influenza A virus infection is found within the promoter of the *IFITM3* gene and is thought to reduce expression of IFITM3 [281].

It was suggested that the rs12252-C allele encoded an IFITM3 protein with a disrupted YXXF motif in the N-terminal domain required for proper localisation. Everitt *et al* have reported reduced antiviral activity of this mutant IFITM3 but several studies have since reported that the predicted truncated transcripts are not detectable in cells homozygous for the C allele [309, 318]. Mis-localisation impacting function and disease severity would be supported by our observation that IFITM1 function is tied closely to its proper subcellular localisation.

To date there are no studies linking SNPs in either *IFITM1* or *IFITM2* to any clinical conditions. The studies of *IFITM3* highlight the need for study of a variety of populations to properly assess SNP impact.

5.4 Antiviral Activity of IFI44 and IFI44L

5.4.1 How Does IFI44 Impact RSV Polymerase Activity?

IFI44 and IFI44L were both observed to restrict RSV infection at an early time point (Fig 4.26) and to reduce activity of an RSV minigenome system (Fig 4.28), suggesting these ISGs reduce activity of the viral polymerase.

Initially restriction of RSV infection was observed in IFN-I-deficient stably transduced Vero cell lines, with levels of viral RNA reduced by 18% ($P < 0.05$, Fig 4.6c), but only when cells were pre-treated with IFN-I. This may be due to differences in proliferation rates between vector-transduced and IFI44L-expressing cell lines affecting initial m.o.i. and subsequent ratio of viral RNA to host RNA. An alternative is that IFI44L may require additional IFN-induced host factors for its antiviral activity. However, in transiently transduced cells treated with ruxolitinib (Fig 4.10d) or stably transduced A549s IFI44 or IFI44L expression reduced viral RNA and the proportion of infected cells ($P < 0.05$, Fig 4.13). As such, our data suggest IFI44 and IFI44L function independently of IFN responses to mediate antiviral activity.

Schoggins *et al* have previously reported that lentiviral transduction with the same IFI44 and IFI44L vectors used in this study does not restrict RSV infection [150]. However, in this high-throughput screen different lentivirus stocks were not titrated or normalised. In addition, protein expression was not confirmed following transduction. Interestingly the screen by Schoggins *et al* also reported no antiviral activity during RSV infection for several ISGs previously shown to restrict RSV including OASL [175, 176, 204], Viperin [205], IFITM1 [207, 208], and IFITM3 [207-209]. This may be due to differences in cell lines, levels of protein expression, or differences in viral load. This study used stably-transduced cell lines of a relevant origin with confirmed constitutive expression of either IFI44 or IFI44L mRNA and IFI44 protein. In addition, siRNA knockdown of both IFI44 and IFI44L using two different siRNA formulations resulted in significant enhancement of viral RNA (Fig 4.14-15). Knockout cell lines were also more susceptible to RSV infection across multiple assay readouts (Fig 4.24). These loss-of-function studies further our understanding of IFI44 proteins and provide novel tools for further work to investigate their function and range of antiviral activity. I believe

this study provides convincing evidence that IFI44 and IFI44L are antiviral during RSV infection, building on the previous observation by McDonald *et al* [204].

RSV infection was restricted by IFI44 and IFI44L at an early point which may have resulted from reduced viral attachment and subsequent entry. There was no observable reduction in virion attachment to IFI44 or IFI44L-expressing cells (Fig 4.27). To date there remain no confirmed mechanism of ISG function that reduces initial virion attachment.

When considering the reduction in minigenome activity in IFI44 or IFI44L-expressing cells, there are several possibilities. First, this difference may be due to an overall dampening of cellular translation. However, β-galactosidase expression driven by a host polymerase was comparable between WT and IFI44 or IFI44L-expressing cells suggesting that this is not the case (Fig 4.28f).

Second, IFI44 proteins may impact directly on activity of the viral polymerase by interacting with the viral genome or other viral proteins required for optimal replication or transcription. The minigenome construct used is unable to differentiate between an impact on replication or transcription due to the presence of both Leader and Trailer regions. IFI44 has been reported to interact with genome-integrated HIV-1 DNA [257], specifically in a promoter region, and so it may be that these proteins bind a similar region in the RSV genome such as the Leader or Trailer promoter regions. However, it may be that the pull-down of IFI44 with HIV-1 DNA was a result of an indirect interaction, with IFI44 bound to the host RNA polymerase II or accessory host or viral factors directing transcription from the viral promoter region.

IFI44 was initially identified as a microtubular aggregate protein. Microtubules, the largest of the cytoskeletal filaments, play a role in a variety of viral infections including

internalisation [319, 320], trafficking viral proteins, nucleocapsids [321, 322], or mature virions throughout the cytoplasm [323], assembly, and budding [79]. Normal microtubule function has been shown to be important for both entry and early replicative stages of the RSV life cycle, although no direct impact on genome transcription or replication has been reported [324]. As such, it seems unlikely that IFI44 or IFI44L mediate their activity directly by interacting with microtubules or other elements of the host cytoskeleton. Further work would be required to expand our understanding of how and why IFI44 proteins interact with the cytoskeleton, and whether this contributes to antiviral defence.

Finally, we hypothesised that as IFI44 and IFI44L are predicted GTPases they may deplete the available pool of cytoplasmic GTP required for viral transcription and genome amplification. Capping of viral mRNAs relies on the addition of guanine nucleotides to the 5' end of nascent mRNAs and subsequent methylation by the viral polymerase [53]. Depletion of guanine nucleotide levels by IFI44 or IFI44L could disrupt this process leaving viral mRNAs more susceptible to recognition by uncapped RNA sensors such as RIG-I [100]. Antiviral activity of several IFN-inducible GTPases such as MXA and GBP1 requires a complete G1 motif [325, 326], with deletion of the conserved lysine residue reducing the antiviral activity of both ISGs. However, deletion of the entire G1 motif of IFI44 resulted in no loss of antiviral activity (Fig 4.32). As such, the mechanism by which IFI44 inhibits RSV genome transcription or replication remains undefined.

5.4.2 IFI44 Proteins as Regulators of IFN Responses

A very recently published pair of studies have suggested a role for IFI44 and IFI44L as negative regulators of IFN responses [327, 328]. IFI44 and IFI44L overexpression was reported to reduce ISG and IFN-III induction by IFN-I treatment, with the opposite

effect seen with siRNA-mediated knockdown. However, I have observed no significant effect on IFN responses in *in vitro* assays or in *Ifi44*$^{-/-}$ mice. Stable overexpression of IFI44 and IFI44L was associated with no significant difference in levels of *MX1* mRNA either at rest or following IFN-I stimulation, although there was a trend towards increased *MX1* expression in IFI44L-expressing cells (Fig 4.11c). Similarly, in knockout cell lines only the loss of *IFI44L* was associated with a trend towards reduced ISG expression (Fig 4.23e). In addition, IFN-β and IFN-γ levels were no different in *Ifi44*$^{-/-}$ mice following four (Fig 4.37a-b) or seven (Fig 4.41f-g) days of RSV infection. DeDiego *et al* did not assess levels of IFN-I or IFN-II expression but did look at IFN-λ1 expression, although their reasoning for choosing this subtype of IFN was not explained [327].

It is unclear whether proliferation of the cell lines assayed by DeDiego *et al* was altered by IFI44 or IFI44L expression as seen in our overexpressing or knockout cell lines. If this was not accounted for then differences in cell number could explain some observations of reduced IFN signalling. Overall my *in vitro* and *in vivo* data do not support a role for IFI44 proteins as negative regulators of ISG responses.

5.4.3 Anti-Proliferative Function of IFI44 Proteins

The anti-proliferative impact of IFN signalling was first described in 1962, with a reversible dose-dependent decline in growth rates observed in L cells treated with IFN [329]. Prolonged treatment resulted in a near complete halt of cellular division. IFN-I stimulation is now known to promote p53 activity, phosphatidylinositol 3-kinase (PI3K) signalling and expression of several cycle cell regulatory and pro-apoptotic factors in order to regulate cell proliferation and apoptosis [330]. Another layer of regulation is that several antiviral ISG products have also been reported to modulate cellular proliferation including OASL [331], IFITM1 [332], IFITs [333], and PKR [334].

Stably transduced clonal A549 cell lines expressing IFI44 or IFI44L were shown to proliferate at a slower rate than vector transduced cells (Fig 4.12). Several of the assays used assess the number of viable cells in the culture well which could have been affected by an increase in cell death instead of just a reduction in metabolic activity and proliferation. However, there was no increase in cytotoxicity associated with either IFI44 or IFI44L expression (Fig 4.12e). Interestingly, knockout of either or both ISGs resulted in enhanced rates of proliferation even in the absence of IFN stimulation suggesting that basal levels of IFI44 and IFI44L are sufficient to impact on proliferation (Fig 4.23a-c). This is the first study to characterise the impact of loss of both ISGs on cell proliferation *in vitro*. *IFI44* expression alone has previously been reported to reduce proliferation of two melanoma cell lines, although the effect was relatively minor (~20% reduction vs control) [256]. In addition, *IFI44L* expression has been examined in liver and hepatocellular carcinoma tumours [261]. An association was described between low levels of *IFI44L* mRNA and increased tumour size, suggestive of an impact on proliferation. Knockdown of IFI44L in hepatocyte-derived cell lines also showed increased migration and invasion ability, along with enhanced activation of the Met/Src signalling pathway. IFI44L may inhibit this signalling pathway, previously shown to modulate proliferation, in order to reduce cell growth. Although the molecular mechanisms and interacting host factors involved have yet to be identified. Met/Src signalling has not been studied in IFI44-expressing cells.

The question remains as to whether the antiproliferative function of these ISGs plays any role in their antiviral activity. Arresting the cell cycle can increase availability of host machinery required for viral genome replication and viral assembly [335]. During RSV infection the matrix protein induces cell cycle arrest through activation of p53/p21 resulting in enhanced infection [336, 337].

Unlike IFI44L, IFI44 contains an N-terminal TLDc domain, although this only shares some 15% amino acid identity with other TLDc proteins such as NCOA7 and OXR1 [338]. TLDc proteins are thought to be involved in protection from oxidative stress by modulating levels of reactive oxygen species (ROS). High levels of ROS can cause damage to cellular proteins, lipids, and DNA, leading to apoptosis [339]. However, low levels of ROS can in fact promote proliferation whereas intermediate levels of ROS can induce growth arrest not associated with cell death. As such, manipulation of ROS levels could explain the antiproliferative function of IFI44, although it is perhaps more likely that IFI44 and IFI44L impact proliferation through similar mechanisms. Murine IFI44L is annotated with an N-terminal TLDc domain and deletion of this region in human IFI44L resulted in a loss of antiviral activity in stably transduced cells compared to cell expressing WT IFI44L (Fig 4.34). However, protein expression of the IFI44L mutant protein could not be confirmed or compared to that of the WT protein.

ROS formation is induced during RSV and is thought to promote autophagy which in turn inhibits apoptosis, promoting viral replication [206]. Mutagenesis approaches should be used to examine whether the TLDc domain contributes to the antiproliferative function of IFI44 and whether this also confers antiviral activity. N-terminal deletion IFI44 mutants were designed during this study but were not completed in time for inclusion in this thesis.

5.4.4 The Role of IFI44 *in Vivo*

Single gene knockout mouse strains of ISGs *Ifitm3* [209], *Ifitm1* [207], and regulatory genes including *Irf7* [204] exhibit signs of enhanced RSV disease severity, often characterised by increased weight loss and viral load. In addition, changes in cytokine production and T cell responses have been associated with disease severity and

delayed viral clearance *in vivo*. This study reported a similar phenotype in *Ifi44*$^{-/-}$ mice, suggesting a role for IFI44 *in vivo*.

Ifi44$^{-/-}$ mice lost significantly more weight than age and sex-matched controls in one experiment (Fig 4.41a), although this was not seen in a repeat infection (Fig 4.43a). However, the difference remains significant when combining data from both independent infections. Weight loss is often used as a readout of disease severity and is caused by inappetence linked to $CD8^+$ T cells [340].

Studies of *IFI44* function in cell culture in this study suggested an early role for IFI44 in restricting initial replication of the viral genome within infected epithelial cells (Fig 4.26). Loss of *Ifi44 in vivo* was associated with elevated viral titre in lung tissue at the peak of infection (Fig 4.36b), which may be a result of a loss of this early control mechanism. However, this may also be a result of altered activation of an innate response during infection as a decrease in IL-1β (Fig 4.36e) and CXCL10 (Fig 4.36g) was also observed at this point of infection. Blockade of IL-1β prior to RSV infection can increase viral load [341]. IL-1β is produced in response to inflammasome activation which can also result in pyroptosis and subsequent release of DAMPs into the tissue microenvironment. Reduced IL-1β may be a result of reduced inflammasome activation and a reduction in DAMP release in the lung could reduce priming of uninfected cells which could result in enhanced viral spread, compounding the impact of increased intracellular RSV genome amplification. However, RSVΔSH has been shown to elicit greater IL-1β production *in vitro*, suggesting that WT RSV may inhibit IL-1β production [341]. As such increased viral replication as a result of the loss of *Ifi44* expression may be dampening IL-1β secretion by lung cells. Similarly, this study cannot determine whether the altered levels of CXCL10 are a result of the loss of *Ifi44* directly or indirectly following increased viral replication.

Interestingly, both IL-1β and CXCL10 are important for immune cell recruitment but no difference was seen in cell counts in either BALF or lung tissue suggesting no widespread changes in inflammation throughout the infected tissue. However, a reduction in the total number of $CD4^+$ T cells was noted in one experiment (Fig 4.43e), along with a concordant increase in the percentage of total live lung cells that were $CD8^+$ T cells (Fig 4.43d).

Both $CD4^+$ and $CD8^+$ T cells have been shown to be important for reducing the duration of viral shedding and amount of weight loss during murine RSV infection [298]. In children immunodeficiencies impacting T cell function have also been associated with increased RSV disease severity [21]. RSV infection of human DCs impairs their ability to promote $CD4^+$ T cell proliferation which may be exacerbated by the increased viral load in *Ifi44*$^{-/-}$ mice [342].

5.5 Limitations and Future Work: IFI44 Proteins

5.5.1 Clonal Cell Lines

One limitation of the *in vitro* work in this study is the use of clonal cell lines. Clones may deviate from the parental polyclonal cell line and differences may have contributed towards differences in susceptibility to infection and proliferation rates. However, observations in clonal cell lines were also replicated in polyclonal populations using transient transduction to overexpress IFI44 or siRNA to knockdown either IFI44 or IFI44L expression. It would be useful to assess an impact on proliferation following IFI44 transduction.

To better understand the contribution of IFI44 and IFI44L it would be interesting to develop a dual overexpression assay where each gene could be expressed. Further,

adapting this system to IFN deficient cell lines such as Vero cells, or generating *STAT1*$^{-/-}$ A549 cells, would allow confirmation of any requirement for IFN-inducible host factors for the antiviral activity of IFI44 or IFI44L.

5.5.2 Gene Knockout Validation

A549 and HEp-2 knockout clones generated using CRISPR-Cas9 were validated by PCR and sequencing of the targeted genomic region. A549 ΔIFI44ΔIFI44L were not verified by sequencing as the targeted region was not able to be amplified by PCR. However, each A549 knockout cell line was also validated by the loss of IFI44 or IFI44L protein expression following IFN-I stimulation. The validity of all knockout cell lines could be further corroborated by sequencing of cDNA isolates instead of genomic DNA. This would allow sequencing of each actively transcribed allele in polyploidy A549 cells but would require next generation sequence approaches or the use of demultiplexing software, which requires high quality trace signatures following Sanger sequencing. The use of transfected plasmid DNA to deliver the Cas9 enzyme and gRNA has also been improved upon by several studies using direct delivery of gRNA:Cas9 ribonucleoprotein complexes. This approach is reported to result in significantly higher rates of editing which can allow for analysis with minimal clonal selection.

A whole genome sequencing approach should be utilised in future work generating CRISPR-Cas9-edited cell lines to screen for off-target activity. Guide RNA sequences were selected that had low predicted off-target activity, but this study was unable to verify that there were no off-target effects that may have influenced the subsequent infectivity and proliferation assays.

5.5.3 RSV Infection

Cells infected with rgRSV expressed GFP, but this does not necessarily confirm the establishment of viral transcription and productive infection. The coding sequence of GFP is at the 3' end of the modified viral genome so it is expressed first. Transcription of viral mRNAs and replication of the viral genome cannot be confirmed by the measurement of GFP alone. Therefore, I utilised multiple readouts for infection including measurement of L gene RNA and the presence of infectious virus in cell supernatants. RSV A2 and rgRSV stocks were produced by the collection of supernatant from infected HEp-2 cells. The medium was not cleared by centrifugation or the virus otherwise purified. As such, the virus stocks may have included immunostimulatory molecules derived from infected cells. This may have further reduced the range of assays aiming to detect immunomodulatory or moderately antiviral ISGs.

5.5.4 L Gene qPCR

PCR of viral L gene cDNA amplifies both antigenome-derived and L gene mRNA cDNA. As such, this qPCR is not a pure readout of either viral transcription or genome amplification. To measure viral transcription a specific purification of mRNAs would be required. Genome amplification could also be measured by using primers binding intergenic sequences not present in viral mRNAs.

5.5.5 Minigenome Studies

Minigenome studies compared stably transduced clonal cell lines to parental polyclonal cells, which may have had differences aside from IFI44 or IFI44L expression affecting minigenome activity. Comparison of multiple clonal populations expressing IFI44 or IFI44L to several clonal controls and the polyclonal parental cell

line could improve this analysis. In addition, the pTRIP lentiviral transfer vectors used in this study could be modified to encode an antibiotic resistance factor to allow selection using antibiotics instead of FACS which would produce a polyclonal population of stably transduced cells. Minigenome activity was also only assessed at a single time point. Assaying activity at earlier time points could improve our understanding of when during infection IFI44 or IFI44L are active.

As discussed previously there are multiple explanations for how IFI44 or IFI44L may have affected minigenome activity. To examine whether these ISGs inhibit polymerase activity directly or indirectly each RSV protein expressed as part of the minigenome system should be expressed with an epitope tag allowing co-immunoprecipitation and immunofluorescence to confirm any interaction or co-localisation. In addition, examining the amounts of each viral protein could reveal whether IFI44 or IFI44L impact expression of a specific protein. This could be by promoting degradation of proteins or by reducing translation of viral mRNAs. A gel-shift assay, or equivalent could be used to investigate whether these ISGs interact directly with the viral genome to inhibit replication or transcription. Further, a modified minigenome lacking the Trailer region and thus unable to replicate could be used to identify if IFI44 or IFI44L have differential impacts on RSV genome replication and transcription of viral mRNAs. Alternatively, a strand-specific qPCR could be developed to specifically assess levels of viral transcription and genome replication [343].

5.5.6 Virus Entry

Any impact of IFI44 or IFI44L on RSV cell entry was assessed indirectly through virus binding assays or implied through minigenome assays where virus entry is bypassed. To further investigate whether these ISGs impact RSV entry, pseudotyped viruses could be used. These could include pseudotyped RSV particles (e.g. expressing VSV-

G) or a lentiviral vector pseudotyped with RSV glycoproteins. This approach has been used previously in the study of IFITM antiviral tropism [219, 221, 235].

5.5.7 Proliferation

Proliferation was enhanced or reduced in IFI44 or IFI44L knockout or overexpressing clonal cell lines respectively. However, when siRNA was used to knockdown expression of either or both ISGs, only the knockdown of IFI44L resulted in trend of increased proliferation. This may be due to the knockdown of IFI44 being associated with enhanced IFI44L expression, which may have reduced cellular proliferation. However, the knockdown of both ISGs also resulted in reduced proliferation. siRNA transfection can induce significant toxicity and so to properly interpret these data any toxicity should be separated from a reduction in proliferation. There may also have been off-target knockdowns that could have influenced cell survival and proliferation.

The reduced proliferation of overexpressing cell lines was also examined using CellTrace Violet dye perfusion and dilution. A limitation of this approach was the use of distinct cell lines which may have altered levels of dye uptake, influencing the final fluorescence distribution plot.

To examine how IFI44 and IFI44L impact proliferation, levels of p53 and cell cycle regulators could be examined. Measuring levels of certain cyclins could determine if cells are halted at a certain point of the cell cycle, which may in turn provide a clue as to the host factors and pathways involved. IFI44L is thought to influence proliferation of hepatocyte-derived cells by influencing Met/Src signalling which should be examined in additional lung-derived cell lines for confirmation [261]. Any impact of IFI44 on Met/Src signalling should also be investigated as it is likely these proteins influence proliferation through similar mechanisms.

5.5.8 Mutagenesis and Mechanistic Investigations

This study could not confirm the antiviral contribution of the N-terminal domain of IFI44L due to the lack of an effective antibody. The stably transduced cell line had comparable levels of IFI44L mRNA but without confirmation of comparable protein levels, conclusions could not be properly drawn. All mutagenesis studies could be improved by the inclusion of appropriate terminal epitope tags. Deletion of the TLDc domain of IFI44 should be a priority along with mutation of the equivalent N-terminal domain of IFI44L.

Studies of the G1 motif of a predicted GTPase domain in IFI44 suggested that this motif had no impact on antiviral activity. Expression of IFI44L$_{\Delta 200\text{-}208}$ in stably transduced cells could not be confirmed, although cells were no more resistant to infection than vector transduced controls.

Expression of additional GTPase mutant proteins, with G2, G3, and G4 motif mutations, could be used to further characterise the contribution of the GTPase domains to IFI44 and IFI44L antiviral or anti-proliferative functions. It would be important to investigate how GTP-binding and hydrolysis was affected with each mutation. To assess the functionality of the predicted GTPase domains of IFI44 and IFI44L, whole cell nucleotide levels could be analysed to determine changes in GTPase activity [344]. *In vitro* expression and purification of IFI44 and IFI44L proteins could be pursued in order to directly assay any GTPase or GTP-binding activity.

5.5.9 Human Studies

To determine whether *IFI44* and *IFI44L* activity is important for control of RSV infection in humans, infants with severe RSV infection could be examined for SNPs within these genes. Mutant proteins could then be assayed *in vitro* to confirm any impact on antiviral

activity. One study has examined a single SNP of *IFI44* in a cohort of German infants with severe RSV infection [345]. The SNP rs11577395 was not associated with severe infection, although why only this SNP was studied was not explained. rs11577395 is a non-coding SNP located at the 3' end of an intron between exons 7 and 8 of *IFI44*. As such, rs1157739 may perturb transcript processing or stability but no direct role for influencing IFI44 expression or function has been reported.

Interestingly, the missense coding SNP rs273259 in *IFI44L* has been associated with altered measles virus antibody levels and febrile seizures following MMR vaccination [346, 347]. The A allele was associated with increased risk of seizure, increased antibody titre, and reduced expression of *IFI44L* exon 2 which results in altered levels of IFI44L isoforms. This variant demonstrated no altered antiviral activity against measles virus infection *in vitro*, although it would be interesting to investigate the impact of altered isoform levels on antiviral activity of IFI44 and IFI44L during RSV infection.

In parallel with my IFI44 study, collaborators examined a published gene expression dataset to examine *IFI44* and *IFI44L* expression in a cohort of infants with RSV infection (Fig 5.1a). There was a significant decrease in expression of both *IFI44* and *IFI44L* in those infants requiring admission to a paediatric intensive care unit (PICU) relative to infants with confirmed RSV infection that required general admission (Fig 5.1b-c). *IFI44* expression correlated with *IFI44L* expression across both moderate and severe RSV patients (Fig 5.1d). Lower expression levels of antiviral ISGs may explain some of the heterogeneity in disease severity and predispose to severe RSV. The observed reduction in *IFI44* and *IFI44L* expression may be a result of reduced IFN activity as a whole, which has been observed in another cohort of infants with severe RSV infection [129]. To understand the impact of reduced *IFI44* and *IFI44L* expression

would require further work with cohorts including healthy controls and those with mild RSV illness not requiring hospitalisation.

a

	Definite RSV with no co-infection
Number of patients	18
Age – mo. median (IQR)	3.6 (1.2-6.9)
Male – No. (%)	11 (61%)
Ethnicity Caucasian – No. (%)	9 (50%)
Intensive care – No. (%)	12 (67%)
Deaths – No. (%)	0 (0%)
Neutrophil % - median (IQR)	43.3 (40-54.3)
Lymphocyte % - median (IQR)	42.4 (32.7-50.7)
Monocyte % - median (IQR)	10 (4.3-15)

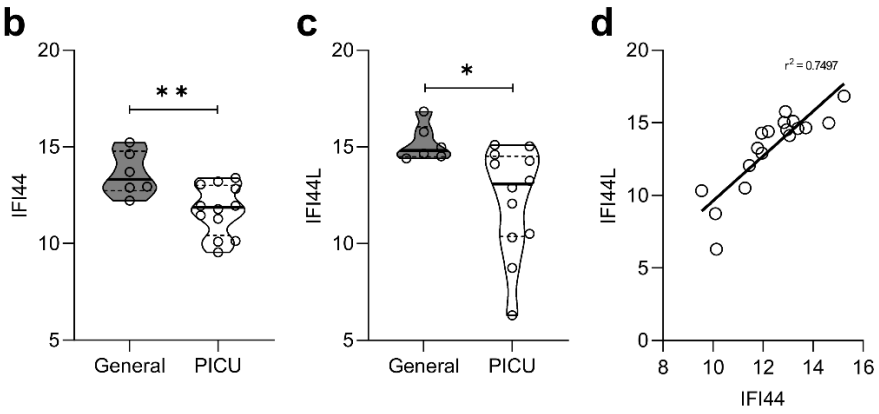

Figure 5.1. IFI44 and IFI44L expression is reduced in infants with severe RSV infection. (a) Demographic and clinical features of patient group. Patients are febrile children with immunofluorescence-confirmed RSV infection. Patients with suspected or confirmed bacterial co-infection were excluded (n = 4) and are not included in this table. **(b)** IFI44 or **(c)** IFI44L expression levels in either patients admitted to a general ward with mild RSV illness or admitted to a paediatric intensive care unit (PICU) at the same hospital. Significance by unpaired t-test. **(d)** Pearson correlation analysis of expression of IFI44 and IFI44L. P < 0.001 (analysis by D. Habgood-Coote, Imperial College London).

5.6 Implications for Antiviral Therapy

The studies described in this thesis demonstrate that there are additional ISGs that restrict RSV infection, and that their function can be relevant to disease severity *in vivo*. Additional screening should be undertaken to identify novel antiviral ISGs and even extended to genes of unknown function that are modulated by IFN treatment, even if lacking the classical ISRE or GAS promoter sequences of an ISG.

The breadth and variety of ISG function is a potential untapped source for the design of novel antiviral therapies. This study has shown that IFI44 and IFI44L impact RSV replication which results in reduced activity of the viral polymerase or reduced translation of viral mRNAs. Understanding how IFI44 and IFI44L impact on RSV replication could provide additional strategies for the development of polymerase inhibitors. Of course, it should be considered that, if IFI44 and IFI44L modulate IFN responses either positively or negatively as proposed in other studies [327, 328], adapting their antiviral mechanism may result in dysregulated IFN responses which could result in enhanced immunopathology or reduced viral control.

Targeting the function of the viral polymerase is an attractive option for an antiviral therapy due to the essential function of this protein complex. This is especially true for treatment of RNA viruses which employ RNA-dependent RNA polymerases not found in human cells. The development of an RSV polymerase inhibitor AL-8176, a nucleoside analogue, has recently been abandoned by Johnson & Johnson [348]. This was the first RSV polymerase inhibitor to report a reduction in viral load in nasal washes in a trial of RSV inoculated adults, providing proof of concept for the therapeutic benefit of targeting of the RSV polymerase [349]. The RSV polymerase catalyses RNA synthesis as well as the addition of a guanosine cap to the 5’ end of

viral mRNAs and subsequent methylation of this cap [350]. As such, non-nucleoside inhibitors have been proposed that may inhibit these additional capping and methylation reactions, although only one (PC786) [351] appears to have progressed past pre-clinical study (Table 5.1). An analysis of 173 registered clinical trials (https://clinicaltrials.gov/) investigating RSV infections revealed the majority of antivirals tested (12 candidate therapies) target the RSV F protein, with three candidate N protein inhibitors also progressing to phase II trials. Combining an anti-F antiviral with a polymerase inhibitor could have a synergistic effect by targeting stages both before and after establishment of infection. This approach would be like that mounted by the host cell, with antiviral ISGs targeting multiple stages of the viral life cycle.

Name	Development phase	Mechanism of Action	Reference
PC786	Phase II	Uncharacterised	[351]
BI-D	Pre-clinical (*in vitro* and mouse model)	Inhibits transcription and replication. Inhibits capping, causes abortive RNA synthesis	[352, 353]
YM-53403	Pre-clinical (*in vitro*)	Uncharacterised	[354]
AZ-27	Pre-clinical (*in vitro*)	Inhibits transcription and replication by interfering with initiation.	[355]

Table 5.1 Development of RSV polymerase inhibitors.

5.7 Redundancy in Antiviral Defence

An interesting point raised by this study of IFI44 proteins and IFITM1 is one of redundancy of ISGs in the control of infection. Additional studies of ISG knockout mice including *Ifitm3* [209] and *Irf7* [204] demonstrate enhanced RSV disease severity. This is also seen for influenza [241], West Nile virus, and alphavirus infection with *Ifitm3* [209]. Considering the scale of the ISG gene network one could assume that single gene loss would not result in the loss of viral control. Even primary immunodeficiencies in humans caused by mutations in IFN sensing or signalling pathways (e.g. *STAT1* and *TLR3*) only result in incomplete penetrance with individuals displaying specific susceptibilities [356]. The use of a mouse model of RSV infection may exacerbate the role of individual genes through the relatively large volumes of viral inoculums and high doses of virus which may stress the system more than would occur in a natural infection setting. ISGs likely work in concert to control natural infection, with multiple ISGs able to counter different steps of a viral life cycle.

5.8 Concluding Remarks

Intrinsic antiviral responses driven by IFN are clearly important during a variety of viral infections. However, there remain many uncharacterised antiviral ISGs. The studies presented here further characterise the antiviral activity of IFITM1, IFI44, and IFI44L while also providing the first indication that these genes contribute towards disease severity *in vivo*. Understanding which ISGs restrict RSV infection and how they do so would improve our understanding of how host responses contribute to RSV disease and interindividual variety.

6 References

1. Cockburn, W.C. and F. Assaad, *Some observations on the communicable diseases as public health problems.* Bull World Health Organisation, 1973. **49**(1): p. 1-12.
2. Troeger, C., et al., *Estimates of the global, regional, and national morbidity, mortality, and aetiologies of lower respiratory tract infections in 195 countries: a systematic analysis for the Global Burden of Disease Study 2015.* The Lancet Infectious Diseases, 2017. **17**(11): p. 1133-1161.
3. Patwa, A. and A. Shah, *Anatomy and physiology of respiratory system relevant to anaesthesia.* Indian J Anaesth, 2015. **59**(9): p. 533-41.
4. Tregoning, J.S. and J. Schwarze, *Respiratory viral infections in infants: causes, clinical symptoms, virology, and immunology.* Clin Microbiol Rev, 2010. **23**(1): p. 74-98.
5. Hall, C.B., et al., *Respiratory syncytial virus-associated hospitalizations among children less than 24 months of age.* Pediatrics, 2013. **132**(2): p. e341-8.
6. Everard, M.L., *Paediatric respiratory infections.* Eur Respir Rev, 2016. **25**(139): p. 36-40.
7. van Benten, I., et al., *Predominance of rhinovirus in the nose of symptomatic and asymptomatic infants.* Pediatr Allergy Immunol, 2003. **14**(5): p. 363-70.
8. Jartti, T., et al., *Persistence of rhinovirus and enterovirus RNA after acute respiratory illness in children.* J Med Virol, 2004. **72**(4): p. 695-9.
9. Estripeaut, D., et al., *Respiratory syncytial virus persistence in the lungs correlates with airway hyperreactivity in the mouse model.* J Infect Dis, 2008. **198**(10): p. 1435-43.
10. Gadomski, A.M., A.L. Bhasale, and A.M. Gadomski, *Bronchodilators for bronchiolitis.* 2006.
11. Karadag, B., et al., *Efficacy of salbutamol and ipratropium bromide in the management of acute bronchiolitis - A clinical trial.* Respiration, 2008. **76**(3): p. 283-287.
12. Levin, D.L., et al., *A prospective randomized controlled blinded study of three bronchodilators in infants with respiratory syncytial virus bronchiolitis on mechanical ventilation.* Pediatr Crit Care Med, 2008. **9**(6): p. 598-604.
13. Schuh, S., et al., *A single versus multiple doses of dexamethasone in infants wheezing for the first time.* Pediatr Pulmonol, 2008. **43**(9): p. 844-50.
14. Glezen, W.P., et al., *Risk of primary infection and reinfection with respiratory syncytial virus.* Am J Dis Child, 1986. **140**(6): p. 543-6.
15. Paes, B.A., et al., *A decade of respiratory syncytial virus epidemiology and prophylaxis: Translating evidence into everyday clinical practice.* Canadian Respiratory Journal, 2011. **18**(2): p. E10-E19.
16. Bont, L., et al., *Defining the Epidemiology and Burden of Severe Respiratory Syncytial Virus Infection Among Infants and Children in Western Countries.* Infect Dis Ther, 2016. **5**(3): p. 271-98.
17. Hall, C.B., et al., *The burden of respiratory syncytial virus infection in young children.* N Engl J Med, 2009. **360**(6): p. 588-98.
18. Shi, T., et al., *Global, regional, and national disease burden estimates of acute lower respiratory infections due to respiratory syncytial virus in young children in 2015: a systematic review and modelling study.* Lancet, 2017. **390**(10098): p. 946-958.

19. Eisenhut, M., *Extrapulmonary manifestations of severe respiratory syncytial virus infection--a systematic review.* Crit Care, 2006. **10**(4): p. R107.

20. Xing, Y. and M. Proesmans, *New therapies for acute RSV infections: where are we?* Eur J Pediatr, 2019. **178**(2): p. 131-138.

21. Lanari, M., et al., *Respiratory syncytial virus infections in infants affected by primary immunodeficiency.* J Immunol Res, 2014. **2014**: p. 850831.

22. Janssen, R., et al., *Genetic susceptibility to respiratory syncytial virus bronchiolitis is predominantly associated with innate immune genes.* Journal of Infectious Diseases, 2007. **196**(6): p. 826-834.

23. Simoes, E.A., *Environmental and demographic risk factors for respiratory syncytial virus lower respiratory tract disease.* J Pediatr, 2003. **143**(5 Suppl): p. S118-26.

24. El Saleeby, C.M., et al., *Respiratory syncytial virus load, viral dynamics, and disease severity in previously healthy naturally infected children.* J Infect Dis, 2011. **204**(7): p. 996-1002.

25. Murray, J., et al., *Risk factors for hospital admission with RSV bronchiolitis in England: a population-based birth cohort study.* PLoS One, 2014. **9**(2): p. e89186.

26. Griffiths, C., S.J. Drews, and D.J. Marchant, *Respiratory Syncytial Virus: Infection, Detection, and New Options for Prevention and Treatment.* Clin Microbiol Rev, 2017. **30**(1): p. 277-319.

27. Ostadabbas, S., et al., *A Passive Quantitative Measurement of Airway Resistance using Depth Data.* 2014 36th Annual International Conference of the Ieee Engineering in Medicine and Biology Society (Embc), 2014: p. 5743-5747.

28. Lambert, L., et al., *Immunity to RSV in Early-Life.* Front Immunol, 2014. **5**: p. 466.

29. Mansbach, J.M., et al., *Prospective multicenter study of children with bronchiolitis requiring mechanical ventilation.* Pediatrics, 2012. **130**(3): p. e492-500.

30. Bulkow, L.R., et al., *Risk factors for severe respiratory syncytial virus infection among Alaska Native children.* Pediatrics, 2002. **109**(2): p. 210-216.

31. Lanari, M., et al., *Prevalence of respiratory syncytial virus infection in Italian infants hospitalized for acute lower respiratory tract infections, and association between respiratory syncytial virus infection risk factors and disease severity.* Pediatric Pulmonology, 2002. **33**(6): p. 458-465.

32. Law, B.J., X. Carbonell-Estrany, and E.A.F. Simoes, *An update on respiratory syncytial virus epidemiology: a developed country perspective.* Respiratory Medicine, 2002. **96**: p. S1-S7.

33. Shi, T., et al., *Risk factors for respiratory syncytial virus associated with acute lower respiratory infection in children under five years: Systematic review and meta-analysis.* J Glob Health, 2015. **5**(2): p. 020416.

34. Chatzis, O., et al., *Burden of severe RSV disease among immunocompromised children and adults: a 10 year retrospective study.* BMC Infect Dis, 2018. **18**(1): p. 111.

35. Sommer, C., B. Resch, and E.A. Simoes, *Risk factors for severe respiratory syncytial virus lower respiratory tract infection.* Open Microbiol J, 2011. **5**: p. 144-54.

36. MacDonald, N.E., et al., *Respiratory syncytial viral infection in infants with congenital heart disease.* N Engl J Med, 1982. **307**(7): p. 397-400.

37. Navas, L., et al., *Improved outcome of respiratory syncytial virus infection in a high-risk hospitalized population of Canadian children. Pediatric Investigators Collaborative Network on Infections in Canada.* J Pediatr, 1992. **121**(3): p. 348-54.

38. Resch, B., *Respiratory Syncytial Virus Infection in High-risk Infants - an Update on Palivizumab Prophylaxis.* Open Microbiol J, 2014. **8**: p. 71-7.

39. Hiatt, P.W., et al., *Effects of viral lower respiratory tract infection on lung function in infants with cystic fibrosis.* Pediatrics, 1999. **103**(3): p. 619-26.

40. Roca, A., et al., *Prevalence of respiratory syncytial virus IgG antibodies in infants living in a rural area of Mozambique.* J Med Virol, 2002. **67**(4): p. 616-23.

41. Stensballe, L.G., et al., *Seasonal variation of maternally derived respiratory syncytial virus antibodies and association with infant hospitalizations for respiratory syncytial virus.* J Pediatr, 2009. **154**(2): p. 296-8.

42. Munoz, F.M., *Respiratory syncytial virus in infants: is maternal vaccination a realistic strategy?* Curr Opin Infect Dis, 2015. **28**(3): p. 221-4.

43. Glezen, W.P., et al., *Risk of respiratory syncytial virus infection for infants from low-income families in relationship to age, sex, ethnic group, and maternal antibody level.* J Pediatr, 1981. **98**(5): p. 708-15.

44. Simoes, E.A., et al., *Preterm twins and triplets. A high-risk group for severe respiratory syncytial virus infection.* Am J Dis Child, 1993. **147**(3): p. 303-6.

45. Colosia, A.D., et al., *Residential crowding and severe respiratory syncytial virus disease among infants and young children: A systematic literature review.* Bmc Infectious Diseases, 2012. **12**.

46. Lofgren, J., et al., *Association between surfactant protein A gene locus and severe respiratory syncytial virus infection in infants.* Journal of Infectious Diseases, 2002. **185**(3): p. 283-289.

47. Lahti, M., et al., *Surfactant protein D gene polymorphism associated with severe respiratory syncytial virus infection.* Pediatr Res, 2002. **51**(6): p. 696-9.

48. Puthothu, B., et al., *Haplotypes of surfactant protein C are associated with common paediatric lung diseases.* Pediatr Allergy Immunol, 2006. **17**(8): p. 572-7.

49. Miyairi, I. and J.P. DeVincenzo, *Human genetic factors and respiratory syncytial virus disease severity.* Clin Microbiol Rev, 2008. **21**(4): p. 686-703.

50. Ciencewicki, J.M., et al., *A genetic model of differential susceptibility to human respiratory syncytial virus (RSV) infection.* FASEB J, 2014. **28**(4): p. 1947-56.

51. Blount, R.E., Jr., J.A. Morris, and R.E. Savage, *Recovery of cytopathogenic agent from chimpanzees with coryza.* Proc Soc Exp Biol Med, 1956. **92**(3): p. 544-9.

52. Chanock, R., B. Roizman, and R. Myers, *Recovery from infants with respiratory illness of a virus related to chimpanzee coryza agent (CCA). I. Isolation, properties and characterization.* Am J Hyg, 1957. **66**(3): p. 281-90.

53. Collins, P.L., R. Fearns, and B.S. Graham, *Respiratory syncytial virus: virology, reverse genetics, and pathogenesis of disease.* Curr Top Microbiol Immunol, 2013. **372**: p. 3-38.

54. Rima, B., et al., *ICTV Virus Taxonomy Profile: Pneumoviridae.* J Gen Virol, 2017. **98**(12): p. 2912-2913.

55. Zhang, L., et al., *Respiratory syncytial virus infection of human airway epithelial cells is polarized, specific to ciliated cells, and without obvious cytopathology.* J Virol, 2002. **76**(11): p. 5654-66.

56. Malhotra, R., et al., *Isolation and characterisation of potential respiratory syncytial virus receptor(s) on epithelial cells.* Microbes Infect, 2003. **5**(2): p. 123-33.

57. Kurt-Jones, E.A., et al., *Pattern recognition receptors TLR4 and CD14 mediate response to respiratory syncytial virus.* Nat Immunol, 2000. **1**(5): p. 398-401.

58. Behera, A.K., et al., *Blocking intercellular adhesion molecule-1 on human epithelial cells decreases respiratory syncytial virus infection.* Biochem Biophys Res Commun, 2001. **280**(1): p. 188-95.

59. Krusat, T. and H.J. Streckert, *Heparin-dependent attachment of respiratory syncytial virus (RSV) to host cells.* Arch Virol, 1997. **142**(6): p. 1247-54.

60. Johnson, S.M., et al., *Respiratory Syncytial Virus Uses CX3CR1 as a Receptor on Primary Human Airway Epithelial Cultures.* Plos Pathogens, 2015. **11**(12).

61. Zhang, L., et al., *Infection of ciliated cells by human parainfluenza virus type 3 in an in vitro model of human airway epithelium.* J Virol, 2005. **79**(2): p. 1113-24.

62. Das, S., et al., *Respiratory syncytial virus infection of newborn CX3CR1-deficient mice induces a pathogenic pulmonary innate immune response.* JCI Insight, 2017. **2**(17).

63. Techaarpornkul, S., N. Barretto, and M.E. Peeples, *Functional analysis of recombinant respiratory syncytial virus deletion mutants lacking the small hydrophobic and/or attachment glycoprotein gene.* J Virol, 2001. **75**(15): p. 6825-34.

64. Tayyari, F., et al., *Identification of nucleolin as a cellular receptor for human respiratory syncytial virus.* Nature Medicine, 2011. **17**(9): p. 1132-U140.

65. Marchant, D., et al., *Toll-like receptor 4-mediated activation of p38 mitogen-activated protein kinase is a determinant of respiratory virus entry and tropism.* J Virol, 2010. **84**(21): p. 11359-73.

66. San-Juan-Vergara, H., et al., *Cholesterol-rich microdomains as docking platforms for respiratory syncytial virus in normal human bronchial epithelial cells.* J Virol, 2012. **86**(3): p. 1832-43.

67. Krzyzaniak, M.A., et al., *Host cell entry of respiratory syncytial virus involves macropinocytosis followed by proteolytic activation of the F protein.* PLoS Pathog, 2013. **9**(4): p. e1003309.

68. Kolokoltsov, A.A., et al., *Small interfering RNA profiling reveals key role of clathrin-mediated endocytosis and early endosome formation for infection by respiratory syncytial virus.* J Virol, 2007. **81**(14): p. 7786-800.

69. Chernomordik, L.V. and M.M. Kozlov, *Membrane hemifusion: crossing a chasm in two leaps.* Cell, 2005. **123**(3): p. 375-82.

70. Harrison, S.C., *Viral membrane fusion.* Nat Struct Mol Biol, 2008. **15**(7): p. 690-8.

71. Bakker, S.E., et al., *The respiratory syncytial virus nucleoprotein-RNA complex forms a left-handed helical nucleocapsid.* J Gen Virol, 2013. **94**(Pt 8): p. 1734-8.

72. Grosfeld, H., M.G. Hill, and P.L. Collins, *Rna Replication by Respiratory Syncytial Virus (Rsv) Is Directed by the N-Protein, P-Protein, and L Protein - Transcription Also Occurs under These Conditions but Requires Rsv Superinfection for Efficient Synthesis of Full-Length Messenger-Rna.* Journal of Virology, 1995. **69**(9): p. 5677-5686.

73. Morin, B., et al., *The polymerase of negative-stranded RNA viruses.* Curr Opin Virol, 2013. **3**(2): p. 103-10.

74. Richard, C.A., et al., *RSV hijacks cellular protein phosphatase 1 to regulate M2-1 phosphorylation and viral transcription.* PLoS Pathog, 2018. **14**(3): p. e1006920.

75. Mitra, R., et al., *The Human Respiratory Syncytial Virus Matrix Protein Is Required for Maturation of Viral Filaments.* Journal of Virology, 2012. **86**(8): p. 4432-4443.

76. Marty, A., et al., *Association of matrix protein of respiratory syncytial virus with the host cell membrane of infected cells.* Arch Virol, 2004. **149**(1): p. 199-210.

77. Ghildyal, R., et al., *Interaction between the respiratory syncytial virus G glycoprotein cytoplasmic domain and the matrix protein.* Journal of General Virology, 2005. **86**: p. 1879-1884.

78. Utley, T.J., et al., *Respiratory syncytial virus uses a Vps4-independent budding mechanism controlled by Rab11-FIP2.* Proc Natl Acad Sci U S A, 2008. **105**(29): p. 10209-14.

79. Shahriari, S., J. Gordon, and R. Ghildyal, *Host cytoskeleton in respiratory syncytial virus assembly and budding.* Virol J, 2016. **13**(1): p. 161.

80. Nicod, L.P., *Lung defences: an overview.* European Respiratory Review, 2005. **14**(95): p. 45-50.

81. Zanin, M., et al., *The Interaction between Respiratory Pathogens and Mucus.* Cell Host & Microbe, 2016. **19**(2): p. 159-168.

82. Widdicombe, J., *Relationships among the Composition of Mucus, Epithelial Lining Liquid, and Adhesion of Microorganisms.* American Journal of Respiratory and Critical Care Medicine, 1995. **151**(6): p. 2088-2093.

83. Jacquot, J., et al., *Effect of human airway lysozyme on the in vitro growth of type I Streptococcus pneumoniae.* Eur J Respir Dis, 1987. **71**(4): p. 295-305.

84. Ellison, R.T., 3rd and T.J. Giehl, *Killing of gram-negative bacteria by lactoferrin and lysozyme.* J Clin Invest, 1991. **88**(4): p. 1080-91.

85. Kota, S., et al., *Role of human beta-defensin-2 during tumor necrosis factor-alpha/NF-kappaB-mediated innate antiviral response against human respiratory syncytial virus.* J Biol Chem, 2008. **283**(33): p. 22417-29.

86. Han, S. and R.K. Mallampalli, *The Role of Surfactant in Lung Disease and Host Defense against Pulmonary Infections.* Ann Am Thorac Soc, 2015. **12**(5): p. 765-74.

87. LeVine, A.M., et al., *Surfactant protein-A enhances respiratory syncytial virus clearance in vivo.* J Clin Invest, 1999. **103**(7): p. 1015-21.

88. Glasser, S.W., et al., *Surfactant protein C-deficient mice are susceptible to respiratory syncytial virus infection.* Am J Physiol Lung Cell Mol Physiol, 2009. **297**(1): p. L64-72.

89. LeVine, A.M., et al., *Surfactant protein-d enhances phagocytosis and pulmonary clearance of respiratory syncytial virus.* Am J Respir Cell Mol Biol, 2004. **31**(2): p. 193-9.

90. Kim, T.H. and H.K. Lee, *Innate immune recognition of respiratory syncytial virus infection.* BMB Rep, 2014. **47**(4): p. 184-91.

91. Janeway, C.A., Jr. and R. Medzhitov, *Innate immune recognition.* Annu Rev Immunol, 2002. **20**: p. 197-216.

92. Rock, K.L., J.J. Lai, and H. Kono, *Innate and adaptive immune responses to cell death.* Immunol Rev, 2011. **243**(1): p. 191-205.

93. Kawasaki, T. and T. Kawai, *Toll-like receptor signaling pathways.* Front Immunol, 2014. **5**: p. 461.

94. Motshwene, P.G., et al., *An oligomeric signaling platform formed by the Toll-like receptor signal transducers MyD88 and IRAK-4.* J Biol Chem, 2009. **284**(37): p. 25404-11.

95. Haynes, L.M., et al., *Involvement of toll-like receptor 4 in innate immunity to respiratory syncytial virus.* J Virol, 2001. **75**(22): p. 10730-7.

96. Murawski, M.R., et al., *Respiratory syncytial virus activates innate immunity through Toll-like receptor 2.* J Virol, 2009. **83**(3): p. 1492-500.

97. Liu, P., et al., *Retinoic acid-inducible gene I mediates early antiviral response and Toll-like receptor 3 expression in respiratory syncytial virus-infected airway epithelial cells.* J Virol, 2007. **81**(3): p. 1401-11.

98. Rudd, B.D., et al., *Deletion of TLR3 alters the pulmonary immune environment and mucus production during respiratory syncytial virus infection.* J Immunol, 2006. **176**(3): p. 1937-42.

99. Lukacs, N.W., et al., *Respiratory virus-induced TLR7 activation controls IL-17-associated increased mucus via IL-23 regulation.* J Immunol, 2010. **185**(4): p. 2231-9.

100. Chow, K.T., M. Gale, Jr., and Y.M. Loo, *RIG-I and Other RNA Sensors in Antiviral Immunity.* Annu Rev Immunol, 2018. **36**: p. 667-694.

101. Goubau, D., et al., *Antiviral immunity via RIG-I-mediated recognition of RNA bearing 5'-diphosphates.* Nature, 2014. **514**(7522): p. 372-375.

102. Hornung, V., et al., *5'-Triphosphate RNA is the ligand for RIG-I.* Science, 2006. **314**(5801): p. 994-7.

103. Pichlmair, A., et al., *RIG-I-mediated antiviral responses to single-stranded RNA bearing 5'-phosphates.* Science, 2006. **314**(5801): p. 997-1001.

104. Kato, H., et al., *Length-dependent recognition of double-stranded ribonucleic acids by retinoic acid-inducible gene-I and melanoma differentiation-associated gene 5.* J Exp Med, 2008. **205**(7): p. 1601-10.

105. Saito, T., et al., *Regulation of innate antiviral defenses through a shared repressor domain in RIG-I and LGP2.* Proceedings of the National Academy of Sciences of the United States of America, 2007. **104**(2): p. 582-587.

106. Satoh, T., et al., *LGP2 is a positive regulator of RIG-I- and MDA5-mediated antiviral responses.* Proc Natl Acad Sci U S A, 2010. **107**(4): p. 1512-7.

107. Rodriguez, K.R., A.M. Bruns, and C.M. Horvath, *MDA5 and LGP2: accomplices and antagonists of antiviral signal transduction.* J Virol, 2014. **88**(15): p. 8194-200.

108. Scagnolari, C., et al., *Gene expression of nucleic acid-sensing pattern recognition receptors in children hospitalized for respiratory syncytial virus-associated acute bronchiolitis.* Clin Vaccine Immunol, 2009. **16**(6): p. 816-23.

109. Loo, Y.M., et al., *Distinct RIG-I and MDA5 signaling by RNA viruses in innate immunity.* J Virol, 2008. **82**(1): p. 335-45.

110. Grandvaux, N., et al., *Sustained activation of interferon regulatory factor 3 during infection by paramyxoviruses requires MDA5.* J Innate Immun, 2014. **6**(5): p. 650-62.

111. Bhoj, V.G., et al., *MAVS and MyD88 are essential for innate immunity but not cytotoxic T lymphocyte response against respiratory syncytial virus.* Proc Natl Acad Sci U S A, 2008. **105**(37): p. 14046-51.

112. Kirsebom, F.C.M., et al., *Neutrophil recruitment and activation are differentially dependent on MyD88/TRIF and MAVS signaling during RSV infection.* Mucosal Immunol, 2019. **12**(5): p. 1244-1255.

113. Sun, Q., et al., *The specific and essential role of MAVS in antiviral innate immune responses.* Immunity, 2006. **24**(5): p. 633-42.

114. Sabbah, A., et al., *Activation of innate immune antiviral responses by Nod2.* Nat Immunol, 2009. **10**(10): p. 1073-80.

115. Johnson, T.R., J.S. McLellan, and B.S. Graham, *Respiratory syncytial virus glycoprotein G interacts with DC-SIGN and L-SIGN to activate ERK1 and ERK2.* J Virol, 2012. **86**(3): p. 1339-47.

116. Monteiro, J.T. and B. Lepenies, *Myeloid C-Type Lectin Receptors in Viral Recognition and Antiviral Immunity.* Viruses, 2017. **9**(3).

117. Schoggins, J.W., *Interferon-stimulated genes: roles in viral pathogenesis.* Curr Opin Virol, 2014. **6**: p. 40-6.

118. Schoggins, J.W., *Interferon-Stimulated Genes: What Do They All Do?* Annu Rev Virol, 2019.

119. Isaacs, A. and J. Lindenmann, *Virus interference. I. The interferon.* Proc R Soc Lond B Biol Sci, 1957. **147**(927): p. 258-67.

120. Isaacs, A., J. Lindenmann, and R.C. Valentine, *Virus interference. II. Some properties of interferon.* Proc R Soc Lond B Biol Sci, 1957. **147**(927): p. 268-73.

121. Ivashkiv, L.B. and L.T. Donlin, *Regulation of type I interferon responses.* Nat Rev Immunol, 2014. **14**(1): p. 36-49.

122. Schroder, K., et al., *Interferon-gamma: an overview of signals, mechanisms and functions.* J Leukoc Biol, 2004. **75**(2): p. 163-89.

123. Zanoni, I., F. Granucci, and A. Broggi, *Interferon (IFN)-lambda Takes the Helm: Immunomodulatory Roles of Type III IFNs.* Front Immunol, 2017. **8**: p. 1661.

124. Makris, S., M. Paulsen, and C. Johansson, *Type I Interferons as Regulators of Lung Inflammation.* Front Immunol, 2017. **8**: p. 259.

125. Ye, L., D. Schnepf, and P. Staeheli, *Interferon-lambda orchestrates innate and adaptive mucosal immune responses.* Nat Rev Immunol, 2019.

126. Jewell, N.A., et al., *Differential type I interferon induction by respiratory syncytial virus and influenza a virus in vivo.* J Virol, 2007. **81**(18): p. 9790-800.

127. Goritzka, M., et al., *Alveolar macrophage-derived type I interferons orchestrate innate immunity to RSV through recruitment of antiviral monocytes.* Journal of Experimental Medicine, 2015. **212**(5): p. 699-714.

128. Cormier, S.A., et al., *Limited type I interferons and plasmacytoid dendritic cells during neonatal respiratory syncytial virus infection permit immunopathogenesis upon reinfection.* J Virol, 2014. **88**(16): p. 9350-60.

129. Thwaites, R.S., et al., *Reduced Nasal Viral Load and IFN Responses in Infants with Respiratory Syncytial Virus Bronchiolitis and Respiratory Failure.* Am J Respir Crit Care Med, 2018. **198**(8): p. 1074-1084.

130. Boyapalle, S., et al., *Respiratory syncytial virus NS1 protein colocalizes with mitochondrial antiviral signaling protein MAVS following infection.* PLoS One, 2012. **7**(2): p. e29386.

131. Ban, J., et al., *Human Respiratory Syncytial Virus NS 1 Targets TRIM25 to Suppress RIG-I Ubiquitination and Subsequent RIG-I-Mediated Antiviral Signaling.* Viruses, 2018. **10**(12).

132. Ling, Z., K.C. Tran, and M.N. Teng, *Human respiratory syncytial virus nonstructural protein NS2 antagonizes the activation of beta interferon transcription by interacting with RIG-I.* J Virol, 2009. **83**(8): p. 3734-42.

133. Chirkova, T., et al., *Respiratory syncytial virus G protein CX3C motif impairs human airway epithelial and immune cell responses.* J Virol, 2013. **87**(24): p. 13466-79.

134. Groskreutz, D.J., et al., *Respiratory syncytial virus limits alpha subunit of eukaryotic translation initiation factor 2 (eIF2alpha) phosphorylation to maintain translation and viral replication.* J Biol Chem, 2010. **285**(31): p. 24023-31.

135. Lindquist, M.E., et al., *Respiratory syncytial virus induces host RNA stress granules to facilitate viral replication.* J Virol, 2010. **84**(23): p. 12274-84.

136. Lifland, A.W., et al., *Human respiratory syncytial virus nucleoprotein and inclusion bodies antagonize the innate immune response mediated by MDA5 and MAVS.* J Virol, 2012. **86**(15): p. 8245-58.

137. Lee, A.J. and A.A. Ashkar, *The Dual Nature of Type I and Type II Interferons.* Front Immunol, 2018. **9**: p. 2061.

138. Wilmes, S., et al., *Receptor dimerization dynamics as a regulatory valve for plasticity of type I interferon signaling.* J Cell Biol, 2015. **209**(4): p. 579-93.

139. Yan, H., et al., *Phosphorylated interferon-alpha receptor 1 subunit (IFNaR1) acts as a docking site for the latent form of the 113 kDa STAT2 protein.* Embo Journal, 1996. **15**(5): p. 1064-1074.

140. Li, X., et al., *Functional subdomains of STAT2 required for preassociation with the alpha interferon receptor and for signaling.* Mol Cell Biol, 1997. **17**(4): p. 2048-56.

141. Improta, T., et al., *Transcription Factor Isgf-3 Formation Requires Phosphorylated Stat91 Protein, but Stat113 Protein Is Phosphorylated Independently of Stat91 Protein.* Proceedings of the National Academy of Sciences of the United States of America, 1994. **91**(11): p. 4776-4780.

142. Au-Yeung, N., R. Mandhana, and C.M. Horvath, *Transcriptional regulation by STAT1 and STAT2 in the interferon JAK-STAT pathway.* JAKSTAT, 2013. **2**(3): p. e23931.

143. Reich, N., et al., *Interferon-induced transcription of a gene encoding a 15-kDa protein depends on an upstream enhancer element.* Proc Natl Acad Sci U S A, 1987. **84**(18): p. 6394-8.

144. Gonzalez-Navajas, J.M., et al., *Immunomodulatory functions of type I interferons.* Nat Rev Immunol, 2012. **12**(2): p. 125-35.

145. Decker, T., P. Kovarik, and A. Meinke, *GAS elements: a few nucleotides with a major impact on cytokine-induced gene expression.* J Interferon Cytokine Res, 1997. **17**(3): p. 121-34.

146. Zhou, Z., et al., *Type III interferon (IFN) induces a type I IFN-like response in a restricted subset of cells through signaling pathways involving both the Jak-STAT pathway and the mitogen-activated protein kinases.* J Virol, 2007. **81**(14): p. 7749-58.

147. Platanitis, E. and T. Decker, *Regulatory Networks Involving STATs, IRFs, and NFkappaB in Inflammation.* Front Immunol, 2018. **9**: p. 2542.

148. Orzalli, M.H., et al., *An Antiviral Branch of the IL-1 Signaling Pathway Restricts Immune-Evasive Virus Replication.* Mol Cell, 2018. **71**(5): p. 825-840 e6.

149. Shaw, A.E., et al., *Fundamental properties of the mammalian innate immune system revealed by multispecies comparison of type I interferon responses.* PLoS Biol, 2017. **15**(12): p. e2004086.

150. Schoggins, J.W., et al., *Pan-viral specificity of IFN-induced genes reveals new roles for cGAS in innate immunity.* Nature, 2014. **505**(7485): p. 691-5.

151. Schoggins, J.W., et al., *A diverse range of gene products are effectors of the type I interferon antiviral response.* Nature, 2011. **472**(7344): p. 481-5.

152. Bailey, C.C., et al., *IFITM-Family Proteins: The Cell's First Line of Antiviral Defense.* Annu Rev Virol, 2014. **1**: p. 261-283.

153. Doyle, T., et al., *The interferon-inducible isoform of NCOA7 inhibits endosome-mediated viral entry.* Nature Microbiology, 2018. **3**(12): p. 1369-1376.

154. Liu, S.Y., et al., *Interferon-inducible cholesterol-25-hydroxylase broadly inhibits viral entry by production of 25-hydroxycholesterol.* Immunity, 2013. **38**(1): p. 92-105.

155. Chemudupati, M., et al., *From APOBEC to ZAP: Diverse mechanisms used by cellular restriction factors to inhibit virus infections.* Biochim Biophys Acta Mol Cell Res, 2019. **1866**(3): p. 382-394.

156. Verhelst, J., P. Hulpiau, and X. Saelens, *Mx proteins: antiviral gatekeepers that restrain the uninvited.* Microbiol Mol Biol Rev, 2013. **77**(4): p. 551-66.

157. Haller, O., et al., *Mx GTPases: dynamin-like antiviral machines of innate immunity.* Trends Microbiol, 2015. **23**(3): p. 154-63.

158. Yu, Z., et al., *GTPase activity is not essential for the interferon-inducible MxA protein to inhibit the replication of hepatitis B virus.* Arch Virol, 2008. **153**(9): p. 1677-84.

159. Kochs, G., et al., *Antivirally active MxA protein sequesters La Crosse virus nucleocapsid protein into perinuclear complexes.* Proceedings of the National Academy of Sciences of the United States of America, 2002. **99**(5): p. 3153-3158.

160. Atreya, P.L. and S. Kulkarni, *Respiratory syncytial virus strain A2 is resistant to the antiviral effects of type I interferons and human MxA.* Virology, 1999. **261**(2): p. 227-241.

161. Zhao, H., et al., *Inhibition of human parainfluenza virus-3 replication by interferon and human MxA.* Virology, 1996. **220**(2): p. 330-8.

162. Wang, J., et al., *Cholesterol 25-hydroxylase acts as a host restriction factor on pseudorabies virus replication.* J Gen Virol, 2017. **98**(6): p. 1467-1476.

163. Shrivastava-Ranjan, P., et al., *25-Hydroxycholesterol Inhibition of Lassa Virus Infection through Aberrant GP1 Glycosylation.* MBio, 2016. **7**(6).

164. Shu, Q., et al., *ADAP2 Is an Interferon Stimulated Gene That Restricts RNA Virus Entry.* PLoS Pathog, 2015. **11**(9): p. e1005150.

165. Pertel, T., et al., *TRIM5 is an innate immune sensor for the retrovirus capsid lattice.* Nature, 2011. **472**(7343): p. 361-5.

166. Maida, Y., et al., *An RNA-dependent RNA polymerase formed by TERT and the RMRP RNA.* Nature, 2009. **461**(7261): p. 230-5.

167. Lahouassa, H., et al., *SAMHD1 restricts the replication of human immunodeficiency virus type 1 by depleting the intracellular pool of deoxynucleoside triphosphates.* Nat Immunol, 2012. **13**(3): p. 223-228.

168. Ryoo, J., et al., *The ribonuclease activity of SAMHD1 is required for HIV-1 restriction.* Nature Medicine, 2014. **20**(8): p. 936-941.

169. Batra, J., et al., *Protein Interaction Mapping Identifies RBBP6 as a Negative Regulator of Ebola Virus Replication.* Cell, 2018. **175**(7): p. 1917-+.

170. Dutrieux, J., et al., *PML/TRIM19-Dependent Inhibition of Retroviral Reverse-Transcription by Daxx.* PLoS Pathog, 2015. **11**(11): p. e1005280.

171. Masroori, N., N. Merindol, and L. Berthoux, *The interferon-induced antiviral protein PML (TRIM19) promotes the restriction and transcriptional silencing of lentiviruses in a context-specific, isoform-specific fashion.* Retrovirology, 2016. **13**: p. 19.

172. Scherer, M. and T. Stamminger, *Emerging Role of PML Nuclear Bodies in Innate Immune Signaling.* J Virol, 2016. **90**(13): p. 5850-5854.

173. Maroui, M.A., M. Pampin, and M.K. Chelbi-Alix, *Promyelocytic leukemia isoform IV confers resistance to encephalomyocarditis virus via the sequestration of 3D polymerase in nuclear bodies.* J Virol, 2011. **85**(24): p. 13164-73.

174. Gariano, G.R., et al., *The intracellular DNA sensor IFI16 gene acts as restriction factor for human cytomegalovirus replication.* PLoS Pathog, 2012. **8**(1): p. e1002498.

175. Dhar, J., et al., *2'-5'-Oligoadenylate Synthetase-Like Protein Inhibits Respiratory Syncytial Virus Replication and Is Targeted by the Viral Nonstructural Protein 1.* J Virol, 2015. **89**(19): p. 10115-9.

176. Behera, A.K., et al., *2'-5' Oligoadenylate synthetase plays a critical role in interferon-gamma inhibition of respiratory syncytial virus infection of human epithelial cells.* J Biol Chem, 2002. **277**(28): p. 25601-8.

177. Kajaste-Rudnitski, A., et al., *The 2',5'-oligoadenylate synthetase 1b is a potent inhibitor of West Nile virus replication inside infected cells.* J Biol Chem, 2006. **281**(8): p. 4624-37.

178. Silverman, R.H., *Viral encounters with 2',5'-oligoadenylate synthetase and RNase L during the interferon antiviral response.* J Virol, 2007. **81**(23): p. 12720-9.

179. Nordmann, A., et al., *A new splice variant of the human guanylate-binding protein 3 mediates anti-influenza activity through inhibition of viral transcription and replication.* Faseb Journal, 2012. **26**(3): p. 1290-1300.

180. Wang, K., et al., *Interferon-stimulated TRIM69 interrupts dengue virus replication by ubiquitinating viral nonstructural protein 3.* PLoS Pathog, 2018. **14**(8): p. e1007287.

181. Gonzalez-Sanz, R., et al., *ISG15 Is Upregulated in Respiratory Syncytial Virus Infection and Reduces Virus Growth through Protein ISGylation.* Journal of Virology, 2016. **90**(7): p. 3428-3438.

182. Mears, H.V. and T.R. Sweeney, *Better together: the role of IFIT protein-protein interactions in the antiviral response.* J Gen Virol, 2018. **99**(11): p. 1463-1477.

183. Hovanessian, A.G., *On the discovery of interferon-inducible, double-stranded RNA activated enzymes: the 2'-5'oligoadenylate synthetases and the protein kinase PKR.* Cytokine Growth Factor Rev, 2007. **18**(5-6): p. 351-61.

184. Dauber, B. and T. Wolff, *Activation of the Antiviral Kinase PKR and Viral Countermeasures.* Viruses, 2009. **1**(3): p. 523-44.

185. Li, M., et al., *Codon-usage-based inhibition of HIV protein synthesis by human schlafen 11.* Nature, 2012. **491**(7422): p. 125-8.

186. Mounce, B.C., et al., *Interferon-Induced Spermidine-Spermine Acetyltransferase and Polyamine Depletion Restrict Zika and Chikungunya Viruses.* Cell Host Microbe, 2016. **20**(2): p. 167-77.

187. Suzuki, Y., et al., *Characterization of RyDEN (C19orf66) as an Interferon-Stimulated Cellular Inhibitor against Dengue Virus Replication.* Plos Pathogens, 2016. **12**(1).

188. Wang, X., et al., *Regulation of HIV-1 Gag-Pol Expression by Shiftless, an Inhibitor of Programmed -1 Ribosomal Frameshifting.* Cell, 2019. **176**(3): p. 625-635 e14.

189. Gizzi, A.S., et al., *A naturally occurring antiviral ribonucleotide encoded by the human genome.* Nature, 2018. **558**(7711): p. 610-614.

190. Chaurasiya, K.R., et al., *Oligomerization transforms human APOBEC3G from an efficient enzyme to a slowly dissociating nucleic acid-binding protein.* Nat Chem, 2014. **6**(1): p. 28-33.

191. Espert, L., et al., *ISG20, a new interferon-induced RNase specific for single-stranded RNA, defines an alternative antiviral pathway against RNA genomic viruses.* J Biol Chem, 2003. **278**(18): p. 16151-8.

192. Richardson, R.B., et al., *A CRISPR screen identifies IFI6 as an ER-resident interferon effector that blocks flavivirus replication.* Nature Microbiology, 2018. **3**(11): p. 1214-1223.

193. Meyerson, N.R., et al., *Nuclear TRIM25 Specifically Targets Influenza Virus Ribonucleoproteins to Block the Onset of RNA Chain Elongation.* Cell Host Microbe, 2017. **22**(5): p. 627-638 e7.

194. Li, M.M., et al., *TRIM25 Enhances the Antiviral Action of Zinc-Finger Antiviral Protein (ZAP).* PLoS Pathog, 2017. **13**(1): p. e1006145.

195. Fu, B., et al., *TRIM32 Senses and Restricts Influenza A Virus by Ubiquitination of PB1 Polymerase.* PLoS Pathog, 2015. **11**(6): p. e1004960.

196. Subramanian, G., et al., *A new mechanism of interferon's antiviral action: Induction of autophagy, essential for paramyxovirus replication, is inhibited by the interferon stimulated gene, TDRD7.* PLoS Pathog, 2018. **14**(1): p. e1006877.

197. Wang, X., E.R. Hinson, and P. Cresswell, *The interferon-inducible protein viperin inhibits influenza virus release by perturbing lipid rafts.* Cell Host Microbe, 2007. **2**(2): p. 96-105.

198. Krapp, C., et al., *Guanylate Binding Protein (GBP) 5 Is an Interferon-Inducible Inhibitor of HIV-1 Infectivity.* Cell Host Microbe, 2016. **19**(4): p. 504-14.

199. Wilson, S.J., et al., *Inhibition of HIV-1 particle assembly by 2',3'-cyclic-nucleotide 3'-phosphodiesterase.* Cell Host Microbe, 2012. **12**(4): p. 585-97.

200. Dittmann, M., et al., *A serpin shapes the extracellular environment to prevent influenza A virus maturation.* Cell, 2015. **160**(4): p. 631-643.

201. Ning, S., L.E. Huye, and J.S. Pagano, *Regulation of the transcriptional activity of the IRF7 promoter by a pathway independent of interferon signaling.* J Biol Chem, 2005. **280**(13): p. 12262-70.

202. Fang, L., et al., *Ataxia telangiectasia mutated kinase mediates NF-kappaB serine 276 phosphorylation and interferon expression via the IRF7-RIG-I amplification loop in paramyxovirus infection.* J Virol, 2015. **89**(5): p. 2628-42.

203. Honda, K., et al., *IRF-7 is the master regulator of type-I interferon-dependent immune responses.* Nature, 2005. **434**(7034): p. 772-777.

204. McDonald, J.U., et al., *A Simple Screening Approach To Prioritize Genes for Functional Analysis Identifies a Role for Interferon Regulatory Factor 7 in the Control of Respiratory Syncytial Virus Disease.* mSystems, 2016. **1**(3).

205. McGillivary, G., et al., *Replication of respiratory syncytial virus is inhibited by the host defense molecule viperin.* J Innate Immun, 2013. **5**(1): p. 60-71.

206. Li, M., et al., *Respiratory Syncytial Virus Replication Is Promoted by Autophagy-Mediated Inhibition of Apoptosis.* J Virol, 2018. **92**(8).

207. Smith, S.E., et al., *Interferon-Induced Transmembrane Protein 1 Restricts Replication of Viruses That Enter Cells via the Plasma Membrane.* J Virol, 2019. **93**(6).

208. Zhang, W., et al., *Human respiratory syncytial virus infection is inhibited by IFN-induced transmembrane proteins.* Journal of General Virology, 2015. **96**: p. 170-182.

209. Everitt, A.R., et al., *Defining the Range of Pathogens Susceptible to Ifitm3 Restriction Using a Knockout Mouse Model.* Plos One, 2013. **8**(11).

210. Friedman, R.L., et al., *Transcriptional and posttranscriptional regulation of interferon-induced gene expression in human cells.* Cell, 1984. **38**(3): p. 745-55.

211. Alber, D. and P. Staeheli, *Partial inhibition of vesicular stomatitis virus by the interferon-induced human 9-27 protein.* J Interferon Cytokine Res, 1996. **16**(5): p. 375-80.

212. Hickford, D., et al., *Evolution of vertebrate interferon inducible transmembrane proteins.* BMC Genomics, 2012. **13**: p. 155.

213. Benfield, C.T., et al., *Bat and pig IFN-induced transmembrane protein 3 restrict cell entry by influenza virus and lyssaviruses.* J Gen Virol, 2015. **96**(Pt 5): p. 991-1005.

214. Zhang, Z., et al., *Evolutionary dynamics of the interferon-induced transmembrane gene family in vertebrates.* PLoS One, 2012. **7**(11): p. e49265.

215. Smith, S.E., et al., *Chicken interferon-inducible transmembrane protein 3 restricts influenza viruses and lyssaviruses in vitro.* J Virol, 2013. **87**(23): p. 12957-66.

216. Smith, J., et al., *A comparative analysis of host responses to avian influenza infection in ducks and chickens highlights a role for the interferon-induced transmembrane proteins in viral resistance.* BMC Genomics, 2015. **16**: p. 574.

217. Blyth, G.A., et al., *Duck Interferon-Inducible Transmembrane Protein 3 Mediates Restriction of Influenza Viruses.* J Virol, 2016. **90**(1): p. 103-16.

218. Hanagata, N., et al., *Characterization of the osteoblast-specific transmembrane protein IFITM5 and analysis of IFITM5-deficient mice.* J Bone Miner Metab, 2011. **29**(3): p. 279-90.

219. Desai, T.M., et al., *IFITM3 restricts influenza A virus entry by blocking the formation of fusion pores following virus-endosome hemifusion.* PLoS Pathog, 2014. **10**(4): p. e1004048.

220. Li, K., et al., *IFITM proteins restrict viral membrane hemifusion.* PLoS Pathog, 2013. **9**(1): p. e1003124.

221. Feeley, E.M., et al., *IFITM3 inhibits influenza A virus infection by preventing cytosolic entry.* PLoS Pathog, 2011. **7**(10): p. e1002337.

222. John, S.P., et al., *The CD225 Domain of IFITM3 Is Required for both IFITM Protein Association and Inhibition of Influenza A Virus and Dengue Virus Replication.* Journal of Virology, 2013. **87**(14): p. 7837-7852.

223. Sallman Almen, M., et al., *The dispanins: a novel gene family of ancient origin that contains 14 human members.* PLoS One, 2012. **7**(2): p. e31961.

224. Yount, J.S., R.A. Karssemeijer, and H.C. Hang, *S-palmitoylation and ubiquitination differentially regulate interferon-induced transmembrane protein 3 (IFITM3)-mediated resistance to influenza virus.* J Biol Chem, 2012. **287**(23): p. 19631-41.

225. Chen, Y.X., et al., *Induction of T cell aggregation by antibody to a 16kd human leukocyte surface antigen.* J Immunol, 1984. **133**(5): p. 2496-501.

226. Weston, S., et al., *A membrane topology model for human interferon inducible transmembrane protein 1.* PLoS One, 2014. **9**(8): p. e104341.

227. Li, K., et al., *A sorting signal suppresses IFITM1 restriction of viral entry.* J Biol Chem, 2015. **290**(7): p. 4248-59.

228. Jia, R., et al., *The C-terminal sequence of IFITM1 regulates its anti-HIV-1 activity.* PLoS One, 2015. **10**(3): p. e0118794.

229. Mudhasani, R., et al., *IFITM-2 and IFITM-3 but not IFITM-1 restrict Rift Valley fever virus.* J Virol, 2013. **87**(15): p. 8451-64.

230. Lu, J., et al., *The IFITM proteins inhibit HIV-1 infection.* J Virol, 2011. **85**(5): p. 2126-37.

231. Weidner, J.M., et al., *Interferon-induced cell membrane proteins, IFITM3 and tetherin, inhibit vesicular stomatitis virus infection via distinct mechanisms.* J Virol, 2010. **84**(24): p. 12646-57.

232. Brass, A.L., et al., *The IFITM proteins mediate cellular resistance to influenza A H1N1 virus, West Nile virus, and dengue virus.* Cell, 2009. **139**(7): p. 1243-54.

233. Li, C., et al., *The Host Restriction Factor Interferon-Inducible Transmembrane Protein 3 Inhibits Vaccinia Virus Infection.* Front Immunol, 2018. **9**: p. 228.

234. Bailey, C.C., et al., *Ifitm3 limits the severity of acute influenza in mice.* PLoS Pathog, 2012. **8**(9): p. e1002909.

235. Jia, R., et al., *The N-terminal region of IFITM3 modulates its antiviral activity by regulating IFITM3 cellular localization.* J Virol, 2012. **86**(24): p. 13697-707.

236. Hach, J.C., et al., *Palmitoylation on conserved and nonconserved cysteines of murine IFITM1 regulates its stability and anti-influenza A virus activity.* J Virol, 2013. **87**(17): p. 9923-7.

237. Bogdanov, M., P.N. Heacock, and W. Dowhan, *Study of polytopic membrane protein topological organization as a function of membrane lipid composition.* Methods Mol Biol, 2010. **619**: p. 79-101.

238. Savidis, G., et al., *The IFITMs Inhibit Zika Virus Replication.* Cell Rep, 2016. **15**(11): p. 2323-30.

239. Anafu, A.A., et al., *Interferon-inducible transmembrane protein 3 (IFITM3) restricts reovirus cell entry.* J Biol Chem, 2013. **288**(24): p. 17261-71.

240. Weston, S., et al., *Alphavirus Restriction by IFITM Proteins.* Traffic, 2016. **17**(9): p. 997-1013.

241. Everitt, A.R., et al., *IFITM3 restricts the morbidity and mortality associated with influenza.* Nature, 2012. **484**(7395): p. 519-23.

242. Wakim, L.M., et al., *Enhanced survival of lung tissue-resident memory CD8(+) T cells during infection with influenza virus due to selective expression of IFITM3.* Nat Immunol, 2013. **14**(3): p. 238-45.

243. Gorman, M.J., et al., *The Interferon-Stimulated Gene Ifitm3 Restricts West Nile Virus Infection and Pathogenesis.* J Virol, 2016. **90**(18): p. 8212-25.

244. Poddar, S., et al., *The Interferon-Stimulated Gene IFITM3 Restricts Infection and Pathogenesis of Arthritogenic and Encephalitic Alphaviruses.* J Virol, 2016. **90**(19): p. 8780-94.

245. Huang, I.C., et al., *Distinct patterns of IFITM-mediated restriction of filoviruses, SARS coronavirus, and influenza A virus.* PLoS Pathog, 2011. **7**(1): p. e1001258.

246. McMichael, T.M., et al., *IFITM3 Restricts Human Metapneumovirus Infection.* J Infect Dis, 2018. **218**(10): p. 1582-1591.

247. Yao, L., et al., *Identification of the IFITM3 gene as an inhibitor of hepatitis C viral translation in a stable STAT1 cell line.* Journal of Viral Hepatitis, 2011. **18**(10): p. E523-E529.

248. Narayana, S.K., et al., *The Interferon-induced Transmembrane Proteins, IFITM1, IFITM2, and IFITM3 Inhibit Hepatitis C Virus Entry.* J Biol Chem, 2015. **290**(43): p. 25946-59.

249. Wrensch, F., et al., *Interferon-Induced Transmembrane Protein-Mediated Inhibition of Host Cell Entry of Ebolaviruses.* J Infect Dis, 2015. **212 Suppl 2**: p. S210-8.

250. Xu-Yang, Z., et al., *Interferon-Induced Transmembrane Protein 3 Inhibits Hantaan Virus Infection, and Its Single Nucleotide Polymorphism rs12252 Influences the Severity of Hemorrhagic Fever with Renal Syndrome.* Front Immunol, 2016. **7**: p. 535.

251. Forn-Cuni, G., et al., *Liver immune responses to inflammatory stimuli in a diet-induced obesity model of zebrafish.* J Endocrinol, 2015. **224**(2): p. 159-70.

252. McDowell, I.C., et al., *Multi-species protein similarity clustering reveals novel expanded immune gene families in the eastern oyster Crassostrea virginica.* Fish Shellfish Immunol, 2016. **53**: p. 13-23.

253. Takahashi, K., et al., *Cloning, sequencing and expression in Escherichia coli of cDNA for a non-A, non-B hepatitis-associated microtubular aggregates protein.* J Gen Virol, 1990. **71 (Pt 9)**: p. 2005-11.

254. Honda, Y., et al., *Isolation and purification of a non-A, non-B hepatitis-associated microtubular aggregates protein.* J Gen Virol, 1990. **71 (Pt 9)**: p. 1999-2004.

255. Kitamura, A., et al., *Induction of the human gene for p44, a hepatitis-C-associated microtubular aggregate protein, by interferon-alpha/beta.* Eur J Biochem, 1994. **224**(3): p. 877-83.

256. Hallen, L.C., et al., *Antiproliferative activity of the human IFN-alpha-inducible protein IFI44.* J Interferon Cytokine Res, 2007. **27**(8): p. 675-80.

257. Power, D., et al., *IFI44 suppresses HIV-1 LTR promoter activity and facilitates its latency.* Virology, 2015. **481**: p. 142-50.

258. Daumke, O. and G.J. Praefcke, *Invited review: Mechanisms of GTP hydrolysis and conformational transitions in the dynamin superfamily.* Biopolymers, 2016. **105**(8): p. 580-93.

259. Blaise, M., et al., *Crystal structure of the TLDc domain of oxidation resistance protein 2 from zebrafish.* Proteins, 2012. **80**(6): p. 1694-8.

260. Jamaluddin, M., et al., *Respiratory syncytial virus infection induces a reactive oxygen species-MSK1-phospho-Ser-276 RelA pathway required for cytokine expression.* J Virol, 2009. **83**(20): p. 10605-15.

261. Huang, W.C., et al., *IFI44L is a novel tumor suppressor in human hepatocellular carcinoma affecting cancer stemness, metastasis, and drug resistance via regulating met/Src signaling pathway.* BMC Cancer, 2018. **18**(1): p. 609.

262. Sacco, J.J. and M.J. Clague, *Dysregulation of the Met pathway in non-small cell lung cancer: implications for drug targeting and resistance.* Transl Lung Cancer Res, 2015. **4**(3): p. 242-52.

263. Carlton-Smith, C. and R.M. Elliott, *Viperin, MTAP44, and protein kinase R contribute to the interferon-induced inhibition of Bunyamwera Orthobunyavirus replication.* J Virol, 2012. **86**(21): p. 11548-57.

264. Guu, T.S., W. Zheng, and Y.J. Tao, *Bunyavirus: structure and replication.* Adv Exp Med Biol, 2012. **726**: p. 245-66.

265. Rossetti, M., et al., *HIV-1-derived lentiviral vectors directly activate plasmacytoid dendritic cells, which in turn induce the maturation of myeloid dendritic cells.* Hum Gene Ther, 2011. **22**(2): p. 177-88.

266. Agudo, J., et al., *A TLR and non-TLR mediated innate response to lentiviruses restricts hepatocyte entry and can be ameliorated by pharmacological blockade.* Mol Ther, 2012. **20**(12): p. 2257-67.

267. Hallak, L.K., et al., *Glycosaminoglycan sulfation requirements for respiratory syncytial virus infection.* J Virol, 2000. **74**(22): p. 10508-13.

268. Livak, K.J. and T.D. Schmittgen, *Analysis of relative gene expression data using real-time quantitative PCR and the 2(-Delta Delta C(T)) Method.* Methods, 2001. **25**(4): p. 402-8.

269. Zhao, Y., et al., *RIG-I like receptor sensing of host RNAs facilitates the cell-intrinsic immune response to KSHV infection.* Nature Communications, 2018. **9**(1): p. 4841.

270. Fu, B., et al., *ZMPSTE24 defends against influenza and other pathogenic viruses.* J Exp Med, 2017. **214**(4): p. 919-929.

271. Liao, J.Y., et al., *Inosine-containing RNA is a novel innate immune recognition element and reduces RSV infection.* PLoS One, 2011. **6**(10): p. e26463.

272. Steegenga, W.T., et al., *Structural, functional and molecular analysis of the effects of aging in the small intestine and colon of C57BL/6J mice.* BMC Med Genomics, 2012. **5**: p. 38.

273. Zhu, F.G., et al., *Sin3a-Tet1 interaction activates gene transcription and is required for embryonic stem cell pluripotency.* Nucleic Acids Research, 2018. **46**(12): p. 6026-6040.

274. Lin, C.C., et al., *Bhlhe40 controls cytokine production by T cells and is essential for pathogenicity in autoimmune neuroinflammation.* Nat Commun, 2014. **5**: p. 3551.

275. Maloney, N.S., et al., *Essential cell-autonomous role for interferon (IFN) regulatory factor 1 in IFN-gamma-mediated inhibition of norovirus replication in macrophages.* J Virol, 2012. **86**(23): p. 12655-64.

276. Pott, J., et al., *IFN-lambda determines the intestinal epithelial antiviral host defense.* Proc Natl Acad Sci U S A, 2011. **108**(19): p. 7944-9.

277. Qiu, Y., et al., *Dynamic DNA Methylation Changes of Tbx21 and Rorc during Experimental Autoimmune Uveitis in Mice.* Mediators Inflamm, 2018. **2018**: p. 9129163.

278. Xin, Q., et al., *miR-155 Deficiency Ameliorates Autoimmune Inflammation of Systemic Lupus Erythematosus by Targeting S1pr1 in Faslpr/lpr Mice.* J Immunol, 2015. **194**(11): p. 5437-45.

279. Ayadi, A., et al., *Mouse large-scale phenotyping initiatives: overview of the European Mouse Disease Clinic (EUMODIC) and of the Wellcome Trust Sanger Institute Mouse Genetics Project.* Mamm Genome, 2012. **23**(9-10): p. 600-10.

280. White, J.K., et al., *Genome-wide generation and systematic phenotyping of knockout mice reveals new roles for many genes.* Cell, 2013. **154**(2): p. 452-64.

281. Allen, E.K., et al., *SNP-mediated disruption of CTCF binding at the IFITM3 promoter is associated with risk of severe influenza in humans.* Nat Med, 2017. **23**(8): p. 975-983.

282. Culley, F.J., J. Pollott, and P.J. Openshaw, *Age at first viral infection determines the pattern of T cell-mediated disease during reinfection in adulthood.* J Exp Med, 2002. **196**(10): p. 1381-6.

283. Danis, B., et al., *Interferon regulatory factor 7-mediated responses are defective in cord blood plasmacytoid dendritic cells.* Eur J Immunol, 2008. **38**(2): p. 507-17.

284. Lange, U.C., et al., *Normal germ line establishment in mice carrying a deletion of the Ifitm/Fragilis gene family cluster.* Mol Cell Biol, 2008. **28**(15): p. 4688-96.

285. Groves, H.T., et al., *Mouse Models of Influenza Infection with Circulating Strains to Test Seasonal Vaccine Efficacy.* Front Immunol, 2018. **9**: p. 126.

286. van Ooyen, A., et al., *Comparison of total sequence of a cloned rabbit beta-globin gene and its flanking regions with a homologous mouse sequence.* Science, 1979. **206**(4416): p. 337-44.

287. Lu, S. and B.R. Cullen, *Analysis of the stimulatory effect of splicing on mRNA production and utilization in mammalian cells.* RNA, 2003. **9**(5): p. 618-30.

288. Merzlyak, E.M., et al., *Bright monomeric red fluorescent protein with an extended fluorescence lifetime.* Nat Methods, 2007. **4**(7): p. 555-7.

289. Mandal, P.K., et al., *Efficient ablation of genes in human hematopoietic stem and effector cells using CRISPR/Cas9.* Cell Stem Cell, 2014. **15**(5): p. 643-52.

290. Zhang, T., et al., *Production of Guide RNAs in vitro and in vivo for CRISPR Using Ribozymes and RNA Polymerase II Promoters.* Bio-Protocol, 2017. **7**(4).

291. Sanjana, N.E., O. Shalem, and F. Zhang, *Improved vectors and genome-wide libraries for CRISPR screening.* Nat Methods, 2014. **11**(8): p. 783-4.

292. Dou, D., et al., *Influenza A Virus Cell Entry, Replication, Virion Assembly and Movement.* Front Immunol, 2018. **9**: p. 1581.

293. McGivern, D.R., P.L. Collins, and R. Fearns, *Identification of internal sequences in the 3' leader region of human respiratory syncytial virus that enhance transcription and confer replication processivity.* J Virol, 2005. **79**(4): p. 2449-60.

294. Fearns, R., P.L. Collins, and M.E. Peeples, *Functional analysis of the genomic and antigenomic promoters of human respiratory syncytial virus.* J Virol, 2000. **74**(13): p. 6006-14.

295. Skarnes, W.C., et al., *A conditional knockout resource for the genome-wide study of mouse gene function.* Nature, 2011. **474**(7351): p. 337-42.

296. Bult, C.J., et al., *Mouse Genome Database (MGD) 2019.* Nucleic Acids Res, 2019. **47**(D1): p. D801-D806.

297. Malarkannan, S., et al., *Differences that Matter.* Immunity, 2000. **13**(3): p. 333-344.

298. Openshaw, P.J. and C. Chiu, *Protective and dysregulated T cell immunity in RSV infection.* Curr Opin Virol, 2013. **3**(4): p. 468-74.

299. Marques, J.T., et al., *A structural basis for discriminating between self and nonself double-stranded RNAs in mammalian cells.* Nature Biotechnology, 2006. **24**(5): p. 559-565.

300. Olejniczak, M., P. Galka, and W.J. Krzyzosiak, *Sequence-non-specific effects of RNA interference triggers and microRNA regulators.* Nucleic Acids Res, 2010. **38**(1): p. 1-16.

301. Young, D.F., et al., *The switch between acute and persistent paramyxovirus infection caused by single amino acid substitutions in the RNA polymerase P subunit.* PLoS Pathog, 2019. **15**(2): p. e1007561.

302. Langereis, M.A., et al., *Knockout of cGAS and STING Rescues Virus Infection of Plasmid DNA-Transfected Cells.* J Virol, 2015. **89**(21): p. 11169-73.

303. Yount, J.S., et al., *Palmitoylome profiling reveals S-palmitoylation-dependent antiviral activity of IFITM3.* Nat Chem Biol, 2010. **6**(8): p. 610-4.

304. Ernst, A.M., et al., *S-Palmitoylation Sorts Membrane Cargo for Anterograde Transport in the Golgi.* Dev Cell, 2018. **47**(4): p. 479-493 e7.

305. Slade, D.J., et al., *Chemical and biological methods to detect post-translational modifications of arginine.* Biopolymers, 2014. **101**(2): p. 133-43.

306. Chesarino, N.M., et al., *IFITM3 requires an amphipathic helix for antiviral activity.* EMBO Rep, 2017.

307. Stacey, M.A., et al., *The antiviral restriction factor IFN-induced transmembrane protein 3 prevents cytokine-driven CMV pathogenesis.* J Clin Invest, 2017. **127**(4): p. 1463-1474.

308. Zhang, Y.H., et al., *Interferon-induced transmembrane protein-3 genetic variant rs12252-C is associated with severe influenza in Chinese individuals.* Nat Commun, 2013. **4**: p. 1418.

309. Randolph, A.G., et al., *Evaluation of IFITM3 rs12252 Association With Severe Pediatric Influenza Infection.* J Infect Dis, 2017. **216**(1): p. 14-21.

310. Mills, T.C., et al., *IFITM3 and susceptibility to respiratory viral infections in the community.* J Infect Dis, 2014. **209**(7): p. 1028-31.

311. Carter, T.C., et al., *Pilot screening study of targeted genetic polymorphisms for association with seasonal influenza hospital admission.* J Med Virol, 2018. **90**(3): p. 436-446.

312. Lopez-Rodriguez, M., et al., *IFITM3 and severe influenza virus infection. No evidence of genetic association.* European Journal of Clinical Microbiology & Infectious Diseases, 2016. **35**(11): p. 1811-1817.

313. Gaio, V., et al., *Hospitalization Risk Due to Respiratory Illness Associated with Genetic Variation at IFITM3 in Patients with Influenza A(H1N1)pdm09 Infection: A Case-Control Study.* Plos One, 2016. **11**(6).

314. David, S., et al., *Population genetics of IFITM3 in Portugal and Central Africa reveals a potential modifier of influenza severity.* Immunogenetics, 2018. **70**(3): p. 169-177.

315. Pan, Y., et al., *IFITM3 Rs12252-C Variant Increases Potential Risk for Severe Influenza Virus Infection in Chinese Population.* Front Cell Infect Microbiol, 2017. **7**: p. 294.

316. Lee, N., et al., *IFITM3, TLR3, and CD55 Gene SNPs and Cumulative Genetic Risks for Severe Outcomes in Chinese Patients With H7N9/H1N1pdm09 Influenza.* J Infect Dis, 2017. **216**(1): p. 97-104.

317. Wang, Z.F., et al., *Early hypercytokinemia is associated with interferon-induced transmembrane protein-3 dysfunction and predictive of fatal H7N9 infection.* Proceedings of the National Academy of Sciences of the United States of America, 2014. **111**(2): p. 769-774.

318. Makvandi-Nejad, S., et al., *Lack of Truncated IFITM3 Transcripts in Cells Homozygous for the rs12252-C Variant That is Associated With Severe Influenza Infection.* Journal of Infectious Diseases, 2018. **217**(2): p. 257-262.

319. Ohka, S., et al., *Receptor (CD155)-dependent endocytosis of poliovirus and retrograde axonal transport of the endosome.* J Virol, 2004. **78**(13): p. 7186-98.

320. Grassme, H., et al., *Rhinoviruses infect human epithelial cells via ceramide-enriched membrane platforms.* J Biol Chem, 2005. **280**(28): p. 26256-62.

321. Sodeik, B., M.W. Ebersold, and A. Helenius, *Microtubule-mediated Transport of Incoming Herpes Simplex Virus 1 Capsids to the Nucleus.* The Journal of Cell Biology, 1997. **136**(5): p. 1007-1021.

322. Chambers, R. and T. Takimoto, *Trafficking of Sendai Virus Nucleocapsids Is Mediated by Intracellular Vesicles.* Plos One, 2010. **5**(6).

323. Sanderson, C.M., M. Hollinshead, and G.L. Smith, *The vaccinia virus A27L protein is needed for the microtubule-dependent transport of intracellular mature virus particles.* Journal of General Virology, 2000. **81**: p. 47-58.

324. Kallewaard, N.L., A.L. Bowen, and J.E. Crowe, Jr., *Cooperativity of actin and microtubule elements during replication of respiratory syncytial virus.* Virology, 2005. **331**(1): p. 73-81.

325. Pitossi, F., et al., *A functional GTP-binding motif is necessary for antiviral activity of Mx proteins.* J Virol, 1993(Nov): p. 6726-6732.

326. Li, L.F., et al., *Guanylate-Binding Protein 1, an Interferon-Induced GTPase, Exerts an Antiviral Activity against Classical Swine Fever Virus Depending on Its GTPase Activity.* J Virol, 2016. **90**(9): p. 4412-4426.

327. DeDiego, M.L., L. Martinez-Sobrido, and D.J. Topham, *Novel Functions of the Interferon-Induced Protein 44-Like (Ifi44l) as a Feedback Regulator of Host Antiviral Responses.* J Virol, 2019.

328. DeDiego, M.L., et al., *Interferon-Induced Protein 44 Interacts with Cellular FK506-Binding Protein 5, Negatively Regulates Host Antiviral Responses, and Supports Virus Replication.* MBio, 2019. **10**(4).

329. Paucker, K., K. Cantell, and W. Henle, *Quantitative studies on viral interference in suspended L cells. III. Effect of interfering viruses and interferon on the growth rate of cells.* Virology, 1962. **17**: p. 324-34.

330. Echebli, N., et al., *Stage-specific IFN-induced and IFN gene expression reveal convergence of type I and type II IFN and highlight their role in both acute and chronic stage of pathogenic SIV infection.* PLoS One, 2018. **13**(1): p. e0190334.

331. Wong, M.T. and S.S. Chen, *Emerging roles of interferon-stimulated genes in the innate immune response to hepatitis C virus infection.* Cell Mol Immunol, 2016. **13**(1): p. 11-35.

332. Yang, G., et al., *IFITM1 plays an essential role in the antiproliferative action of interferon-gamma.* Oncogene, 2007. **26**(4): p. 594-603.

333. Fensterl, V. and G.C. Sen, *The ISG56/IFIT1 gene family.* J Interferon Cytokine Res, 2011. **31**(1): p. 71-8.

334. Meurs, E.F., et al., *Tumor suppressor function of the interferon-induced double-stranded RNA-activated protein kinase.* Proc Natl Acad Sci U S A, 1993. **90**(1): p. 232-6.

335. Chulu, J.L., et al., *Avian reovirus nonstructural protein p17-induced G(2)/M cell cycle arrest and host cellular protein translation shutoff involve activation of p53-dependent pathways.* J Virol, 2010. **84**(15): p. 7683-94.

336. Bian, T., et al., *Respiratory syncytial virus matrix protein induces lung epithelial cell cycle arrest through a p53 dependent pathway.* PLoS One, 2012. **7**(5): p. e38052.

337. Gibbs, J.D., et al., *Cell Cycle Arrest by Transforming Growth Factor beta 1 Enhances Replication of Respiratory Syncytial Virus in Lung Epithelial Cells.* Journal of Virology, 2009. **83**(23): p. 12424-12431.

338. Finelli, M.J. and P.L. Oliver, *TLDc proteins: new players in the oxidative stress response and neurological disease.* Mamm Genome, 2017. **28**(9-10): p. 395-406.

339. Day, R.M. and Y.J. Suzuki, *Cell proliferation, reactive oxygen and cellular glutathione.* Dose Response, 2006. **3**(3): p. 425-42.

340. Groves, H.T., et al., *Respiratory viral infection alters the gut microbiota by inducing inappetence.* 2019.

341. Russell, R.F., et al., *Partial Attenuation of Respiratory Syncytial Virus with a Deletion of a Small Hydrophobic Gene Is Associated with Elevated Interleukin-1beta Responses.* J Virol, 2015. **89**(17): p. 8974-81.

342. Guerrero-Plata, A., et al., *Differential response of dendritic cells to human metapneumovirus and respiratory syncytial virus.* Am J Respir Cell Mol Biol, 2006. **34**(3): p. 320-9.

343. Vashist, S., L. Urena, and I. Goodfellow, *Development of a strand specific real-time RT-qPCR assay for the detection and quantitation of murine norovirus RNA.* J Virol Methods, 2012. **184**(1-2): p. 69-76.

344. del Val, I.J., et al., *An optimized method for extraction and quantification of nucleotides and nucleotide sugars from mammalian cells.* Anal Biochem, 2013. **443**(2): p. 172-80.

345. Mailaparambil, B., et al., *Polymorphisms of interferons and their receptors in the genetics of severe RSV-associated diseases.* Archives of Virology, 2008. **153**(11): p. 2133-2137.

346. Feenstra, B., et al., *Common variants associated with general and MMR vaccine-related febrile seizures.* Nat Genet, 2014. **46**(12): p. 1274-82.

347. Haralambieva, I.H., et al., *Genome-wide associations of CD46 and IFI44L genetic variants with neutralizing antibody response to measles vaccine.* Hum Genet, 2017. **136**(4): p. 421-435.

348. Joseph, S.S. *J&J to record $700 million charge related to abandoned drug program*. Business News 2019 [cited 2019 20.9.19]; Available from: https://uk.reuters.com/article/uk-johnson-johnson-charge/jj-to-record-700-million-charge-related-to-abandoned-drug-program-idUKKCN1R22M3.

349. DeVincenzo, J.P., et al., *Activity of Oral ALS-008176 in a Respiratory Syncytial Virus Challenge Study.* N Engl J Med, 2015. **373**(21): p. 2048-58.

350. Fearns, R. and J. Deval, *New antiviral approaches for respiratory syncytial virus and other mononegaviruses: Inhibiting the RNA polymerase.* Antiviral Res, 2016. **134**: p. 63-76.

351. Coates, M., et al., *Preclinical Characterization of PC786, an Inhaled Small-Molecule Respiratory Syncytial Virus L Protein Polymerase Inhibitor.* Antimicrob Agents Chemother, 2017. **61**(9).

352. Liuzzi, M., et al., *Inhibitors of respiratory syncytial virus replication target cotranscriptional mRNA guanylylation by viral RNA-dependent RNA polymerase.* J Virol, 2005. **79**(20): p. 13105-15.

353. Braun, M.R., et al., *RNA elongation by respiratory syncytial virus polymerase is calibrated by conserved region V.* PLoS Pathog, 2017. **13**(12).

354. Sudo, K., et al., *YM-53403, a unique anti-respiratory syncytial virus agent with a novel mechanism of action.* Antiviral Res, 2005. **65**(2): p. 125-31.

355. Noton, S.L., et al., *Respiratory Syncytial Virus Inhibitor AZ-27 Differentially Inhibits Different Polymerase Activities at the Promoter.* J Virol, 2015. **89**(15): p. 7786-98.

356. Casanova, J.L. and L. Abel, *Human genetics of infectious diseases: Unique insights into immunological redundancy.* Seminars in Immunology, 2018. **36**(C): p. 1-12.

8 Appendix

Copyright Clearance Center

Note: Copyright.com supplies permissions but not the copyrighted content itself.

1 PAYMENT 2 REVIEW **3 CONFIRMATION**

Step 3: Order Confirmation

Thank you for your order! A confirmation for your order will be sent to your account email address. If you have questions about your order, you can call us 24 hrs/day, M-F at +1.855.239.3415 Toll Free, or write to us at info@copyright.com. This is not an invoice.

Confirmation Number: 11851356
Order Date: 09/16/2019

If you paid by credit card, your order will be finalized and your card will be charged within 24 hours. If you choose to be invoiced, you can change or cancel your order until the invoice is generated.

Payment Information

David Busse
Imperial College London
+44 7794775746
Payment Method: n/a

Order Details

Annual review of immunology

Order detail ID:	72010555
Order License Id:	4670750221685
ISSN:	1545-3278
Publication Type:	e-Journal
Volume:	
Issue:	
Start page:	
Publisher:	ANNUAL REVIEWS

Permission Status: Granted
Permission type: Republish or display content
Type of use: Thesis/Dissertation

Requestor type	Academic institution
Format	Electronic
Portion	chart/graph/table/figure
Number of charts/graphs/tables/figures	1
The requesting person/organization	Mr David Busse
Title or numeric reference of the portion(s)	Figure 4.
Title of the article or chapter the portion is from	Interferon-Stimulated Genes: A Complex Web of Host Defenses
Editor of portion(s)	N/A
Author of portion(s)	William M. Schneider, Meike Dittmann Chevillotte, and Charles M. Rice
Volume of serial or monograph	32
Page range of portion	524
Publication date of portion	February 6, 2014
Rights for	Main product
Duration of use	Life of current and all future editions
Creation of copies for the disabled	yes
With minor editing privileges	no

For distribution to	Worldwide
In the following language(s)	Original language of publication
With incidental promotional use	no
Lifetime unit quantity of new product	More than 2,000,000
Title	Functional Characterisation of interferon stimulated genes in respiratory viral infection
Institution name	Imperial College London
Expected presentation date	Jan 2020

Note: This item will be invoiced or charged separately through CCC's **RightsLink** service. More info **$ 0.00**

This is not an invoice.

Total order items: 1 **Order Total: 0.00 USD**